Dissertation
submitted to the
Combined Faculties of the Natural Sciences and Mathematics
of the
Ruperto-Carola-University of Heidelberg, Germany
for the degree of
Doctor of Natural Sciences

Put forward by

Matthias Kronenwett, MSc
born in Eberbach, Germany

Oral examination: 19 January 2011

Far-from-equilibrum dynamics of ultra-cold Fermi gases

Referees: apl. Prof. Dr. Thomas Gasenzer
Prof. Dr. Markus Oberthaler

Matthias Kronenwett

Institut für Theoretische Physik
Philosophenweg 16
D-69120 Heidelberg
Germany

Supervisor

apl. Prof. Dr. Thomas Gasenzer

Institut für Theoretische Physik
Philosophenweg 16
D-69120 Heidelberg
Germany

Abstract

In this thesis, far-from-equilibrium dynamics of fermionic quantum gases is discussed utilising functional quantum field theoretical methods. Employing the Schwinger-Keldysh path integral, real-time Schwinger-Dyson/Kadanoff-Baym dynamic equations for the two-point correlation functions are derived from the two-particle irreducible (2PI) effective action. For two specific models, these dynamic equations are investigated further. (a) For an $\mathcal{N}$-fold spin-degenerate ultra-cold Fermi gas, non-perturbative approximation schemes based on either a loop or a $1/\mathcal{N}$ expansion of the 2PI effective action are presented. Adopting these approximations, the long-time evolution of a homogeneous Fermi gas with $\mathcal{N} = 2$ after an initial preparation far from thermal equilibrium is thoroughly studied in one spatial dimension. Depending on the total energy, the gas is found to evolve into thermal as well as non-thermal states, the latter becoming manifest in violating the fluctuation-dissipation relation. (b) A similar $1/\mathcal{N}$ expansion is derived for the $SU(\mathcal{N})$ symmetric Kondo lattice model. At leading order, the mean-field dynamic equations of the $U = 0$ Anderson model are recovered. At next-to-leading order (NLO), both spin-flip and direct interactions between localised atoms and conduction band atoms are taken into account non-perturbatively into the dynamic equations. This allows future studies of possibly existing novel phases in coupling regimes where the Kondo screening and RKKY-type interactions are competing.

Kurzzusammenfassung

In dieser Arbeit wird die Nichtgleichgewichtsdynamik fermionischer Quantengase anhand funktionaler Methoden der Quantenfeldtheorie diskutiert. Mit Hilfe des Schwinger-Keldysh-Pfadintegrals werden dynamische Schwinger-Dyson/Kadanoff-Baym-Gleichungen für die Zweipunktsfunktionen aus der zweiteilchen-irreduziblen (2PI) effektiven Wirkung abgeleitet. Diese Gleichungen werden für zwei spezielle Modelle näher untersucht. (a) Für ein $\mathcal{N}$-fach entartetes, ultrakaltes Fermigas werden nichtstörungstheoretische Näherungsverfahren, denen entweder eine Schleifen- oder eine $1/\mathcal{N}$-Entwicklung der 2PI effektiven Wirkung zugrunde liegt, betrachtet. Als Anwendung dieser Näherungen wird die Langzeitentwicklung eines homogenen Fermigases mit $\mathcal{N} = 2$ in einer Raumdimension von einem anfänglichen Zustand, der weit entfernt eines thermischen Gleichgewichtszustands liegt, detailliert untersucht. Abhängig von der Gesamtenergie entwickelt sich das Gas mit der Zeit in thermische und nichtthermische Zustände, wobei sich die Letzteren durch eine Verletzung der Fluktuations-Dissipations-Beziehung auszeichnen. (b) Eine ähnliche $1/\mathcal{N}$-Entwicklung wird für das $SU(\mathcal{N})$-symmetrische Modell des Kondo-Gitters abgeleitet. In führender Ordnung werden die Molekularfeldgleichungen des $U = 0$ Anderson-Modells gefunden. In der nächsthöheren Ordnung werden sowohl spinaustauschende als auch spinbeibehaltende Wechselwirkungen zwischen lokalisierten Atomen und Leitungsbandatomen nichtstörungstheoretisch berücksichtigt. Dies erlaubt zukünftige Untersuchungen möglicher neuer Phasen in Wechselwirkungsbereichen, in denen Kondo-Abschirmung und eine RKKY-artige Wechselwirkung konkurrieren.

Für meine Eltern

Preface

The dynamics of interacting quantum many-body systems far from thermal equilibrium is a subject of great interest for a deeper understanding of nature and has various applications within the whole range of physics. Examples are cosmology, where the inflationary epoch during the very early evolution of our universe requires a quantum dynamical description [1, 2], high energy and particle physics, where the interest in non-equilibrium dynamics mainly originates from relativistic heavy-ion collision experiments [1, 3, 4, 5], molecular physics, where the understanding of many-body processes is important to analyse molecular reactions (e. g. metabolism in biology) [6], condensed matter physics, where ultrashort-time spectroscopy techniques using pulsed lasers with pulse durations and delay times in the attosecond range enable to probe electron dynamics [7, 8, 9], and AMO physics, where experiments with ultra-cold atomic quantum gases allow to study strongly interacting model Hamiltonians [10].

In spite of this diversity of applications, non-equilibrium physics still poses a challenge both for theory and experiment and requires deeper understanding. Two of the fundamental questions concern the long-time evolution of an isolated interacting quantum many-body system: Given that it starts in some deliberately chosen initial non-equilibrium configuration, will the interactions force the system to evolve into a stationary long-time behaviour, i. e. will *equilibration* take place? If yes, is this steady state in agreement with a standard statistical ensemble like the micro-canonical or (grand-)canonical ensemble, i. e. did *thermalisation* occur? For classical integrable systems, such problems have been studied intensively since the pioneering work of Fermi, Pasta, and Ulam [11, 12]. However, the time evolution of quantum systems remains much more elusive. In a closed system with unitary time evolution, no information is lost, irrespective whether or not the system is integrable. Thus, the system cannot show dissipation or reach thermal equilibrium at a fundamental level. Nonetheless, we can pose the question whether a closed and finite but sufficiently large system with a ground state shows, at least approximately, equilibration to a thermal or to some alternative quasi-stationary state before its unitary time evolution causes revivals [13]—and if so, we can ask on what time scale this happens. In this thesis, we will pursue these questions in the context of ultra-cold Fermi gases.

In recent years, new experimental techniques have been developed for ultra-cold atomic gases and solid-state physics that allow to precisely study quantum many-body dynamics. In the field of ultra-cold atomic gases, the combination of various trapping techniques with methods to manipulate the inter-atomic interaction strength opened a huge variety of possibilities to prepare ultra-cold atomic Bose and Fermi gases in non-

equilibrium initial states and investigate important aspects of the subsequent dynamics. This allows to examine dynamical theories for many-body systems whose parameters like the particle density and interaction strength can be precisely varied over wide ranges. In turn, an improved understanding of the capabilities and limitations of the dynamical theories allows to better interpret the results of other non-equilibrium experiments whose initial states and system parameters are much less tunable, e. g. in relativistic heavy-ion collision experiments.

Non-equilibrium experiments with ultra-cold gases have focused on the question of the equilibration of a one-dimensional quantum gas with quadratic dispersion in which isolated binary collisions of the particles would not change their momenta owing to the restrictions of simultaneous momentum and energy conservation [14, 15]. Many of the past experiments with ultra-cold gases can be approximately described by semi-classical approximations of the quantum many-body field equations such as the Gross-Pitaevskii, Hartree-Fock-Bogoliubov, or Bardeen-Cooper-Schrieffer theories [16, 17]. The description of the dynamics of many-body systems of sufficiently weakly interacting particles is usually based on perturbative approximations that rely on an expansion in powers of some dimensionless parameter that measures the binary interaction strength. These approximations are generically based on the smallness of statistical fluctuations. In the limit of infinitely strong interactions, a number of approaches exist—in particular for systems in only one or two spatial dimensions—that allow dual descriptions in which approximations rely on the smallness of the inverse of the coupling strength [18, 19].

For intermediate interaction strengths, only a few approaches exist. In this regime, quantum as well as strong classical fluctuations generally play an important rôle. Prime examples for systems in this regime are ultra-cold gases driven into the vicinity of Feshbach-Fano scattering resonances [20, 21, 22, 23], lattice-trapped gases in between the superfluid and Mott insulator regimes [24, 25, 26], and low-dimensional gases in regimes where the transverse confinement strongly affects the binary scattering dynamics of the particles [15, 17, 27, 28, 29, 30]. Ultra-cold Fermi gases have been studied extensively in the vicinity of the BEC-BCS crossover, i. e. superfluid-superconducting crossover [31, 32, 33, 34, 35, 36, 37, 38]. They currently attract increasing interest, for example, in the context of Kondo phenomena in lattice environments [39] studied also in this thesis. To appropriately model these experiments, it is crucial to include the quantum and strong classical fluctuations into the description. As discussed below, taking into account higher-order classical and quantum fluctuations is also important for describing the late-time behaviour of initially strongly perturbed as well as of continuously driven systems. This is the subject of non-equilibrium quantum field theory.

In quantum field theoretic descriptions of non-equilibrium physics, the quantities of interest are different from those in quantum field theory applied to, for example, high-energy reactions. In the latter, the primary concerns are cross sections of scattering processes between particles. These cross sections are related to transition amplitudes between asymptotically defined initial and final states. In non-equilibrium quantum

field theory, the main focus lies on the time evolution of expectation values of physical observables. In this case, only the initial state (density matrix) of the system is specified, and no information about the final state is available in the first instance. An adequate method to study the non-equilibrium dynamics for these kind of initial value problems is the closed-time-path (CTP) formalism developed by Schwinger [40], Bakshi and Mahanthappa [41, 42, 43], and Keldysh [44]. In this formalism, the initial conditions are specified by a density matrix that can be far from equilibrium. And the time evolution is governed by causal equations of motion that are completely determined by the classical action.

To describe the late-time behaviour of initially strongly perturbed as well as of continuously driven systems, standard perturbation theory approaches to describe non-equilibrium quantum field theories suffer from various problems. For example, the appearance of artificial, so-called secular, terms during the time evolution leads to a break down of the correct description even for weakly coupled systems after some evolution time, see e. g. Refs. [45, 46]. The reason for this is that the perturbative expansion parameter is generically of the type 'coupling multiplied by evolution time', which is no longer small at sufficiently late times however small the coupling is. Another example is the presence of pinch singularities [47]. However, these kind of problems can be resolved by resorting to self-consistent methods. A prominent example for a self-consistent method discussed in detail in the literature is the time-dependent Hartree approximation, which qualitatively reproduces the early-time behaviour to equilibrium but has problems to correctly describe the late-time behaviour of the dynamics quantitatively because it includes insufficiently scattering [48, 49, 50, 51, 52]. A quantitative description of the late-time behaviour needs to be consistent with vital conservation laws such as, for example, the conservation of the total energy.

A compelling method taking into account the effects of scattering between particles as well as quantum effects is the two-particle irreducible (2PI) effective action approach [53, 54, 55, 56, 57]. The 2PI effective action approach extends self-consistent mean-field formulations like the Hartree approximation by including the effects of scattering between particles to the desired order of approximation. The 2PI effective action represents the complete theory in terms of dressed one- and two-point correlation functions. Exact non-equilibrium dynamic equations for these correlation functions can be derived from the 2PI effective action using the CTP formulation. Approximations to these dynamic equations can be obtained by truncating the effective action and obtaining time evolution equations by subsequent functional derivations with respect to the desired correlation functions. Performing the approximation on the level of the effective action has two main advantages. First, the resulting equations are self-consistent and do not suffer from secular problems. And second, the variational procedure to derive the equation of motion ensures that they preserve the global symmetries of the action; therefore, they also fulfil the conservation laws associated with these symmetries through Noether's theorem. In particular, for a non-relativistic gas, the dynamic equations respect the local conservation of the

particle density-current vector as well as of the energy-momentum tensor.

Functional integral techniques based on the 2PI effective action enable an efficient embedding of summations of infinite series of perturbative processes. In recent years, systematic non-perturbative expansions of the 2PI effective action to next-to-leading order in inverse powers of the number of field components [58] have allowed substantial progress [59, 60]: after first successful applications of these non-perturbative expansions to the study of far-from-equilibrium dynamics as well as thermalisation in relativistic bosonic [60, 61, 62, 63] and fermionic [64, 65] theories, they have recently been employed in the context of ultra-cold bosonic quantum gases [66, 67, 68, 69, 70, 71]. A related alternative approach based on renormalisation-group-like flow equations was presented in Refs. [72, 73]. For introductory texts, see, e. g. Refs. [74, 75].

In this thesis, we present a self-consistent formulation of the non-equilibrium dynamics of ultra-cold Fermi gases in terms of beyond-mean-field Schwinger-Dyson/Kadanoff-Baym equations for correlation functions derived from the 2PI effective action.

Chapter 1 In the first chapter, we present a derivation of an exact non-equilibrium dynamical equation—an integro-differential Schwinger-Dyson/Kadanoff-Baym dynamic equation—for the two-point Green function of a non-relativistic Fermi gas. Thereby, we review the general framework for deriving this type of equation from the two-particle irreducible (2PI) effective action. The calculations and formulae in this chapter are model independent in the sense that we do not specify to any particular interaction between the fermions.

As pointed out above, the 2PI effective action approach to non-equilibrium dynamics is well established in the literature. The 2PI effective action for non-relativistic fermions is also known in the literature [76, 77], where it is discussed in the context of collective excitations in low-energy nuclear physics but not in the context of non-equilibrium dynamics. The main task in Ch. 1 was to combine this knowledge in a coherent presentation, and introduce the reader to the topic. To our knowledge, however, the derivation of the energy-momentum tensor for non-relativistic fermions from the 2PI effective action, which we present in Sec. 1.7, has never been shown explicitly.

The dynamical equation derived in the first chapter can generally not be solved exactly due to the complexity of the proper self-energy appearing therein. In order to be able to (numerically) solve the dynamical equation, some approximation of the proper self-energy is necessary. This requires a specification of a precise model in the first place. In the remainder of this thesis, we specifically investigate two types of models.

The first model, studied in Ch. 2 and Ch. 3, is an $\mathcal{N}$-component ultra-cold Fermi gas, where the individual components could be, for example, hyperfine states of fermionic atoms.

Chapter 2 In the second chapter, we begin with introducing the model for an ultra-cold Fermi gas containing $\mathcal{N}$ spin components that mutually interact through local s-wave contact collisions. We present two types of non-perturbative approximations of the 2PI effective action. The first type of approximation is based on a coupling expansion of the 2PI effective action, and a subsequent truncation of this expansion at a certain order. In the lowest-order approximation, we recover the self-consistent Hartree-Fock-Bogoliubov equation of motion. The second type of approximation is based on an expansion of the 2PI effective action in powers of $1/\mathcal{N}$. Considering the case of a degeneracy in the $\mathcal{N}$ spin degrees of freedom, we derive the 2PI effective action to next-to-leading order (NLO) in this expansion. While the $1/\mathcal{N}$ expansion is entirely classical in leading order approximation, classical fluctuations and corrections induced by quantum fluctuations, both of which are introduced by scattering, are included in NLO in a non-perturbative manner.

For the model of a non-relativistic Fermi gas with $\mathcal{N}$ components, the loop expansion of the 2PI effective action is briefly discussed in the literature [76, 77]; however, for example, the explicit form of the real-time dynamical equations beyond the first-order (Hartree-Fock-Bogoliubov) loop approximation has not been given there. Deriving the Schwinger-Dyson/Kadanoff-Baym equations up to next-to-leading (NLO) order $1/\mathcal{N}$ approximation of the 2PI effective action for non-relativistic Fermi gas with $\mathcal{N}$ components is original work. A major part of the work for my thesis project was the efficient numerical implementation of the dynamic equations up to 3rd-order in the loop expansion and up to NLO in the $1/\mathcal{N}$ approximation.

For our numerical investigations, we specify to the most fundamental but also particular interesting version of this model: a spatially homogeneous gas with two spin components in one spatial dimension (1D). In this version, the model is integrable in the sense that it has as many conserved quantities as there are degrees of freedom [78]. Since the model is integrable, it is expected not to thermalise in general if prepared out of equilibrium [79, 80, 81, 82]. The low-energy properties of the considered 1D Fermi gas can be approximated by a Tomonaga-Luttinger liquid (TLL) model [83] that contains a linear free dispersion. The approximating TLL model is known to form a low-energy fixed point of the full interacting one-dimensional Fermi gas, and its non-equilibrium dynamics has been studied [84, 85]. Its long-time evolution after an interaction quench approaches a generalised Gibbs ensemble [82] accounting for the conserved quasi-particle numbers. In this thesis, however, we consider the dynamic evolution described by the full interacting fermionic Hamiltonian, approaching the problem of equilibration from the high-energy end. Our analysis applies away from zero temperature in a regime of energies where the non-linearity of the dispersion becomes relevant; therefore, we do not expect to recover the TLL model. For our analysis, we employ Schwinger-Dyson/Kadanoff-Baym dynamic equations in the 2PI next-to-leading order $1/\mathcal{N}$ approximation. These equations are generally considered

to describe thermalisation. We find, however, that the correlation functions emerging at late times become incompatible with a thermal ensemble at low energies by analysing the fluctuation-dissipation relation. Non-thermal stationary states have also been found in a number of other models, both integrable and non-integrable [82, 84, 85, 86, 87, 88, 89].

Chapter 3 In the third chapter, we study the long-time evolution of a homogeneous one-dimensional Fermi gas with two-fold spin degeneracy from an initial state that is far from thermal equilibrium. We numerically solve the dynamical equations for such a gas employing the Schwinger-Dyson/Kadanoff-Baym dynamic equations in next-to-leading order $1/\mathcal{N}$ approximation of the 2PI effective action. We analyse the dependence of the late-time behaviour of the dynamics on the details of the initial state, on the total energy of the system, and on the strength of the interactions. At low energies, the high-momentum tail of the single-particle momentum distribution develops a power-law behaviour reminiscent of the p^{-4} power law of Tan's relation. By analysing the fluctuation-dissipation relation, we find furthermore that the correlation functions emerging at late times are incompatible with a thermal ensemble if the total energy of the system is sufficiently low.

Large parts of the original work presented in the first three chapters of this thesis are going to be published in the article [90].

The second model that we study in this thesis is the $SU(\mathcal{N})$ symmetric Kondo lattice model (KLM). This model has recently attracted interest in the cold-atom community because a fermionic quantum gas that is described by the KLM can be realised in experiments with the help of alkaline-earth-metal atoms trapped in optical lattice potentials [39, 91, 92, 93]. Alkaline-earth-metal atoms make an exceptional system to systematically study models with a global $SU(\mathcal{N} \geq 2)$ symmetry in experiments.

The ground-state phase diagram for the KLM in $d > 1$ spatial dimensions is not yet well understood. While the different phases for both sufficiently weak and stronger coupling can be well described, the understanding of the quantum phase transition that separates these two phases is the main outstanding challenge in KLM research. And the $1/\mathcal{N}$ expansion of the 2PI effective action beyond the leading-order approximation is a promising tool to tackle this challenge. In this thesis, we lay the foundations for this tackle.

Chapter 4 In the fourth chapter, we derive non-equilibrium dynamical equations for an ultra-cold Fermi gas that can be described by the $SU(\mathcal{N})$ symmetric Kondo lattice model (KLM). We first give a general motivation why the KLM recently attracted attention in the cold-atom community. We also discuss relevant properties of fermionic alkaline-earth-metal atoms that allow to simulate the KLM using optical lattice potentials.

Afterwards, we review the KLM more formally and show how different representations of the Kondo lattice Hamiltonian that can be found in the literature are linked to each other. Subsequently, we derive the dynamic equations using the $1/\mathcal{N}$ expansion of the 2PI effective action. In leading-order approximation of the $1/\mathcal{N}$ expansion, we recover the mean-field dynamic equations of the $U = 0$ Anderson model used in Ref. [93] to describe Kondo lattice dynamics. Finally, we derive the dynamic equations in next-to-leading order approximation. We discuss how the $1/\mathcal{N}$ expansion of the 2PI effective action beyond the leading-order approximation is a promising tool to tackle yet outstanding challenges in KLM research like, for example, the characterisation of possible novel phases outside the heavy-Fermi-liquid phase at strong interactions and the dynamics between these phases.

Our conclusions are drawn in the last chapter of this thesis. In the appendices, we review relevant properties of the ideal non-relativistic Fermi gas in d spatial dimensions and of Graßmann variables.

I would like to acknowledge and thank the people that have contributed to the content of my thesis. First and foremost, I would like to thank my supervisor Thomas Gasenzer for giving me a rich learning experience, and for his guidance and support during this project. I also would like to thank my co-adviser Markus Oberthaler for helpful discussions and for writing the joint report. Over the last few years, many discussions with different people positively influenced my thesis work; I would like to thank Cédric Bodet, Sebastian Bock, Michael Foss-Feig, Fabian Gross, Fabienne Haupert, Murray Holland, Selim Jochim, Stefan Kessler, Thomas Lübbert, Andreas von Manteuffel, Behnam Nikoobakht, Boris Nowak, Jan Pawlowski, Ana Maria Rey, Konrad Schade, Denes Sexty, and Martin Trappe. I would like to thank JILA and CU Boulder for their hospitality during my months in Boulder and the Heidelberg Graduate School for Fundamental Physics and the German Academic Exchange Service (DAAD) for financially supporting my stay at JILA. I would like to thank the bwGRiD project for providing computational resources that were essential for the numerical parts of my thesis project.

Matthias Kronenwett

Heidelberg, Germany
8 November 2010

Contents

List of figures

Chapter 1

Two-particle irreducible (2PI) effective action approach to non-equilibrium dynamics

In this first chapter, we present a derivation of an exact non-equilibrium dynamical equation for the two-point function of a non-relativistic Fermi gas. Thereby, we review the general framework for obtaining an exact dynamical equation for the two-point function from the two-particle irreducible (2PI) effective action. The calculations and formulae in this chapter are model independent in the sense that we do not specify any particular interaction between the fermions.

We start with a presentation of the general Lagrangian density for non-relativistic fermions (Sec. 1.1). Even though the explicit form of this general Lagrangian density is not needed for our discussion in this chapter (except for the last section), it allows us to remark on some basic and general properties of the specific models we investigate in the following chapters of this thesis. In particular, we discuss the symmetries of the Lagrangian density since it is crucial that also the dynamic equations derived later on need to respect them in order to appropriately describe the dynamics.

Our main interest is in the dynamic evolution of the lowest-order correlation functions since most of the experimentally relevant observables are determined by these functions. Due to the Pauli exclusion principle, which states that no two identical fermions can occupy the same quantum state simultaneously, there is no macroscopic field for fermions unlike it can be the case for bosons. And thus, for fermions, the lowest correlation function of our interest is the two-point (Green) function. We introduce the two-point Green function and its decomposition into the spectral function and the statistical propagator in Sec. 1.2.

The ensuing four sections are devoted to the derivation of the exact dynamic equation for the two-point Green function—approximations of the otherwise generally unsolvable equation are model dependent and are, therefore, discussed in the respective chapters (in Ch. 2 for the spin degenerate Fermi gas and in Ch. 4 for the Kondo lattice gas). In Sec. 1.3, we derive the non-equilibrium generating functional for connected Green functions using the Schwinger-Keldysh closed time path formulation suitable for initial value problems. Specifying to Gaussian initial states (in Sec. 1.4), which permit

to specify (one- and) two-point functions as initial conditions, allows us to write the generating functional in a much simpler form. However, written in a real-time path integral formulation, the generating functional still involves an integration over a fluctuating field; therefore, it can generally not be directly evaluated[1]. A solution is to introduce an effective action that incorporates these fluctuations without the need for an explicit path integral. As we will see in Sec. 1.5, the 2PI effective action is a suitable effective action when Gaussian initial states are considered. Similar to Hamilton's principle for the classical action, one can determine the exact dynamic equation for the two-point Green function from the effective action by solving a variational problem. This is shown in Sec. 1.6. The resulting dynamic equation for the two-point Green function involves a time integration along the closed time path; however, it can be transformed into two coupled integro-differential equations for the statistical propagator and the spectral function that involve only standard time integrals. This neat feature is especially helpful when solving the (at that time necessarily approximate) dynamic equations numerically.

Deriving the dynamic equations from the effective action functional has the substantial advantage that approximations can be made on the level of a functional. The 2PI effective action is constructed in such a way that it, as well as any truncation of it, owns the same global symmetries as the underlying classical action that specifies the model. Thus, starting with any truncation of the functional, the variational procedure then ensures that the resulting equations of motion still preserve the global symmetries. And hence, the Noether currents associated with these symmetries are also conserved. This is crucial for an accurate description of long-time and out-of-equilibrium dynamics. In Sec. 1.7, we discuss and give explicit expressions for the conserved total particle number, total energy, and total momentum.

1.1 General Lagrangian density for non-relativistic fermions

In this section, we motivate our choice of Lagrangian density for a fermionic field obeying the (non-relativistic) Schrödinger equation. Excluding interactions, we first observe that a continuity equation can be derived from the Schrödinger equation. The continuity equation implies the existence of a conserved current. And from the existence of a conserved current follows that the action (i. e. the Lagrangian density integrated over space-time) must be invariant under some continuous symmetry transformation. The fact that continuous symmetries of the action lead to conserved currents is known as Noether's theorem. After an obvious educated guess of the symmetry associated with the conserved current, we use Noether's theorem to derive the desired Lagrangian density. Having derived the Lagrangian density for the

[1] This is in contrast to a path integral formulation in equilibrium. In the latter, one can go over to an imaginary time description, in which the Euclidean action becomes positive definite and can be interpreted as a probability distribution. This allows to employ Monte-Carlo techniques to evaluate the path integral.

non-interacting fermionic fields, we then discuss the inclusion of interactions at cold temperatures.

We consider an ultra-cold Fermi gas of atoms. For the physical processes discussed in this thesis, we take all atoms to be of the same kind in the sense that they have the same masses and several internal states, e. g. fine and hyperfine states, to which we refer with small Greek letters in this chapter. Over large parts of this thesis, we will be concerned with a functional integral formulation of the dynamical field theory. In this formulation, the dynamics of an ultra-cold Fermi gas of atoms translates to the time evolution of complex Graßmann fields $\psi_\alpha(x)$, where the index α counts the internal states, and $x = (x_0, \mathbf{x}) = (t, \mathbf{x})$ is a space-time coordinate. If there is no risk of confusion, we use the time coordinates x_0 and t synonymously in the following. As an important property of complex Graßmann fields, the fields $\psi_\alpha(x)$ obey the anti-commutation relations

$$\psi_\alpha(x)\psi_\beta(y) + \psi_\beta(y)\psi_\alpha(x) = \psi_\alpha(x)\psi^*_\beta(y) + \psi^*_\beta(y)\psi_\alpha(x) = 0 \tag{1.1}$$

for any combination of α, β, x, and y. Here, the asterisk denotes complex conjugation. Further properties of Graßmann fields that are relevant for our discussion can be found in App. B.

The Hamiltonian for a single non-relativistic particle in the internal state α that is exposed to a possibly time-dependent external (e. g. trapping) potential $V_{\mathrm{ext},\alpha}(x)$ is

$$H^{\mathrm{1B}}_\alpha(x) = -\frac{(\hbar\nabla_{\mathbf{x}})^2}{2m} + V_{\mathrm{ext},\alpha}(x)\,. \tag{1.2}$$

The field equation for non-interaction fields $\psi_\alpha(x)$ is given by

$$\mathrm{i}\hbar\partial_t\psi_\alpha(x) = -\frac{\hbar^2}{2m}\nabla^2_{\mathbf{x}}\psi_\alpha(x) + V_{\mathrm{ext},\alpha}(x)\psi_\alpha(x)\,. \tag{1.3}$$

This equation is of the same form as the single-particle Schrödinger equation, but the interpretation is completely different: $\psi_\alpha(x)$ are fields describing the ultra-cold Fermi gas and is not a single-particle wave function.

As a first step towards the derivation of a Lagrangian density from the field equation, we recover a continuity equation and therewith a conserved current from Eq. (1.3). For this purpose, we multiply the field equation with ψ^*_α from the left. Subsequently, we subtract the complex conjugate of the resulting equation from itself (using $(\psi_\alpha\psi_\beta)^* \equiv \psi^*_\beta\psi^*_\alpha$). If we assume $V_{\mathrm{ext},\alpha}(x)$ to be real then this yields

$$\begin{aligned}
\partial_t\big(\psi^*_\alpha(x)\psi_\alpha(x)\big) &= \psi^*_\alpha(x)\big(\partial_t\psi_\alpha(x)\big) + \big(\partial_t\psi^*_\alpha(x)\big)\psi_\alpha(x) \\
&= \frac{\mathrm{i}\hbar}{2m}\Big(\psi^*_\alpha(x)\big(\nabla^2_{\mathbf{x}}\psi_\alpha(x)\big) - \big(\nabla^2_{\mathbf{x}}\psi^*_\alpha(x)\big)\psi_\alpha(x)\Big) \\
&= \frac{\mathrm{i}\hbar}{2m}\nabla_{\mathbf{x}}\cdot\Big(\psi^*_\alpha(x)\big(\nabla_{\mathbf{x}}\psi_\alpha(x)\big) - \big(\nabla_{\mathbf{x}}\psi^*_\alpha(x)\big)\psi_\alpha(x)\Big)\,.
\end{aligned} \tag{1.4}$$

This is a continuity equation of the form

$$\partial_t j^0_\alpha(x) + \nabla_{\mathbf{x}} \cdot \mathbf{j}_\alpha(x) = 0 \,, \tag{1.5}$$

where the charge density $j^0_\alpha(x)$ and the conventional current density $\mathbf{j}_\alpha(x)$ for the spin component α are given by

$$j^0_\alpha(x) = \psi^*_\alpha(x)\psi_\alpha(x) \tag{1.6}$$

$$\mathbf{j}_\alpha(x) = -\frac{\mathrm{i}\hbar}{2m}\Big(\psi^*_\alpha(x)\big(\nabla_{\mathbf{x}}\psi_\alpha(x)\big) - \big(\nabla_{\mathbf{x}}\psi^*_\alpha(x)\big)\psi_\alpha(x)\Big) \,. \tag{1.7}$$

Since the conserved current involves both $\psi_\alpha(x)$ and its complex conjugate $\psi^*_\alpha(x)$, both of them will appear in the Lagrangian density. To identify the symmetry of the action associated with the conserved charge, we note that both the field equation and the conserved current are invariant under a multiplication of the field with a global phase. This suggests that a global invariance of the action under the transformation

$$\psi_\alpha(x) \to \psi'_\alpha(x) = \mathrm{e}^{-\mathrm{i}\vartheta_\alpha/\hbar}\psi_\alpha(x) \approx \psi_\alpha(x)(1 - \mathrm{i}\vartheta_\alpha/\hbar) \tag{1.8}$$

$$\psi^*_\alpha(x) \to \psi'^*_\alpha(x) = \mathrm{e}^{\mathrm{i}\vartheta_\alpha/\hbar}\psi^*_\alpha(x) \approx \psi^*_\alpha(x)(1 + \mathrm{i}\vartheta_\alpha/\hbar) \tag{1.9}$$

where $\hbar$ and ϑ_α are real constants, generates the conserved current found above as a result of the symmetry. Generally, continuous symmetries of the action and conserved currents are related to each other through Noether's theorem.

Noether's theorem: Consider a Lagrangian density $\mathcal{L}(\psi_s, \partial_\mu\psi_s, x^\mu)$ that depends on several fields ψ_s distinguished by the index s, on the temporal and spatial derivatives of these fields $\partial_\mu\psi_s$ where $(\partial_\mu) = (\partial_t, \nabla)$, and on the space-time coordinates x^μ. If the action $S = \int \mathrm{d}x\, \mathcal{L}$, where $\int \mathrm{d}x$ denotes integration over space and time, is invariant under the transformations

$$x^\mu \to x'^\mu = x^\mu + \delta x^\mu \,, \qquad \delta x^\nu = X^\nu_a \delta\varepsilon_a \,, \tag{1.10}$$

$$\psi_s(x) \to \psi'_s(x) = \psi_s(x) + \Delta\psi_s(x) \,, \qquad \Delta\psi_s(x) = \Psi_{sa}(x)\delta\varepsilon_a \,, \tag{1.11}$$

where X and Ψ are matrices, and $\delta\varepsilon_a$ are infinitesimal parameters, then there exists the conserved current[2]

$$j^\mu_a(x) = \Psi_{sa}(x)\frac{\partial\mathcal{L}}{\partial(\partial_\mu\psi_s(x))} - T^\mu_\nu(x)X^\nu_a \tag{1.12}$$

such that $\partial_\mu j^\mu_a(x) = 0$. ◁

[2] In Eq. (1.12), $T^\mu_\nu(x) = (\partial\mathcal{L}/\partial(\partial_\mu\psi_s(x)))\partial_\nu\psi_s(x) - g^\mu_\nu\mathcal{L}$ is the energy-momentum tensor, where $g^{\mu\nu}$ is the metric tensor. In our case, we use flat Minkowski space-time where $(g^{\mu\nu}) = \mathrm{diag}\{1, -1, -1, -1\}$ such that $g^\mu_\nu = \delta^\mu_\nu$.

According to Noether's theorem, the transformation considered in Eqs. (1.8) and (1.9) yields

$$X_{\nu a} = 0\,, \quad \Psi(x) = (1/\mathrm{i}\hbar)\psi_\alpha(x)\,, \quad \Psi^*(x) = -(1/\mathrm{i}\hbar)\psi^*_\alpha(x)\,, \quad \delta\varepsilon_a = \vartheta_\alpha\,, \tag{1.13}$$

and the expression for the conserved Noether current is

$$\begin{aligned} j^\mu_\alpha(x) &= \Psi(x)\frac{\partial\mathcal{L}}{\partial(\partial_\mu\psi_\alpha(x))} + \Psi^*(x)\frac{\partial\mathcal{L}}{\partial(\partial_\mu\psi^*_\alpha(x))} \\ &= \frac{1}{\mathrm{i}\hbar}\left(\psi_\alpha(x)\frac{\partial\mathcal{L}}{\partial(\partial_\mu\psi_\alpha(x))} - \psi^*_\alpha(x)\frac{\partial\mathcal{L}}{\partial(\partial_\mu\psi^*_\alpha(x))}\right). \end{aligned} \tag{1.14}$$

Using Eq. (1.14) and Eqs. (1.6) and (1.7), one can now work backwards to find the Lagrangian density. Comparing the left-hand side and the right-hand side of the two expressions for $j^0_\alpha(x)$,

$$\begin{aligned} &\frac{1}{2}\Big(\psi^*_\alpha(x)\psi_\alpha(x) + \psi^*_\alpha(x)\psi_\alpha(x)\Big) \\ &= \frac{1}{\mathrm{i}\hbar}\left(\psi_\alpha(x)\frac{\partial\mathcal{L}_{\text{free}}}{\partial(\partial_t\psi_\alpha(x))} - \psi^*_\alpha(x)\frac{\partial\mathcal{L}_{\text{free}}}{\partial(\partial_t\psi^*_\alpha(x))}\right), \end{aligned} \tag{1.15}$$

and $j^i_\alpha(x)$,

$$\begin{aligned} &\frac{\mathrm{i}\hbar}{2m}\Big(\big(\partial_i\psi^*_\alpha(x)\big)\psi_\alpha(x) - \psi^*_\alpha(x)\big(\partial_i\psi_\alpha(x)\big)\Big) \\ &= \frac{1}{\mathrm{i}\hbar}\left(\psi_\alpha(x)\frac{\partial\mathcal{L}_{\text{free}}}{\partial(\partial_i\psi_\alpha(x))} - \psi^*_\alpha(x)\frac{\partial\mathcal{L}_{\text{free}}}{\partial(\partial_i\psi^*_\alpha(x))}\right), \end{aligned} \tag{1.16}$$

it is evident that the Lagrangian density $\mathcal{L}_{\text{free}}$ is given by

$$\begin{aligned} \mathcal{L}_{\text{free}} = {}& \frac{\mathrm{i}\hbar}{2}\Big(\psi^*_\alpha(x)\big(\partial_t\psi_\alpha(x)\big) - \big(\partial_t\psi^*_\alpha(x)\big)\psi_\alpha(x)\Big) \\ &+ \frac{(\mathrm{i}\hbar)^2}{2m}\big(\partial_i\psi^*_\alpha(x)\big)\big(\partial_i\psi_\alpha(x)\big) + \mathcal{L}(\psi,\psi^*)\,. \end{aligned} \tag{1.17}$$

Thus, from the conserved Noether current, the resulting Lagrangian density is determined up to a term $\mathcal{L}(\psi,\psi^*)$ that depends on the fields only (and a total divergence, which we did not write down). Since applying the variational principle $\delta S/\delta\psi^*_\alpha$ and $\delta S/\delta\psi_\alpha$ should give the field equation and its complex conjugate, respectively, the Lagrangian density is given by

$$\begin{aligned} \mathcal{L}_{\text{free}} = {}& \frac{\mathrm{i}\hbar}{2}\Big(\psi^*_\alpha(x)\big(\partial_t\psi_\alpha(x)\big) - \big(\partial_t\psi^*_\alpha\big)\psi_\alpha(x)\Big) \\ &- \frac{\hbar^2}{2m}\big(\nabla\psi^*_\alpha(x)\big)\cdot\big(\nabla\psi_\alpha(x)\big) - \psi^*_\alpha(x)V_{\text{ext},\alpha}(x)\psi_\alpha(x)\,. \end{aligned} \tag{1.18}$$

In the next sections, we choose the field basis $\psi_{\alpha,i}$ where the index i distinguishes real and imaginary parts of the quantum field,

$$\psi_{\alpha,1}(x) \equiv \sqrt{2}\,\mathrm{Re}[\psi_\alpha(x)]\,, \tag{1.19}$$

$$\psi_{\alpha,2}(x) \equiv \sqrt{2}\,\mathrm{Im}[\psi_\alpha(x)]\,. \tag{1.20}$$

To simplify the notation, we include the hyperfine index α and the field index i into a single index $a = (\alpha, i)$. Sums over a imply a sum over α and one over $i \in \{1, 2\}$. In this field basis, the Lagrangian density can be written as

$$\mathcal{L}_{\mathrm{free}} = \frac{1}{2}\int_y \overline{\psi}_a(x)\mathrm{i}G^{-1}_{0,ab}(x,y)\psi_b(y)\,, \tag{1.21}$$

where the inverse free propagator $\mathrm{i}G^{-1}_{0,ab}(x,y)$ is given by

$$\mathrm{i}G^{-1}_{0,ab}(x,y) = \delta(x-y)\big(\mathrm{i}\hbar\tau_{ab}\partial_{x_0} - \delta_{ab}H^{\mathrm{1B}}_\alpha(x)\big)\,, \tag{1.22}$$

where $\int_y \equiv \int \mathrm{d}y_0 \int \mathrm{d}^d y$ denotes the integration over the region of space-time under consideration (with d spatial dimensions), $\overline{\psi}_a(x) = \psi_b(x)\tau_{ba}$ with

$$\tau_{ab} \equiv -\delta_{\alpha\beta}\sigma^2_{i_a i_b}\,, \qquad \sigma^2 \equiv \begin{pmatrix} 0 & -\mathrm{i} \\ \mathrm{i} & 0 \end{pmatrix}\,, \tag{1.23}$$

$\delta_{ab} = \delta_{i_a i_b}\delta_{\alpha\beta}$, and $\delta(x-y) \equiv \delta(x_0 - y_0)\delta^{(d)}(\mathbf{x}-\mathbf{y})$ denotes the $(d+1)$-dimensional Dirac distribution. Note that the notation of overlined fields is introduced in order to diagonalise the Hamiltonian part of the free inverse propagator; this choice is commonly preferred in the literature.

Once we take interactions into account, additional terms $\mathcal{L}_{\mathrm{int}}(\psi, \psi^*)$ will appear in the Lagrangian density. If their dependence on the fields only is of such that $\mathcal{L}_{\mathrm{int}}(\psi, \psi^*)$ also respects the global invariance discussed above, e. g. $\mathcal{L}_{\mathrm{int}}(\psi, \psi^*) = \mathcal{L}_{\mathrm{int}}(\psi^*_\alpha \psi_\alpha)$, then the conserved current discussed above will remain a conserved current.

The microscopic interactions we are interested throughout this thesis are contact interactions where two particles meet to interact. Thus, the corresponding contribution to the Lagrangian density reads

$$\mathcal{L}_{\mathrm{int}} = \frac{\lambda_{\alpha\beta\gamma\delta}(x)}{2}\psi^*_\alpha(x)\psi^*_\beta(x)\psi_\gamma(x)\psi_\delta(x) + \mathrm{c.\,c.}\,, \tag{1.24}$$

where $\lambda_{\alpha\beta\gamma\delta}(x)$ is the coupling constant and c. c. denotes the complex conjugate of the first term. The detailed form of $\lambda_{\alpha\beta\gamma\delta}(x)$—in particular, which of these elements are non-vanishing—determines the specific model one is looking at. In the following chapters of this thesis, we will consider a spin-degenerate Fermi gas and a Kondo lattice gas, for which the specific forms of the interactions are given in Eq. (2.1) and Eq. (4.5), respectively.

Canonical quantisation

In the next sections, we sometimes resort to field operators rather than Graßmann fields. Therefore, we derive the canonical anti-commutation relation for the field operators that results from the Lagrangian density in the real field basis introduced in Eqs. (1.19) and (1.20) in the following.

Since the considered interactions in Eq. (1.24) do not depend on time-derivatives of the fields, the canonical momentum $\pi_a(x)$ to the field $\psi_a(x)$ obtained from the Lagrangian density in Eq. (1.21) is

$$\pi_a(x) = \frac{\delta\mathcal{L}}{\delta(\partial_{x_0}\psi_a(x))} = -\frac{\mathrm{i}\hbar}{2}\overline{\psi}_b(x)\tau_{ba} = -\frac{\mathrm{i}\hbar}{2}\psi_a(x)\,. \tag{1.25}$$

The minus sign in Eq. (1.25) is due to the fact that $\partial_{x_0}\psi$ needs to be anti-commuted with $\overline{\psi}$ in the Lagrangian density in order to perform the functional derivative. We see that the canonical momenta are given by the fields themselves. In the Dirac classification, this implies the second-class constraint

$$\chi_a(x) = \pi_a(x) + \frac{\mathrm{i}\hbar}{2}\psi_a(x) = 0\,, \tag{1.26}$$

which means that the classical Dirac brackets

$$\{A, B\}_D \equiv \{A, B\}_P - \{A, \chi_a\}_P (C^{-1})_{ab} \{\chi_b, B\}_P\,, \tag{1.27}$$

where C^{-1} is the inverse of the matrix $C_{ab} = \{\chi_a, \chi_b\}_P$, rather than the Poisson brackets $\{\cdot,\cdot\}_P$ need to be employed for the quantisation procedure [94, 95]. In our case, the Dirac brackets evaluate to

$$\{\pi_a(x), \psi_b(y)\}_D = -\frac{1}{2}\delta_{ab}\delta(x-y)\,. \tag{1.28}$$

Replacing the Dirac brackets by $(-\mathrm{i}/\hbar)$ times anti-commutation relations and promoting both the Graßmann fields and the canonical momenta to operators yields the equal-time anti-commutation relation

$$\left[\hat{\pi}_a(\mathbf{x},t), \hat{\Psi}_b(\mathbf{y},t)\right]_+ = -\frac{\mathrm{i}\hbar}{2}\delta_{ab}\delta(\mathbf{x}-\mathbf{y}) \tag{1.29}$$

$$\Leftrightarrow \quad \left[\hat{\Psi}_a(\mathbf{x},t), \hat{\Psi}_b(\mathbf{y},t)\right]_+ = \delta_{ab}\delta(\mathbf{x}-\mathbf{y}) \tag{1.30}$$

$$\Leftrightarrow \quad \left[\hat{\Psi}_a(\mathbf{x},t), \hat{\overline{\Psi}}_b(\mathbf{y},t)\right]_+ = \tau_{ab}\delta(\mathbf{x}-\mathbf{y})\,, \tag{1.31}$$

where $\hat{\overline{\Psi}}_b(y) = \hat{\Psi}_c(y)\tau_{cb}$, and $[\cdot,\cdot]_+$ denotes the anti-commutator.

1.2 Two-point Green function

Ultimately, we are interested in the description of the time evolution of expectation values of observables. These expectation values can be calculated from the time

evolution of the density matrix. In general, one can express any density matrix with the set of n-point Green functions; therefore, the knowledge of the dynamical evolution of all Green functions amounts to a complete dynamical solution. Our main interest is in the dynamic evolution of the lowest-order correlation functions since most of the experimentally relevant observables are determined by these functions. For fermions, there is no macroscopic field. And the lowest correlation function of our interest is the two-point function.

At the beginning of this section, we introduce the two-point Green function G, its statistical and spectral components F and ρ, respectively, and some of their properties that we use later in this thesis. And at the end, we show how F and ρ are related by the fluctuation-dissipation relation if the system is in thermal equilibrium.

1.2.1 Two-point Green function and its spectral and statistical components

The two-point Green function G is defined as the time-ordered expectation value of two fields at two points in space-time,

$$G_{ab}(x,y) = \langle \mathcal{T}_{\mathcal{C}} \hat{\Psi}_a(x) \hat{\overline{\Psi}}_b(y) \rangle \,, \tag{1.32}$$

where $\mathcal{T}_{\mathcal{C}}$ denotes time ordering along the time contour $\mathcal{C}$. Our discussion in this section will be general and we do not need to specify the time contour here. Both the time contour and the evaluation of the expectation value will be discussed in Sec. 1.3. For our purposes in this section, we only need to know that, for Graßmann fields, the time ordering is defined as

$$\mathcal{T}_{\mathcal{C}} \hat{\Psi}_a(x) \hat{\overline{\Psi}}_b(y) = \begin{cases} \hat{\Psi}_a(x) \hat{\overline{\Psi}}_b(y) & \text{if } \operatorname{sgn}_{\mathcal{C}}(x_0 - y_0) = 1 \\ -\hat{\overline{\Psi}}_b(y) \hat{\Psi}_a(x) & \text{if } \operatorname{sgn}_{\mathcal{C}}(x_0 - y_0) = -1 \,, \end{cases} \tag{1.33}$$

where $\operatorname{sgn}_{\mathcal{C}}(x_0 - y_0)$ denotes the sign function along the time contour $\mathcal{C}$ and evaluates to 1 (-1) if x_0 is posterior (prior) to y_0. Note that G is automatically connected[3] since there are no fermionic field expectation values, i. e. $\langle \hat{\Psi}_a(x) \rangle = 0$, for the situations relevant to us; however, for higher n-point functions, there is a difference between the full and the connected function.

At equal times, the time ordering is ill-defined; in other words, the two-point Green function G defined above is singular at $x_0 = y_0$. Particularly, but not only, for numerical implementations we are aiming at later on, it is convenient to make the singularity explicit and to decompose G into its non-singular spectral and statistical components. The spectral function ρ contains information about the spectrum of the theory, i. e. the energies and decay times of the states, and the statistical propagator

[3] In the language of probability theory or statistics, one would refer to the connected n-point function as the nth cumulant.

F accounts for the respective occupation numbers. They are defined as

$$\rho_{ab}(x,y) \equiv \mathrm{i}\langle\big[\hat{\Psi}_a(x), \hat{\overline{\Psi}}_b(y)\big]_+\rangle\,, \tag{1.34}$$

$$F_{ab}(x,y) \equiv \frac{1}{2}\langle\big[\hat{\Psi}_a(x), \hat{\overline{\Psi}}_b(y)\big]_-\rangle\,, \tag{1.35}$$

where $[\cdot,\cdot]_-$ denotes the commutator and $[\cdot,\cdot]_+$ the anti-commutator. Since the time ordering defined in Eq. (1.33) can be rewritten as

$$\mathcal{T}_\mathcal{C}\hat{\Psi}_a(x)\hat{\overline{\Psi}}_b(y) = \frac{1}{2}\Big(\big[\hat{\Psi}_a(x), \hat{\overline{\Psi}}_b(y)\big]_- + \big[\hat{\Psi}_a(x), \hat{\overline{\Psi}}_b(y)\big]_+ \operatorname{sgn}_\mathcal{C}(x_0 - y_0)\Big)\,, \tag{1.36}$$

one finds the decomposition identity

$$G_{ab}(x,y) = F_{ab}(x,y) - \frac{\mathrm{i}}{2}\rho_{ab}(x,y)\operatorname{sgn}_\mathcal{C}(x_0 - y_0)\ . \tag{1.37}$$

The sign function accounts now explicitly for the time ordering and the associated discontinuity at $x_0 = y_0$.

Finally, we remark some properties of the two-point functions that we will frequently use.

From the definitions of the two-point functions follow immediately the symmetry relations

$$G_{ab}(x,y) = \tau_{bc}G_{cd}(y,x)\tau_{da} = (-1)^{i_a+i_b}G_{\bar{b}\bar{a}}(y,x)\,, \tag{1.38a}$$

$$F_{ab}(x,y) = \tau_{bc}F_{cd}(y,x)\tau_{da} = (-1)^{i_a+i_b}F_{\bar{b}\bar{a}}(y,x)\,, \tag{1.38b}$$

$$\rho_{ab}(x,y) = \tau_{bc}\rho_{cd}(y,x)\tau_{da} = (-1)^{i_a+\bar{i}_b}\rho_{\bar{b}\bar{a}}(y,x)\,, \tag{1.38c}$$

where, for $a = (\alpha, i_a)$, we introduced $\bar{a} = (\alpha, \bar{i}_a)$ and $\bar{i}_a = 3 - i_a$.

In the definitions of ρ and F, the operator product is not time ordered. Therefore, the expectation values cannot be *directly* evaluated in the path integral formalism. However, expectation values of equal-time anti-commutators of Graßmann fields can be evaluated using the Bjorken-Johnson-Low theorem [96, 97]. These anti-commutation relations are consistent with the anti-commutation relations found in the canonical quantisation approach, cf. Eq. (1.31). Thus, the spectral density function fulfils

$$\rho_{ab}(x,y)\big|_{x_0=y_0} = \mathrm{i}\tau_{ab}\delta^{(d)}(\mathbf{x}-\mathbf{y})\,. \tag{1.39}$$

In the derivation of the equations of motion, we make use of this relation when applying the identity

$$\rho_{ab}(x,y)\partial_{x_0}\operatorname{sgn}_\mathcal{C}(x_0 - y_0) = 2\rho_{ab}(x,y)\delta_\mathcal{C}(x_0 - y_0) = 2\mathrm{i}\tau_{ab}\delta_\mathcal{C}(x-y)\,. \tag{1.40}$$

1.2.2 Fluctuation-dissipation relation in thermal equilibrium

Later in this thesis, when we look at the non-equilibrium dynamics of an interacting Fermi gas, we want to decide whether or not an equilibrated system is thermalised—in our terminology, "equilibrated" refers to "observables are stationary in time", whereas "thermalised" refers to "observables can also be obtained from one of the standard statistical ensembles" and requires equilibration. For an interacting system, especially if the interactions are strong, the single-particle modes are not the eigenmodes of the Hamiltonian. Hence, a comparison between the occupation number distribution of the single-particle modes and a Fermi-Dirac distribution cannot be consulted to decide whether the equilibrated state is thermalised.

Without assuming a particular particle number choice, a necessary condition for a state to be described as a (grand-)canonical ensemble with density operator $\hat{\rho} = \exp(-\beta\hat{H} - \mu N)$ is the Callen-Welton fluctuation-dissipation relation [98, 99]

$$F_{\alpha\alpha}(X_0;\omega,p) = -\mathrm{i}\left(\frac{1}{2} - n_{\mathrm{FD}}(\omega-\mu)\right)\rho_{\alpha\alpha}(X_0;\omega,p)\,, \tag{1.41}$$

which connects the statistical propagator F and the spectral function ρ via the Fermi-Dirac distribution $n_{\mathrm{FD}}(\omega) = (\exp(\beta\omega)+1)^{-1}$ with the inverse temperature $\beta = (k_B T)^{-1}$. Here,

$$F_{\alpha\alpha}(X_0;\omega,p) = \int \mathrm{d}s\, \exp(\mathrm{i}\omega s) F_{\alpha\alpha}(X_0 + s/2, X_0 - s/2; p)\,, \tag{1.42}$$

$$F_{\alpha\alpha}(t,t';p) = \frac{1}{2}\langle \big[\hat{\Psi}^\dagger_\alpha(t,p), \hat{\Psi}_\alpha(t',p)\big]_- \rangle\,, \tag{1.43}$$

and similar for $\rho_{\alpha\alpha}(t,t';p) = \mathrm{i}\langle[\hat{\Psi}^\dagger_\alpha(t,p), \hat{\Psi}_\alpha(t',p)]_+\rangle$. That means, to see if a system is possibly thermalised, one should look at the fluctuation-dissipation relation because it is not based on the choice of a particular field basis.

1.3 Non-equilibrium generating functional

In this section, we derive the Schwinger functional W, which is the generating functional for connected Green functions in the presence of a classical two-point field K. To describe non-equilibrium physics, where one typically specifies an initial state, we use the closed-time-path (CTP) formulation developed by Schwinger [40], Bakshi and Mahanthappa [41, 42, 43], and Keldysh [44], and show how the CTP formulation emerges naturally when calculating n-point functions. Furthermore, we want to use a path integral formulation in which time ordering is intrinsically built in (and the n-point functions we are interested in are expectation values of time-ordered field operators).

Since we look at non-equilibrium dynamics after the preparation of an initial state given by the initial density matrix $\hat{\rho}_D(t_0)$ at time t_0, expectation values need to be

evaluated with respect to the initial density matrix $\hat{\rho}_D(t_0)$, i. e.

$$\langle\cdot\rangle \equiv \mathrm{Tr}\left[\hat{\rho}_D(t_0)\cdot\right] . \tag{1.44}$$

Therefore, it is convenient to evaluate the trace in the basis of eigenstates of the Heisenberg field operators at the initial time, i. e. $\hat{\Psi}_a(0,\mathbf{x})|\psi_0^{(\pm)}\rangle = \psi_{0,a}^{(\pm)}(\mathbf{x})|\psi_0^{(\pm)}\rangle$, such that the matrix elements of $\hat{\rho}_D(t_0)$ can be evaluated with respect to them. For example, for the two-point function, we have

$$\begin{aligned}\langle\mathcal{T}_{\mathcal{C}}\hat{\overline{\Psi}}_a(x)\hat{\Psi}_b(y)\rangle &= \mathrm{Tr}\left[\hat{\rho}_D(t_0)\mathcal{T}_{\mathcal{C}}\hat{\overline{\Psi}}_a(x)\hat{\Psi}_b(y)\right] \\ &= \int \mathcal{D}\psi_0^{(+)}\mathcal{D}\psi_0^{(-)}\Big(\langle-\psi_0^{(+)}|\hat{\rho}_D(t_0)|\psi_0^{(-)}\rangle \\ &\qquad\qquad \times\langle\psi_0^{(-)}|\mathcal{T}_{\mathcal{C}}\hat{\overline{\Psi}}_a(x)\hat{\Psi}_b(y)|\psi_0^{(+)}\rangle\Big) ,\end{aligned} \tag{1.45}$$

where we inserted unity in the form $\int\mathcal{D}\psi_0^{(-)}|\psi_0^{(-)}\rangle\langle\psi_0^{(-)}| = 1$, cf. Eq. (B.26). Note that at this stage, the superscripts $(\pm)$ simply distinguish between the two different integration fields; but soon, they are promoted to label the two branches of a closed time path. The differential parts of the path integral measures in Eq. (1.45) are defined as $\mathcal{D}\psi_0^{(\pm)} = \prod_{\alpha,\mathbf{x}}(\mathrm{i}/2)\mathrm{d}\psi_{\alpha,1}^{(\pm)}(\mathbf{x},t_0)\mathrm{d}\psi_{\alpha,2}^{(\pm)}(\mathbf{x},t_0)$, cf. Eq. (B.22).

In the second line on the r. h. s. of Eq. (1.45), the time ordering operator $\mathcal{T}_{\mathcal{C}}$ still appears in the matrix elements. As mentioned before, the time ordering operator is ill-defined if the field operators have the same time arguments; therefore, we want to circumvent the explicit appearance of it in our expressions. In order to get rid of the time ordering operator, we aim to rewrite the matrix elements as a path integral expression since path integrals are intrinsically time ordered. The first step is to introduce the closed time path. For this purpose, we note that the involved field operators, in the Heisenberg picture, are evaluated at different times—after a transformation into the Schrödinger picture, this translates to additional time-evolution operators $\hat{U}(t,t') = \mathcal{T}\exp[-\mathrm{i}\int_t^{t'}H\mathrm{d}t'']$ between the field operators. For example, if $x_0 > y_0$ then

$$\begin{aligned}&\langle\psi_0^{(-)}|\mathcal{T}_{\mathcal{C}}\hat{\overline{\Psi}}_a(x)\hat{\Psi}_b(y)|\psi_0^{(+)}\rangle \\ &= \langle\psi_0^{(-)}|\hat{U}(t_0,x_0)\hat{\overline{\Psi}}_a(x)\hat{U}(x_0,y_0)\hat{\Psi}_b(y)\hat{U}(y_0,t_0)|\psi_0^{(+)}\rangle .\end{aligned} \tag{1.46}$$

Since the density matrix elements $\langle-\psi_0^{(+)}|\hat{\rho}_D(t_0)|\psi_0^{(-)}\rangle$ are taken on both sides with respect to states at time t_0, the combination of the time-evolution operators in Eq. (1.46) form a closed time path (CTP), the so-called closed Schwinger-Keldysh real-time path [40, 44] denoted by $\mathcal{C}$ in the following—$\mathcal{C}$ for 'contour'. The closed time path starts at t_0, runs to the maximum time appearing $t_{\max}$ in the arguments of the field operators, and then back to t_0. As depicted in Fig. 1.1, the branch of the time path that runs from t_0 to $t_{\max}$, is denoted as $\mathcal{C}^{(+)}$, and the branch that runs

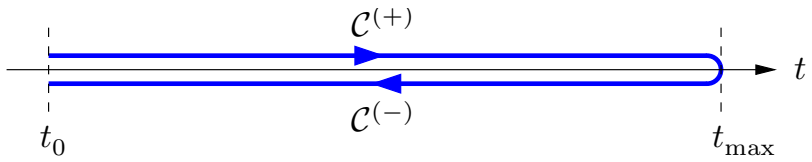

Figure 1.1: Illustration of the Schwinger-Keldysh closed real-time path (CTP). The CTP starts at the initial time t_0, runs to the maximum time $t_{\max}$ appearing in the arguments of the field operators, and then back to t_0. The branch of the time path that runs from t_0 to $t_{\max}$, is denoted as $\mathcal{C}^{(+)}$, and the branch that runs back to t_0 is denoted as $\mathcal{C}^{(-)}$. The branches are depicted above and below the time axis only in order to make them separately visible.

back to t_0 is denoted as $\mathcal{C}^{(-)}$, such that

$$\int_{\mathcal{C},x} = \int_{\mathcal{C},x_0} \int_{\mathbf{x}} \qquad \text{with} \qquad \int_{\mathcal{C},x_0} = \int_{\mathcal{C}^{(+)},x_0} + \int_{\mathcal{C}^{(-)},x_0} \tag{1.47}$$

where

$$\int_{\mathcal{C}^{(+)},x_0} = \int_{t_0}^{t_{\max}} \mathrm{d}x_0 \qquad \text{and} \qquad \int_{\mathcal{C}^{(-)},x_0} = \int_{t_{\max}}^{t_0} \mathrm{d}x_0 \,. \tag{1.48}$$

In the example discussed above, cf. Eq. (1.46), we have generically chosen the time arguments of the field operators to lie on $\mathcal{C}^+$; however, this can be generalized such that the time arguments of the operators can lie anywhere on $\mathcal{C}$. We want to consider this generalization, see, e. g. Ref. [66] for a discussion of it. Therefore, we have employed the contour time-ordering operator $\mathcal{T}_\mathcal{C}$ in the definition of the two-point Green function in Eq. (1.32) in the first place. Contour time-ordering along the CTP implies that operators evaluated at later times on the CTP stand to the left of those evaluated at earlier times.

Having introduced the notion of the CTP $\mathcal{C}$, we are in the position to lift the contour time-ordering operator $\mathcal{T}_\mathcal{C}$ in Eq. (1.45) by writing the matrix elements as a path integral expression,

$$\langle \psi_0^{(-)} | \mathcal{T}_\mathcal{C} \hat{\overline{\Psi}}_a(x) \hat{\Psi}_b(y) | \psi_0^{(+)} \rangle = \int_{\psi_0^{(+)}}^{\psi_0^{(-)}} \mathcal{D}\psi \, \overline{\psi}_a(x) \psi_b(y) \exp\left[\mathrm{i} \int_{\mathcal{C},x} \mathcal{L} \right], \tag{1.49}$$

where $\mathcal{L}$ is the Lagrangian density of the system. The path integral measure $\mathcal{D}\psi$ in Eq. (1.49) is defined on the complete CTP, i. e. $\mathcal{D}\psi = \prod_{\alpha,\mathbf{x},x_0\in\mathcal{C}} (\mathrm{i}/2) \mathrm{d}\psi_{\alpha,1}(x) \mathrm{d}\psi_{\alpha,2}(x)$. Thus, Eq. (1.45) can be rewritten as

$$\begin{aligned} \langle \mathcal{T}_\mathcal{C} \hat{\overline{\Psi}}_a(x) \hat{\Psi}_b(y) \rangle = & \int \mathcal{D}\psi_0^{(+)} \mathcal{D}\psi_0^{(-)} \langle \psi_0^{(+)} | \hat{\rho}_D(t_0) | \psi_0^{(-)} \rangle \\ & \times \int_{\psi_0^{(+)}}^{\psi_0^{(-)}} \mathcal{D}'\psi \, \overline{\psi}_a(x) \psi_b(y) \exp\left[\mathrm{i} S_\mathcal{C}[\psi] \right], \end{aligned} \tag{1.50}$$

where the action on the CTP is defined as

$$S_{\mathcal{C}}[\psi] = \int_{\mathcal{C},x} \mathcal{L}[\psi_\alpha, \psi_\alpha^*] \,. \tag{1.51}$$

Since the fields $\psi_0^{(\pm)}$ are now not only integration fields appearing in the matrix elements of the initial density matrix but also the (upper and lower) limits of the dynamical functional integral, the primed measure of this integral needs to exclude these initial-time fields, i. e. $\mathcal{D}'\psi = \prod_{\alpha,\mathbf{x},x_0\in\mathcal{C}\setminus\{t_0\}} (\mathrm{i}/2)\mathrm{d}\psi_{\alpha,1}(x)\mathrm{d}\psi_{\alpha,2}(x)$.

Knowing how the two-point function can be written as a path integral expression, cf. Eq. (1.50), it is self-evident that the desired non-equilibrium generating functional $Z[K;\hat{\rho}_D]$ is given by

$$\begin{aligned} Z[K;\hat{\rho}_D(t_0)] = \int \mathcal{D}\psi_0^{(+)}\mathcal{D}\psi_0^{(-)} \langle -\psi_0^{(+)}|\hat{\rho}_D(t_0)|\psi_0^{(-)}\rangle \\ \times \int_{\psi_0^{(+)}}^{\psi_0^{(-)}} \mathcal{D}'\psi \, \exp\left[\mathrm{i}S_{\mathcal{C}}[\psi] + \frac{\mathrm{i}}{2}\int_{\mathcal{C},xy} \overline{\psi}_a(x) K_{ab}(x,y)\psi_b(y)\right] . \end{aligned} \tag{1.52}$$

In Eq. (1.52), the classical external two-point field $K_{ab}(x,y) = \tau_{bc}K_{cd}(y,x)\tau_{da}$ is introduced to allow for the generation of correlation functions of order $2n$:

$$\begin{aligned} &\langle \mathcal{T}_{\mathcal{C}} \hat{\overline{\Psi}}_{a_1}(x_1)\hat{\Psi}_{b_1}(y_1)\cdots\hat{\overline{\Psi}}_{a_n}(x_n)\hat{\Psi}_{b_n}(y_n)\rangle \\ &= \frac{2^n}{Z} \left.\frac{\delta^n Z[K;\hat{\rho}_D(t_0)]}{\mathrm{i}\delta K_{a_1b_1}(x_1,y_1)\cdots\mathrm{i}\delta K_{a_nb_n}(x_n,y_n)}\right|_{K\equiv 0} . \end{aligned} \tag{1.53}$$

This implies that the connected two-point Green function in the presence of the external two-point field K can be derived by a functional differentiation,

$$-\frac{1}{2}G_{ba}(y,x;K) = \frac{\delta W[K]}{\delta K_{ab}(x,y)} \,, \tag{1.54}$$

of the Schwinger functional

$$W[K;\hat{\rho}_D] = -\mathrm{i}\ln Z[K;\hat{\rho}_D] \,. \tag{1.55}$$

Therefore, the Schwinger functional W is the generating functional for G. Note that for fermionic fields, the two-point Green function G is identical to the connected two-point function since the field expectation value always vanishes; however, for higher n-point functions, there is a distinction. Also note that the external two-point field K is introduced only for the technical reason of deriving the two-particle irreducible effective action in the following—the physical situation corresponds to the absence of external two-point fields, i. e. to $K = 0$. Finally note that two-point Green function defined in the previous section coincides with the one defined in Eq. (1.54) for a vanishing external two-point field, i. e.

$$G_{ab}(x,y) = G_{ab}(x,y;K=0) \,. \tag{1.56}$$

Before discussing the initial conditions in the next section, we like to close this section with some further remarks on the non-equilibrium generating functional in Eq. (1.52):

- ▷ The functional integral with action $S_{\mathcal{C}}$, i. e. the second line of the r. h. s. of Eq. (1.52), embeds the quantum fluctuations of the quantum dynamics. And the weighted average with the initial-time elements, i. e. the first line of the r. h. s. of Eq. (1.52), incorporates the statistical fluctuations.
- ▷ Causality requires that the contributions from the time path vanish for all times exceeding the largest time argument of the n-point function. This can be achieved by setting the external two-point field K to zero for these times such that the time evolution operators on the $\mathcal{C}^{(+)}$ and $\mathcal{C}^{(-)}$ branch of the CTP cancel each other.

1.4 Gaussian initial states

The non-equilibrium generating functional, Eq. (1.52), derived in the last section allows arbitrary initial conditions. When aiming to describe experimental relevant scenarios, it is however often enough to specify only a few of the lowest n-point functions. Often Gaussian initial states, where up to two-point functions are specified (for example, mode occupation numbers or pair correlation functions), are sufficient. In this section, we show how considering Gaussian initial states, for which we can combine the initial density matrix with the external two-point field K, allows to write the generating functional, Eq. (1.52), in a much simpler form [Eq. (1.61)].

The most general initial density matrix can be parametrised as

$$\langle -\psi_0^{(+)}|\hat{\rho}_D(t_0)|\psi_0^{(-)}\rangle = \mathcal{N}_0 \exp\big[\mathrm{i} f_{\mathcal{C}}[\psi]\big] \tag{1.57}$$

with normalization factor $\mathcal{N}_0$ and a functional $f_{\mathcal{C}}[\psi]$ that can be expanded in powers of the fields,

$$f_{\mathcal{C}}[\psi] = \alpha^{(0)} + \sum_{n=1}^{\infty} \frac{1}{n!} \int_{\mathcal{C},x^{(1)}\cdots x^{(n)}} \alpha^{(n)}_{a_1\cdots a_n}(x^{(1)},\ldots,x^{(n)}) \prod_{m=1}^{n} \psi_{a_m}(x^{(m)})\,. \tag{1.58}$$

In the integral, the boundary conditions $\psi_{a_m}(x_0^{(m)} \in \mathcal{C}^+, \mathbf{x}^{(m)}) = \psi_0^{(+)}(t_0,\mathbf{x})$ and $\psi_{a_m}(x_0^{(m)} \in \mathcal{C}^-, \mathbf{x}^{(m)}) = \psi_0^{(-)}(t_0,\mathbf{x})$ as well as summations over repeated indices are implied. The cumulants $\alpha^{(n)}_{a_1\cdots a_n}(x^{(1)},\ldots,x^{(n)})$ are non-zero only at time t_0 (at both ends of the CTP) since the density matrix $\hat{\rho}_D(t_0)$ is only specified at the initial time t_0. Note that for a physical density matrix, hermiticity implies that the cumulants are related amongst each other.

If the cumulants $\alpha^{(n)}_{a_1\cdots a_n}(x^{(1)},\ldots,x^{(n)})$ vanish for all $n > 2$ also at time t_0 then the initial density matrix is said to be Gaussian—and we talk about a Gaussian initial

state. For a fermionic theory, where the vanishing macroscopic field allows to set $\alpha^{(1)} = 0$, the generating functional with a Gaussian initial state can then be written as

$$Z[K;\rho_D(t_0)] = \mathcal{N}_0 \int_{\psi_0^{(+)}}^{\psi_0^{(-)}} \mathcal{D}\psi \, \exp\Bigg[\mathrm{i}\alpha^{(0)} + \frac{\mathrm{i}}{2}\int_{\mathcal{C},xy} \alpha^{(2)}_{ab}(x,y)\psi_a(x)\psi_b(y) + \mathrm{i}S_{\mathcal{C}}[\psi] + \frac{\mathrm{i}}{2}\int_{\mathcal{C},xy} \overline{\psi}_a(x)K_{ab}(x,y)\psi_b(y)\Bigg] . \tag{1.59}$$

Here, the path integral measure $\mathcal{D}\psi$ also includes the fields at time t_0. Compared to Eq. (1.50), this is now possible because the fields $\psi_0^{(\pm)}$ only appear as limits of the path integral and no longer as parts of the matrix elements of the initial density matrix—the implementation of the initial conditions is now completely determined by the cumulants. Finally, we absorb the normalization factor $\mathcal{N}_0$ and the cumulant $\alpha^{(0)}$ into the normalization of the path integral. And finally, we combine the remaining contribution of the initial density matrix $\rho_D(t_0)$ with the external two-point field R by defining the non-local source

$$R_{ab}(x,y) = K_{ab}(x,y) - \tau_{ac}\alpha^{(2)}_{cb}(x,y) . \tag{1.60}$$

This allows to write the generating functional in the simpler form

$$Z[R] = \int_{\psi_0^{(+)}}^{\psi_0^{(-)}} \mathcal{D}\psi \, \exp\Bigg[\mathrm{i}S_{\mathcal{C}}[\psi] + \frac{\mathrm{i}}{2}\int_{\mathcal{C},xy} \overline{\psi}_a(x)R_{ab}(x,y)\psi_b(y)\Bigg] . \tag{1.61}$$

As we have seen, the non-local source R allows to specify the initial conditions for the connected two-point function G of a Gaussian initial state in a very elementary way. And at the same time, a Gaussian initial state simplifies the generating functional. These are two of the main reasons why we introduce the two-particle irreducible (2PI) effective action in the next section to describe non-equilibrium dynamics. In the case where higher (say, up to n) cumulants need to be specified to describe the initial state, the most convenient way is to use the generalization of this approach to the nPI effective action [100]. Alternatively, staying within the 2PI effective action approach, one could also specify an artificial past that describes the desired higher cumulants at time t_0 through the time integrals over the artificial past in the dynamic equations; however, to find such an appropriate specification is practically very difficult if not impossible.

1.5 Non-equilibrium two-particle irreducible effective action

In the previous two sections, we first derived the non-equilibrium generating functional, and then simplified it by specifically looking at Gaussian initial states, cf. Eqs. (1.52)

and (1.61). But still, directly evaluating the full quantum real-time path integral in the simplified generating functional is in general not feasible because the oscillating complex measure is not positive definite and, thus, represents a variant of the sign problem [101, 102, 103]. One therefore needs to resort to analytical approaches in evaluating the dynamics in regimes where quantum fluctuations are relevant. This is in particular the case for long-time evolutions and where interactions become strong. Whereas, if quantum fluctuations are small then the quantum part of the fluctuating fields can be integrated out leading to a classical path integral that can be computed using Monte Carlo techniques [66, 104, 105, 106, 107].

We aim to simplify the path integral in the generating functional, Eq. (1.61). Instead of using the classical action $S_\mathcal{C}$ and a path integral over the fluctuating field ψ, we want to introduce an effective action Γ that incorporates the fluctuations such that the only contribution to the path integral comes from the path along the classical field[4] ϕ for which $\delta S_\mathcal{C}[\phi] = 0$; i. e. suggestively written, we take the step

$$\int \mathcal{D}\psi \, \exp\big[S_\mathcal{C}[\psi]\big] \longrightarrow \int \mathcal{D}\psi \, \delta(\psi - \phi) \exp\big[\Gamma[\psi]\big] \,, \tag{1.62}$$

and the path integration becomes trivial. Furthermore, the goal in constructing an effective action is not only to simplify the path integral in the generating functional but also to allow, similar to Hamilton's principle in the Lagrangian formulation of classical mechanics, to derive the quantum dynamic equation for the correlation function G from the effective action, i. e.

$$\frac{\delta\Gamma[G]}{\delta G} = 0 \,. \tag{1.63}$$

These requirements are fulfilled by the two-particle irreducible (2PI) effective action [53, 56, 57], which is defined by a Legendre transform of the Schwinger functional $W[R] = -\mathrm{i} \ln Z[R]$ with respect to the non-local source R defined in Eq. (1.60),

$$\Gamma[G] = W[R] - \int_{\mathcal{C},xy} \frac{\delta W[R]}{\delta R_{ab}(x,y)} R_{ab}(x,y) = W[R] + \frac{1}{2} \operatorname{Tr}\left[GR\right] \,, \tag{1.64}$$

where we have used Eq. (1.54), and where it is implied that

$$-\frac{1}{2} G_{ba}(y,x;R) = \frac{\delta W[R]}{\delta R_{ab}(x,y)} \tag{1.65}$$

can be inverted to give R as a function of G. The trace in Eq. (1.64) denotes a summation over all field and spin indices, and an integration over all spatial coordinates and over all times along the CTP. Note that, as compared to the Bose case, there is no Legendre transform with respect to the one-point source $J_a(x)$ as

[4] In the fermionic case we consider, the classical field, i. e. the field expectation value of the fluctuating quantum field, vanishes.

there is no field expectation value, either. Also note that the stationarity condition derived from Eq. (1.64),

$$\frac{\delta\Gamma[G]}{\delta G_{ba}(y,x;R)} = \frac{1}{2}R_{ab}(x,y)\,, \tag{1.66}$$

becomes the requested stationarity condition in Eq. (1.63) for a vanishing source R.

Next, to get more familiar with Eq. (1.64), we directly evaluate Γ to one-loop order. For this purpose, we divide the action in Eq. (1.61) into a free part and an interaction part

$$S_{\mathcal{C}}[\psi] = \frac{1}{2}\int_{\mathcal{C},xy} \overline{\psi}_a(x)\mathrm{i}G^{-1}_{0,ab}(x,y)\psi_b(y) + S_{\mathcal{C},\mathrm{int}}[\psi]\,, \tag{1.67}$$

where we introduced the free inverse propagator G_0^{-1} in the free part of the action. Taylor expanding the term $\exp[\mathrm{i}S_{\mathcal{C},\mathrm{int}}]$, the generating functional in Eq. (1.61) can be rewritten as

$$\begin{aligned} Z[R] = &\int_{\psi_0^{(+)}}^{\psi_0^{(-)}} \mathcal{D}\psi\, \exp\left[-\frac{1}{2}\int_{\mathcal{C},xy} \overline{\psi}_a(x)\big(G^{-1}_{0,ab}(x,y) - \mathrm{i}R_{ab}(x,y)\big)\psi_b(y)\right] \\ &+ \int_{\psi_0^{(+)}}^{\psi_0^{(-)}} \mathcal{D}\psi\, \exp\left[-\frac{1}{2}\int_{\mathcal{C},xy} \overline{\psi}_a(x)\big(G^{-1}_{0,ab}(x,y) - \mathrm{i}R_{ab}(x,y)\big)\psi_b(y)\right] \\ &\times \sum_{n=1}^{\infty} \frac{(\mathrm{i}S_{\mathcal{C},\mathrm{int}})^n}{n!}\,. \end{aligned} \tag{1.68}$$

The first term on the r. h. s. of this equation is is of one-loop order and involves a Gaussian functional integral that can be written as a functional determinant [95, 108, 109]. The second term is beyond one-loop order for the kind of interactions we are interested in, cf. Eq. (1.24). Neglecting the beyond one-loop order term, we find the generating functional up to one-loop order,

$$\begin{aligned} Z^{(1\,\mathrm{loop})}[R] &= \det{}^{1/2}\big[G^{-1}_{0,ab}(x,y) - \mathrm{i}R_{ab}(x,y)\big] \\ &= \exp\left[\frac{1}{2}\,\mathrm{Tr}\,\big[\ln\big(G^{-1}_{0,ab}(x,y) - \mathrm{i}R_{ab}(x,y)\big)\big]\right]. \end{aligned} \tag{1.69}$$

Correspondingly, the Schwinger functional to one-loop order is

$$W^{(1\,\mathrm{loop})}[R] = -\mathrm{i}\ln Z^{(1\,\mathrm{loop})}[R] = -\frac{\mathrm{i}}{2}\,\mathrm{Tr}\,\big[\ln\big(G^{-1}_{0,ab}(x,y) - \mathrm{i}R_{ab}(x,y)\big)\big]\,. \tag{1.70}$$

And thus, the 2PI effective action to one-loop order is given by

$$\begin{aligned} \Gamma^{(1\,\mathrm{loop})}[G] &= W^{(1\,\mathrm{loop})}[R] + \frac{1}{2}\,\mathrm{Tr}\,[GR] \\ &= -\frac{\mathrm{i}}{2}\,\mathrm{Tr}\,\big[\ln(G^{-1}) + (G_0^{-1} - G^{-1})G\big]\,, \end{aligned} \tag{1.71}$$

where in the last step we set $G^{-1} = G_0^{-1} - \mathrm{i}R$, which is justified since the stationarity condition, Eq. (1.66), at one-loop order then gives

$$\begin{aligned} \frac{\delta \Gamma^{(1\,\mathrm{loop})}[G]}{\delta G_{ba}(y,x;R)} &= \frac{\mathrm{i}}{2}\Big(G_{ab}^{-1}(x,y) - G_{0,ab}^{-1}(x,y)\Big) = \frac{1}{2}R_{ab}(x,y) \\ &\Rightarrow \quad G^{-1} = G_0^{-1} - \mathrm{i}R\,. \end{aligned} \tag{1.72}$$

Here, we used

$$\frac{\delta\,\mathrm{Tr}\,[\ln(G^{-1})]}{\delta G_{ba}(y,x;R)} = -G_{ab}^{-1}(x,y;R)\,. \tag{1.73}$$

To go beyond the one-loop order, the 2PI effective action Γ is conveniently written as the one-loop contribution plus a rest term Γ_2, which includes *per se* everything beyond one-loop,

$$\Gamma[G] = -\frac{\mathrm{i}}{2}\,\mathrm{Tr}\,\big[\ln(G^{-1}) + (G_0^{-1} - G^{-1})G\big] + \Gamma_2[G]\,. \tag{1.74}$$

The constant term $\mathrm{Tr}\,[G^{-1}G]$ is irrelevant for the dynamics. While the one-loop term remains within the mean-field approximation, scattering effects are contained in $\Gamma_2[G]$.

Before deriving the actual dynamic equations for the two-point Green function G in the next section, we discuss the rest term $\Gamma_2[G]$ a bit further. A particularly illustrative description is to write $\Gamma_2[G]$ in terms of Feynman diagrams. Since the effective action $\Gamma_2[G]$ is a functional, only closed loop diagrams can contribute[5]. In fact, $\Gamma_2[G]$ can be written as the series of all closed 2PI diagrams constructed from the Green function G and the bare vertices defined by the model Lagrangian [56, 110]—in the next section, we find another justification why all diagrams contributing to $\Gamma_2[G]$ are 2PI. A diagram is 2PI if it does not fall apart on opening two of its lines. Written as a formula, it is

$$\Gamma_2[G] = -\mathrm{i}\Big\langle \sum_{n=1}^{\infty} \frac{(\mathrm{i}S_{\mathrm{int}})^n}{n!} \Big\rangle_{\mathrm{2PI}\ \&\ G}\,, \tag{1.75}$$

where $\langle\cdot\rangle_{\mathrm{2PI}\ \&\ G}$ means that only closed 2PI diagrams contribute in which all lines are full propagators G. The specific form of a diagrammatic expansion of $\Gamma_2[G]$ depends on the considered model that specifies S_{int}. In this thesis, we will consider models with contact interactions that translate in a diagrammatic language to vertices where four propagator lines meet, cf. Eq. (1.24). For these models, Fig. 1.2 shows the leading diagrams in the series ordered by the number of bare vertices per diagram.

[5] Open diagrams would furthermore depend on space-time coordinates.

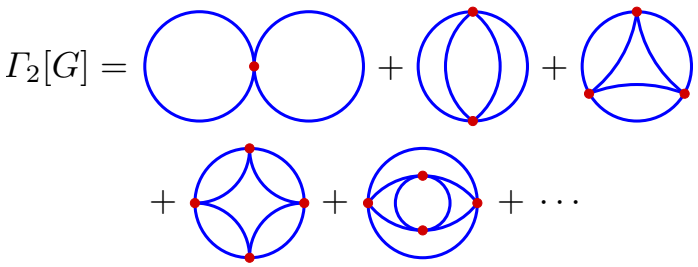

Figure 1.2: Diagrammatic expansion of the two-particle irreducible (2PI) part Γ_2 of the effective action (1.74) in terms of closed 2PI diagrams. (Blue) solid lines stand for the full Green function G, and (red) dots for the bare interaction vertex λ. Explicitly shown are all diagrams that contain up to four vertices. All factors that determine the relative weights of the diagrams are omitted.

1.6 Exact dynamic equations

In the previous section, we derived the two-particle irreducible (2PI) effective action that takes into account quantum effects. At this stage, we want to point out that no approximation of the 2PI effective action $\Gamma[G]$ has been made. The 2PI effective action provides an exact representation of the full theory. In this section, we derive the dynamic equation for the two-point function G (and later for its statistical and spectral components F and ρ) from the stationarity condition of the 2PI effective action, which also involves no approximation. Thus, the resulting dynamic equation provides an exact description of the dynamics. Our specification to Gaussian initial conditions still allows for higher irreducible correlations to be build up during the time evolution. These higher correlations are crucial for possible equilibration processes and, therefore, need to be taken into account by the quantum dynamics. Specifying the initial density matrix does not approximate the quantum dynamics.

1.6.1 Exact dynamic equation for the Green function

Given the effective action Γ, the stationarity condition in Eq. (1.66) determines G for a given non-local source R. For a given initial state, Eq. (1.66) represents the equation of motion for the Green function G. Deriving the equation of motion through a variational procedure (i. e. applying the stationarity condition) ensures that the global symmetries of the effective action are still preserved by the resulting equation of motion. As we will see in Sec. 1.7, this implies that the derived dynamic equation respects the conservation laws associated with these global symmetries.

Substituting the effective action of Eq. (1.74) into the stationarity condition in Eq. (1.66), one finds the real-time Schwinger-Dyson/Kadanoff-Baym-type equation

$$G^{-1}_{ab}(x,y;R) = G^{-1}_{0,ab}(x,y) - \mathrm{i}R_{ab}(x,y) - \Sigma_{ab}(x,y;G)\,, \tag{1.76}$$

where

$$\Sigma_{ab}(x,y;G) = -2\mathrm{i}\frac{\delta\Gamma_2[G]}{\delta G_{ba}(y,x;R)} \tag{1.77}$$

denotes the one-particle irreducible (1PI) self-energy[6]. From the last equation, we can infer that $\Gamma_2[G]$ is two-particle irreducible (2PI). Since a functional derivative with respect to the full propagator G is equivalent to cutting one propagator line in a Feynman diagram, the 1PI property of the self-energy requires $\Gamma_2[G]$ to be 2PI.

In order to derive a partial differential equation as dynamical equation for the two-point Green function G that is suitable for initial-value problems, we convolve Eq. (1.76) with G, which yields

$$\begin{aligned}\int_{\mathcal{C},z} \mathrm{i}G^{-1}_{0,ac}(x,z)G_{cb}(z,y;R) = \mathrm{i}\delta_{\mathcal{C}}(x-y)\delta_{ab} \\ + \mathrm{i}\int_{\mathcal{C},z}\big(\Sigma_{ac}(x,z;G) + \mathrm{i}R_{ac}(x,z)\big)G_{cb}(z,y;R)\,.\end{aligned} \tag{1.78}$$

Equation (1.78) now also clearly highlights how the information about the initial-time density matrix enters the dynamics. For a closed system (i. e. a vanishing external two-point field $K = 0$), the source term $R_{ac}(x,z)$ is non-vanishing only at $x_0 = z_0 = t_0$ where it is determined by the initial-time density matrix. Hence, the source term R fixes the initial values for the two-point function G. At all later times $x_0 > t_0$, no explicit dependence on R remains in the evolution equation since the term $\int_{\mathcal{C},z} R_{ac}(x,z)G_{cb}(z,y;R)$ vanishes for vanishing R.

Note that the (non-relativistic) free inverse propagator, cf. Eq. (1.22), contains a first-order time derivative. Since the free inverse propagator is otherwise diagonal in $(x-y)$, the integral on the left-hand side can be carried out, revealing the integro-differential structure of Eq. (1.78).

Despite the dynamic equation [Eq. (1.78)] being exact, to be solved, it requires knowledge of the self-energy and therefore of the 2PI part Γ_2 of the effective action. For practical computations, truncations of the series of 2PI diagrams are chosen—for a spin degenerate Fermi gas, some possible truncation schemes are discussed in the next chapter, and for a Kondo lattice gas in Ch. 4. It is crucial that these approximations are made on the level of the effective action, i. e. on the level of a functional. Deriving the approximated self-energy from an approximated functional and through a variational procedure has the advantage that conservation laws associated with the symmetries of the original effective action are automatically fulfilled by the resulting approximated dynamic equation [68, 111, 112, 113].

Next, in Sec. 1.6.2, we will rewrite the dynamic equation for the two-point function G as two equations for the spectral (ρ) and statistical (F) parts of G and thereby

[6] In Eq. (1.76), Σ must the self-energy because G_0^{-1} is the free inverse propagator and G^{-1} the inverse full propagator.

simplifying the time integrals over the CTP into standard time integrals. For this purpose, it is convenient to separate out the local contributions to the proper self-energy,

$$\Sigma_{ab}(x,y;G) = -\mathrm{i}\Sigma^{(0)}_{ab}(x;G)\delta_{\mathcal{C}}(x-y) + \overline{\Sigma}_{ab}(x,y;G)\,, \tag{1.79}$$

and include them together with the one-body Hamiltonian term of G_0^{-1} in the matrix

$$M_{ab}(x,y;G) = \delta_{\mathcal{C}}(x-y)\Big(\delta_{i_a i_b}H^{\mathrm{1B}}_{\alpha\beta}(x) + \Sigma^{(0)}_{ab}(x;G)\Big)\,. \tag{1.80}$$

For a closed system ($K=0$), the dynamic equation for G, Eq. (1.78), then takes the compact form

$$\begin{aligned}&\mathrm{i}\tau_{ac}\partial_{x_0}G_{cb}(x,y) - \mathrm{i}\delta_{ab}\delta_{\mathcal{C}}(x-y)\\ &= \int_{\mathcal{C},z}\big(M_{ac}(x,z;G) + \mathrm{i}\overline{\Sigma}_{ac}(x,z;G)\big)\,G_{cb}(z,y)\,,\end{aligned} \tag{1.81}$$

where

$$G_{ab}(x,y) = G_{ab}(x,y;R[K=0])\,. \tag{1.82}$$

We now left out the term $\int KG$ completely since it has (as we discussed above) no influence on the dynamics of G; but we keep in mind that we are allowed to specify G at the initial time t_0.

Note that the dynamic equation [Eq. (1.81)] reduces to a local differential equation in time if $\overline{\Sigma}$ is neglected. In contrast, a non-vanishing $\overline{\Sigma}$ introduces memory of the past evolution of G into the equation. This will be seen explicitly in the following. Because of the integration over the past evolution, we refer to $\int \overline{\Sigma}G$ as the so-called memory integral.

1.6.2 Exact dynamic equations for the statistical propagator and the spectral function

We employ the decomposition of the full Green function G into the statistical correlation function F and the spectral function ρ, cf. Eq. (1.37). In order to derive the contributions to the dynamic equations for F and ρ, one also decomposes $\overline{\Sigma}$ into its statistical and spectral parts,

$$\overline{\Sigma}_{ab}(x,y) = \overline{\Sigma}^{F}_{ab}(x,y) - \frac{\mathrm{i}}{2}\overline{\Sigma}^{\rho}_{ab}(x,y)\,\mathrm{sgn}_{\mathcal{C}}(x_0-y_0)\;. \tag{1.83}$$

Finally, inserting the decomposition identities of G, Eq. (1.37), and of $\overline{\Sigma}$, Eq. (1.83), into the dynamic equation for G, Eq. (1.81), one finds the dynamic equations for F

and ρ,

$$\begin{aligned}\big[\mathrm{i}\tau_{ac}\partial_{x_0} - M_{ac}(x;G)\big]F_{cb}(x,y) &= \int_{t_0}^{x_0}\mathrm{d}z\,\overline{\Sigma}^{\rho}_{ac}(x,z;G)F_{cb}(z,y) \\ &\quad - \int_{t_0}^{y_0}\mathrm{d}z\,\overline{\Sigma}^{F}_{ac}(x,z;G)\rho_{cb}(z,y)\,,\end{aligned} \tag{1.84}$$

$$\big[\mathrm{i}\tau_{ac}\partial_{x_0} - M_{ac}(x;G)\big]\rho_{cb}(x,y) = \int_{y_0}^{x_0}\mathrm{d}z\,\overline{\Sigma}^{\rho}_{ac}(x,z;G)\rho_{cb}(z,y)\,, \tag{1.85}$$

where $\int_t^{t'}\mathrm{d}x \equiv \int_t^{t'}\mathrm{d}x_0\int_{\mathbf{x}}$. There are now two dynamic equations, one for F and one for ρ, since after the insertion of the decomposition identities into the dynamic equation for G there are terms that involve the sign-function and others that do not. These two types of terms need to fulfil the equal sign independent of each other in order that the equation holds as a whole. The terms not involving the sign-function lead to the dynamic equation for F and the others to the dynamic equation for ρ. In deriving Eqs. (1.84) and (1.85), the decomposition of G and $\overline{\Sigma}$ into their statistical and spectral parts also allows to rewrite time integrals over the CTP into standard time integrals since

$$\int_{\mathcal{C}}\mathrm{d}z_0\,\mathrm{sgn}_{\mathcal{C}}(x_0-z_0) = 2\int_{t_0}^{x_0}\mathrm{d}z_0\,, \tag{1.86}$$

and

$$\int_{\mathcal{C}}\mathrm{d}z_0\,\mathrm{sgn}_{\mathcal{C}}(x_0-z_0)\;\mathrm{sgn}_{\mathcal{C}}(z_0-y_0) = 2\,\mathrm{sgn}_{\mathcal{C}}(x_0-y_0)\int_{y_0}^{x_0}\mathrm{d}z_0\,. \tag{1.87}$$

The right-hand sides of Eqs. (1.84) and (1.85) introduce scattering effects in form of memory integrals that render the equations non-Markovian. The form of Eqs. (1.84) and (1.85) is independent of the order of approximation chosen for Γ_2.

From the non-equilibrium dynamic equations (1.84) and (1.85), standard quantum kinetic (Boltzmann) equations can be derived for the mode occupation numbers $n_\alpha(\mathbf{p},t)$. This is achieved by a transformation to Wigner space, neglecting initial-time and non-Markovian effects in a gradient expansion with respect to the absolute time $T = (x_0+y_0)/2$, and making a quasi-particle ansatz—see, e. g. Refs. [74, 114] for details. The relevance of non-Markovian and initial-time effects provided by the full dynamic equations has been discussed, for bosonic theories, in Refs. [67, 115]. For concise discussions of kinetic equations, we refer to Refs. [116, 117].

Before discussing possible approximation schemes of Γ_2, which enable us to solve Eqs. (1.84) and (1.85) numerically, in the next chapter, we discuss the conservation of the total particle number, the energy, and the momentum in the next section.

1.7 Conservation laws

For a theory of dynamics to be physically meaningful, it is crucial to respect the conservation laws prescribed by the symmetries present in nature. For example,

for a system that is closed with respect to the exchange of particles and energy with its surroundings, a theoretical description of its dynamics needs to reflect the conservation of particle number and energy irrespective of the approximation chosen. In the preceding section, we have derived (exact) dynamic equations for the two-point functions from the two-particle irreducible (2PI) effective action. In the present section, we show how these equation fulfil crucial conservation laws for the total particle number, the total energy, and the total momentum. Our discussion also points out these quantities are also conserved at any order of truncation of the 2PI effective action. To take into account other independent conserved quantities, a generalization of the 2PI effective action approach to nPI effective actions is required [100]. In the remainder of this chapter, we assume a vanishing external field, i. e. $V_{\text{ext}} = 0$.

1.7.1 Particle number conservation

According to Noether's theorem, a symmetry of the Lagrangian density with respect to global $U(1)$ transformations of the complex fields ψ_α implies the conservation of the total particle number in component α, cf. Sec. 1.1. This symmetry is transferred to the effective action. And from there, it is passed on to the dynamic equations through the stationary condition (1.66). A global $U(1)$ symmetry of the Lagrangian density requires, of course, that also the interaction part of the Lagrangian density is $U(1)$ symmetric. Thus, the discussion of the particle number is model dependent. We postpone, therefore, the details of the discussion about the conservation of the particle number until we introduced specific models in the later chapters of this thesis. However, we present the general idea how the conservation of the total particle number can be shown in the following.

For a closed system ($K = 0$), we can construct the vanishing expression

$$0 = -2\mathrm{i}\tau_{ab} \int_y \frac{\delta \Gamma[G]}{\delta G_{cb}(y,x)} G_{ca}(y,x) \tag{1.88}$$

from the stationary condition of the effective action, Eq. (1.66). Substituting the right-hand side of Eq. (1.74) for Γ into this expression and using the identities

$$\partial_\mu^x G_{aa}(x,y)\Big|_{y=x} = \frac{1}{2}\Big(\partial_\mu^x G_{aa}(x,y) + \partial_\mu^y G_{aa}(x,y)\Big)\Big|_{y=x}, \tag{1.89}$$

$$\tau_{ab} G_{ba}(y,x) = -\tau_{ab} G_{ba}(x,y), \tag{1.90}$$

$$\partial_\mu^z f(z) = \big(\partial_\mu^x + \partial_\mu^y\big) f(x,y)\Big|_{x=y=z} \qquad \text{for } f(z) = f(x,y)\Big|_{x=y=z}, \tag{1.91}$$

one finds

$$\partial_{x_0} n_\alpha(x) + \frac{1}{m}\partial_k^x T^{0k,\alpha}(x) = 2\mathrm{i}\tau_{ab} \int_y \frac{\delta \Gamma_{\text{int}}[G]}{\delta G_{cb}(y,x)} G_{ca}(y,x) \tag{1.92}$$

with the particle density $n_\alpha(x)$ of the component α,

$$n_\alpha(x) = \frac{1}{2}\Big(1 - G_{aa}(x,x)\Big)\,, \tag{1.93}$$

the momentum density $T^{0k,\alpha}(x)$ of the component α,

$$T^{0k,\alpha}(x) = \frac{\mathrm{i}\tau_{ab}}{2}\partial_k^z G_{ba}(z,y)\Big|_{z=y=x}\,, \tag{1.94}$$

and $\Gamma_{\mathrm{int}}[G]$ defined as

$$\Gamma_{\mathrm{int}}[G] = \Gamma[G] + \frac{\mathrm{i}}{2}\,\mathrm{Tr}\left[G_0^{-1}G\right]\,. \tag{1.95}$$

In Eqs. (1.92), (1.93), and (1.94), it is $a = (\alpha, i_a)$ and $b = (\beta, i_b)$, and summations over i_a, i_b, β, but not α are implied.

With this, the general framework is set. If we can show that the r. h. s. of Eq. (1.92) vanishes (due to the $U(1)$ symmetry) then Eq. (1.92) becomes the continuity equation and the total particle number of component α is conserved. Substituting the 2PI effective action Γ from Eq. (1.74) into the definition of Γ_{int} in Eq. (1.95), and making use of the identity of Eq. (1.73), the r. h. s. of Eq. (1.92) can be rewritten as

$$\begin{aligned}
&2\mathrm{i}\tau_{ab}\int_y \frac{\delta\Gamma_{\mathrm{int}}[G]}{\delta G_{cb}(y,x)}G_{ca}(y,x)\\
&= -\tau_{ab}\int_y G^{-1}_{bc}(x,y)G_{ca}(y,x) + 2\mathrm{i}\tau_{ab}\int_y \frac{\delta\Gamma_2[G]}{\delta G_{cb}(y,x)}G_{ca}(y,x)\\
&= 2\mathrm{i}\tau_{ab}\int_y \frac{\delta\Gamma_2[G]}{\delta G_{cb}(y,x)}G_{ca}(y,x) = -\tau_{ab}\int_y \Sigma_{bc}(x,y)G_{ca}(y,x)\,,
\end{aligned} \tag{1.96}$$

where, like above, summations over i_a, i_b, β, but not α are implied. In the step from the second to the third line, we used that $\int_y G^{-1}_{bc}(x,y)G_{ca}(y,x) = \delta_{ba}$ is symmetric under an exchange of i_a and i_b while τ_{ab} is anti-symmetric under such an exchange; therefore, summing over i_a and i_b sets $\tau_{ab}\delta_{ba}$ to zero and the first term vanishes. Thus, it is left to show that, due to the $U(1)$ symmetry, also the integrand of Eq. (1.96) is symmetric under an exchange of i_a and i_b. As mentioned, this argumentation is done in the model dependent chapters since the symmetries of Γ_2 depend on the considered interactions. We will find that the argumentation is independent of the specific approximations made to Γ_2.

1.7.2 Energy and momentum conservation

For a time independent Lagrangian density, the system is time translation invariant. This implies energy conservation. Here, we consider the invariance under general translations in continuous space and time that vanish at the boundary, $x^\mu \to x^\mu + \epsilon^\mu(x)$,

where $\epsilon^\mu(x)$ is a time- and space-dependent infinitesimal $(d+1)$-vector. To leading order in ϵ, the Green function transforms under these translations as

$$G_{ab}(x,y) \to G_{ab}(x,y) + \epsilon^\nu(x)\partial_\nu^x G_{ab}(x,y) + \epsilon^\nu(y)\partial_\nu^y G_{ab}(x,y)\,, \tag{1.97}$$

where $\partial_\nu^x = \partial/\partial x_\nu$. We will see that under these transformations the variation of the 2PI effective action Γ can be written as $\Gamma[G] \to \Gamma[G] + \delta\Gamma[G]$, with

$$\delta\Gamma[G] = \int_x T^{\mu\nu}(x)\,\partial_\mu^x \epsilon_\nu(x)\,. \tag{1.98}$$

Since, by virtue of the stationarity condition (1.66), the variation $\delta\Gamma$ vanishes for all solutions of the equation of motion for G, an integration by parts shows that $T^{\mu\nu}$ is the conserved Noether current for the space-time translations:

$$\delta\Gamma[G] = -\int_x \epsilon_\nu(x)\,\partial_\mu^x T^{\mu\nu}(x) = 0\,. \tag{1.99}$$

$T^{\mu\nu}(x)$ is identified as the energy-momentum tensor. From the invariance of the theory under time translations follows a continuity equation for the energy density T^{00} and the energy flux T^{i0},

$$\partial_0^x T^{00}(x) + \partial_i^x T^{i0}(x) = 0\,, \tag{1.100}$$

with the total energy $\int \mathrm{d}^{(d)}x\, T^{00}(t,\vec{x})$ as the conserved charge. And from the invariance of the theory under space translations follows a continuity equation for the momentum density T^{0i} and the momentum flux (or stress tensor) T^{ij},

$$\partial_0^x T^{0i}(x) + \partial_j^x T^{ji}(x) = 0\,, \tag{1.101}$$

with the total momentum $\int \mathrm{d}^{(d)}x\, T^{0i}(t,\vec{x})$ as the conserved charge. The Eqs. (1.100) and (1.101) can be combined as $\partial_\mu^x T^{\mu\nu}(x) = 0$.

To derive explicit expressions for the components of the energy-momentum tensor, we split the variation of the effective action Γ under space-time translations into terms,

$$\delta\Gamma[G] = -\frac{\mathrm{i}}{2}\delta\,\mathrm{Tr}\left[\ln G^{-1}\right] - \frac{\mathrm{i}}{2}\delta\,\mathrm{Tr}\left[G_0^{-1}G\right] + \delta\Gamma_2[G]\,. \tag{1.102}$$

The contributions from the particular terms are as follows.

▷ To obtain the contribution to $T^{\mu\nu}$ arising from the one-loop term, we use Eq. (1.98) and observe that the term $\delta\,\mathrm{Tr}\left[\ln G^{-1}\right]$ in Eq. (1.102) does not contribute to $T^{\mu\nu}$.

▷ The term $\mathrm{Tr}\left[G_0^{-1}G\right]$ can be written as

$$\delta\left(-\frac{\mathrm{i}}{2}\,\mathrm{Tr}\left[G_0^{-1}(x,y)G(y,x)\right]\right) = -\frac{1}{2}\int_{xy}\mathrm{i}G^{-1}_{0,ab}(x,y)\delta G_{ba}(y,x) \tag{1.103}$$

with

$$\mathrm{i}G^{-1}_{0,ab}(x,y) = \delta(x-y)\Big(\mathrm{i}\tau_{ab}\partial_0^y + \delta_{ab}\frac{1}{2m}\partial_k^y\partial_k^y\Big)\,, \tag{1.104}$$

$$\delta G_{ab}(x,y) = \Big(\epsilon^\lambda(x)\partial_\lambda^x + \epsilon^\lambda(y)\partial_\lambda^y\Big)G_{ab}(x,y)\,. \tag{1.105}$$

Integration by parts and the identity

$$\int_x \partial_k^y[\delta(x-y)G(y,x)] = \int_x \delta(x-y)(\partial_k^x + \partial_k^y)G(y,x) \tag{1.106}$$

allows to rewrite the r. h. s. of Eq. (1.103) in the form of Eq. (1.98). The resulting contribution to the energy-momentum tensor are

$$T^{00}_{(G_0^{-1}G)}(x) = \frac{\partial_k^y\partial_k^x}{4m}G_{aa}(x,y)\bigg|_{y=x}\,, \tag{1.107}$$

$$T^{k0}_{(G_0^{-1}G)}(x) = -\frac{\partial_k^y\partial_0^x}{2m}G_{aa}(x,y)\bigg|_{y=x}\,, \tag{1.108}$$

$$T^{0j}_{(G_0^{-1}G)}(x) = \frac{\mathrm{i}\tau_{ab}}{2}\partial_j^x G_{ba}(x,y)\bigg|_{y=x}\,, \tag{1.109}$$

$$T^{kj}_{(G_0^{-1}G)}(x) = \left(-\delta_{ba}\frac{\partial_k^y\partial_j^x}{2m} - \frac{\delta_{kj}}{2}\left(\mathrm{i}\tau_{ab}\partial_0^x + \delta_{ab}\frac{\partial_l^y\partial_l^x}{2m}\right)\right)G_{ba}(x,y)\bigg|_{y=x}\,. \tag{1.110}$$

▷ As shown in Ref. [61], the contribution from the Γ_2 term to the energy-momentum tensor is given by

$$T^{\mu\nu}_{(\Gamma_2)}(x) = g^{\mu\nu}\frac{\delta\Gamma_2}{\delta\xi(x)}\bigg|_{\xi=1}\,, \tag{1.111}$$

where $\xi(x)$ is a scale factor introduced at every interaction vertex as $\lambda \to \xi(x)\lambda$ and $g^{\mu\nu}(x) = \mathrm{diag}\{1,-1,-1,-1\}$ the metric tensor of Minkowski space-time. In the Feynman graph language, the r. h. s. of Eq. (1.111) means that the diagram is left unchanged with an additional factor being pulled out. If the diagram has n vertices then the factor pulled out is n.

For the interactions considered by us, only vertices at which four propagator lines meet appear in the Feynman graphs contributing to Γ_2, cf. Fig. 1.2. In

this case, leaving a diagram unchanged up to a factor can also be achieved by cutting and repasting a propagator line, i. e.

$$\left.\frac{\delta\Gamma_2}{\delta\xi(x)}\right|_{\xi=1} = \frac{1}{2}\int_{\mathcal{C},y} \underbrace{\frac{\delta\Gamma_2[G]}{\delta G_{ab}(x,y)}}_{\text{cut}} \underbrace{G_{ab}(x,y)}_{\substack{\text{repaste} \\ (\text{together with } \int_{\mathcal{C},y})}} \quad . \tag{1.112}$$

The factor $1/2$ is required since there are $2n$ propagators for a diagram with n vertices; therefore, without the factor $1/2$, the pulled out factor would be $2n$ rather than n. Hence, using the definition of the proper self-energy, we can rewrite the contribution from Γ_2 to the energy-momentum tensor as

$$\begin{aligned} T^{\mu\nu}_{(\Gamma_2)}(x) &= \frac{g^{\mu\nu}}{2}\int_{\mathcal{C},y} \frac{\delta\Gamma_2[G]}{\delta G_{ba}(y,x)} G_{ba}(y,x) \\ &= \frac{\mathrm{i}g^{\mu\nu}}{4}\int_{\mathcal{C},y} \Sigma_{ab}(x,y)G_{ba}(y,x)\,. \end{aligned} \tag{1.113}$$

Putting the above results together, the energy-momentum tensor is given by

$$T^{\mu\nu}(x) = T^{\mu\nu}_{(\mathrm{Tr}[G_0^{-1}G])}(x) + T^{\mu\nu}_{(G_0^{-1}G)}(x) + T^{\mu\nu}_{(\Gamma_2)}(x)\,, \tag{1.114}$$

and its individual components are

$$T^{00}(x) = \frac{\partial_k^y\partial_k^x}{4m}G_{aa}(x,y)\bigg|_{y=x} + \frac{\mathrm{i}}{4}\int_{\mathcal{C},y}\Sigma_{ab}(x,y)G_{ba}(y,x)\,, \tag{1.115}$$

$$T^{i0}(x) = -\frac{\partial_i^y\partial_0^x}{2m}G_{aa}(x,y)\bigg|_{y=x}\,, \tag{1.116}$$

$$T^{0j}(x) = \frac{\mathrm{i}\tau_{ab}}{2}\partial_j^x G_{ba}(x,y)\bigg|_{y=x}\,, \tag{1.117}$$

$$\begin{aligned} T^{ij}(x) = &-\left(\delta_{ba}\frac{\partial_i^y\partial_j^x}{2m} + \frac{\delta_{ij}}{2}\left(\mathrm{i}\tau_{ab}\partial_0^x - \delta_{ab}\frac{\partial_k^y\partial_k^x}{2m}\right)\right)G_{ba}(x,y)\bigg|_{y=x} \\ &- \frac{\mathrm{i}\delta_{ij}}{4}\int_{\mathcal{C},y}\Sigma_{ab}(x,y)G_{ba}(y,x)\,. \end{aligned} \tag{1.118}$$

Note that in the non-relativistic energy-momentum tensor of a Galilean invariant theory, the energy flux does not necessarily coincide with the momentum density, i. e. generally $T^{i0}(x) \neq T^{0i}(x)$, unlike it is the case in a Lorentz invariant theory. However, the stress tensor $T^{ij}(x)$ is symmetric, which reflects the rotational invariance of the theory.

1.8 Summary

In this chapter, we presented a derivation of an exact non-equilibrium dynamical equation—an integro-differential Schwinger-Dyson/Kadanoff-Baym equation—for

the two-point Green function of a non-relativistic Fermi gas without specifying any specific model for the interactions. Thereby, we reviewed the general framework for obtaining an exact dynamical equation for the two-point function from the two-particle irreducible (2PI) effective action.

First, we derived the general Lagrangian density for non-relativistic fermions. Second, we introduced the two-point Green function G, its decomposition into the statistical propagator F and the spectral function ρ, and showed how F and ρ are related through the fluctuation-dissipation relation if the system is in a (grand-)canonical thermal state. Then, we derived the non-equilibrium generating functional for connected Green functions using the Schwinger-Keldysh closed time path (CTP) formulation suitable for initial value problems. After specifying to Gaussian initial states, we introduced the two-particle (2PI) effective action, which incorporates the quantum fluctuations and allows to circumvent the direct evaluation of a path integral. Using a variational procedure, we derived the exact dynamic equations for the two-point Green function from the 2PI effective action. We showed how this equation can be transformed into two coupled integro-differential equations for the statistical propagator and the spectral function. These two equations involve only standard time integrals rather than time integrals along the CTP. The latter fact will be helpful when numerically solving the then approximated equations later on.

Chapter 2

Non-perturbative approximations of the 2PI effective action for a Fermi gas with $\mathcal{N}$-fold spin degeneracy

In the previous chapter, we derived an exact non-equilibrium dynamical equation for the two-point function of a non-relativistic Fermi gas [Eq. (1.81)]. However, this dynamical equation can generally not be solved exactly due to the complexity of the proper self-energy contribution $\overline{\Sigma}$ appearing therein. In order to be able to (numerically) solve the dynamical equation, some approximation of the proper self-energy is necessary. This requires a specification of a precise model in the first place. In this and the next chapter, we look into the non-equilibrium dynamics of a non-relativistic Fermi gas with $\mathcal{N}$-fold spin degeneracy. The model for such a gas is introduced in Sec. 2.1.

The main focus of this chapter is a discussion of different possible approximation schemes of the two-particle irreducible (2PI) effective action Γ, which lead to an approximated proper self-energy. Each of these approximations is characterised by a certain truncation of the expansion of the 2PI part Γ_2 of the 2PI effective action in terms of 2PI diagrams. As we discussed in the previous chapter, it is a crucial advantage to first approximate the functional Γ_2 and then derive the corresponding (approximated) proper self-energy from the approximated Γ_2 rather than directly approximating the proper self-energy. The advantage is that the resulting approximated dynamic equation still preserves the global symmetries of the original model and, therefore, fulfils the conservation laws associated with these symmetries.

We describe two approximation schemes of the 2PI effective action in detail. Both of them are non-perturbative. The first approximation scheme, discussed in Sec. 2.2, is a loop expansion. In this expansion, the contributions to the 2PI part Γ_2 of the 2PI effective action are ordered as a power series in the number of explicitly appearing bare coupling constants λ. This is very similar to the standard loop or coupling expansion with the only difference that now only 2PI graphs are considered and the full propagator G is used for all propagator lines in a diagram. And since the

full propagator itself contains the bare coupling constant λ to all orders, the loop expansion using the full propagator is non-perturbative in the coupling even for small λ. We discuss the first-order (Hartree-Fock-Bogoliubov) approximation in the loop expansion and obtain dynamic equations for the single particle density and an anomalous pair-correlation function. In the next order of this approximation, the resulting coupled equations for the statistical propagator F and spectral function ρ generalise the quantum Boltzmann kinetic equation for multi-component fermions by including non-Markovian[1] corrections to the propagation kernel as well as many-body corrections to the two-body T matrix. At the end of this section, we briefly comment on higher-order loop approximations. It is important to note that the loop expansion requires a small coupling constant in order to be a controlled approximation.

The second approximation scheme, discussed in Sec. 2.3, is a controlled non-perturbative approximation, in which the expansion parameter is not based on the coupling (and which is, therefore, not restricted to the weak coupling regime). Instead, the 2PI part Γ_2 of the effective action is expanded in powers of the inverse number of spin states $\mathcal{N}$, i. e. in powers of $1/\mathcal{N}$. We derive the 2PI effective action to next-to-leading order (NLO) in this so-called $1/\mathcal{N}$ expansion [58][2]. At NLO, an infinite number of diagrams is resummed and both scattering and memory effects are included. The dynamic equations derived from the NLO approximation in the $1/\mathcal{N}$ expansion of the 2PI effective action are suitable for a numerical evaluation, as it was first shown in Refs. [59, 60, 74] for relativistic models. At the end of this section, we give a short discussion on how to go beyond the NLO approximation of the $1/\mathcal{N}$ expansion.

Using the non-perturbative approximation schemes discussed in the current chapter, we present our numerical results for a one-dimensional Fermi gas with two-fold spin degeneracy in the next chapter.

2.1 Fermi gas with $\mathcal{N}$-fold spin degeneracy

The Lagrangian for a non-interacting Fermi gas is given in Eq. (1.18), where the Greek indices are now spin labels, i. e. $\alpha \in \{1, 2, \ldots, \mathcal{N}\}$. In a physical system, the spin label could, for example, count $\mathcal{N}$ different atomic hyperfine states that can be populated. In this section, we first characterise the interactions for such a Fermi gas at ultra-cold temperatures, and discuss the symmetries of the corresponding Lagrangian. Afterwards, we comment on the structure of the interaction vertex and introduce a special graphical representation for the vertex in Feynman diagrams. This representation is especially helpful in the discussion of the $1/\mathcal{N}$ expansion of the 2PI effective action in Sec. 2.3.

[1] The term "non-Markovian" refers to the property of a system that its near-future evolution is not only determined by the present state of the system but also by its past evolution.

[2] In the literature, the truncated $1/\mathcal{N}$ expansion introduced in Ref. [58] is often also referred to as the *GW* approximation (GWA).

2.1.1 The model Lagrangian and its symmetries

Since we consider an ultra-cold gas of fermionic atoms, s-wave contact interactions between atoms in different hyperfine states are assumed, while Pauli's principle forbids s-wave collisions between fermions that are internally in the same state. p-wave and higher-order partial-wave contributions are neglected. Our formalism, though, can be readily extended to more complicated interaction potentials. In the contact potential approximation, the interactions in the channel characterised by the asymptotic hyperfine states α and β are described by the potential $V_{\mathrm{int},\alpha\beta}(\mathbf{x}-\mathbf{y},t) = g_{\alpha\beta}(t)\delta(\mathbf{x}-\mathbf{y})$ with a possibly time-dependent coupling strength $g_{\alpha\beta}(t)$. In three spatial dimensions, for example, the coupling strength is related to the scattering length $a_{\alpha\beta}$ between states α and β by the relation $g_{\alpha\beta} = 4\pi\hbar^2 a_{\alpha\beta}/m$. Hence, the interaction Hamiltonian reads

$$H_{\mathrm{int}}(t) = \frac{g_{\alpha\beta}(t)}{2}\int_{\mathbf{x}} \hat{\Psi}^\dagger_\alpha(\mathbf{x})\hat{\Psi}^\dagger_\beta(\mathbf{x})\hat{\Psi}_\beta(\mathbf{x})\hat{\Psi}_\alpha(\mathbf{x})\,, \tag{2.1}$$

where we used the shorthand notation $\int_{\mathbf{x}} \equiv \int \mathrm{d}^d x$ for the spatial integration in d dimensions.

Furthermore, we generalise the possibly time-dependent trapping potentials or other external-field matrix elements V_{ext} in Eq. (1.18) such that they can also pairwise couple between the hyperfine levels, i. e. $V_{\mathrm{ext}} = V_{\mathrm{ext},\alpha\beta}(x)$, which can be realised in an experiment, for example, by a magnetic field.

For the contact interactions considered above and the generalisation of the external potential, the resulting Lagrangian for the $\mathcal{N}$-component ultra-cold Fermi gas reads

$$\begin{aligned} L = \int_{\mathbf{x}} \Bigg(& \frac{\mathrm{i}}{2}\Big(\psi^*_\alpha(x)\partial_{x_0}\psi_\alpha(x) - \big(\partial_{x_0}\psi^*_\alpha(x)\big)\psi_\alpha(x)\Big) + \psi^*_\alpha(x)\frac{\nabla^2}{2m}\psi_\alpha(x) \\ & - \psi^*_\alpha(x)V_{\mathrm{ext},\alpha\beta}(x)\psi_\beta(x) - \frac{\lambda_{\alpha\beta}}{2\mathcal{N}}\psi^*_\alpha(x)\psi^*_\beta(x)\psi_\beta(x)\psi_\alpha(x)\Bigg)\,, \end{aligned} \tag{2.2}$$

where ∂_{x_0} denotes the partial derivative with respect to time, and summations over repeated indices are implied. A factor of $1/\mathcal{N}$ has been taken out of the couplings $\lambda_{\alpha\beta} = \mathcal{N} g_{\alpha\beta}$ in order to make the relative weight of the interaction to the quadratic terms in the Lagrangian invariant under a rescaling of $\mathcal{N}$. This will be of use when considering the expansion of the 2PI effective action in powers of $1/\mathcal{N}$ in Sec. 2.3.

Three symmetries of the Lagrangian play an important rôle:

1. The Lagrangian possesses a global $U(1)$ symmetry ($\psi = (\psi_1, \ldots, \psi_{\mathcal{N}})^T \to \mathrm{e}^{\mathrm{i}\theta}\psi$), and in the case where V_{ext} does not couple different hyperfine levels, i. e. where $V_{\mathrm{ext},\alpha\beta}(x) = \delta_{\alpha\beta}V_{\mathrm{ext},\alpha}(x)$, the Lagrangian density possesses a global $U(1)$ symmetry even within each hyperfine subspace ($\psi_\alpha \to \mathrm{e}^{\mathrm{i}\theta_\alpha}\psi_\alpha$). Together with the linear time derivative, this $U(1)$ symmetry implies the conservation of the total particle number in both cases, and the total particle number even within each hyperfine state in the latter case, cf. Sec. 1.1.

Note that in relativistic physics, where one has a second-order time derivative in the Lagrangian, the global $U(1)$ symmetry imposes a conserved current with charge density $\langle\psi\partial_t\psi^\dagger - \psi^\dagger\partial_t\psi\rangle$. In this case the total particle number is not a conserved quantity, but rather the difference in the total particle number and the total anti-particle number.

2. For vanishing external fields and time-independent interactions, the Lagrangian is Galilei invariant. This symmetry implies a local conservation of the energy-momentum tensor, cf. Secs. 1.7.2 and 1.7.1.

3. If the couplings between the hyperfine levels through both the external field $V_{\mathrm{ext},\alpha\beta}$ and the interactions $\lambda_{\alpha\beta}$ are all equal to each other, the Lagrangian has an additional $O(\mathcal{N})$ symmetry under rotations in the space of the hyperfine states.

   Note that for the interactions considered here, see Eqs. (2.1) and (2.2), the fermionic property of the interaction (that two fermions of the same spin component do not interact with each other) is implemented in the fields since $\hat{\Psi}_\alpha(\mathbf{x})\hat{\Psi}_\alpha(\mathbf{x}) = 0$ and $\psi_\alpha(x)\psi_\alpha(x) = 0$; therefore, it is unnecessary to additionally require $\lambda_{\alpha\alpha}$, and all couplings $\lambda_{\alpha\beta}$ can indeed be chosen to be equal.

As in the previous chapter, we change to the field basis $\psi_{\alpha,i}$ where the index i distinguishes real and imaginary parts of the quantum field,

$$\psi_{\alpha,1}(x) \equiv \sqrt{2}\,\mathrm{Re}[\psi_\alpha(x)]\,, \tag{2.3}$$

$$\psi_{\alpha,2}(x) \equiv \sqrt{2}\,\mathrm{Im}[\psi_\alpha(x)]\,. \tag{2.4}$$

To simplify the notation, we include the hyperfine index α and the field index i into a single index $a = (\alpha, i)$. Sums over a imply a sum over $\alpha \in \{1, \ldots, \mathcal{N}\}$ and one over $i \in \{1, 2\}$.

The Graßmann action

$$S[\psi] = \int_{x_0} L[\psi_\alpha, \psi^*_\alpha]\,, \tag{2.5}$$

where $\int_{x_0} \equiv \int \mathrm{d}x_0$, associated with the Lagrangian in Eq. (2.2) then reads

$$S[\psi] = \frac{1}{2}\int_{xy} \overline{\psi}_a(x)\mathrm{i}G^{-1}_{0,ab}(x,y)\psi_b(y) + S_{\mathrm{int}}[\psi]\,. \tag{2.6}$$

Here, the inverse free fermionic propagator is given by

$$\mathrm{i}G^{-1}_{0,ab}(x,y) = \delta(x-y)\big(\mathrm{i}\tau_{ab}\partial_{x_0} - \delta_{i_a i_b}H^{\mathrm{1B}}_{\alpha\beta}(x)\big)\,, \tag{2.7}$$

with the one-body Hamiltonian

$$H^{\mathrm{1B}}_{\alpha\beta}(x) = -\frac{\nabla^2_{\mathbf{x}}}{2m}\delta_{\alpha\beta} + V_{\mathrm{ext},\alpha\beta}(x)\,, \tag{2.8}$$

$\int_x \equiv \int \mathrm{d}x_0 \int \mathrm{d}^d x$ denotes the integration over the region of space-time under consideration, $\delta_{ab} = \delta_{\alpha\beta}\delta_{i_a i_b}$, and

$$\tau_{ab} \equiv -\delta_{\alpha\beta}\sigma^2_{i_a i_b}\,, \qquad \text{with } \sigma^2 \equiv \begin{pmatrix} 0 & -\mathrm{i} \\ \mathrm{i} & 0 \end{pmatrix}\,. \tag{2.9}$$

Furthermore, $\delta(x-y) \equiv \delta(x_0-y_0)\delta^{(d)}(\mathbf{x}-\mathbf{y})$ denotes the $(d+1)$-dimensional Dirac distribution and $\overline{\psi}_a(x) = \psi_b(x)\tau_{ba}$. The interaction part $S_{\mathrm{int}}[\psi]$ corresponding to the Lagrangian in Eq. (2.2) is

$$S_{\mathrm{int}}[\psi] = -\frac{\lambda_{\alpha\beta}}{8\mathcal{N}} \int_x \overline{\psi}_a(x)\overline{\psi}_b(x)\psi_b(x)\psi_a(x)\,. \tag{2.10}$$

For the sake of completeness, we note that the action for a Fermi gas trapped in a lattice potential has the same form as in Eq. (2.6) if the tight binding approximation is applied. In this case, the free inverse propagator is given by

$$\mathrm{i}G^{-1}_{0,ab}(x,y) = \mathrm{i}\tau_{ab}\partial_{x_0}\delta(x-y) - \delta_{ab}H^{\mathrm{1B}}_{\alpha}(x,y)\delta(x_0-y_0)\,, \tag{2.11}$$

where

$$H^{\mathrm{1B}}_{\alpha}(x,y) = -J\delta^{(d)}_{\langle \mathbf{n},\mathbf{m}\rangle} + \epsilon_{\alpha,n}\delta^{(d)}_{\mathbf{nm}} \tag{2.12}$$

is the one-body Hamiltonian. Here, $x = (x_0, \mathbf{n})$ and $y = (y_0, \mathbf{m})$ denote the lattice space-time coordinates, $\delta(x-y) = \delta^{(d)}_{\mathbf{nm}}\delta(x_0-y_0)$, and $\delta^{(d)}_{\langle \mathbf{n},\mathbf{m}\rangle} = 1$ if and only if, in the single-band approximation, $\mathbf{n}$ and $\mathbf{m}$ denote adjacent sites in the d-dimensional lattice; otherwise, $\delta^{(d)}_{\langle \mathbf{n},\mathbf{m}\rangle} = 0$. The site dependent energy $\epsilon_{\alpha,\mathbf{n}}$ describes, for example, an additional external trapping potential for hyperfine mode α, and we neglect spin mixing by this potential. All other previous and subsequent equations carry over to the lattice case when spatial integrals are replaced by sums over the lattice sites.

2.1.2 Structure of the interaction vertex

Having chosen a model, we are now in the position to discuss possible approximations and truncation schemes of the two-particle irreducible effective action. To be precise, we approximate the infinite sum in Eq. (1.75),

$$\Gamma_2[G] = -\mathrm{i}\left\langle \sum_{n=1}^{\infty} \frac{(\mathrm{i}S_{\mathrm{int}})^n}{n!} \right\rangle_{\text{2PI \& } G}\,, \tag{(1.75)}$$

with S_{int} given by the equivalent of Eq. (2.10) in a field operator language. In the process of evaluating the expectation values of the approximated sum, we use Wick's theorem to reduce products of field operators to sums of products of pairs of these operators (where the two-point Green function G defined in Eq. (1.32) is used for the expectation value of each of these pairs). For this discussion, it is convenient to reveal the specific structure of the point interaction vertex and to represent the vertex

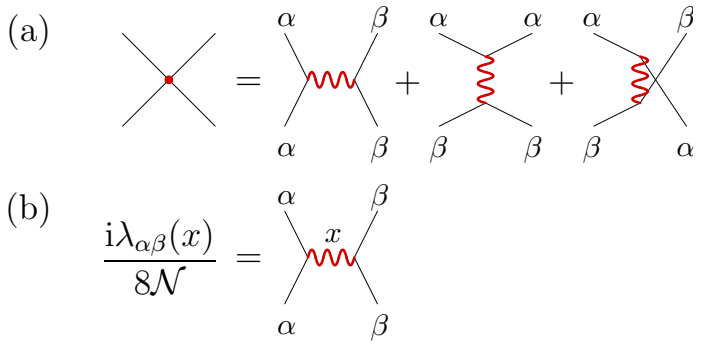

Figure 2.1: (a) Decomposition of the bare vertex λ (red dot) as a sum of the three possible spin-index contractions. (b) The point interaction vertex $\lambda_{\alpha\beta}(x)$ is represented by a squiggly line at each end of which spin and field indices are conserved and summed over. In all diagrams, thin black (propagator) lines are not part of the diagrams themselves—they are only shown to illustrate the possible connections of the diagrams if embedded into larger diagrams. Furthermore, all field indices are suppressed.

by a squiggly line where spins are conserved at each end of the vertex—however, to make this clear, the squiggly line still represents a point interaction. As depicted in Fig. 2.1, each vertex enables three possible index contractions. The choice of a spin conservation at each end of a squiggly line is especially useful in Sec. 2.3 when classifying diagrams according to their contributions in powers of $1/\mathcal{N}$.

2.2 Loop expansion of the 2PI effective action

The expansion of Γ_2 in terms of two-particle irreducible (2PI) diagrams can be ordered as a power series in the bare coupling constant λ explicitly appearing in the diagrams. This is like in the standard loop or coupling expansion but now with the restriction that

- ▷ only 2PI graphs are considered and
- ▷ the full propagator G is used for all propagator lines in a diagram.

Rewriting Eq. (1.75) as

$$\Gamma_2[G] = \sum_{n=2}^{\infty} \Gamma_2^{(n)}[G]\,, \tag{2.13}$$

with

$$\Gamma_2^{(n)}[G] = -\mathrm{i}\left\langle \frac{(\mathrm{i}S_{\mathrm{int}})^{n-1}}{(n-1)!} \right\rangle_{\text{2PI \& } G}\,, \tag{2.14}$$

the n-loop approximation of Γ_2 is given by

$$\Gamma_2^{(n\text{ loop})}[G] = \sum_{m=2}^{n} \Gamma_2^{(m)}[G]\,. \tag{2.15}$$

From Eq. (2.14), it is evident that each diagram contributing to $\Gamma_2^{(n)}$ contains $n-1$ explicit interaction vertices λ. Nevertheless, even for small λ, the expansion in Eq. (2.13) does not constitute a perturbation expansion in powers of λ since the Green function G entering the diagrams is the full propagator, which is determined self-consistently by Eq. (1.81). Due to this self-consistency, each Green function G, and thereby each diagram that involves G, contains contributions up to arbitrarily high powers in the coupling[3]—this is why, in our case, "loop expansion" might be the more adequate name for this expansion than "coupling expansion". Although the loop expansion is a non-perturbative expansion in powers of λ, it is, however, a controlled expansion only if both the coupling is small and the dynamic equation exhibits G to be a bounded function. Here, 'controlled' means that one has a certain criteria why the left out contributions are less important contributions than the ones taken into account. Such a controlled expansion can then effectively be viewed to be perturbative.

2.2.1 Hartree-Fock-Bogoliubov approximation

As a first step, we recover the dynamic equations in the Hartree-Fock-Bogoliubov (HFB) approximation [118, 119, 120]. Retaining only the lowest-order diagram of the loop expansion of Γ_2, that is, the double-bubble contribution shown as the most left graph in Fig. 1.2, is known as the HFB mean-field approximation. Due to the structure of the interaction vertex, see Eq. (2.10) and Fig. 2.1, this contribution consists of two qualitatively different diagrams, see Fig. 2.2a, and reads

$$\begin{aligned}\Gamma_2^{\text{HFB}}[G] &= \Gamma_2^{(2\text{ loop})}[G] \\ &= -\frac{\lambda_{\alpha\beta}}{8\mathcal{N}} \int_x \Big(G_{aa}(x,x)G_{bb}(x,x) - 2G_{ab}(x,x)G_{ba}(x,x) \Big)\,,\end{aligned} \tag{2.16}$$

where it is summed over $a=(\alpha,i_a)$ and $b=(\beta,i_b)$, and the relative minus sign occurs due to the Graßmann nature of the fields when performing the contractions in order

[3] To make these contributions more evident note that Eq. (1.81) is equivalent to Eq. (1.76) (for $K=0$). The latter can be rewritten as

$$\begin{aligned}G &= (G_0^{-1} - \mathrm{i}R)^{-1} + (G_0^{-1} - \mathrm{i}R)^{-1}\Sigma G \\ &= (G_0^{-1} - \mathrm{i}R)^{-1} + (G_0^{-1} - \mathrm{i}R)^{-1}\Sigma (G_0^{-1} - \mathrm{i}R)^{-1} \\ &\quad + (G_0^{-1} - \mathrm{i}R)^{-1}\Sigma (G_0^{-1} - \mathrm{i}R)^{-1}\Sigma (G_0^{-1} - \mathrm{i}R)^{-1} + \cdots\,,\end{aligned}$$

where an obvious matrix notation is employed. Thus, the full propagator G can be written as an infinite series containing the bare propagator $(G_0^{-1} - \mathrm{i}R)^{-1}$ and the proper self-energy Σ. And since the proper self-energy consists of 1PI diagrams that themselves contains contributions up to arbitrarily high powers in the coupling, the full propagator also contains these contributions.

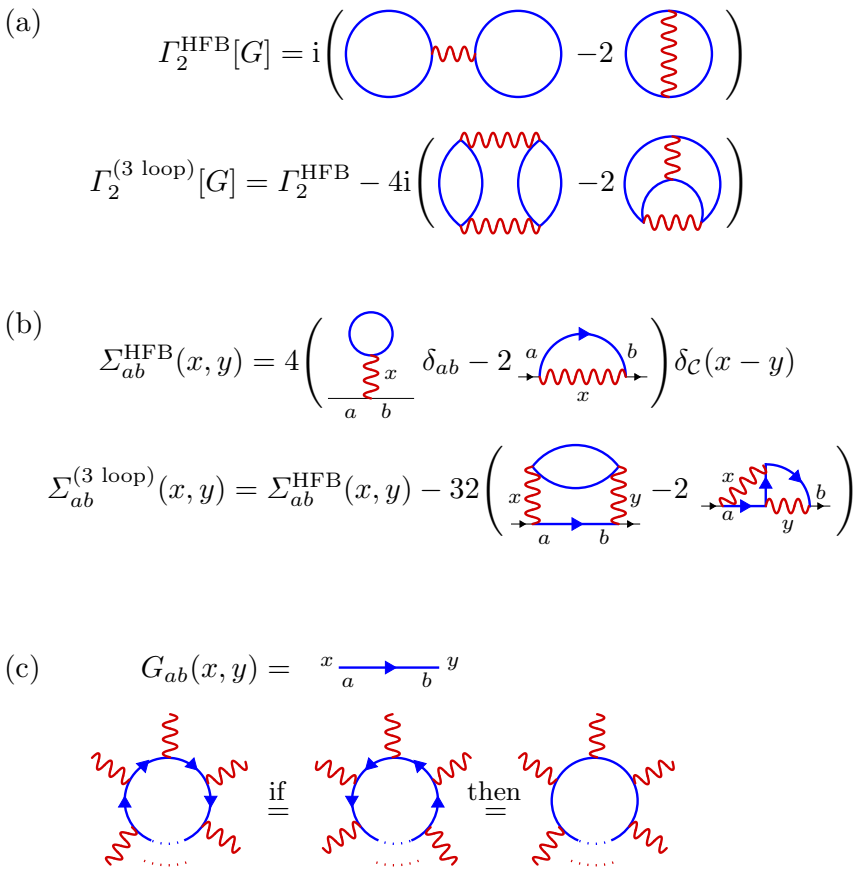

Figure 2.2: Diagrammatic representation of (a) the two-loop (Hartree-Fock-Bogoliubov) and three-loop approximation to Γ_2 in the loop expansion, (b) their respective self-energy contributions, and (c) the full propagator—since generally $G_{ab}(x,y) \neq G_{ba}(y,x)$, an arrow is required for clearness; however, if the orientation of propagator loops are redundant, the arrows are omitted. In all diagrams, thick wiggly red lines represent the local vertex λ, see Fig. 2.1(b). Thin black (propagator) lines are not part of the diagrams themselves—they are only shown to illustrate the possible connections of the diagrams if embedded into larger diagrams.

to rewrite the expectation value. The self-energy derived from Eq. (2.16) is

$$\Sigma_{ab}^{\mathrm{HFB}}(x,y;G) = -\mathrm{i}\Sigma_{ab}^{\mathrm{HFB}(0)}(x;G)\delta_{\mathcal{C}}(x-y)\,, \tag{2.17}$$

$$\Sigma_{ab}^{\mathrm{HFB}(0)}(x;G) = -\frac{\lambda_{\alpha\gamma}}{2\mathcal{N}}\Big(\delta_{ab}G_{cc}(x,x) - 2\delta_{\gamma\beta}G_{ab}(x,x)\Big)\,, \tag{2.18}$$

where it is summed only over $c = (\gamma, i_c)$. Hence, the HFB self-energy reduces to its local part $\Sigma^{\mathrm{HFB}(0)}$.

Inserting the decomposition of Eq. (1.37) into the dynamic equation for G and using Eq. (1.40), we find the time-dependent Hartree-Fock-Bogoliubov equations for ρ and F,

$$\big[\mathrm{i}\tau_{ac}\partial_{x_0} - M_{ac}^{\mathrm{HFB}}(x;G)\big]\,F_{cb}(x,y) = 0\,, \tag{2.19}$$

$$\big[\mathrm{i}\tau_{ac}\partial_{x_0} - M_{ac}^{\mathrm{HFB}}(x;G)\big]\,\rho_{cb}(x,y) = 0\,, \tag{2.20}$$

where $M^{\mathrm{HFB}}(x;G)$ is obtained by Eq. (1.80), with $\Sigma^{(0)}(x;G) = \Sigma^{\mathrm{HFB}(0)}(x;G)$ as given in Eq. (2.18). As the non-local self-energy contribution vanishes in the HFB approximation, the dynamic equations for F and ρ decouple. At equal times, $x_0 = y_0$, the spectral function ρ is fixed by the anti-commutation relations, cf. Eq. (1.39). Hence, one finds that the single-particle density matrix $n_{\alpha\beta}(\mathbf{x},\mathbf{y},t) = \langle\hat{\Psi}_\alpha^\dagger(\mathbf{x})\hat{\Psi}_\beta(\mathbf{y})\rangle_t$ is solely determined by the statistical correlation function:

$$\begin{aligned} n_{\alpha\beta}(\mathbf{x},\mathbf{y},t) - \frac{1}{2}\delta_{\alpha\beta}\delta(\mathbf{x}-\mathbf{y}) = -\frac{1}{2}\delta_{i_a 1}\delta_{i_b 1}\Big(&F_{ab}(\mathbf{x},\mathbf{y},t) + F_{\bar{a}\bar{b}}(\mathbf{x},\mathbf{y},t) \\ &+ \mathrm{i}\big(F_{a\bar{b}}(\mathbf{x},\mathbf{y},t) - F_{\bar{a}b}(\mathbf{x},\mathbf{y},t)\big)\Big)\,, \end{aligned} \tag{2.21}$$

where $\bar{a} = (\alpha, 3-i_a)$, and it is summed over i_a and i_b. This includes the density of particles in mode α at point $(\mathbf{x},t)$, $n_\alpha(\mathbf{x},t) \equiv n_{\alpha\alpha}(\mathbf{x},\mathbf{x},t)$. Moreover, the anomalous density matrix or pair function $m_{\alpha\beta}(\mathbf{x},\mathbf{y},t) = \langle\hat{\Psi}_\alpha(\mathbf{x})\hat{\Psi}_\beta(\mathbf{y})\rangle_t$ is given as

$$\begin{aligned} m_{\alpha\beta}(\mathbf{x},\mathbf{y},t) = -\frac{1}{2}\delta_{i_a 1}\delta_{i_b 1}\Big(&F_{ab}(\mathbf{x},\mathbf{y},t) - F_{\bar{a}\bar{b}}(\mathbf{x},\mathbf{y},t) \\ &+ \mathrm{i}\big(F_{a\bar{b}}(\mathbf{x},\mathbf{y},t) + F_{\bar{a}b}(\mathbf{x},\mathbf{y},t)\big)\Big)\,, \end{aligned} \tag{2.22}$$

where it is summed over i_a and i_b. Adding Eq. (2.19) and its transpose, one obtains

the set of coupled HFB equations for $n_{\alpha\beta}(\mathbf{x},\mathbf{y},t)$ and $m_{\alpha\beta}(\mathbf{x},\mathbf{y},t)$:

$$\begin{aligned}
&\big(\mathrm{i}\partial_t + H^{\mathrm{1B}}_{\alpha\alpha}(x) - H^{\mathrm{1B}}_{\beta\beta}(y)\big)\tilde{n}_{\alpha\beta}(\mathbf{x},\mathbf{y},t) \\
&= \Big\{\frac{2\lambda_{\alpha\gamma}}{\mathcal{N}}\Big(-\tilde{n}_{\gamma\gamma}(\mathbf{x},\mathbf{x},t)\tilde{n}_{\alpha\beta}(\mathbf{x},\mathbf{y},t) + m^*_{\alpha\gamma}(\mathbf{x},\mathbf{x},t)m_{\gamma\beta}(\mathbf{x},\mathbf{y},t) \\
&\qquad\qquad + \tilde{n}_{\alpha\gamma}(\mathbf{x},\mathbf{x},t)\tilde{n}_{\gamma\beta}(\mathbf{x},\mathbf{y},t)\Big)\Big\} \\
&\quad - \big\{(\alpha,\mathbf{x}) \leftrightarrow (\beta,\mathbf{y})\big\}^*\,,
\end{aligned} \tag{2.23}$$

$$\begin{aligned}
&\big(\mathrm{i}\partial_t - H^{\mathrm{1B}}_{\alpha\alpha}(x) - H^{\mathrm{1B}}_{\beta\beta}(y)\big)m_{\alpha\beta}(\mathbf{x},\mathbf{y},t) \\
&= \Big\{\frac{2\lambda_{\alpha\gamma}}{\mathcal{N}}\Big(\tilde{n}_{\gamma\gamma}(\mathbf{x},\mathbf{x},t)m_{\alpha\beta}(\mathbf{x},\mathbf{y},t) - \tilde{n}^*_{\alpha\gamma}(\mathbf{x},\mathbf{x},t)m_{\gamma\beta}(\mathbf{x},\mathbf{y},t) \\
&\qquad\qquad - m_{\alpha\gamma}(\mathbf{x},\mathbf{x},t)\tilde{n}_{\gamma\beta}(\mathbf{x},\mathbf{y},t)\Big)\Big\} \\
&\quad - \big\{(\alpha,\mathbf{x}) \leftrightarrow (\beta,\mathbf{y})\big\}\,,
\end{aligned} \tag{2.24}$$

where it is summed only over γ, and $\tilde{n}_{\alpha\beta}(\mathbf{x},\mathbf{y},t) \equiv n_{\alpha\beta}(\mathbf{x},\mathbf{y},t) - \delta_{\alpha\beta}\delta(\mathbf{x}-\mathbf{y})/2$. The last term in Eq. (2.24) (Eq. (2.23)) denotes (the complex conjugate of) the first term in curly brackets with α and β, and $\mathbf{x}$ and $\mathbf{y}$ interchanged.

Note that for the case of space-translational invariant two-point functions describing a spatially homogeneous Fermi gas, the two-point functions only depend on the spatial relative coordinate $\mathbf{x}-\mathbf{y}$, and Eqs. (2.19) and (2.20) are conveniently solved in momentum space. The solutions are

$$F_{ab}(\mathbf{p},t) = \big(\exp[-\mathrm{i}\tau M^{\mathrm{HFB}}(\mathbf{p})t]\big)_{ac} F_{cb}(\mathbf{p},t)\,, \tag{2.25}$$

$$\rho_{ab}(\mathbf{p},t) = \big(\exp[-\mathrm{i}\tau M^{\mathrm{HFB}}(\mathbf{p})t]\big)_{ac} \rho_{cb}(\mathbf{p},t)\,, \tag{2.26}$$

with

$$M^{\mathrm{HFB}}_{ab}(\mathbf{p},t) = \delta_{ab}\left(\frac{\mathbf{p}^2}{2m} - \frac{\lambda_{\alpha\gamma}(t)}{2\mathcal{N}}\int_{\mathbf{q}} F_{cc}(\mathbf{q},t)\right) + \frac{\lambda_{\alpha\beta}(t)}{\mathcal{N}}\int_{\mathbf{q}} F_{ab}(\mathbf{q},t)\,, \tag{2.27}$$

where $\int_{\mathbf{q}} = (2\pi)^{-d}\int \mathrm{d}^d q$, and it is summed over $c = (\gamma, i_c)$. Inserting the solution for F into $n_\alpha(\mathbf{p},t) = [1 - F_{(\alpha,1)(\alpha,1)}(\mathbf{p},t) - F_{(\alpha,2)(\alpha,2)}(\mathbf{p},t)]/2$, cf. Eq. (2.21), we recover that the HFB equations, which exclude multiple scattering events, leave all momentum-mode occupation numbers invariant.

Alternative derivation of the HFB equations

The HFB equations, Eqs. (2.23) and (2.24), can also be derived from the Liouville equation[4] for the density matrix $\rho_D(t)$,

$$\mathrm{i}\partial_t \rho_D(t) = \big[H(t), \rho_D(t)\big]_-\,, \tag{2.28}$$

[4]The Liouville equation is valid for both equilibrium and non-equilibrium systems.

and a Weyl ordered Hamiltonian H, i. e.

$$\begin{aligned} H_{\text{int, Weyl}}(t) = \frac{\lambda_{\alpha\beta}(t)}{24\mathcal{N}} \int_{\mathbf{x}} \Big(& \hat{\Psi}^\dagger_\alpha(\mathbf{x})\hat{\Psi}^\dagger_\beta(\mathbf{x})\big[\hat{\Psi}_\beta(\mathbf{x}), \hat{\Psi}_\alpha(\mathbf{x})\big]_- \\ & + \hat{\Psi}^\dagger_\alpha(\mathbf{x})\hat{\Psi}_\beta(\mathbf{x})\big[\hat{\Psi}_\alpha(\mathbf{x}), \hat{\Psi}^\dagger_\beta(\mathbf{x})\big]_- \\ & + \hat{\Psi}^\dagger_\alpha(\mathbf{x})\hat{\Psi}_\alpha(\mathbf{x})\big[\hat{\Psi}^\dagger_\beta(\mathbf{x}), \hat{\Psi}_\beta(\mathbf{x})\big]_- \\ & + \hat{\Psi}_\alpha(\mathbf{x})\hat{\Psi}^\dagger_\beta(\mathbf{x})\big[\hat{\Psi}^\dagger_\alpha(\mathbf{x}), \hat{\Psi}_\beta(\mathbf{x})\big]_- \\ & + \hat{\Psi}_\alpha(\mathbf{x})\hat{\Psi}^\dagger_\alpha(\mathbf{x})\big[\hat{\Psi}_\beta(\mathbf{x}), \hat{\Psi}^\dagger_\beta(\mathbf{x})\big]_- \\ & + \hat{\Psi}_\alpha(\mathbf{x})\hat{\Psi}_\beta(\mathbf{x})\big[\hat{\Psi}^\dagger_\beta(\mathbf{x}), \hat{\Psi}^\dagger_\alpha(\mathbf{x})\big]_- \Big)\,, \end{aligned} \tag{2.29}$$

where we used the commutators only for the reason of compressing the equation. Using the Liouville equation, the time-evolution of the single-particle density matrix is given by

$$\begin{aligned} \mathrm{i}\partial_t n_{\alpha\beta}(\mathbf{x},\mathbf{y},t) &= \mathrm{i}\partial_t \,\mathrm{Tr}\left[\rho_D(t)\hat{\Psi}^\dagger_\alpha(\mathbf{x})\hat{\Psi}_\beta(\mathbf{y})\right] = \mathrm{Tr}\left[\big[H,\rho_D(t)\big]_-\hat{\Psi}^\dagger_\alpha(\mathbf{x})\hat{\Psi}_\beta(\mathbf{y})\right] \\ &= \mathrm{Tr}\left[\rho_D(t)\big[\hat{\Psi}^\dagger_\alpha(\mathbf{x})\hat{\Psi}_\beta(\mathbf{y}), H\big]_-\right] \\ &= -\big\langle\big[H,\hat{\Psi}^\dagger_\alpha(\mathbf{x})\hat{\Psi}_\beta(\mathbf{y})\big]_-\big\rangle \end{aligned} \tag{2.30}$$

and similarly the time-evolution of $m_{\alpha\beta}(\mathbf{x},\mathbf{y},t)$.When evaluating the expectation value in Eq. (2.30) for the interaction Hamiltonian of Eq. (2.29), the operator identity

$$\begin{aligned} & \big[\hat{A}\hat{B}\hat{C}\hat{D},\hat{E}\hat{F}\big]_- \\ &= \hat{A}\hat{B}\Big(\big[\hat{C},\hat{D}\big]_+\hat{E} - \hat{E}\big[\hat{C},\hat{D}\big]_+ + \big[\hat{E},\hat{D}\big]_+\hat{C} - \hat{D}\big[\hat{C},\hat{E}\big]_+\Big)\hat{F} \\ &\quad + \Big(\big[\hat{A},\hat{B}\big]_+\hat{E} - \hat{E}\big[\hat{A},\hat{B}\big]_+ + \big[\hat{E},\hat{B}\big]_+\hat{A} - \hat{B}\big[\hat{A},\hat{E}\big]_+\Big)\hat{C}\hat{D}\hat{F} \\ &\quad + \hat{A}\hat{E}\hat{B}\Big(\big[\hat{C},\hat{D}\big]_+\hat{F} - \hat{F}\big[\hat{C},\hat{D}\big]_+ + \big[\hat{F},\hat{D}\big]_+\hat{C} - \hat{D}\big[\hat{C},\hat{F}\big]_+\Big) \\ &\quad + \hat{E}\Big(\big[\hat{A},\hat{B}\big]_+\hat{F} - \hat{F}\big[\hat{A},\hat{B}\big]_+ + \big[\hat{F},\hat{B}\big]_+\hat{A} - \hat{B}\big[\hat{A},\hat{F}\big]_+\Big)\hat{C}\hat{D} \end{aligned} \tag{2.31}$$

together with the fermionic anti-commutation relation is very useful to rewrite the expectation value with six operators as a sum of expectation values with four operators. The Hartree-Fock-Bogoliubov approximation then consists of neglecting all joint cumulants higher than second order, i. e.

$$\begin{aligned} \big\langle\hat{A}\hat{B}\hat{C}\hat{D}\big\rangle &= \big\langle\hat{A}\hat{B}\big\rangle_c\big\langle\hat{C}\hat{D}\big\rangle_c - \big\langle\hat{A}\hat{C}\big\rangle_c\big\langle\hat{B}\hat{D}\big\rangle_c + \big\langle\hat{A}\hat{D}\big\rangle_c\big\langle\hat{B}\hat{C}\big\rangle_c + \big\langle\hat{A}\hat{B}\hat{C}\hat{D}\big\rangle_c \\ &\approx \big\langle\hat{A}\hat{B}\big\rangle_c\big\langle\hat{C}\hat{D}\big\rangle_c - \big\langle\hat{A}\hat{C}\big\rangle_c\big\langle\hat{B}\hat{D}\big\rangle_c + \big\langle\hat{A}\hat{D}\big\rangle_c\big\langle\hat{B}\hat{C}\big\rangle_c\,, \end{aligned} \tag{2.32}$$

where $\langle\cdot\rangle_c$ denotes the joint cumulant, and where we also used that joint cumulants with an odd number of fermionic operators vanish. For related discussions in the context of cold gases, see, e. g. Refs. [68, 121, 122, 123, 124].

2.2.2 Second-order loop approximation

Going beyond the mean-field Hartree-Fock-Bogoliubov contribution to Γ_2 discussed so far, we now additionally take into account the second-order (three loop) diagram that contains two explicit bare couplings and is shown in Fig. 2.2:

$$\Gamma_2^{(3\text{ loop})}[G] = \Gamma_2^{\text{HFB}}[G] + \Gamma_2^{(3)}[G] \tag{2.33}$$

with

$$\begin{aligned}\Gamma_2^{(3)}[G] = &\frac{\mathrm{i}\lambda_{\alpha\beta}(x)\lambda_{\gamma\delta}(y)}{16\mathcal{N}^2}\int_{xy} G_{bc}(x,y)G_{cb}(y,x)G_{da}(x,y)G_{ad}(y,x) \\ &- \frac{\mathrm{i}\lambda_{\alpha\beta}(x)\lambda_{\gamma\delta}(y)}{8\mathcal{N}^2}\int_{xy} G_{ad}(x,y)G_{db}(y,x)G_{bc}(x,y)G_{ca}(y,x)\,,\end{aligned} \tag{2.34}$$

where it is summed over $a = (\alpha, i_a)$, $b = (\beta, i_b)$, $c = (\gamma, i_c)$, and $d = (\delta, i_d)$. Taking the functional derivative with respect to G, the additional term yields the non-local self-energy

$$\begin{aligned}\overline{\Sigma}_{ab}(x,y) = &\frac{\lambda_{\gamma\beta}(y)}{\mathcal{N}}\Pi_{\alpha\gamma}(x,y)G_{ab}(x,y) \\ &- \frac{\lambda_{\alpha\gamma}(x)\lambda_{\delta\beta}(y)}{\mathcal{N}^2}G_{ad}(x,y)G_{dc}(y,x)G_{cb}(x,y)\end{aligned} \tag{2.35}$$

with

$$\Pi_{\alpha\beta}(x,y) = \frac{\lambda_{\alpha\gamma}(x)}{2\mathcal{N}}G_{(\gamma,i)(\beta,j)}(x,y)G_{(\beta,j)(\gamma,i)}(y,x)\,, \tag{2.36}$$

where sums over γ, δ, i_c, and i_d are implied in Eq. (2.35), and over i, j, and γ in Eq. (2.36).

Finally, we want to derive the statistical and spectral components for the non-local self-energy $\overline{\Sigma}$ since they are required in the dynamic equations, Eqs. (1.84) and (1.85). For this purpose, we need to decompose Π into its statistical and spectral components,

$$\Pi_{\alpha\beta}(x,y) = \Pi^F_{\alpha\beta}(x,y) - \frac{\mathrm{i}}{2}\Pi^\rho_{\alpha\beta}(x,y)\,\mathrm{sgn}_{\mathcal{C}}(x_0 - y_0)\,, \tag{2.37}$$

like the two-point Green function G and the non-local self-energy $\overline{\Sigma}$ in Eqs. (1.37) and (1.83), respectively. The resulting statistical and spectral components for the

non-local self-energy $\overline{\Sigma}$ are

$$\begin{aligned}\overline{\Sigma}^F_{ab}(x,y) = &\frac{\lambda_{\gamma\beta}(y)}{\mathcal{N}}\left(\Pi^F_{\alpha\gamma}(x,y)F_{ab}(x,y) - \frac{1}{4}\Pi^\rho_{\gamma\delta}(x,y)\rho_{ab}(x,y)\right)\\ &- \frac{\lambda_{\alpha\gamma}(x)\lambda_{\delta\beta}(y)}{2\mathcal{N}^2}\left(2P^F_{a\delta c}(x,y)F_{cb}(x,y) - \frac{1}{2}P^\rho_{a\delta c}(x,y)\rho_{cb}(x,y)\right),\end{aligned} \tag{2.38}$$

$$\begin{aligned}\overline{\Sigma}^\rho_{ab}(x,y) = &\frac{\lambda_{\gamma\beta}(y)}{\mathcal{N}}\left(\Pi^F_{\gamma\delta}(x,y)\rho_{ab}(x,y) + \Pi^\rho_{\gamma\delta}(x,y)F_{ab}(x,y)\right)\\ &- \frac{\lambda_{\alpha\gamma}(x)\lambda_{\delta\beta}(y)}{\mathcal{N}^2}\left(P^F_{a\delta c}(x,y)\rho_{cb}(x,y) + P^\rho_{a\delta c}(x,y)F_{cb}(x,y)\right),\end{aligned} \tag{2.39}$$

with

$$P^F_{a\delta c}(x,y) = F_{a(\delta,i)}(x,y)F_{(\delta,i)c}(y,x) + \frac{1}{4}\rho_{a(\delta,i)}(x,y)\rho_{(\delta,i)c}(y,x)\,, \tag{2.40}$$

$$P^\rho_{a\delta c}(x,y) = \rho_{a(\delta,i)}(x,y)F_{(\delta,i)c}(y,x) - F_{a(\delta,i)}(x,y)\rho_{(\delta,i)c}(y,x)\,, \tag{2.41}$$

and

$$\begin{aligned}\Pi^F_{\alpha\beta}(x,y) = &\frac{\lambda_{\alpha\gamma}(x)}{2\mathcal{N}}\Big(F_{(\gamma,i)(\beta,j)}(x,y)F_{(\beta,j)(\gamma,i)}(y,x)\\ &+ \frac{1}{4}\rho_{(\gamma,i)(\beta,j)}(x,y)\rho_{(\beta,j)(\gamma,i)}(y,x)\Big),\end{aligned} \tag{2.42}$$

$$\begin{aligned}\Pi^\rho_{\alpha\beta}(x,y) = &\frac{\lambda_{\alpha\gamma}(x)}{2\mathcal{N}}\Big(\rho_{(\gamma,i)(\beta,j)}(x,y)F_{(\beta,j)(\gamma,i)}(y,x)\\ &- F_{(\gamma,i)(\beta,j)}(x,y)\rho_{(\beta,j)(\gamma,i)}(y,x)\Big),\end{aligned} \tag{2.43}$$

where $a = (\alpha, i)$, $b = (\beta, j)$, and $c = (\gamma, k)$. And on the right-hand sides of Eqs. (2.38)–(2.43), it is summed over all indices not appearing on the respective left-hand sides.

In the second-order loop approximation introduced above, the Schwinger-Dyson/Kadanoff-Baym equations of motion, Eqs. (1.84) and (1.85), form a closed set of integro-differential dynamic equations. Unlike the dynamic equations in the HFB approximation, these equations of motion now include both non-Markovian corrections to the propagation kernel and many-body corrections to the dynamics through the non-vanishing memory integrals $\int \overline{\Sigma}G$.

Before proceeding to a brief comment on higher-order loop approximations, we remark on the relation to the quantum Boltzmann approximation and the BBGKY hierarchy.

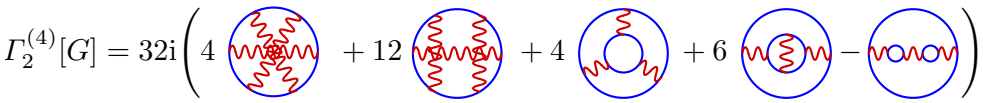

Figure 2.3: Diagrammatic representation of the third-order (four-loop) contributions $\Gamma_2^{(4)}$ to Γ_2 in the loop expansion.

Relation to quantum Boltzmann approximation and BBGKY hierarchy

In the second-order loop approximation discussed in this section, standard quantum Boltzmann equations can be derived from the dynamic equations (1.84) and (1.85) after choosing a kinetic approximation—i. e. neglecting initial-time effects, going over to a quasi-particle basis, and considering the Markovian limit—which is generically justified for near-equilibrium situations [74, 114]. The relevance of non-Markovian and initial-time effects has been discussed, for an ultra-cold Bose gas, in Refs. [67, 115].

An alternative possibility to go beyond the Hartree-Fock-Bogoliubov (HFB) approximation is the so-called Bogoliubov-Born-Green-Kirkwood-Yvon (BBGKY) hierarchy [125, 126, 127, 128, 129]. The Liouville equation, Eq. (2.28), can be transformed into a hierarchy of coupled differential equations for general $2n$th-order correlation functions $\mathrm{Tr}[\hat{\rho}_D(t)\hat{\overline{\Psi}}_{a_1}(\mathbf{x}_1)\hat{\Psi}_{b_1}(\mathbf{y}_1)\cdots\hat{\overline{\Psi}}_{a_n}(\mathbf{x}_n)\hat{\Psi}_{b_n}(\mathbf{y}_n)]$ that are local in time. Solving this BBGKY hierarchy of equations is as difficult as solving the Liouville equation; however, approximating the BBGKY hierarchy makes it possible to truncate this hierarchy into a finite system of coupled equations. Truncating this hierarchy, e. g. by neglecting all correlation functions higher than a certain order, and formally solving the equations for functions of order larger than two, one finally arrives at a closed set of non-Markovian integro-differential equations for the two-point functions, see, for example, Ref. [122]. In this truncation scheme, the Hartree-Fock-Bogoliubov (HFB) approximation in Eq. (2.32) is the lowest-order approximation, and the resulting dynamic equations are not yet non-Markovian or integro-differential.

We point out that this approximation procedure is, however, prone to inconsistencies that can lead to equations that do not conserve vital conservation laws. The equations derived from the 2PI effective action, besides being obtained in a technically simpler procedure, do not suffer such problems as we have seen in Sec. 1.7.

2.2.3 Higher-order loop approximation

Following the same lines as in Sec. 2.2.1 and Sec. 2.2.2, higher-order loop approximations can be derived straightforwardly. The resulting equations of motion for the two-point correlation functions have the form as Eqs. (1.84) and (1.85) with modified proper self-energy functions $\overline{\Sigma}^{F,\rho}$. The diagrammatic representation of the third-order (four-loop) contribution $\Gamma_2^{(4)}$ to Γ_2 in the loop expansion is shown in Fig. 2.3.

2.3 $1/\mathcal{N}$ expansion of the 2PI effective action

In this section, we discuss a non-perturbative approximation scheme of the two-particle irreducible action. In this approximation scheme, the expansion parameter is superficially not based on the coupling. Thus, this scheme is generally expected to be useful to describe physics where large fluctuations require a non-perturbative description. For ultra-cold Fermi gases, the dynamics near a Feshbach resonance, where the two-body scattering length diverges, is a prime example.

In the special case that all couplings $\lambda_{\alpha\beta}$ are equal, the Lagrangian considered in Eq. (2.2) has an additional $O(\mathcal{N})$ symmetry in the space of all hyperfine levels $\mathcal{N}$ described by the multi-component field $\psi_\alpha(x)$. This symmetry can be used to derive an expansion of the 2PI part Γ_2 of the effective action in powers of the inverse number of hyperfine levels, i. e. in powers of $1/\mathcal{N}$,

$$\Gamma_2[G] = \underbrace{\Gamma_2^{\mathrm{LO}}[G]}_{\sim\mathcal{N}^1} + \underbrace{\Gamma_2^{\mathrm{NLO}}[G]}_{\sim\mathcal{N}^0} + \underbrace{\Gamma_2^{\mathrm{NNLO}}[G]}_{\sim\mathcal{N}^{-1}} + \underbrace{\Gamma_2^{\mathrm{N^3LO}}[G]}_{\sim\mathcal{N}^{-2}} + \cdots . \tag{2.44}$$

2.3.1 Classification of diagrams

To see how one identifies to which order a contribution of Γ_2 belongs to in the $1/\mathcal{N}$ expansion of the effective action, we consider the two different origins of the powers of $\mathcal{N}$:

1. From the form of the interaction part S_{int} of the considered action, see Eq. (2.10), follows that

   ▷ each vertex contributes a factor of $1/\mathcal{N}$.

2. Using the squiggly line notation for the interaction vertex, it is apparent that each closed propagator loop in a diagram (see, e. g. Fig. 2.4a) is of the form $\mathrm{tr}\,(G^n)$, where the trace applies to hyperfine (and field) indices, e. g. $\mathrm{tr}\,(G^3) = G_{ab}(x,y)G_{bc}(y,z)G_{ca}(z,x)$. Thus, at this stage, each propagator loop of the form $\mathrm{tr}\,(G^n)$ involves n summations over different hyperfine indices. However, one can diagonalise the argument of the trace by making use of the $O(\mathcal{N})$ symmetry for spin balanced situations and a spin-independent coupling. As a result, only one of the n sums over the hyperfine indices remains, i. e.

   ▷ each propagator loop contributes a factor of $\mathcal{N}$.

   Note that for spin balanced initial conditions, the dynamical equations conserve the spin balance at all later times. Thus, for the diagonalisation procedure described above, it is sufficient to require a spin balanced initial state and a spin-independent coupling.

Consequently, all diagrams with one new vertex (i. e. one new squiggly line) appearing for each new propagator loop contribute to Γ_2 at the same order.

We finally note that the one-loop contribution to the 2PI effective action in Eq. (1.74) is proportional to $\mathrm{Tr}\left[\ln(G^{-1}) + G_0^{-1}G\right]$ and scales linear with $\mathcal{N}$, i. e. it contributes at LO. The logarithmic term corresponds, in absence of all other terms, to the free field effective action and scales proportional to $\mathcal{N}$. Since the free inverse propagator is diagonal in the spin index space, it follows that the second term can be written as a trace in the spin index space, which is also proportional to $\mathcal{N}$.

2.3.2 Leading and next-to-leading order approximation

In the following, we derive the leading-order (LO) and next-to-leading-order (NLO) terms of Γ_2 in the 2PI $1/\mathcal{N}$ expansion, i. e. Γ_2^{LO} and Γ_2^{NLO}, respectively. As already indicated in Eq. (2.44), we will see that the leading order is proportional to $\mathcal{N}^1$ and the next-to-leading order is proportional to $\mathcal{N}^0$.

The LO contribution, which is shown in Fig. 2.4, is equivalent to the Hartree part of the Hartree-Fock-Bogoliubov (HFB) diagram,

$$\Gamma_2^{\mathrm{LO}}[G] = -\frac{\lambda_{\alpha\beta}(x)}{8\mathcal{N}} \int_x G_{aa}(x,x) G_{bb}(x,x)\,. \tag{2.45}$$

As there are two sums over $\alpha, \beta \in \{1, \ldots, \mathcal{N}\}$, this contribution is of the same order in $\mathcal{N}$ as the one-loop part of the action. Hence, in the limit $\mathcal{N} \to \infty$, the dynamic equations contain less terms than in the HFB approximation, and the dynamics is entirely mean-field or classical.

At NLO, the diagrams have to have the same number of invariants (closed propagator loops) as number of vertices. Thus, the only type of contributing 2PI diagrams are the so-called ring diagrams depicted in Fig. 2.4a. There are $(n-1)!/2$ possibilities to arrange n vertices as a ring ($1/2$ because of cyclic property, e. g. 1234 is identical to 1432). Within the ring, for $n > 2$, there are $4 \cdot 4^{n-2} \cdot 2$ possible contractions; for $n = 2$ there are $4 \cdot 2$ and for $n = 1$ there are 2. Hence, the NLO contribution reads

$$\begin{aligned}\Gamma_2^{\mathrm{NLO}}[G] = -\mathrm{i} \sum_{n=1}^{\infty} \frac{1}{n!} \frac{4^n (n-1)!}{2} \int_{xy\cdots z} & \frac{\mathrm{i}\lambda_{\alpha\beta}(x)}{8\mathcal{N}} G_{bc}(x,y) G_{cb}(y,x) \\ & \times \frac{\mathrm{i}\lambda_{\gamma\delta}(y)}{8\mathcal{N}} \cdots \frac{\mathrm{i}\lambda_{\eta\epsilon}(z)}{8\mathcal{N}} G_{ea}(z,x) G_{ae}(x,z) \\ = -\frac{\mathrm{i}}{2} \sum_{n=1}^{\infty} \frac{\mathrm{i}^n}{n} \mathrm{Tr}\left[\Pi^n\right]\,. &\end{aligned} \tag{2.46}$$

The trace in Eq. (2.46) is over spin indices as well as over space-time coordinates (e. g. $\mathrm{Tr}\left[\Pi^3\right] = \int_{xyz} \Pi_{\alpha\beta}(x,y)\Pi_{\beta\gamma}(y,z)\Pi_{\gamma\alpha}(z,x)$). $\Pi_{\alpha\beta}(x,y)$ is defined in Eq. (2.36). In the first line of Eq. (2.46), the different factors come from the overall $(-\mathrm{i})$ in the defining functional integral, cf. Eq. (1.55), the remaining power series of the exp-function, the combinatorics, and the vertices. Remarks:

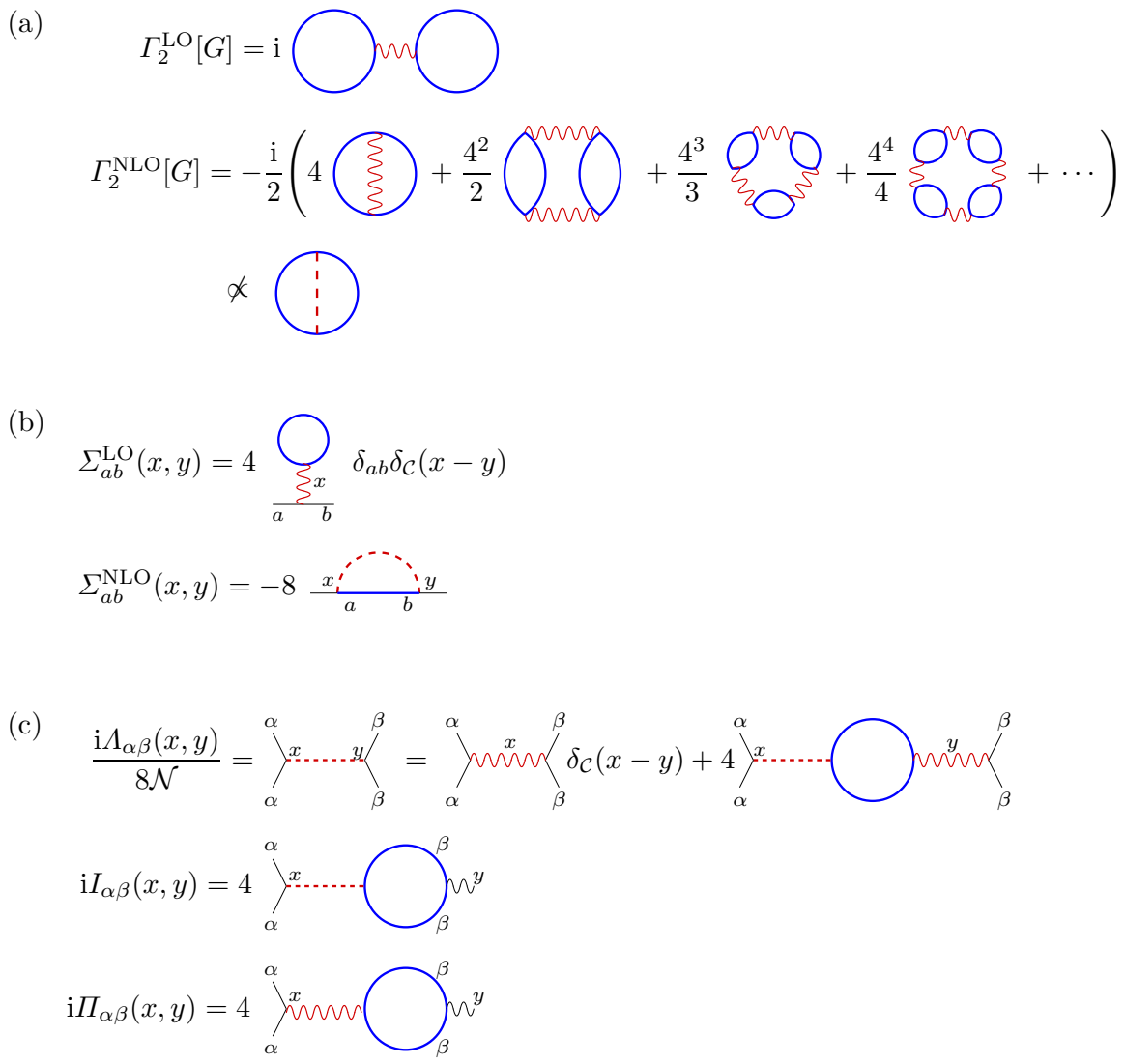

Figure 2.4: Diagrammatic representation of (a) the leading order (LO) and next-to-leading order (NLO) contributions to Γ_2 in the $1/\mathcal{N}$ expansion, (b) their respective self-energies, and (c) the resummed vertex Λ depicted by a dashed red line, the resummed bubble chain I, and the function Π. In all diagrams, thick blue lines represent full propagators and thick wiggly red lines the local vertex λ, see Fig. 2.1(b). Thin black lines (both straight and wiggly) are not part of the diagrams themselves—they are only shown to illustrate the possible connections of the diagrams if embedded into larger diagrams.

1. Since the infinite series in Eq. (2.46) is the Taylor series of the natural logarithm, one can also use the suggestive notation

$$\Gamma_2^{\mathrm{NLO}}[G] = \frac{\mathrm{i}}{2}\,\mathrm{Tr}\left[\ln\left[\mathbb{I} - \mathrm{i}\Pi\right]\right] \tag{2.47}$$

   with $\mathbb{I}_{\alpha\beta}(x,y) = \delta_{\alpha\beta}\delta_{\mathcal{C}}(x-y)$.

2. In the computation of the self-energy in the next step, we make use of the relation

$$\begin{aligned}\frac{\delta\Pi_{\gamma\delta}(u,v)}{\delta G_{ba}(y,x)} = \frac{\lambda_{\gamma\varepsilon}(u)}{2\mathcal{N}}\Big\{&\delta_{\varepsilon\beta}\delta_{\delta\alpha}\delta_{\mathcal{C}}(u-y)\delta_{\mathcal{C}}(v-x)\\ &+\delta_{\varepsilon\alpha}\delta_{\delta\beta}\delta_{\mathcal{C}}(v-y)\delta_{\mathcal{C}}(u-x)\Big\}G_{ab}(x,y)\end{aligned} \tag{2.48}$$

   where $a = (\alpha, i_a)$ and $b = (\beta, i_b)$.

In deriving the NLO contribution, we made use of the property $\lambda_{\alpha\beta}(x) = \lambda_{\beta\alpha}(x)$. In analogy to Eq. (2.44), the proper self-energy has LO and NLO contributions,

$$\Sigma_{ab}(x,y;G) = \Sigma_{ab}^{\mathrm{LO}}(x,y;G) + \Sigma_{ab}^{\mathrm{NLO}}(x,y;G) + \cdots\,, \tag{2.49}$$

with

$$\Sigma_{ab}^{\mathrm{LO}}(x,y;G) = \delta_{ab}\frac{\mathrm{i}\lambda_{\alpha\gamma}(x)}{2\mathcal{N}}G_{cc}(x,x)\delta_{\mathcal{C}}(x-y)\,, \tag{2.50}$$

$$\Sigma_{ab}^{\mathrm{NLO}}(x,y;G) = -\frac{\mathrm{i}\Lambda_{\alpha\beta}(x,y;G)}{\mathcal{N}}G_{ab}(x,y)\,. \tag{2.51}$$

The NLO contribution can be understood as a scattering diagram with the resummed vertex

$$\Lambda_{\alpha\beta}(x,y) = \Big(\delta_{\alpha\gamma}\delta_{\mathcal{C}}(x-y) + \mathrm{i}I_{\alpha\gamma}(x,y;G)\Big)\lambda_{\gamma\beta}\,, \tag{2.52}$$

which is defined through the integral equation

$$I_{\alpha\beta}(x,y;G) = \int_z \frac{\Lambda_{\alpha\gamma}(x,z;G)}{2\mathcal{N}}G_{cb}(z,y)G_{bc}(y,z) \tag{2.53}$$

$$= \Pi_{\alpha\beta}(x,y) + \mathrm{i}\int_z I_{\alpha\gamma}(x,z)\Pi_{\gamma\beta}(z,y)\,, \tag{2.54}$$

cf. Fig. 2.4c, where $a = (\alpha, i_a)$, $b = (\beta, i_b)$, and $c = (\gamma, i_c)$, and it is summed over all indices not appearing on the l. h. s. of the equations. One recovers the Hartree-Fock-Bogoliubov approximation by setting the resummed vertex Λ equal to the bare vertex, $\Lambda_{\alpha\beta}(x,y) = \lambda_{\alpha\beta}(x)\delta(x-y)$.

The self-energy up to NLO has in general both local and non-local contributions, the local one being equivalent to the HFB term,

$$\Sigma_{ab}^{\mathrm{HFB}}(x,y) = \Sigma_{ab}^{\mathrm{LO}}(x,y) + \Sigma_{ab}^{\mathrm{NLO}}(x,y)\big|_{\Lambda=\lambda}\,. \tag{2.55}$$

The non-local beyond-mean-field contribution to the self-energy is given by

$$\overline{\Sigma}_{ab}(x,y;G) = I_{\alpha\gamma}(x,y;G)\frac{\lambda_{\gamma\beta}(y)}{\mathcal{N}}G_{ab}(x,y)\,. \tag{2.56}$$

The real functions $M_{ab}(x;G)$, $\overline{\Sigma}^F_{ab}(x,y;G)$, and $\overline{\Sigma}^\rho_{ab}(x,y;G)$ are all regular in x_0 and are obtained in terms of statistical and spectral functions as follows:

$$M_{ab}(x) = \delta_{ab}\Big(H^{\mathrm{1B}}_{\alpha\beta}(\mathbf{x}) - \frac{\lambda_{\alpha\gamma}(x)}{2\mathcal{N}}F_{cc}(x,x)\Big) + \frac{\lambda_{\alpha\beta}(x)}{\mathcal{N}}F_{ab}(x,x)\,, \tag{2.57}$$

$$\overline{\Sigma}^F_{ab}(x,y) = \frac{\lambda_{\gamma\beta}(y)}{\mathcal{N}}\Big(I^F_{\alpha\gamma}(x,y)F_{ab}(x,y) - \frac{1}{4}I^\rho_{\alpha\gamma}(x,y)\rho_{ab}(x,y)\Big)\,, \tag{2.58}$$

$$\overline{\Sigma}^\rho_{ab}(x,y) = \frac{\lambda_{\gamma\beta}(y)}{\mathcal{N}}\Big(I^F_{\alpha\gamma}(x,y)\rho_{ab}(x,y) + I^\rho_{\alpha\gamma}(x,y)F_{ab}(x,y)\Big)\,, \tag{2.59}$$

where

$$\begin{aligned} I^F_{\alpha\beta}(x,y) = \Pi^F_{\alpha\beta}(x,y) + \bigg(&\int_0^{x_0}\mathrm{d}z\, I^\rho_{\alpha\gamma}(x,z)\Pi^F_{\gamma\beta}(z,y) \\ &- \int_0^{y_0}\mathrm{d}z\, I^F_{\alpha\gamma}(x,z)\Pi^\rho_{\gamma\beta}(z,y)\bigg)\,, \end{aligned} \tag{2.60}$$

$$I^\rho_{\alpha\beta}(x,y) = \Pi^\rho_{\gamma\beta}(x,y) + \int_{y_0}^{x_0}\mathrm{d}z\, I^\rho_{\alpha\gamma}(x,z)\Pi^\rho_{\gamma\beta}(z,y)\,, \tag{2.61}$$

with Π^F and Π^ρ defined in Eqs. (2.42) and (2.43), respectively. We will see soon that the appealing part of the NLO approximation is the recursive expressions for I^F and I^ρ, Eqs. (2.60) and (2.61), without involving any explicit summations. The structure of these expressions further allows to solve the equations numerically without requiring to solve self-consistently any type of gap equation.

Before proceeding to a brief discussion about the beyond-NLO contributions, we provide some helpful considerations for the next chapter, where we numerical solve the equation of motions in NLO of the $1/\mathcal{N}$ expansion in momentum space.

2.3.3 Numerical implementation of the dynamical equations

A good portion of this PhD project was the effective numerical implementation of the dynamical equations derived from the NLO $1/\mathcal{N}$ approximation of the 2PI effective action. We solve the dynamical equations in momentum space after introducing dimensionless variables and transforming the equations into an interaction picture. In this section, we discuss this procedure step by step and provide some remarks important for the actual numerical implementation.

NLO equations in momentum space

In the next chapter, we consider a spatially homogeneous Fermi gas of N particles in a box of volume V with periodic boundary conditions in the absence of external

potentials. In this case, the functions G, Σ, etc. depend only on the relative spatial coordinates; therefore, a Fourier transformation in momentum space almost suggests itself.

In the following, we provide the dynamic equations derived from the 2PI effective action, to next-to-leading order (NLO) in the $1/\mathcal{N}$ expansion, for a spatially homogeneous Fermi gas in momentum space. Note that from a numerical point of view, a convenient side effect of writing the equations in momentum space is the simple form of M, which involves a multiplication with $\mathbf{p}^2$ in momentum space instead of a second-order derivative in position space. The equations in momentum space are

$$\left(\mathrm{i}\hbar\tau_{ac}\partial_{x_0} - M_{ac}(x_0;\mathbf{p})\right)F_{cb}(x_0,y_0;\mathbf{p}) = \frac{1}{\hbar}\int_0^{x_0}\mathrm{d}z_0\,\overline{\Sigma}^{\rho}_{ac}(x_0,z_0;\mathbf{p})F_{cb}(z_0,y_0;\mathbf{p}) - \frac{1}{\hbar}\int_0^{y_0}\mathrm{d}z_0\,\overline{\Sigma}^{F}_{ac}(x_0,z_0;\mathbf{p})\rho_{cb}(z_0,y_0;\mathbf{p}) \tag{2.62}$$

$$\left(\mathrm{i}\hbar\tau_{ac}\partial_{x_0} - M_{ac}(x_0;\mathbf{p})\right)\rho_{cb}(x_0,y_0;\mathbf{p}) = \frac{1}{\hbar}\int_{y_0}^{x_0}\mathrm{d}z_0\,\overline{\Sigma}^{\rho}_{ac}(x_0,z_0;\mathbf{p})\rho_{cb}(z_0,y_0;\mathbf{p}) \tag{2.63}$$

with

$$M_{ab}(x_0;\mathbf{p}) = \delta_{ab}\left(\frac{\mathbf{p}^2}{2m} - \frac{\lambda_{\alpha\delta}(x_0)}{2\mathcal{N}}\int_{\mathbf{q}}F_{dd}(x_0,x_0;\mathbf{q})\right) + \frac{\lambda_{\alpha\beta}(x_0)}{\mathcal{N}}\int_{\mathbf{q}}F_{ab}(x_0,x_0;\mathbf{q})\,, \tag{2.64}$$

$$\overline{\Sigma}^{F}_{ab}(x_0,y_0;\mathbf{p}) = \frac{\lambda_{\gamma\beta}(y_0)}{\mathcal{N}}\int_{\mathbf{q}}\Big(I^{F}_{\alpha\gamma}(x_0,y_0;\mathbf{p}-\mathbf{q})F_{ab}(x_0,y_0;\mathbf{q}) - \frac{1}{4}I^{\rho}_{\alpha\gamma}(x_0,y_0;\mathbf{p}-\mathbf{q})\rho_{ab}(x_0,y_0;\mathbf{q})\Big)\,, \tag{2.65}$$

$$\overline{\Sigma}^{\rho}_{ab}(x_0,y_0;\mathbf{p}) = \frac{\lambda_{\gamma\beta}(y_0)}{\mathcal{N}}\int_{\mathbf{q}}\Big(I^{F}_{\alpha\gamma}(x_0,y_0;\mathbf{p}-\mathbf{q})\rho_{ab}(x_0,y_0;\mathbf{q}) + I^{\rho}_{\alpha\gamma}(x_0,y_0;\mathbf{p}-\mathbf{q})F_{ab}(x_0,y_0;\mathbf{q})\Big)\,, \tag{2.66}$$

and

$$I^{F}_{\alpha\beta}(x_0,y_0;\mathbf{p}) = \Pi^{F}_{\alpha\beta}(x_0,y_0;\mathbf{p}) + \frac{1}{\hbar}\int_{t_0}^{x_0}\mathrm{d}z_0\,I^{\rho}_{\alpha\gamma}(x_0,z_0;\mathbf{p})\Pi^{F}_{\gamma\beta}(z_0,y_0;\mathbf{p}) - \frac{1}{\hbar}\int_{t_0}^{y_0}\mathrm{d}z_0\,I^{F}_{\alpha\gamma}(x_0,z_0;\mathbf{p})\Pi^{\rho}_{\gamma\beta}(z_0,y_0;\mathbf{p})\,, \tag{2.67}$$

$$I^{\rho}_{\alpha\beta}(x_0,y_0;\mathbf{p}) = \Pi^{\rho}_{\alpha\beta}(x_0,y_0;\mathbf{p}) + \frac{1}{\hbar}\int_{y_0}^{x_0}\mathrm{d}z_0\,I^{\rho}_{\alpha\gamma}(x_0,z_0;\mathbf{p})\Pi^{\rho}_{\gamma\beta}(z_0,y_0;\mathbf{p})\,, \tag{2.68}$$

and

$$\Pi^F_{\alpha\beta}(x_0,y_0;\mathbf{p}) = \frac{\lambda_{\alpha\gamma}(x_0)}{2\mathcal{N}}\int_{\mathbf{q}}\Big(F_{(\gamma,i)(\beta,j)}(x_0,y_0;\mathbf{p}-\mathbf{q})F_{(\beta,j)(\gamma,i)}(y_0,x_0;\mathbf{q}) + \frac{1}{4}\rho_{(\gamma,i)(\beta,j)}(x_0,y_0;\mathbf{p}-\mathbf{q})\rho_{(\beta,j)(\gamma,i)}(y_0,x_0;\mathbf{q})\Big)\,, \tag{2.69}$$

$$\Pi^\rho_{\alpha\beta}(x_0,y_0;\mathbf{p}) = \frac{\lambda_{\alpha\gamma}(x_0)}{2\mathcal{N}}\int_{\mathbf{q}}\Big(\rho_{(\gamma,i)(\beta,j)}(x_0,y_0;\mathbf{p}-\mathbf{q})F_{(\beta,j)(\gamma,i)}(y_0,x_0;\mathbf{q}) - F_{(\gamma,i)(\beta,j)}(x_0,y_0;\mathbf{p}-\mathbf{q})\rho_{(\beta,j)(\gamma,i)}(y_0,x_0;\mathbf{q})\Big)\,, \tag{2.70}$$

where

$$\int_{\mathbf{q}} = \begin{cases} \displaystyle\int \frac{\mathrm{d}^d q}{(2\pi\hbar)^d} & \text{in the thermodynamic limit,} \\ \displaystyle\frac{1}{V}\sum_{\mathbf{q}} & \text{for a finite volume } V, \end{cases} \tag{2.71}$$

and all factors $\hbar$ are shown explicitly.

Dimensionless equation

To identify the relevant quantities that characterise the dynamics, it is convenient to introduce dimensionless variables. These above equations can be made dimensionless with the transformations

$$\tilde{t} \equiv \frac{\hbar n_{d\mathrm{D}}^{2/d}}{m}t\,, \tag{2.72}$$

$$\tilde{\mathbf{p}} \equiv \frac{1}{\hbar n_{d\mathrm{D}}^{1/d}}\mathbf{p}\,, \tag{2.73}$$

$$\tilde{M} \equiv \frac{m}{\left(\hbar n_{d\mathrm{D}}^{1/d}\right)^2}M\,, \qquad \tilde{I} \equiv \frac{m}{\left(\hbar n_{d\mathrm{D}}^{1/d}\right)^2}I\,, \qquad \tilde{\Pi} \equiv \frac{m}{\left(\hbar n_{d\mathrm{D}}^{1/d}\right)^2}\Pi\,, \tag{2.74}$$

$$\tilde{\overline{\Sigma}} \equiv \left(\frac{m}{\hbar^2 n_{d\mathrm{D}}^{2/d}}\right)^2\overline{\Sigma}\,, \tag{2.75}$$

where we consider d spatial dimensions. The resulting dimensionless equations of motion are

$$\Big(\mathrm{i}\tau_{ac}\partial_{\tilde{x}_0} - \tilde{M}_{ac}(\tilde{x}_0;\tilde{\mathbf{p}})\Big)F_{cb}(\tilde{x}_0,\tilde{y}_0;\tilde{\mathbf{p}}) = \int_0^{\tilde{x}_0}\mathrm{d}\tilde{z}_0\,\tilde{\overline{\Sigma}}^\rho_{ac}(\tilde{x}_0,\tilde{z}_0;\tilde{\mathbf{p}})F_{cb}(\tilde{z}_0,\tilde{y}_0;\tilde{\mathbf{p}}) - \int_0^{\tilde{y}_0}\mathrm{d}\tilde{z}_0\,\tilde{\overline{\Sigma}}^F_{ac}(\tilde{x}_0,\tilde{z}_0;\tilde{\mathbf{p}})\rho_{cb}(\tilde{z}_0,\tilde{y}_0;\tilde{\mathbf{p}}) \tag{2.76}$$

$$\Big(\mathrm{i}\tau_{ac}\partial_{\tilde{x}_0} - \tilde{M}_{ac}(\tilde{x}_0;\tilde{\mathbf{p}})\Big)\rho_{cb}(\tilde{x}_0,\tilde{y}_0;\tilde{\mathbf{p}}) = \int_{\tilde{y}_0}^{\tilde{x}_0}\mathrm{d}\tilde{z}_0\,\tilde{\overline{\Sigma}}^\rho_{ac}(\tilde{x}_0,\tilde{z}_0;\tilde{\mathbf{p}})\rho_{cb}(\tilde{z}_0,\tilde{y}_0;\tilde{\mathbf{p}}) \tag{2.77}$$

with

$$\tilde{\overline{\Sigma}}^{F}_{ab}(\tilde{x}_0,\tilde{y}_0;\tilde{\mathbf{p}}) = \gamma_{\delta\beta}(\tilde{y}_0)\int_{\tilde{\mathbf{q}}}\Big(\tilde{I}^{F}_{\alpha\delta}(\tilde{x}_0,\tilde{y}_0;\tilde{\mathbf{p}}-\tilde{\mathbf{q}})F_{ab}(\tilde{x}_0,\tilde{y}_0;\tilde{\mathbf{q}}) - \frac{1}{4}\tilde{I}^{\rho}_{\alpha\delta}(\tilde{x}_0,\tilde{y}_0;\tilde{\mathbf{p}}-\tilde{\mathbf{q}})\rho_{ab}(\tilde{x}_0,\tilde{y}_0;\tilde{\mathbf{q}})\Big)\,, \tag{2.78}$$

$$\tilde{\overline{\Sigma}}^{\rho}_{ab}(\tilde{x}_0,\tilde{y}_0;\tilde{\mathbf{p}}) = \gamma_{\delta\beta}(\tilde{y}_0)\int_{\tilde{\mathbf{q}}}\Big(\tilde{I}^{F}_{\alpha\delta}(\tilde{x}_0,\tilde{y}_0;\tilde{\mathbf{p}}-\tilde{\mathbf{q}})\rho_{ab}(\tilde{x}_0,\tilde{y}_0;\tilde{\mathbf{q}}) + \tilde{I}^{\rho}_{\alpha\delta}(\tilde{x}_0,\tilde{y}_0;\tilde{\mathbf{p}}-\tilde{\mathbf{q}})F_{ab}(\tilde{x}_0,\tilde{y}_0;\tilde{\mathbf{q}})\Big)\,, \tag{2.79}$$

and

$$\tilde{I}^{F}_{\alpha\beta}(\tilde{x}_0,\tilde{y}_0;\tilde{\mathbf{p}}) = \tilde{\Pi}^{F}_{\alpha\beta}(\tilde{x}_0,\tilde{y}_0;\tilde{\mathbf{p}}) + \bigg(\int_{\tilde{t}_0}^{\tilde{x}_0}\mathrm{d}\tilde{z}_0\,\tilde{I}^{\rho}_{\alpha\gamma}(\tilde{x}_0,\tilde{z}_0;\tilde{\mathbf{p}})\tilde{\Pi}^{F}_{\gamma\beta}(\tilde{z}_0,\tilde{y}_0;\tilde{\mathbf{p}}) - \int_{\tilde{t}_0}^{\tilde{y}_0}\mathrm{d}\tilde{z}_0\,\tilde{I}^{F}_{\alpha\gamma}(\tilde{x}_0,\tilde{z}_0;\tilde{\mathbf{p}})\tilde{\Pi}^{\rho}_{\gamma\beta}(\tilde{z}_0,\tilde{y}_0;\tilde{\mathbf{p}})\bigg)\,, \tag{2.80}$$

$$\tilde{I}^{\rho}_{\alpha\beta}(\tilde{x}_0,\tilde{y}_0;\tilde{\mathbf{p}}) = \tilde{\Pi}^{\rho}_{\alpha\beta}(\tilde{x}_0,\tilde{y}_0;\tilde{\mathbf{p}}) + \int_{\tilde{y}_0}^{\tilde{x}_0}\mathrm{d}\tilde{z}_0\,\tilde{I}^{\rho}_{\alpha\gamma}(\tilde{x}_0,\tilde{z}_0;\tilde{\mathbf{p}})\tilde{\Pi}^{\rho}_{\gamma\beta}(\tilde{z}_0,\tilde{y}_0;\tilde{\mathbf{p}})\,, \tag{2.81}$$

and

$$\tilde{\Pi}^{F}_{\alpha\beta}(\tilde{x}_0,\tilde{y}_0;\tilde{\mathbf{p}}) = \frac{\gamma_{\alpha\gamma}(\tilde{x}_0)}{2}\int_{\tilde{\mathbf{q}}}\Big(F_{(\gamma,i)(\beta,j)}(\tilde{x}_0,\tilde{y}_0;\tilde{\mathbf{p}}-\tilde{\mathbf{q}})F_{(\beta,j)(\gamma,i)}(\tilde{y}_0,\tilde{x}_0;\tilde{\mathbf{q}}) + \frac{1}{4}\rho_{(\gamma,i)(\beta,j)}(\tilde{x}_0,\tilde{y}_0;\tilde{\mathbf{p}}-\tilde{\mathbf{q}})\rho_{(\beta,j)(\gamma,i)}(\tilde{y}_0,\tilde{x}_0;\tilde{\mathbf{q}})\Big)\,, \tag{2.82}$$

$$\tilde{\Pi}^{\rho}_{\alpha\beta}(\tilde{x}_0,\tilde{y}_0;\tilde{\mathbf{p}}) = \frac{\gamma_{\alpha\gamma}(\tilde{x}_0)}{2}\int_{\tilde{\mathbf{q}}}\Big(\rho_{(\gamma,i)(\beta,j)}(\tilde{x}_0,\tilde{y}_0;\tilde{\mathbf{p}}-\tilde{\mathbf{q}})F_{(\beta,j)(\gamma,i)}(\tilde{y}_0,\tilde{x}_0;\tilde{\mathbf{q}}) - F_{(\gamma,i)(\beta,j)}(\tilde{x}_0,\tilde{y}_0;\tilde{\mathbf{p}}-\tilde{\mathbf{q}})\rho_{(\beta,j)(\gamma,i)}(\tilde{y}_0,\tilde{x}_0;\tilde{\mathbf{q}})\Big)\,, \tag{2.83}$$

where

$$\int_{\tilde{\mathbf{q}}} = \begin{cases} \displaystyle\int\frac{\mathrm{d}^d\tilde{q}}{(2\pi)^d} & \text{in the thermodynamic limit,} \\ \displaystyle\frac{1}{N}\sum_{\tilde{\mathbf{q}}} & \text{for a finite volume } V. \end{cases} \tag{2.84}$$

From the dimensionless equations, it is now evident that the strength of the interaction is governed by the dimensionless coupling constant

$$\gamma_{\alpha\beta}(\tilde{t}) = \frac{m g_{\alpha\beta}(\tilde{t})}{\hbar^2 n_{d\mathrm{D}}^{2/d-1}} = \frac{m\lambda_{\alpha\beta}(\tilde{t})}{\mathcal{N}\hbar^2 n_{d\mathrm{D}}^{2/d-1}}\,. \tag{2.85}$$

From Eq. (2.85), one notices that the dependence of the coupling strength on the density differs significantly for different dimensions. In three spatial dimensions, the

weak-coupling regime ($|\gamma| \ll 1$) corresponds to low densities n_{3D}, and the strong-coupling regime ($|\gamma| \gg 1$) is achieved at high densities. However, in one spatial dimension, the dependence is reversed: the weak-coupling regime corresponds to high densities n_{1D}, and the strong-coupling regime is achieved at low densities. Finally, note that the relation in Eq. (2.85) can also be derived directly from the Hamiltonian in Eq. (2.1) through a simple dimensional analysis.

"Interaction picture" transformation

Whereas the rewriting of the equations in momentum space and the introduction of dimensionless variables had also some physical motivation, the interaction picture discussed below is of sole interest for the numerical implementation of the equations later on. The matrix M in the equations of motion causes fast oscillations of the two-point functions F, ρ, and G in the time plane. And fast oscillations can quickly be a serious problem for any numerical integration of differential equations. Therefore, it is advisable to analytically first separate out these fast oscillations through a transformation into an interaction picture and then perform the numerical integration only on the envelopes of the two-point functions.

In preparation for the transformation, it is convenient to put the $\mathrm{i}\tau$ into the definition of $\tilde{M}$ and $\tilde{\overline{\Sigma}}$:

$$\tilde{M}' \equiv -\mathrm{i}\tau^{-1}\tilde{M} \tag{2.86}$$

$$\tilde{\overline{\Sigma}}' \equiv -\mathrm{i}\tau^{-1}\tilde{\overline{\Sigma}}\,, \tag{2.87}$$

i. e. in the NLO approximation of the $1/\mathcal{N}$ expansion, one has

$$\begin{aligned}\tilde{M}'_{ab}(\tilde{x}_0;\tilde{\mathbf{p}}) = -\mathrm{i}\tau_{ab}^{-1}\left(\frac{\tilde{\mathbf{p}}^2}{2} - \frac{\gamma_{\alpha\delta}(\tilde{x}_0)}{2}\int_{\tilde{\mathbf{q}}} F_{dd}(\tilde{x}_0,\tilde{x}_0;\tilde{\mathbf{q}})\right)\\ - \mathrm{i}\tau_{ac}^{-1}\gamma_{\gamma\beta}(\tilde{x}_0)\int_{\tilde{\mathbf{q}}} F_{cb}(\tilde{x}_0,\tilde{x}_0;\tilde{\mathbf{q}})\,,\end{aligned} \tag{2.88}$$

$$\begin{aligned}\tilde{\overline{\Sigma}}'^{F}_{ab}(\tilde{x}_0,\tilde{y}_0;\tilde{\mathbf{p}}) = -\mathrm{i}\tau_{ac}^{-1}\gamma_{\delta\beta}(\tilde{y}_0)\int_{\tilde{\mathbf{q}}}\Big(\tilde{I}^{F}_{\gamma\delta}(\tilde{x}_0,\tilde{y}_0;\tilde{\mathbf{p}}-\tilde{\mathbf{q}})F_{cb}(\tilde{x}_0,\tilde{y}_0;\tilde{\mathbf{q}})\\ - \frac{1}{4}\tilde{I}^{\rho}_{\gamma\delta}(\tilde{x}_0,\tilde{y}_0;\tilde{\mathbf{p}}-\tilde{\mathbf{q}})\rho_{cb}(\tilde{x}_0,\tilde{y}_0;\tilde{\mathbf{q}})\Big)\,,\end{aligned} \tag{2.89}$$

$$\begin{aligned}\tilde{\overline{\Sigma}}'^{\rho}_{ab}(\tilde{x}_0,\tilde{y}_0;\tilde{\mathbf{p}}) = -\mathrm{i}\tau_{ac}^{-1}\gamma_{\delta\beta}(\tilde{y}_0)\int_{\tilde{\mathbf{q}}}\Big(\tilde{I}^{F}_{\gamma\delta}(\tilde{x}_0,\tilde{y}_0;\tilde{\mathbf{p}}-\tilde{\mathbf{q}})\rho_{cb}(\tilde{x}_0,\tilde{y}_0;\tilde{\mathbf{q}})\\ + \tilde{I}^{\rho}_{\gamma\delta}(\tilde{x}_0,\tilde{y}_0;\tilde{\mathbf{p}}-\tilde{\mathbf{q}})F_{cb}(\tilde{x}_0,\tilde{y}_0;\tilde{\mathbf{q}})\Big)\,.\end{aligned} \tag{2.90}$$

Now, we define the interaction picture by

$$\underline{A}(\tilde{x}_0,\tilde{y}_0;\tilde{\mathbf{p}}) \equiv \exp\left[-\int_{\tilde{t}_0}^{\tilde{x}_0}\mathrm{d}\tilde{t}\tilde{M}'(\tilde{t};\tilde{\mathbf{p}})\right]A(\tilde{x}_0,\tilde{y}_0;\tilde{\mathbf{p}})\exp\left[\int_{\tilde{t}_0}^{\tilde{y}_0}\mathrm{d}\tilde{t}\tilde{M}'(\tilde{t};\tilde{\mathbf{p}})\right]. \tag{2.91}$$

With this definition, the dimensionless equations of motion in the interaction picture are

$$\begin{aligned}\partial_{\tilde{x}_0}\underline{\tilde{F}}_{cb}(\tilde{x}_0,\tilde{y}_0;\tilde{\mathbf{p}}) &= \int_0^{\tilde{x}_0} \mathrm{d}\tilde{z}_0\, \underline{\tilde{\Sigma}}'^{\rho}_{ac}(\tilde{x}_0,\tilde{z}_0;\tilde{\mathbf{p}})\underline{F}_{cb}(\tilde{z}_0,\tilde{y}_0;\tilde{\mathbf{p}}) \\ &\quad - \int_0^{\tilde{y}_0} \mathrm{d}\tilde{z}_0\, \underline{\tilde{\Sigma}}'^{F}_{ac}(\tilde{x}_0,\tilde{z}_0;\tilde{\mathbf{p}})\underline{\rho}_{cb}(\tilde{z}_0,\tilde{y}_0;\tilde{\mathbf{p}})\end{aligned} \tag{2.92}$$

$$\partial_{\tilde{x}_0}\underline{\rho}_{cb}(\tilde{x}_0,\tilde{y}_0;\tilde{\mathbf{p}}) = \int_{\tilde{y}_0}^{\tilde{x}_0} \mathrm{d}\tilde{z}_0\, \underline{\tilde{\Sigma}}'^{\rho}_{ac}(\tilde{x}_0,\tilde{z}_0;\tilde{\mathbf{p}})\underline{\rho}_{cb}(\tilde{z}_0,\tilde{y}_0;\tilde{\mathbf{p}})\,. \tag{2.93}$$

To make the advantage of the transformation into the interaction picture more explicit, we note that, for the special case (which applies in most of the situations we are interested in) of

$$A(\tilde{x}_0,\tilde{y}_0;\tilde{\mathbf{p}}) = \begin{pmatrix} a(\tilde{x}_0,\tilde{y}_0;\tilde{\mathbf{p}}) & b(\tilde{x}_0,\tilde{y}_0;\tilde{\mathbf{p}}) \\ -b(\tilde{x}_0,\tilde{y}_0;\tilde{\mathbf{p}}) & a(\tilde{x}_0,\tilde{y}_0;\tilde{\mathbf{p}}) \end{pmatrix} \tag{2.94}$$

and a time-independent

$$\tilde{M}'(\tilde{t};\tilde{\mathbf{p}}) = \begin{pmatrix} 0 & c(\tilde{\mathbf{p}}) \\ -c(\tilde{\mathbf{p}}) & 0 \end{pmatrix}, \tag{2.95}$$

Eq. (2.91) reduces to

$$\underline{A}(\tilde{x}_0,\tilde{y}_0;\tilde{\mathbf{p}}) = \begin{pmatrix} \cos[c(\tilde{\mathbf{p}})(\tilde{x}_0-\tilde{y}_0)] & -\sin[c(\tilde{\mathbf{p}})(\tilde{x}_0-\tilde{y}_0)] \\ \sin[c(\tilde{\mathbf{p}})(\tilde{x}_0-\tilde{y}_0)] & \cos[c(\tilde{\mathbf{p}})(\tilde{x}_0-\tilde{y}_0)] \end{pmatrix} A(\tilde{x}_0,\tilde{y}_0;\tilde{\mathbf{p}})\,, \tag{2.96}$$

which can be numerically evaluated to a certain accuracy much more easily than a numerical integration of the oscillations in the differential equation.

Further remarks on the numerical implementation

We would like to finish this section on the NLO contributions to the $1/\mathcal{N}$ expansion with some further remarks on the numerical implementation of the equations of motion, Eqs. (2.92) and (2.93).

1. The dynamic equations are differential equations of first-order in the time derivative. Thus, standard integration methods like the fourth-order Runge-Kutta algorithm can be used to discretise and solve them.

2. After discretising the time integrals, the structure of equations allows that all quantities necessary to evolve F and ρ to the next time step can be computed from already known quantities. This is described in detail in Ref. [74] for a relativistic bosonic system, but carries over to our case one by one: at the current time $\tilde{x}_0$, one determines successively
   - ▷ $\tilde{\Pi}^{\rho}_{\alpha\beta}(\tilde{x}_0,\tilde{y}_0)$ and $\tilde{\Pi}^{F}_{\alpha\beta}(\tilde{x}_0,\tilde{y}_0)$ for all $\tilde{y}_0$ with $0 \leq \tilde{y}_0 \leq \tilde{x}_0$ using Eqs. (2.82) and (2.83),

- ▷ $\tilde{I}^{\rho}_{\alpha\beta}(\tilde{x}_0, \tilde{y}_0)$ from $\tilde{I}^{\rho}_{\alpha\beta}(\tilde{x}_0, \tilde{x}_0)$ to $\tilde{I}^{\rho}_{\alpha\beta}(\tilde{x}_0, 0)$ using Eq. (2.81),
- ▷ $\tilde{I}^{F}_{\alpha\beta}(\tilde{x}_0, \tilde{y}_0)$ from $\tilde{I}^{F}_{\alpha\beta}(\tilde{x}_0, 0)$ to $\tilde{I}^{F}_{\alpha\beta}(\tilde{x}_0, \tilde{x}_0)$ using Eq. (2.80),
- ▷ $\tilde{\overline{\Sigma}}'^{\rho}_{ab}(\tilde{x}_0, \tilde{y}_0)$ and $\tilde{\overline{\Sigma}}'^{F}_{ab}(\tilde{x}_0, \tilde{y}_0)$ for all $\tilde{y}_0$ with $0 \leq \tilde{y}_0 \leq \tilde{x}_0$ using Eqs. (2.89) and (2.90),
- ▷ and finally $\partial_{\tilde{x}_0}\underline{\rho}_{ab}(\tilde{x}_0, \tilde{y}_0)$ and $\partial_{\tilde{x}_0}\underline{F}_{ab}(\tilde{x}_0, \tilde{y}_0)$ for all $\tilde{y}_0$ with $0 \leq \tilde{y}_0 \leq \tilde{x}_0$ using Eqs. (2.92) and (2.93).

3. For the time-evolution of $\underline{F}_{ab}(\tilde{x}_0, \tilde{x}_0) = F_{ab}(\tilde{x}_0, \tilde{x}_0)$ and $\underline{\rho}_{ab}(\tilde{x}_0, \tilde{x}_0) = \rho_{ab}(\tilde{x}_0, \tilde{x}_0)$ along the time diagonal, two considerations are especially beneficial to improve the numerical accuracy:

   - ▷ Since $\rho_{ab}(\tilde{x}_0 + \Delta\tilde{t}, \tilde{x}_0 + \Delta\tilde{t})$ is fixed by the anti-commutation relation, Eq. (1.39), it can be evaluated using this relation and no numerical integration is needed.
   - ▷ If the diagonal time step of F is determined according to

$$\begin{aligned} F_{ab}(\tilde{x}_0 + \Delta\tilde{t}, \tilde{x}_0 + \Delta\tilde{t}) = F_{ab}(\tilde{x}_0, \tilde{x}_0) \\ + \Big(F_{ab}(\tilde{x}_0 + \Delta\tilde{t}, \tilde{x}_0) - F_{ab}(\tilde{x}_0, \tilde{x}_0)\Big) \\ + \Big(F_{ab}(\tilde{x}_0, \tilde{x}_0 + \Delta\tilde{t}) - F_{ab}(\tilde{x}_0, \tilde{x}_0)\Big) \end{aligned} \tag{2.97}$$

     then the discretised equations fulfil the same symmetry associated with the particle number conservation as the continuous equations. This enables to conserve the particle number also numerically exactly.

4. The time integrals on the r. h. s. of the equations of motion (and in the equations for the $\tilde{I}$) make the numerical evolution of the equations time consuming. Furthermore, they require to store the whole past of F and ρ (and $\tilde{\Pi}$ for the practical purpose to significantly decrease the run time of the numerical computation). At first sight, this suggests that the maximum possible time evolution is limited by the RAM of the computer. However, for large enough interactions $\gamma_{\alpha\beta}$, $F_{ab}(\tilde{x}_0, \tilde{y}_0)$ and $\rho_{ab}(\tilde{x}_0, \tilde{y}_0)$ are damped for $\tilde{x}_0 \gg \tilde{y}_0$, which allows to keep only a finite memory kernel, i. e. keeping only the near past in the memory, at longer times without changing the numerical accuracy of the resulting dynamics.
   Another possibility, not pursued by us, is to parallelise the computation (for example using MPI) on several computers and distribute the memory kernel on the different RAMs. Such a distributed memory concept with minimum MPI communication is described, for example, in Ref. [130], where dynamical equations of very similar structure as ours are solved. Similar to the distribution of Σ^F, Σ^ρ, F, and ρ described in this reference, one can also distribute I^F, I^ρ, Π^F, and Π^ρ in order to implement their concept for our dynamic equations in the NLO $1/\mathcal{N}$ approximation.

5. We use a shared memory concept to solve the dynamic equations numerically. Thus, we have a high interest in saving memory. A crucial point is to make use of the symmetries of F and ρ. In the time domain, this means that only those entries with $\tilde{x}_0 \geq \tilde{y}_0$ need to be stored. In the field index domain, two values need to be stored, the 11- and the 12-entry, since the other two, the 22- and the 21-entry, are (except a possible sign) identical to them—see Eqs. (1.38b) and (1.38c). In the spin index domain, two values need to be stored, one for $\alpha = \beta$ and one for $\alpha \neq \beta$ for the (spin balanced) initial conditions we are interested. This implies that the memory costs are the same for all $\mathcal{N} \geq 2$.

6. All computations can be performed in both position and momentum space. Practically, one can switch between them using Fast-Fourier-Transform (FFT) algorithms. This is especially recommendable for computations in larger than one dimension where the direct evaluation of convolutions are numerically much more costly. In this case, it is much cheaper to perform an FFT, evaluate the multiplication associated with the convolution, and transform back with another FFT.

2.3.4 Beyond the next-to-leading order approximation

We have seen that the combinatorial factors played an important rôle in allowing a convenient expression of the dynamic equations in the NLO $1/\mathcal{N}$ approximation; more specifically, it is the iterative form of I, which allowed to write all equations without any explicit summation over diagrams. This iterative form for I was possible due to the appearance of adequate combinatorial factors arising when evaluating the diagrams. As we will see in the following, it is straightforward to identify the contributing diagrams at each order if we go beyond NLO; however, to rewrite the resulting dynamic equations without any explicit summation is at least difficult and maybe impossible.

As a first step, we identify the contributing diagrams without taking care about the combinatorial factors.

▷ As we have seen in Sec. 2.3.1, all diagrams with one new vertex (i. e. one new squiggly vertex line) appearing for each new propagator loop contribute to Γ_2 at the same order. In each diagram, a squiggly vertex line can thus be replaced by a bubble chain without changing the order at which the diagram contributes. To identify different types of diagrams contributing at the same order in the $1/\mathcal{N}$ expansion, this motivates to replace squiggly vertex lines in the diagrams by dashed vertex lines. Dashed lines now represent a bubble chain without specifying the number of bubbles, i. e.

and contribute a factor of $1/\mathcal{N}$ to Γ_2. As a consequence, all diagrams now consist of only full propagator lines forming loops that contribute a factor of $\mathcal{N}$

to Γ_2 and dashed vertex lines, where at each end of a dashed vertex line two propagator lines join.

Note that we must not include diagrams in which two dashed vertex lines are connected by a propagator bubble since this diagram is already included by a dashed vertex line itself, i. e.

Since now all vertex lines are dashed, an equivalent statement is that at each propagator loop there must join at least three dashed vertex ends if the diagram contains more than one dashed vertex line.

▷ In this diagrammatic language, a diagram with k propagator loops contributes at $\mathrm{N}^n\mathrm{LO}$ with $n \geq 1$ if and only if it has $n + k - 1$ dashed vertex lines because $\mathcal{N}^k(\mathcal{N}^{-1})^{n+k-1} = \mathcal{N}^{1-n}$ and $\mathrm{N}^n\mathrm{LO}$ is of order $\mathcal{O}(\mathcal{N}^{1-n})$.

Note that this implies that there is only one diagram that contains exactly one dashed vertex line. This diagram has one propagator loop and is the so-called sunset diagram. The sunset diagram is the only contribution at NLO, see Fig. 2.5a.

▷ Beyond NLO, only a finite number of diagrams contribute at each order, which can be seen as follows.

As argued above, there must be more than one dashed vertex line appear in the diagrams at $\mathrm{N}^n\mathrm{LO}$ with $n > 1$. Therefore, there must join at least three vertex ends at each propagator loop, i. e. there must be at least $3k$ dashed vertex ends in a diagram with k propagator loops. And since there are $n + k - 1$ dashed vertex lines (each having two ends) in a diagram with k propagator loops, this implies

$$2(n + k - 1) \geq 3k \qquad \Leftrightarrow \qquad 2(n - 1) \geq k\,. \tag{2.98}$$

Therefore, an upper bound for the number of propagator loops, and therewith also an upper bound for the number of vertices, exists for a given n. Hence, only a finite number of diagrams contribute at each order.

Examples: As depicted in Fig. 2.5, two diagrams contribute at $\mathrm{N}^2\mathrm{LO}$, and ten diagrams contribute at $\mathrm{N}^3\mathrm{LO}$.

With this, we have seen that it is straightforward to identify the contributing diagrams when going beyond the NLO approximation of Γ_2 in the $1/\mathcal{N}$ expansion. Even though there are only a finite number of diagrams at each order, we have to keep in mind that each dashed vertex itself represents a sum over an infinite number of bubble chains. If there is more than one dashed vertex in a diagram then we find that the combinatorial factors appearing when evaluating these diagrams make it unobvious how to write the dynamic equations in a form that does not involve explicit summations over an

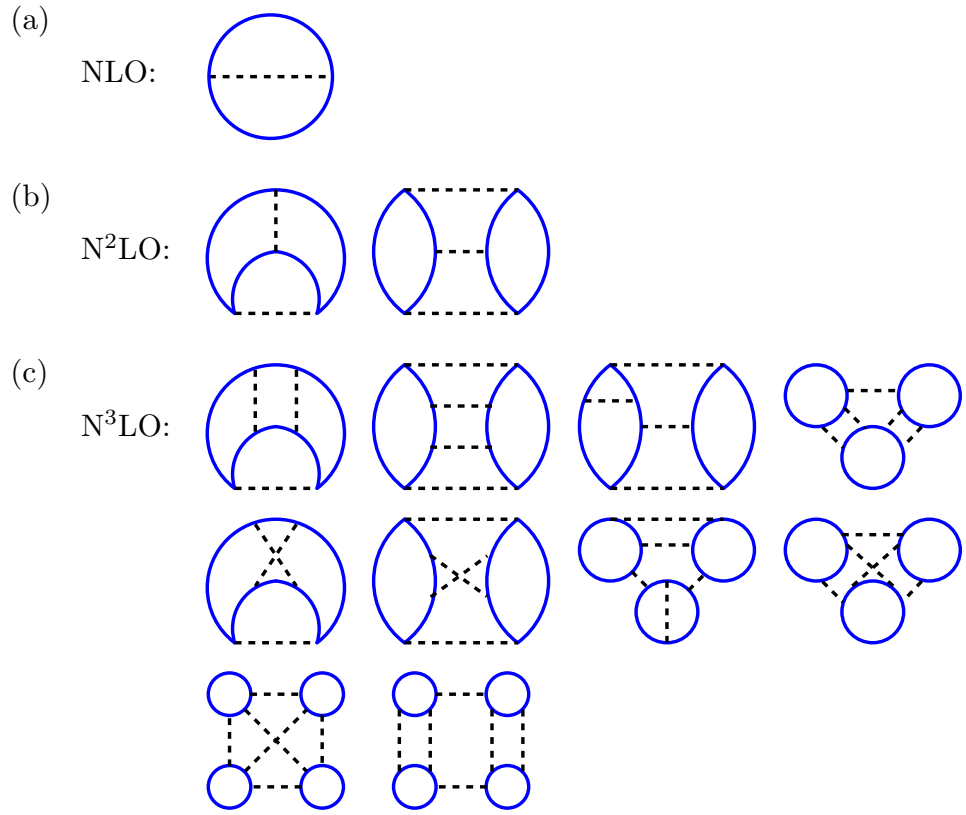

Figure 2.5: Diagrammatic representation of the diagrams contributing at (a) NLO, (b) N^{2}LO, and (c) N^{3}LO to Γ_2 in the $1/\mathcal{N}$ expansion. Thick blue lines represent full propagators and black dashed vertex lines represent a collection of all bubble chains consisting of full propagator loops and bare interaction vertices (see text in main body for details).

infinite number of contributions. These explicit summations make a direct numerical implementation impossible.

An alternative approach to go beyond the NLO approximation in the $1/\mathcal{N}$ expansion of the 2PI effective action is known within the so-called auxiliary-field formalism [59, 131, 132, 133]. It was used in Refs. [134, 135] to derive dynamical equations in N^{2}LO approximation for a relativistic bosonic model with ϕ^4 interactions.

The action needed in the auxiliary-field formalism can be derived from the action S we used via a Hubbard-Stratonovic transformation. Instead of the original four-vertex interaction, one then has a three-vertex interaction. Two legs of the three-vertex are the original fermionic fields. The third leg is the auxiliary-field, which turns out to be identical to the $I_{\alpha\beta}(x,y)$ we introduced in the NLO approximation. All NLO diagrams of the original $1/\mathcal{N}$ expansion are then collected in a single diagram, the sunset diagram. Since this sounds very similar to our discussion above, a word in caution: The NLO contribution to Γ_2 in the auxiliary-field formalism is *not*

identical to the NLO contribution Γ_2 we discussed in this chapter. In the former, the resummed bubble chain appears in the sunset diagram in the from of $I_{\alpha\beta}(x, y)$; in the latter, the bubble chain contributions are, however, differently weighted (with factors $1/2, 1/3, 1/4, \dots$), which is depicted in Fig. 2.4a. In the auxiliary-field formalism, the dynamic equations derived in $\mathrm{N^2LO}$ approximation of the $1/\mathcal{N}$ expansion are in principle suitable for a numerical implementation; however, solving them is numerically very costly due to additional temporal convolutions[5].

2.4 Summary

In this chapter, we discussed different possible approximation schemes of the two-particle irreducible (2PI) effective action Γ for a non-relativistic Fermi gas with $\mathcal{N}$ components that mutually interact through local s-wave contact collisions. These approximations were necessary since the exact dynamical equation derived in the first chapter can generally not be solved exactly due to the complexity of the proper self-energy contribution $\overline{\Sigma}$ appearing therein. The approximated proper self-energies, which we derived from the approximated 2PI effective action discussed in this chapter, enabled us to write the dynamical equation in a form suitable for a numerical integration.

We described two approximation schemes of the 2PI effective action in detail. The first approximation scheme we discussed was a loop expansion in which the contributions to the 2PI effective action were sorted in terms of powers of the bare coupling constant λ. In the first order of this approximation, we derived the well known Hartree-Fock-Bogoliubov dynamic equations for the single particle density and an anomalous pair-correlation function. These equations include neither non-Markovian corrections to the propagation kernel nor many-body corrections to the scattering matrix. Both types of corrections are included, however, in the second order of this approximation, the dynamic equations of which we also derived. We commented on both how these dynamic equations are related to kinetic equations found in the literature and how one proceeds to higher orders in the loop expansion.

The second approximation scheme we discussed is a controlled non-perturbative approximation in which we expanded the effective action in powers of the inverse number of spin states $\mathcal{N}$, i. e. in powers of $1/\mathcal{N}$. This expansion is not based on the coupling and which is, therefore, not restricted to the weak coupling regime. We derived the dynamical equations in leading order and next-to-leading order approximation of this expansion. We showed that at next-to-leading order, an infinite number of diagrams is resummed and, thus, both scattering and memory effects are included. For a homogeneous gas, we presented the dynamical equations in next-to-leading order approximation also in momentum space. Furthermore, We wrote them in dimensionless variables and in an interaction picture. This is especially useful for our numerical investigations, the results of which are presented in the next

[5] In Refs. [134, 135], the numerical solutions of the dynamic equations in NLO approximation neglected for this reason the contributions from the diagrams shown on the right side of Fig. 2.4b.

chapter. Finally, we gave some ideas on how to proceed beyond the next-to-leading order approximation in the $1/\mathcal{N}$ expansion of the 2PI effective action.

Chapter 3

Non-equilibrium time evolution of a one-dimensional Fermi gas

In the previous chapter, we derived non-perturbative approximation schemes for the two-particle irreducible (2PI) effective action of an ultra-cold Fermi gas with $\mathcal{N}$-fold spin degeneracy. The approximation schemes are required in order to be able to solve the dynamical equations for the two-point functions that we derived in Ch. 1. In the present chapter, we apply the dynamic equations derived from the 2PI effective action in next-to-leading order (NLO) approximation of the $1/\mathcal{N}$ expansion to the case of a homogeneous ultra-cold Fermi gas with two-fold hyperfine or spin degeneracy (denoted as $\uparrow$ and $\downarrow$) in one spatial dimension.

The model of a one-dimensional Fermi gas containing two spin components that mutually interact through local repulsive s-wave collisions is considered to be integrable in the sense that it has as many conserved quantities as degrees of freedom [78]. Thus, if such a gas is initially prepared far from an equilibrium state then the gas is expected not to evolve into a late-time state that can be described by a grand-canonical density matrix [79, 81, 82]. Recently, there has been an extensive discussion on the required circumstances that allow the long-time properties of integrable systems to be described by a generalised Gibbs ensemble (GGE) [82, 85, 86, 87, 88, 89, 136, 137]. From the experimental point of view, it might be difficult, however, to rule out the equilibration of the system to a particular statistical ensemble because the expectations of many of the experimentally accessible observables will appear essentially indistinguishable from the ones found from the different ensembles once the system evolved into a steady state [138].

At zero temperature, the one-dimensional Fermi gas containing two spin components that mutually interact through repulsive contact interactions is known to behave as a Tomonaga-Luttinger liquid (TLL) [83, 139, 140], which is obtained by taking the dispersion to be linear in momentum. The TLL Hamiltonian is quadratic and therefore integrable, and its equilibrated maximum-entropy state is naturally described by a GGE [84, 141]. Further away from zero temperature, where our analysis presented in this chapter is performed, we are in a regime of energies in which the non-linearity of the dispersion becomes relevant. In this regime, the applicability of the TLL model has not been shown, and the description of the long-time properties

is still an open question. As we will see, our results indicate that the considered Fermi gas at sufficiently low energies approaches a non-thermal late-time state that does not respect the fluctuation-dissipation theorem. This signature is in principle accessible in experiments.

In our analysis, the Fermi gas is initially assumed to be non-interacting and prepared far from equilibrium, characterised by a non-equilibrium single-particle momentum distribution. In the first section of the present chapter, Sec. 3.1, we discuss how the initial conditions translate into the specification of two-point functions. The homogeneous one-dimensional gas is taken to have a line density $n_{1\mathrm{D}}$, and the constituents have mass m. We assume the interactions to be switched on at the initial time and investigate the long-time evolution of the interacting gas towards equilibrium. We study the dynamics of the gas in a finite-size box with periodic boundary conditions. The numerical implications of this restriction are discussed in Sec. 3.2. The ensuing sections are devoted to the discussion and interpretation of our numerical results.

All runs that we performed evolved into a stationary state once they were insensitive to numerical parameters like the discrete time step size. An exemplary run is discussed in Sec. 3.3. As we show in Sec. 3.4, these stationary states are insensitive to the details of the initial state. They are solely determined by the total energy E_{tot}, the total particle number N (or rather the line density $n_{1\mathrm{D}}$), and the interaction strength γ. In these stationary states, we find that the occupation numbers of the lowest momentum modes coincide with a Fermi-Dirac distribution, with which thermodynamic quantities like the temperature and the chemical potential are connected. This is investigated in Sec. 3.5. The occupation numbers of the higher momentum modes deviate from a Fermi-Dirac distribution. This deviation becomes more and more dominant at lower total energies of the gas. To be more precise, we find that a power-law tail is replacing the exponential decay of a Fermi-Dirac distribution, as we will see in Sec. 3.6.

There are two possible reasons for a deviation of the momentum mode occupation numbers from a Fermi-Dirac distribution. First, the system is in a non-thermal state that cannot be described by a grand-canonical density matrix. Second, the single particle momentum modes are no longer the eigenmodes of the system, which is naturally the case for an interacting system at sufficiently low energies. In the latter case, if the system is in a thermal state then only the occupation numbers of the quasi-particles corresponding to the eigenmodes of the system need to respect a Fermi-Dirac distribution in order that the state can be described by a grand-canonical density matrix. However, for a (strongly) interacting system, the eigenmodes are usually difficult to extract. Thus, it is advisable employ the fluctuation-dissipation theorem, which, for a (grand-)canonical state, is exact and independent of a quasi-particle basis of eigenmodes of the system. In Sec. 3.7, we investigate the fluctuation-dissipation relation for our data. For the runs with very low total energies, i. e. those where the single particle momentum distribution deviates the strongest from a Fermi-Dirac distribution, we also find deviations from the fluctuation-dissipation relation. This indicates that the Fermi gas approaches a non-thermal state at large times.

3.1 Initial conditions

With initial values for the spectral function $\rho(t_0, t_0; p)$ and the statistical propagator $F(t_0, t_0; p)$, Eqs. (2.62) and (2.63) describe the time evolution of the two-time correlation functions including the momentum distribution

$$n_\alpha(t,p) = \frac{1}{2}\big(1 - F_{(\alpha,i)(\alpha,i)}(t,t;p)\big)\,. \tag{3.1}$$

In the following, we will choose different initial momentum distributions $n_\alpha(t_0, p)$ away from thermal equilibrium. Furthermore, we choose the initial coherence between different spins as well as the initial pair correlation function to vanish,

$$\langle \hat\Psi^\dagger_\alpha(\mathbf{x}, t_0)\hat\Psi_\beta(\mathbf{x}, t_0)\rangle = 0 \qquad \text{for } \alpha \neq \beta\,, \tag{3.2}$$

$$\langle \hat\Psi_\alpha(\mathbf{x}, t_0)\hat\Psi_\beta(\mathbf{x}, t_0)\rangle = 0\,. \tag{3.3}$$

$$\tag{3.4}$$

For $\alpha = \beta$, the equal-time pair correlation function always vanishes, which is in accordance with the conservation of the total particle number and a direct consequence of the equal-time property of the spectral function (Eq. (1.39)). For $\alpha \neq \beta$, a non-zero initial pair correlation function would account for BCS-type pairs and imply a non-zero variance of the total particle number. The above initial conditions require

$$F_{(\alpha,i_a)(\beta,i_b)}(t_0, t_0; p) = 0 \qquad \text{for } i_a \neq i_b\,. \tag{3.5}$$

Combining Eqs. (3.1) and (3.5) yields the initial condition

$$F_{(\alpha,1)(\alpha,1)}(t_0, t_0; p) = F_{(\alpha,2)(\alpha,2)}(t_0, t_0; p) = \frac{1}{2} - n_\alpha(t_0, p)\,. \tag{3.6}$$

The equal-time property of the spectral function, Eq. (1.39), requires

$$\rho_{ab}(t_0, t_0; p) = \mathrm{i}\tau_{ab}\,. \tag{3.7}$$

For a homogeneous gas and a $(p \leftrightarrow -p)$-symmetric initial state, F and ρ are invariant under $p \to -p$ at all later times.

The initial conditions in Eqs. (3.2) and (3.2) imply that $F_{(\alpha,i_a)(\beta,i_b)}(t_0, t_0; p)$ and $\rho_{(\alpha,i_a)(\beta,i_b)}(t_0, t_0; p)$ vanishes for $\alpha \neq \beta$ at the initial time t_0. For the model we are considering, the dynamic equations for F and ρ, Eqs. (2.62) and (2.63), conserve this property in time, independent of the approximation chosen for Γ_2. As a consequence of this, only diagrams with an even number of vertices yield a non-vanishing contribution to Γ_2 at NLO of the $1/\mathcal{N}$ expansion. A diagram with an even number of vertices is not sensitive to the sign of the coupling strength γ. Therefore, the dynamical equations derived from either the second-order approximation in the loop-expansion or from the NLO approximation in the $1/\mathcal{N}$ expansion of the 2PI effective action are insensitive to the sign of γ.

3.2 Numerical implementation

We numerically solve the (dimensionless) equations of motion in momentum space, Eqs. (2.92) and (2.93), together with the non-perturbative integral equations for the self-energies, Eqs. (2.78) and (2.79). For this purpose, we need to consider the system to be discretised in time and momentum space.

Discretising the momentum space is equivalent to using a finite sized system in position space, which has automatically discretised momentum modes. If the (one-dimensional) system is of length L in position space and discretised by an even number N_s of equally spaced lattice sites then the discrete physical momenta p_j, whose square corresponds to the lattice Laplacian (i. e. the Fourier transform of the discrete second derivative in position space), are given by

$$\frac{p_j}{n_{1\mathrm{D}}} = \frac{2N_s}{N} \sin(j\pi/N_s)\,, \tag{3.8}$$

where $j \in \{-N_s/2+1, -N_s/2+2, \ldots, N_s/2\}$ labels the momentum modes, $N = \sum_{\alpha,j} n_\alpha(p_j)$ is the total particle number, and $n_{1\mathrm{D}} = N/L$ is the one-dimensional particle density. The lattice provides an infra-red (IR) cut-off at the lowest resolved non-zero momentum

$$\frac{p_1}{n_{1\mathrm{D}}} = \frac{2N_s}{N} \sin(\pi/N_s) \overset{\pi \ll N_s}{\approx} \frac{2\pi}{N} \tag{3.9}$$

and an ultra-violet (UV) cut-off at the highest resolved momentum

$$\frac{p_{N_s/2}}{n_{1\mathrm{D}}} = \frac{2N_s}{N}\,. \tag{3.10}$$

In the last three formulae, the momenta on the left-hand sides of the equations are divided by the particle density in order to remind us that we actually implement the dimensionless equations, i. e. we implement the dimensionless momentum $p/n_{1\mathrm{D}}$ rather than the dimensionfull momentum p. Thus, in the dimensionless equations, the total particle N and the number N_s of lattice sites need to be specified to characterise the lattice—and there is no need to specify explicitly either the length L of the lattice or the lattice spacing L/N_s in position space. N controls the IR cut-off and the ratio N_s/N the UV cut-off. If not stated otherwise, we chose a lattice with $N_s = 128$ sites and used $N = 26$ particles (13 of each spin component) for the results presented in this chapter. We carefully checked that a change in the size of the box and the number of the momentum modes does not lead to a significant change in the results presented, except for finite-size (IR cutoff) effects taken into account explicitly in our analysis. For example, we chose the interaction strength sufficiently weak such that the occupation numbers of momentum modes close to the UV cut-off are small enough not to give rise to UV-cutoff-dependent effects.

Due to the memory integrals, computations are costly, and in computing the results shown below, we kept a finite memory kernel at longer times, checking that an increase in the memory time did not change the results.

In the graphs we show in this chapter, the momenta, the energies, and the temperatures are given in units of the Fermi momentum p_F, the Fermi energy ω_F, and the Fermi temperature T_F, which are defined as

$$\frac{p_F}{n_{1\mathrm{D}}} \equiv \frac{2N_s}{N} \sin\left(\frac{\pi(N-\mathcal{N})}{2\mathcal{N}N_s}\right) \qquad \text{with } \mathcal{N}=2, \tag{3.11}$$

$$\omega_F \equiv \frac{p_F^2}{2m}\,, \tag{3.12}$$

$$T_F \equiv \frac{\omega_F}{k_B}\,, \tag{3.13}$$

where k_B is Boltzmann's constant.

3.3 Time evolution from far-from-equilibrium into a stationary state

In this section, we want to address the question how the Fermi gas evolves in time if it is initially prepared far from an equilibrium state. In particular, it is the question whether or not the Fermi gas will reach a (quasi) stationary state before the finite size of the system causes revivals. To address these questions, we present some typical results that we found when numerically solving the dynamic equations Eqs. (2.62) and (2.63) (in next-to-leading order approximation of the $1/\mathcal{N}$ approximation of the effective action) on the basis of an exemplary but typical run.

Our numerical results for the typical run considered here are shown in Fig. 3.1. As initial state at time $\tilde{t} \equiv n_{1\mathrm{D}}^2 t/m = 0$, we populate all momentum modes of a non-interacting Fermi gas in a certain momentum interval and leave all other modes unpopulated. No further correlations are present in the initial state. The interactions are suddenly switched on at the initial time $\tilde{t} = 0$. Therefore, the chosen initial momentum distribution is clearly far-from-equilibrium. The initial distribution of the momentum mode occupation numbers is shown in Fig. 3.1a together with the numerically determined late-time ($\tilde{t} = 10$) distribution. Since there is a $(p \leftrightarrow -p)$-symmetry, we always show only half of the momentum modes; actually, to be precise, we show $(N_s + 2)/2$ of the N_s momentum modes.

Figure 3.1b shows the numerically determined time evolution of the momentum mode occupation numbers on a double logarithmic plot. After an initial dephasing period where the occupation numbers show fast oscillations, the occupation numbers slowly drift into the late-time state. One can virtually see that this late-time state is stationary. In fact, all runs we performed (i. e. in particular those presented below in this chapter) reached a stationary distribution of the momentum mode occupation numbers once the time evolution was insensitive to numerical parameters like the time step size and the finite size of the memory kernel. Note that a conservative estimate of the recurrence time on the basis of the slowest oscillating discrete mode

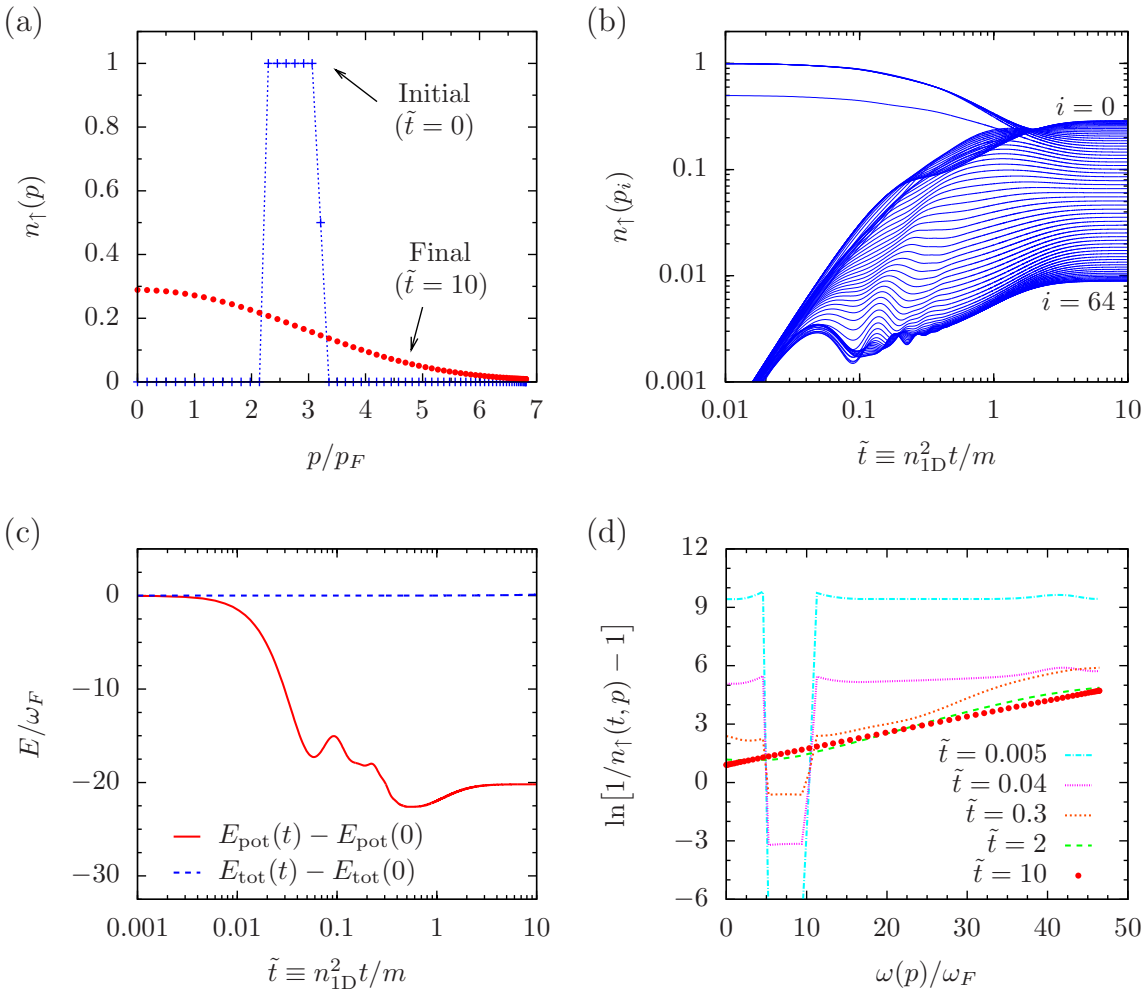

Figure 3.1: Results for a typical run presented in this chapter. The parameters used in this run are: $N_s = 128$ momentum modes, $N = 26$ particles (13 spin up, 13 spin down), interaction strength $|\gamma| = 4$, size of time steps $\Delta\tilde{t} = 0.0015$, and always the most recent 1500 time steps of the past evolution are used in the time integrals over the past (i. e. the size of the memory kernel is $1500\Delta\tilde{t} = 2.25$). (a) Initial ($\tilde{t} \equiv n_{1D}^2 t/m = 0$) far-from-equilibrium and late-time ($\tilde{t} = 10$) distribution of the momentum mode occupation numbers. (b) Numerically determined time evolution of the momentum mode occupation numbers on a double logarithmic plot. The occupation numbers virtually reach a stationary state. (c) Redistribution of the potential and kinetic energy distributions. The total energy remains constant. (d) Inverse slope function at various times. Since it becomes a straight line at late times ($\tilde{t} = 10$), the steady state distribution is a Fermi-Dirac distribution.

of the free gas is two orders of magnitude larger than the shown total evolution time.

During the time evolution, scattering effects lead to a redistribution of the initial potential and kinetic energy distribution. For the typical run, this is shown in Fig. 3.1c. Note that the discrete time steps in the numerics break the continuous symmetry of the equation that is associated with the conservation of the total energy. Hence, the total energy cannot be exactly conserved in the numerics. However, for small enough step sizes, the numerically determined time evolution becomes insensitive to the discreteness of the time. And in this case, the numerics conserves essentially also the total energy.

At this stage, we also want to introduce the inverse slope function $\sigma_\uparrow = \ln[1/n_\uparrow - 1]$. When substituting the inverse slope function for the exponent of the Fermi-Dirac distribution, i. e.

$$n_\uparrow(t,p) = \frac{1}{\exp\{\sigma_\uparrow[\omega(p)]\} + 1}\,, \tag{3.14}$$

it is apparent that $\sigma_\uparrow$, as a function of mode energy $\omega(p)$, reduces to a straight line when the occupation number $n_\uparrow(t,p)$ is a Fermi-Dirac distribution. And in the case where the inverse slope function becomes a straight line, one can extract the inverse temperature $\beta = (k_\mathrm{B})$ and the chemical potential μ according to $\sigma_\uparrow(\omega) = \beta(\omega - \mu)$. In Fig. 3.1d, the inverse slope function of the typical run is shown for various times during the time evolution. For the exemplary run shown here, it becomes a straight line at late times. However, this is not characteristic for any generic run but a distinctive property if the total energy is large enough. We will come back to this property and investigate it further in Secs. 3.6 and 3.7.

3.4 Insensitivity of the final state on the details of the initial state

In this section, we want to address the question how much memory of the initial conditions will remain in the system once it reaches a stationary (or quasi-stationary) state. For this purpose, we study the time-evolution for two initial states—in the following called run A and run B—with the same total particle number, total energy, and interaction strength $|\gamma| = 4$ but different far-from-equilibrium distribution of the initial momentum mode occupation numbers.

The two different initial distributions we consider in this section are shown in Fig. 3.2a. Once the system evolves in time, multiple scattering events lead to a redistribution of momenta until the system reaches a stationary state. In Fig. 3.2b, the numerically determined time evolution of the momentum mode occupation numbers is shown for six of the momentum modes. The final ($n_\mathrm{1D}^2 t/m = 10$) distributions of the

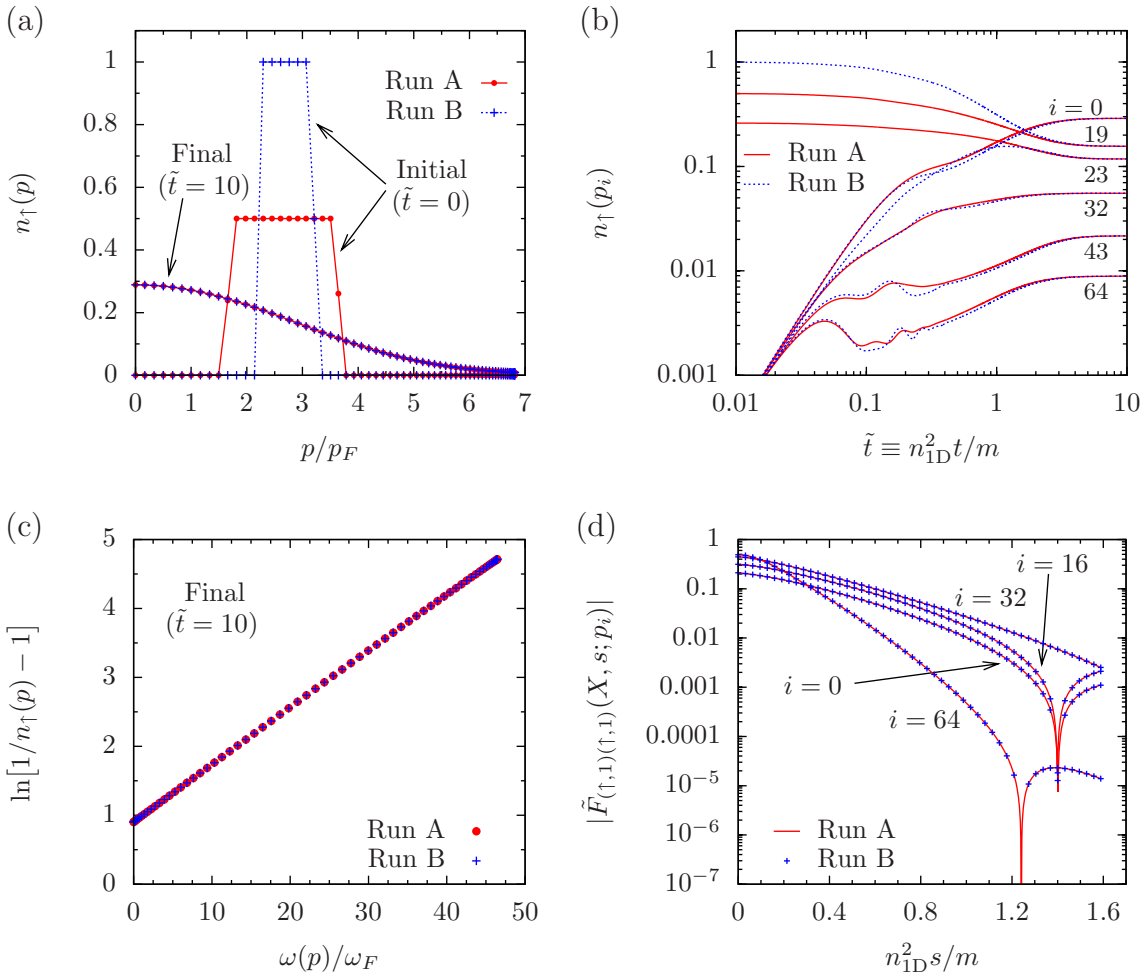

Figure 3.2: Comparison between two runs with the same total energy and coupling constant ($|\gamma| = 4$) but different initial distributions of the momentum mode occupation numbers. (a) Initial ($\tilde{t} \equiv n_{1D}^2 t/m = 0$) and final ($\tilde{t} = 10$) momentum mode occupation numbers. Within the numerical precision, the final momentum distributions are the same for both runs. (b) Numerically determined momentum-mode occupation numbers as a function of time t. (c) Inverse slope function of the final distribution of the momentum mode occupation numbers. (d) Nonlocal-in-time behaviour (i. e. same center but different relative time coordinates) of the statistical propagator $\underline{F}_{(\uparrow,1)(\uparrow,1)}(X, s; p)$ in the interaction picture, cf. Eq. (2.91), at late center times ($n_{1D}^2 X/m = 10$) for four of the momentum modes. Within the numerical precision, the data from the two runs lie on top of each other, which proves (together with an exact match of the other components of $\tilde{F}$ and $\tilde{\rho}$) that the final states of both runs are identical.

momentum mode occupation numbers and the corresponding inverse slope functions are shown in Fig. 3.2a and c, respectively. We find that the steady states of the two runs have within the numerical precision the same momentum-mode occupation numbers at late times.

However, the momentum distribution is just one possible observable. And thus, the fact that the two runs coincide in this observable does not allow the conclusion of the final states being the same. For the two runs, the off-diagonal behaviour is the same as illustrated in Fig. 3.2d. To decide whether the final states are identical, one has not only to look at the momentum-mode occupation numbers, but also to compare the nonlocal-in-time behaviour of the two-point functions $F_{ab}(x_0, y_0; p)$ and $\rho_{ab}(x_0, y_0; p)$ of the two runs. Here, nonlocal-in-time behaviour means same center time coordinates $X \equiv (x_0 + y_0)/2$ but different relative time coordinates $s \equiv x_0 - y_0$. Exemplary, the nonlocal-in-time behaviour of $F_{(\uparrow,1)(\uparrow,1)}(X, s; p)$ at late times ($n_{1\mathrm{D}}^2 X/m = 10$) is depicted in Fig. 3.2d for four of the momentum modes of runs A and B. The data for the two runs lie on top of each other. Since also the other two-point functions of the two runs coincide within the numerical precision at late times, we can conclude that the final states of run A and run B are indeed identical.

The chosen initial conditions for runs A and B allow the Fermi gas to equilibrate over the considered range of momenta into the same final state. We have also compared runs with other sets of parameters (N, N_S, γ) and always found that the late time state, on the one hand, depends only on E_{tot} and γ as soon as the dynamics does not depend on numerical parameters like the size of the time step and the size of the memory kernel, and on the other hand, loses all other details of the initial preparation.

In conclusion, we find that the final state is determined by the values of the conserved quantities in the initial state. All other information about the details of the initial state is lost during the time evolution.

3.5 Thermodynamic properties

In this section, we investigate a few thermodynamic properties of the equilibrated interacting Fermi gas. For this purpose, we performed additional runs with different initial energies but the same total particle number and interaction strength as in runs A and B. Exemplary, the initial momentum distributions of some of these runs are shown in Fig. 3.3a together with the one from run B (= run 10).

All runs virtually reach a stationary state within the times that are numerically accessible before the time discretisation leads to a break-down of the energy conservation (the discrete time breaks the time translational invariance of the action that is related to the energy conservation). Two examples, one for a high initial energy and another for the lowest initial energy, are shown in Fig. 3.1b and Fig. 3.7a, respectively. The late-time momentum distributions look on a first sight like a Fermi-Dirac distributions, see Figs. 3.3b and 3.4a. However, when plotting the inverse slope functions (Figs. 3.3c and 3.4b), we find that the momentum distribution of the runs with lower

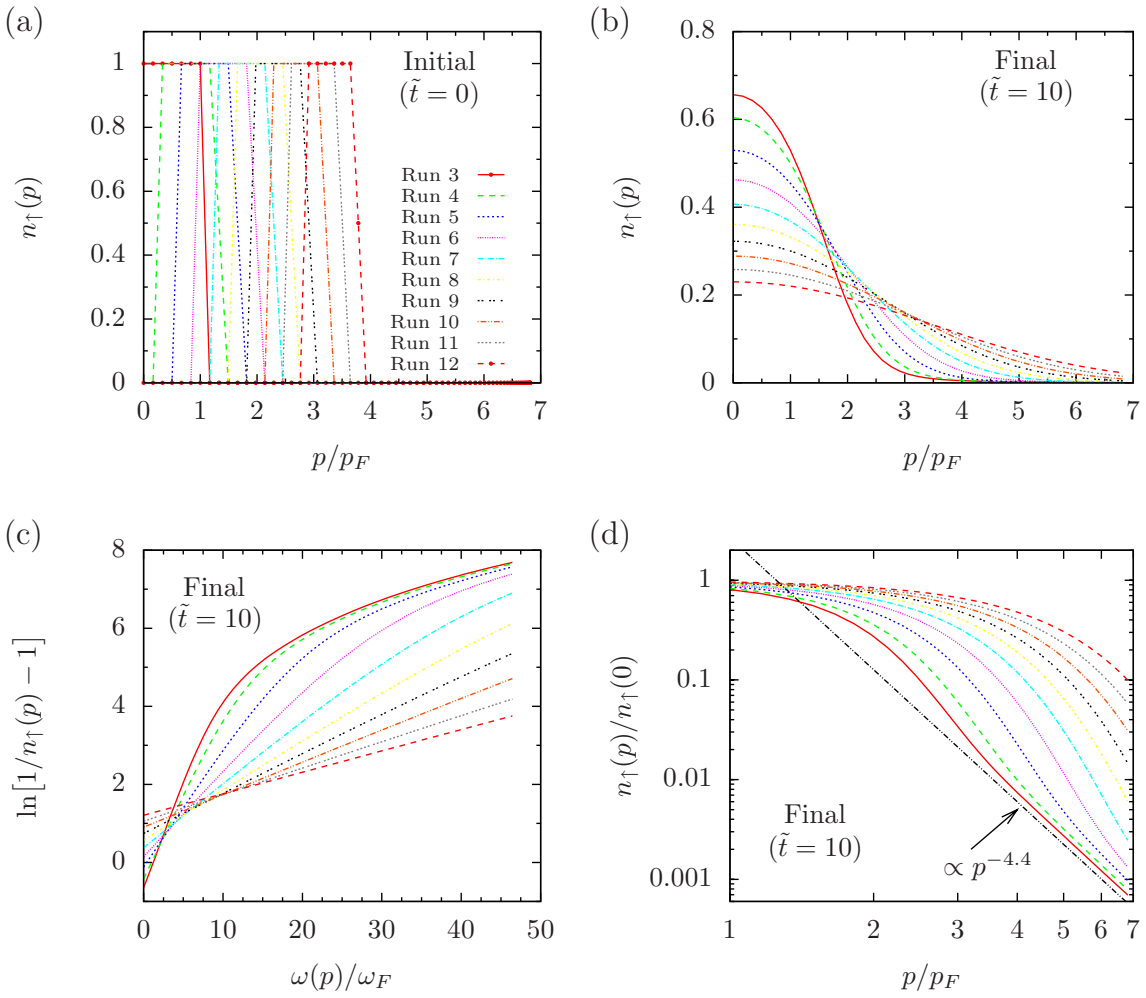

Figure 3.3: Runs with the same total particle number and interaction strength but different initial energies. (a) Initial distribution of the momentum mode occupation numbers. (b) Final ($\tilde{t} = 10$) momentum distributions that look on a first sight like Fermi-Dirac distributions. (c) Inverse slope functions of the final momentum distributions from which it can be seen that the runs with low energies show an excess population in the high momentum modes. (d) Normalised final momentum distribution on a double logarithmic plot. For the runs with low energies, the tail of the momentum distribution is characterised by a power-law decay rather than a Fermi-Dirac distribution.

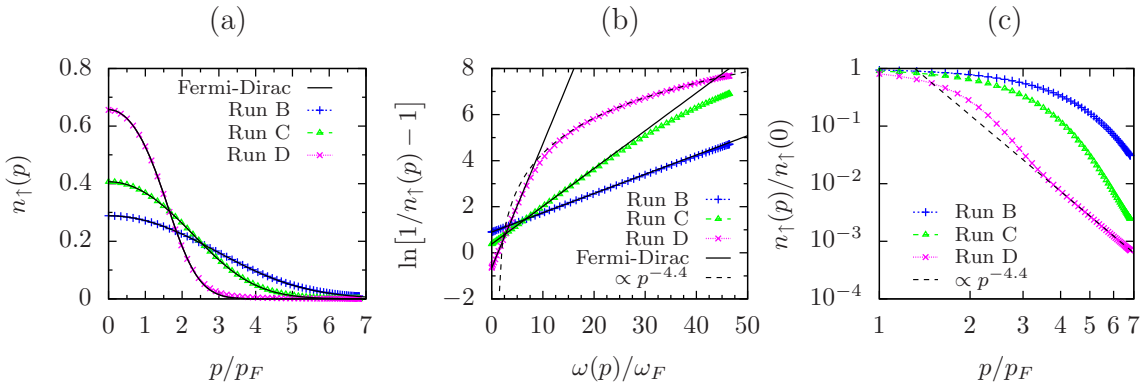

Figure 3.4: Final ($\tilde{t} \equiv n_{1D}^2 t/m = 10$) momentum mode occupation number distributions of runs B, C, and D (= runs 10, 7, and 3). (a) Momentum mode occupation numbers as a function of momentum together with fits of the lowest momentum mode occupation numbers to a Fermi-Dirac distribution. For the fits, the momentum modes with $|p/p_F| \leq 2$ are used. (b) Inverse slope functions together with the Fermi-Dirac and power-law fits from (a) and (c). (c) Normalised momentum mode occupation numbers as a function of momentum together with a power-law fit to the tail of the momentum distribution of run D.

initial energies do not fully settle to Fermi-Dirac distributions. For these runs, the inverse slope function of the lower momentum modes becomes a straight line and thus reaches a Fermi-Dirac distribution, but the higher momentum modes show an excess population, which we characterise further in the next section.

Keeping the total particle number constant, a further reduction of the population in the higher momentum modes will not significantly alter the population in the lower momentum modes since the former are already populated much less than the latter. This suggests that we can extract temperatures and chemical potentials from a fit of the lowest momentum modes (we use the modes with $|p/p_F| \leq 2$) to a Fermi-Dirac distribution as it is shown in Fig. 3.4a and b for three of the runs.

The so found temperature dependence of the chemical potential μ is shown in Fig. 3.5a. For high temperatures, the chemical potential of the interacting gas converges towards the results for an ideal Fermi gas. However, as shown in the inset, it substantially deviates from those of an ideal gas at low temperatures where the finite coupling constant becomes more significant. Note that for the finite size of our system, the results for the ideal Fermi gas in the discrete momentum space (green dashed line in Fig. 3.5) differ from those of an ideal Fermi gas in the thermodynamic limit (blue dashed line in Fig. 3.5), where the momentum space is continuous. Our results extracted from the late-time momentum distribution are sensitive to this finite-size effect, too. For more details on the ideal Fermi gas, see App. A.

In Figs. 3.5b and c, the temperature dependence of the late-time kinetic energy $E_{\text{kin}}^{(\text{eq})}$, and the heat capacity $C_V = k_B \partial E_{\text{tot}}/\partial \beta^{-1}$ at constant volume are depicted. They show the same qualitative features as the chemical potential: they converge

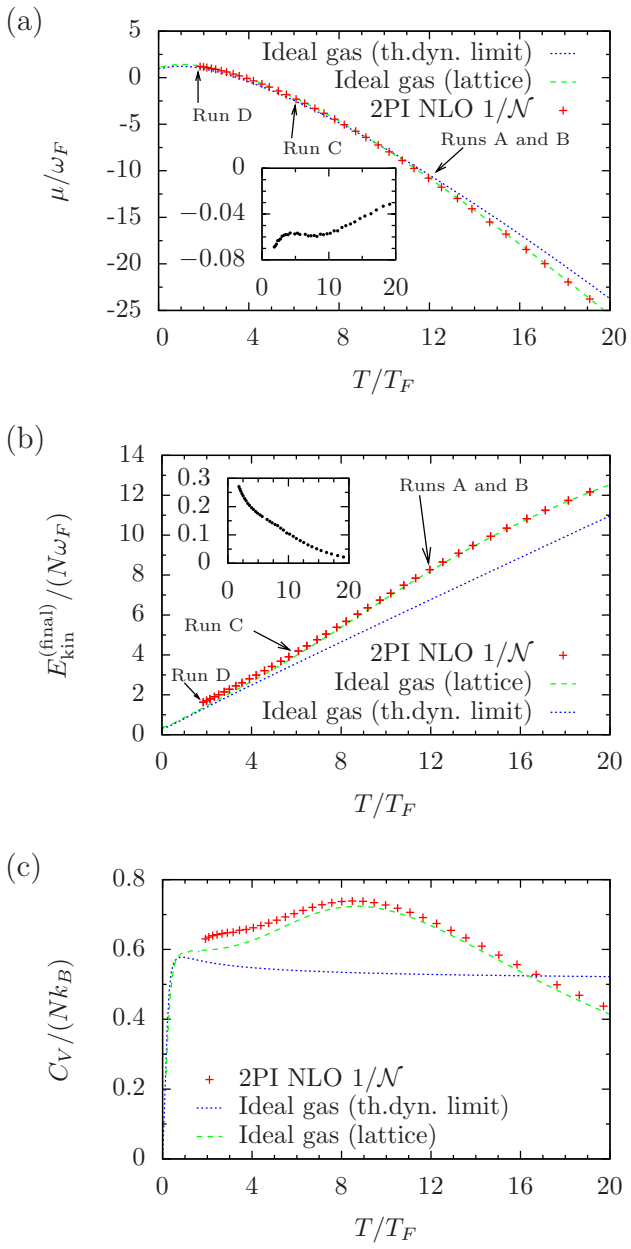

Figure 3.5: Temperature dependence of (a) the mean kinetic energy per particle, (b) the heat capacity per particle, and (c) the chemical potential. The results for the interacting Fermi gas from the 2PI $1/\mathcal{N}$ NLO runs are shown as red dots. For comparison, the exact results for the ideal Fermi gas are shown both for a continuous and a discrete momentum space. The differences between the interacting Fermi gas and the ideal Fermi gas in discrete momentum space are shown in the insets.

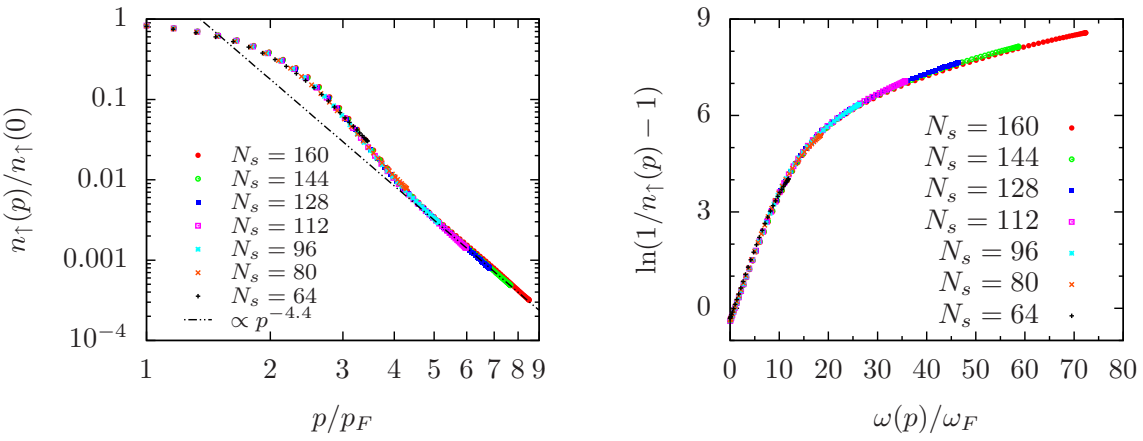

Figure 3.6: Independency check of our results from the chosen UV cut-off. The runs are for the same initial momentum distribution and the same total particle number $N = 26$ but different number N_s of momentum modes. We find that neither the bending of the inverse slope function (right panel) nor the power-law exponent (left panel) of the late-time momentum distribution depends on the UV cut-off. Note that in all other runs presented in this chapter, we always used $N_s = 128$ momentum modes.

to the ideal gas results for high temperatures and deviate from them for lower temperatures.

3.6 Power-law momentum tail

In the previous section, we have seen that thermodynamic quantities can be extracted from the occupation numbers of the low momentum modes by fitting them to a Fermi-Dirac distribution. In this section, we investigate the overpopulation of the occupation numbers at high momenta as compared to a Fermi-Dirac distribution, which occurs for runs with sufficiently small initial energies. From the runs depicted in Fig. 3.3d, we find that the population of more and more momentum modes follow a power law at late times if the total initial energy of the Fermi gas is reduced.

We stress that the data in Fig. 3.3d are extracted at late times where the time evolution of the momentum mode occupation numbers is virtually stationary on a double logarithmic plot. For Run D (= Run 3), which has the smallest total energy of the shown runs, and which therefore takes the longest time to reach a stationary state, the time evolution is shown in Fig. 3.7a. One clearly sees that especially the occupation numbers of the higher momentum modes are stationary. And since the highest momentum modes of this run would need to be less populated by about three orders of magnitude if all momentum modes were required to fulfil a Fermi-Dirac distribution, it is very likely that the overpopulation remains even if the propagation is taken much longer in real time.

We also want to check that neither the overpopulation in general nor the power-law exponent in particular are a result of the UV momentum cut-off. If there was such a dependence, we would expect that for larger UV cut-offs the inverse slope function becomes a straight line extending to higher and higher momenta such that the bending shifts towards higher momenta. To investigate a possible UV cut-off dependence, we performed runs with the same initial far-from-equilibrium momentum distribution but different UV cut-offs characterised by different ratios N_s/N. The resulting equilibrated momentum distributions are shown in Fig. 3.6. We find that neither the bending of the inverse slope function nor the power-law exponent depend significantly on the chosen UV cut-off.

Finally, we show that the power-law tail is present not only in the NLO $1/\mathcal{N}$ approximation. As depicted in Fig. 3.7b, the power-law exponent does not change when diagrams of order γ^3 are included[1] in the effective action. Therefore, the power-law exponent is clearly no artifact of the chosen approximation.

The power-law behaviour for different values of the coupling strength is shown in Fig. 3.8. Within the range of momenta we can resolve, only the runs with smaller couplings, i. e. lower total energies, develop a power-law tail. Once the power-law tail is present, the power-law exponent seems not to be strongly depend on the value of the coupling.

Note that a p^{-4} power law for the high-momentum tail of the single-particle momentum distribution is one of Tan's relations [142, 143, 144, 145, 146] for a strongly correlated two-component Fermi gas (independent of the strength and the sign of the coupling) and is also a feature of the BCS theory.

3.7 Fluctuation-dissipation relation and non-thermal final states

In this section, we address the question whether or not the late-time stationary states can be described by a standard statistical ensemble as, e. g. the micro-canonical, the canonical, or the grand-canonical ensemble. If this is the case, we would speak of thermalisation.

The single-particle momentum mode occupation numbers of an interacting system is not a good indicator whether or not the system is in a thermal state. Since only the the occupation numbers of the eigenmodes need to be Fermi-Dirac distributed in order for the system to be in a thermal state, the single-particle momentum distribution is likely not to be Fermi-Dirac distributed once the interactions become a pronounced feature of the system. The interactions become generically a pronounced feature at sufficiently low energies. Therefore, we have a closer look at the fluctuation-dissipation relation (FDR), Eq. (1.41). The FDR does not depend on a particular field basis,

[1] For the third-order loop approximation, which is sensitive to the sign of the interaction strength, results are shown for positive γ. For negative γ, the numerics turns out to be much more sensitive for the discrete time step size, such that no numerically stable evaluation of the dynamic equations was possible with the computational resources by hand.

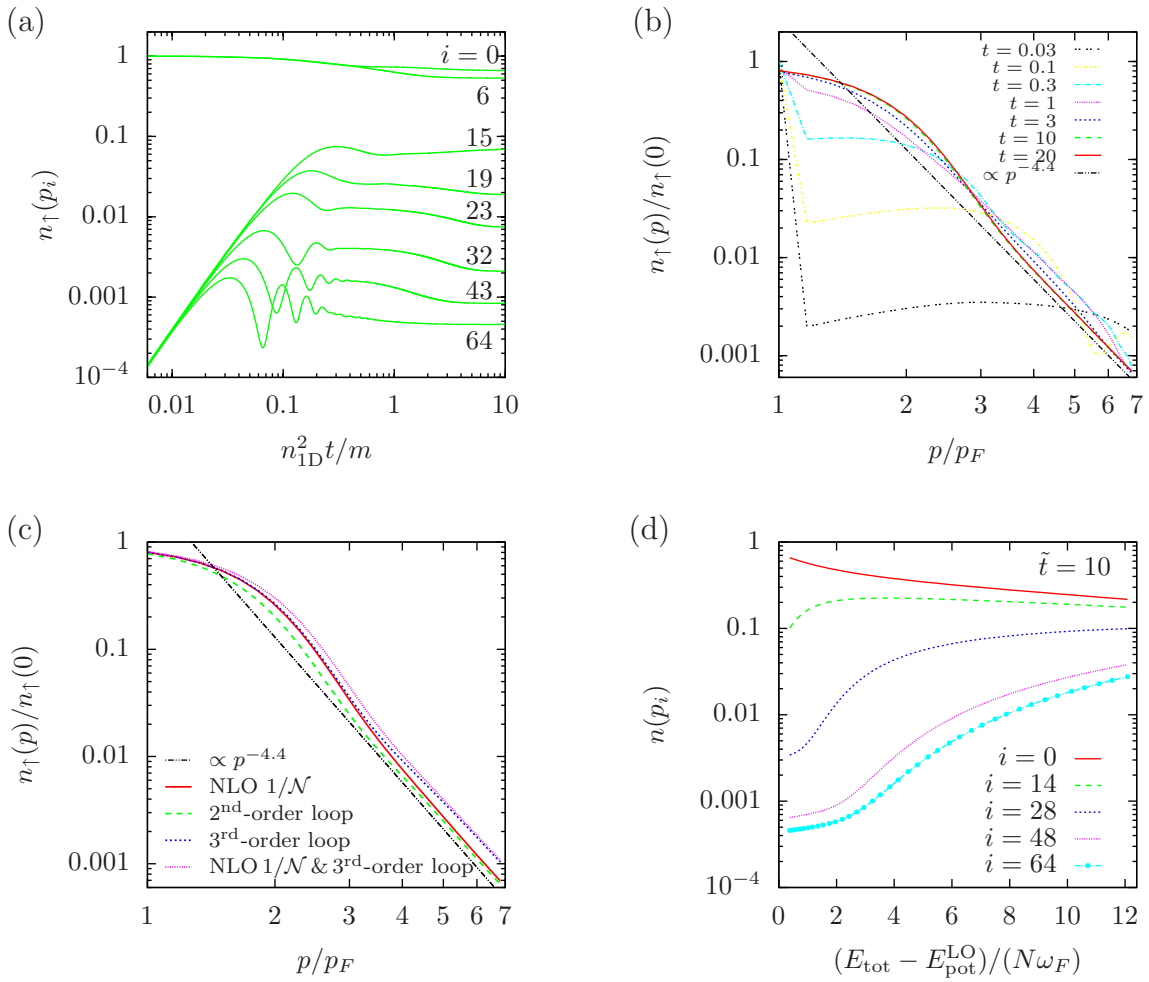

Figure 3.7: (a) Time evolution of the momentum mode occupation numbers of run D in NLO $1/\mathcal{N}$ approximation of the effective action. (b) Snap-shots of the occupation numbers shown in (a) as a function of momentum. This shows how the power-law tail at larger momenta develops in time and becomes stationary. (c) Comparison of the late time ($\tilde{t} = 10$) momentum distribution for different approximation schemes of the effective action for runs with the same initial state as run D. For the third-order loop approximation, which is sensitive to the sign of the interaction strength, results are shown for positive γ. (d) Occupation numbers in NLO $1/\mathcal{N}$ approximation of the effective action at late time ($\tilde{t} = 10$) as a function of the total energy per particle. Here, we subtracted the constant potential energy contribution $E_{\text{pot}}^{\text{LO}}$ from the total energy.

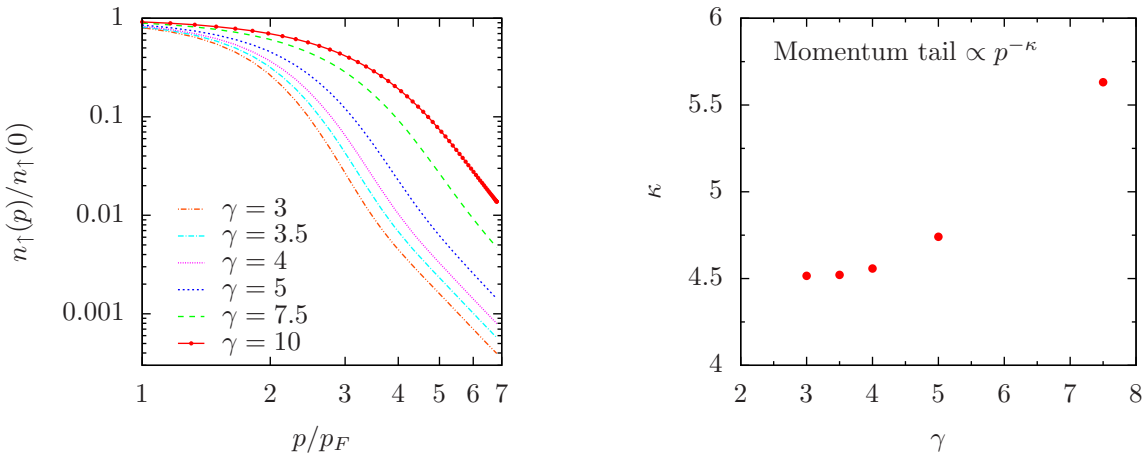

Figure 3.8: Left: Comparison of late-time distributions for runs with same initial momentum distribution as run D but different interaction strengths, and thereby different total energies. Note that only the runs with lower total energy (i. e. smaller coupling strength) develop a power-law tail within the resolved momenta. Right: Power-law exponents extracted from the high momentum tails shown in the left panel.

see Sec. 1.2.2, and does thus not require the knowledge of the eigenmodes of the system. Specifically, we will look at three distinctive runs whose late-time momentum distributions are shown in Fig. 3.4:

- ▷ Run B at a high energy, where the single-particle momentum distribution becomes a Fermi-Dirac distribution and the FDR holds,
- ▷ Run C at an intermediate energy, where the single-particle momentum distribution does not become a Fermi-Dirac distribution but the FDR still holds, and
- ▷ Run D at a low energy, where neither the single-particle momentum distribution becomes a Fermi-Dirac distribution nor the FDR holds. Thus, run D evolves into a non-thermal final state.

For our analysis, it is convenient to introduced the fraction

$$f(\omega, p) = \mathrm{i}F_{\uparrow\uparrow}(X_0; \omega, p)/\rho_{\uparrow\uparrow}(X_0; \omega, p) \tag{3.15}$$

as a function of the frequency ω and momentum p. For the definitions of $F_{\uparrow\uparrow}(X_0; \omega, p)$ and $\rho_{\uparrow\uparrow}(X_0; \omega, p)$, see Eq. (1.42). If the system is in a thermal state, which is described by a (grand-)canonical ensemble, then f is independent of the momentum p and according to the FDR given by

$$f_{\text{thermal}}(\omega, p) \equiv f(\omega) = \frac{1}{2} - n_{\text{FD}}(\omega - \mu) \tag{3.16}$$

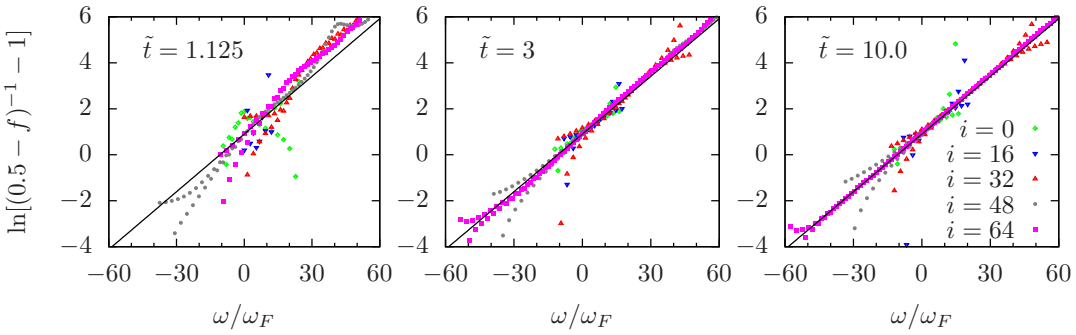

Figure 3.9: Emergence of the fluctuation-dissipation relation for several momentum modes p_i in run B. Left to right: the inverse slope function of the fraction f defined in Eq. (3.15) is plotted for early ($\tilde{t} \equiv n_{1D}^2 t/m = 1.125$), intermediate ($\tilde{t} = 3$), and late times ($\tilde{t} = 10.0$). The black lines indicate the Fermi-Dirac distribution with the same β and μ as in Figs. 3.4a and b.

with the Fermi-Dirac distribution $n_{\mathrm{FD}}(\omega) = (\exp(\beta\omega) + 1)^{-1}$. In the following, f is shown for each momentum mode in a region of frequencies ω around the peaks of the statistical and spectral functions where the argument of the logarithm $\ln[(1/2 - f)^{-1} - 1]$ is positive, i. e. where $|f| < 1/2$. Outside this region, the numerically evaluated argument of the logarithm oscillates around zero due to finite evolution time after the quench. Propagating the dynamic equations further reduces these oscillations.

Figure 3.9b shows the emergence of the fluctuation-dissipation relation at late times for run B. One clearly observes that the inverse-slope function $\ln[(1/2 - f)^{-1} - 1]$ of the fraction f evolves towards a Fermi-Dirac distribution. Note that the Fermi-Dirac distribution shown in the figures as black solid lines is not a fit to the data; rather, it is the distribution we extracted from the low-momentum mode occupation numbers as shown in Figs. 3.4a and b. Hence, the system is approximately thermalised over the depicted range of energies according to the FDR with all minor deviations being due to the finite evolution time. In conclusion, the chosen initial conditions for run B allow the single-particle momentum distributions to thermally equilibrate over the considered range of momenta.

Figure 3.10c shows the inverse-slope function of the fraction $f(\omega, p)$ for run C for five of the momentum modes. Again, f is shown in a region where the argument of the logarithm is positive. The mean $f(\omega)$ of all momentum modes is depicted in Fig. 3.10e. In run C, the inverse-slope function is a straight line at late times over the region of relevant ω and therefore corresponds to a Fermi-Dirac function. As in run B, the system is thermalised over the depicted range of energies, in spite of the signs of a power-law tail in run C. This can be understood by considering the spectral function shown in Fig. 3.10a: The second peak at negative frequencies picks up extra contributions from the Fermi sea thereby causing the power-law overpopulation at

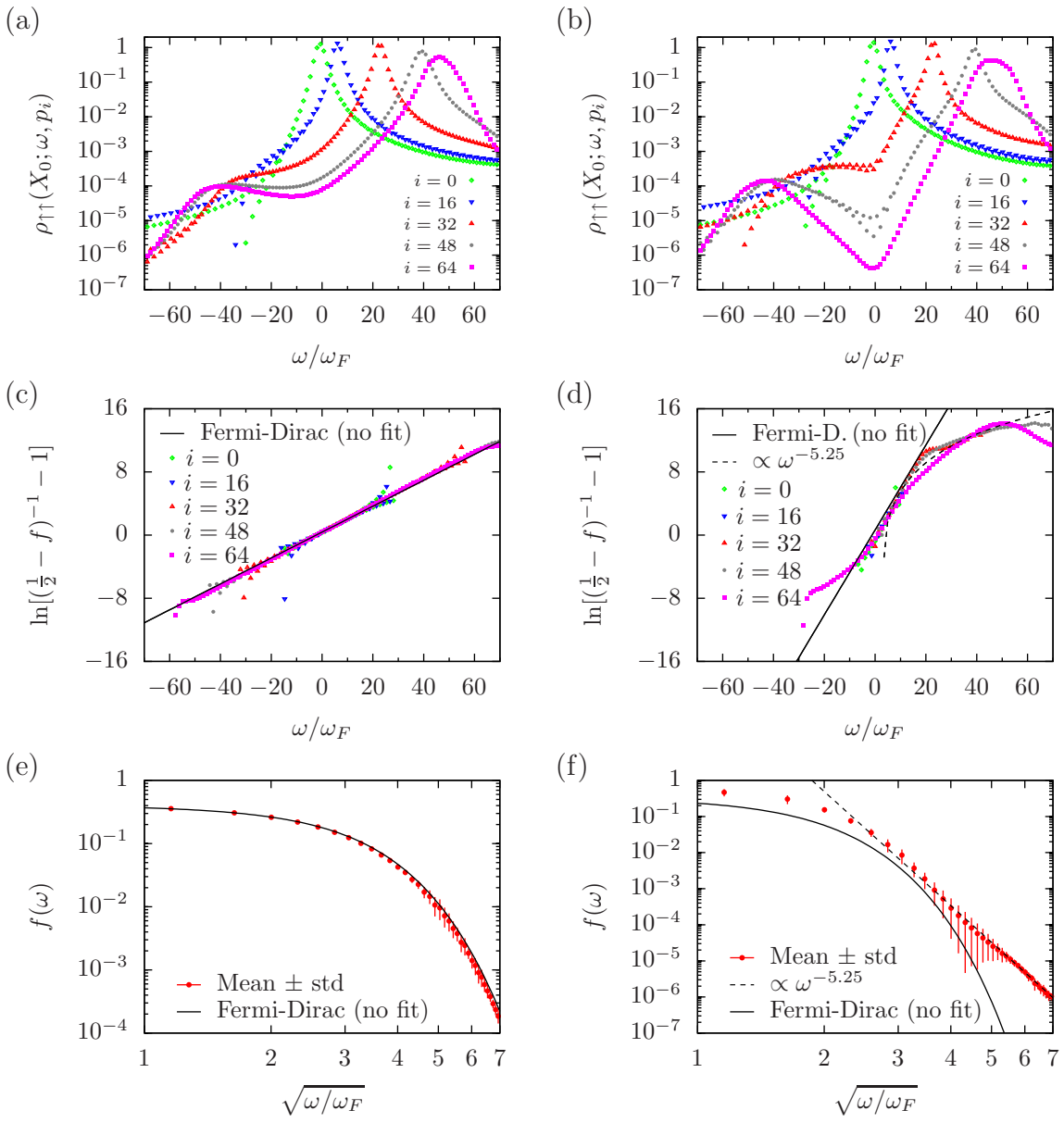

Figure 3.10: (a) Spectral functions as a function of frequency at late time $X_0 = 18.9\, n_{1D}^{-2} m$ in run C for five of the momentum modes p_i. (c) Inverse-slope function of fraction $f(\omega, p_i)$ defined in Eq. (3.15) at $X_0 = 18.9\, n_{1D}^{-2} m$, for the same five momentum modes as in (a). (e) Mean fraction f of all momentum modes, error bars are standard deviations. (b), (d), and (f) are the same as (a), (c), and (e), respectively, but for run D. In all graphs, black solid lines indicate Fermi-Dirac distributions with the same values for β and μ as in Figs. 3.4a and b. In run C, the system thermalises, whereas it does not in run D. Note the exponential decay of the spectral functions away from the peaks in run D.

high momenta. Although the area under the negative-ω peak is reduced by a factor of $\sim 10^{-4}$, it is multiplied by 1 on the filled-sea side of the Fermi-Dirac function in f while the positive-ω peak multiplies the exponentially suppressed tail of the Fermi-Dirac function. Thus, one may pre-conclude from run C that the one-dimensional Fermi gas always thermalises to a grand-canonical ensemble, with the eigenmodes of the strongly interacting system at low temperatures being superpositions of particles and holes. This contains reminiscence of the Bogoliubov depletion at zero temperature that gives a p^{-4} power-law tail of the single-particle momentum distribution for a Fermi gas in the BCS theory.

However, run D performed at even lower energy shows that the system does in general not thermalise to a grand-canonical ensemble. Figure 3.10d shows the inverse-slope function for the fraction f of run D. Even though the momentum overpopulation is again largely produced by the contributions from the Fermi sea, see Fig. 3.10a, also the fraction f shows a power-law tail $\sim \omega^{-5.25} \sim p^{-10.5}$ violating the FDR, see Fig. 3.10f. Despite this, the equilibrated momentum distribution $\propto p^{-4.4}$ at low total energies is still mainly due to the second peak in the spectral function while the contribution from the non-thermal power-law tail of f is suppressed by another 6 powers of p.

We finally note that the spectral functions of the intermediate and high momentum modes of run D in Fig. 3.10b show an interesting exponential decay away from the spectral peaks.

Comparison to Tomonaga-Luttinger liquid model

The model of a homogeneous gas with two spin components in one spatial dimension (1D) is integrable in the sense that it has as many conserved quantities as there are degrees of freedom [78]. Hence, if prepared out of equilibrium, it is expected not to thermalise in general [79, 80, 81, 82]. Its low-energy properties can be approximated by a Tomonaga-Luttinger liquid (TLL) model [83] that contains a linear free dispersion. It is important, however, to clearly separate the TLL model, which is widely discussed in the literature, and the 2PI effective action approach we choose. The approximating TLL model is known to form a low-energy fixed point of the full interacting one-dimensional Fermi gas [84]. Owing to the quadratic form into which the TLL Hamiltonian can be transformed by introducing bosonic particle-hole operators, the occupation numbers of the resulting quasi-particle modes represent conserved quantities. As a consequence, the long-time evolution of TLL fermion and coupled fermion-boson models after an interaction quench is found to approach a generalised Gibbs ensemble [82, 84, 85], which accounts for the conserved quasi-particle numbers. We would like to point out that non-thermal stationary states have also been found in a number of other models, both integrable and non-integrable [86, 87, 88, 89].

In our work, however, we consider the dynamic evolution described by the full interacting fermionic Hamiltonian, approaching the problem of equilibration from the

high-energy end. Our analysis applies away from zero temperature in a regime of energies where the non-linearity of the dispersion becomes relevant; therefore, we do not expect to recover the TLL model.

3.8 Summary

In this chapter, we applied the dynamic equations derived from the 2PI effective action in next-to-leading order (NLO) approximation of the $1/\mathcal{N}$ expansion to a homogeneous ultra-cold Fermi gas with two-fold spin degeneracy in one spatial dimension with contact interactions between fermions in different spin states. In NLO $1/\mathcal{N}$ approximation, these equations are commonly considered to describe thermalisation. At sufficiently high total energies, also we found equilibration of the Fermi gas to a thermal state satisfying the fluctuation-dissipation relation (FDR) for a grand-canonical ensemble. However, at sufficiently low total energies, we observed non-thermal equilibration to a state in which the correlation functions violated the FDR. This signature is in principle amenable to experiments.

We studied the dynamics of the gas in a finite-size box with periodic boundary conditions. All runs that we performed evolved into a stationary state once they were insensitive to numerical parameters like the discrete time step size. These stationary states were insensitive to the details of the initial state and solely determined by the total energy, the line density, and the interaction strength.

In the stationary states, we found that the occupation numbers of the lowest momentum modes coincided with a Fermi-Dirac distribution with which thermodynamic quantities like the temperature and the chemical potential are connected. We also extracted the late-time kinetic energy and the heat capacity at constant volume. The so found thermodynamic quantities had in common that they converged to the ideal gas results for high temperatures and deviate from them for lower temperatures. These deviations were expected since the finite coupling constant becomes more significant at lower temperatures.

In the stationary states, the occupation numbers of the higher momentum modes deviated from a Fermi-Dirac distribution. This feature was more pronounced at lower total energies of the system, and a power-law tail was replacing the exponential decay of the Fermi-Dirac distribution. The power law is reminiscent of the p^{-4} power law for the high-momentum tail of the single-particle momentum distribution in both one of Tan's relations for a strongly correlated two-component Fermi gas and BCS theory. Note that our results do not rule out that a power law ultimately appears also at higher energies in a range of momenta beyond the momentum cut off present in our numerics.

For the runs with very low total energies, we also found deviations from the FDR for a grand-canonical ensemble. This indicated equilibration to a non-thermal state.

Chapter 4

Non-equilibrium dynamics of a Kondo lattice gas

After analysing the model of an $\mathcal{N}$-component Fermi gas in the previous two chapters, we investigate a different model in this chapter. In the following, we treat an ultra-cold Fermi gas on a spatial lattice that can be described by the $SU(\mathcal{N})$ symmetric Kondo lattice model (KLM). The crucial difference to the former model is that now the constituents of the gas have an additional (internal) degree of freedom.

We start, in Sec. 4.1, with a general motivation why the KLM recently attracted attention in the cold atom community. Here, we also discuss relevant properties of fermionic alkaline earth atoms that allow to simulate the KLM using optical lattice potentials. Afterwards, we review the KLM more formally in Sec. 4.2 and show how different representations of the Kondo lattice Hamiltonian are linked with each other. Since we use a complex field basis for our description in this chapter, we briefly review relevant formulae of the 2PI effective action approach in Sec. 4.3 in order to see which formulae change and which do not. Section 4.4 is devoted to the derivation of the dynamic equations using the $1/\mathcal{N}$ expansion of the 2PI effective action. In leading-order approximation of the $1/\mathcal{N}$, we recover the mean-field dynamic equations of the $U = 0$ Anderson model used in Ref. [93] to describe Kondo lattice dynamics. Finally, we derive the dynamic equations in next-to-leading order approximation. We elaborate on how the $1/\mathcal{N}$ expansion of the 2PI effective action beyond the leading-order approximation is a promising tool to tackle yet outstanding challenges in KLM research.

4.1 Motivation: the Kondo lattice model and fermionic alkaline-earth-metal atoms

Simulations of condensed matter systems using ultra-cold atomic quantum gases have become possible through the development of precise optical and magnetical trapping techniques. While single-band Bose and Fermi Hubbard models have already been studied in great variety, the description of specific systems where both spin and orbital electronic degrees of freedom are relevant require the use of more com-

plicated models. Fermionic alkaline-earth-metal atoms have recently been shown to allow simulations of (condensed matter) models with both spin and orbital degrees of freedom [39], the Kondo lattice model (KLM) [147] being a particular example of them.

In the original condensed matter KLM, one studies the interaction of mobile conduction electrons with immobile, i. e. localised, spin-1/2 scattering centers. Depending on the strength (both sign and magnitude) of the interaction between the conduction electrons and the localised impurities, the KLM describes very different physics. For an anti-ferromagnetic interaction, which specifies the sign of the interaction strength and favours a spin anti-alignment between mobile electrons and the localised spins, the KLM has been studied in great detail in the context of so-called heavy-fermion rare-earth and actinoide compounds, see Ref. [148] for a recent review. The term "heavy fermion" [149] refers to a deformed band edge leading to an electronic density of states as much as thousand times larger than in copper, and the conduction electrons behave as if they had an effective mass up to thousand times the free electron mass.

Depending on the magnitude of the anti-ferromagnetic interactions, two different phases exist in the limits of sufficiently weak and strong couplings. At sufficiently weak coupling, the conduction electrons are polarised by the localised spins. Thereby, they mediate Ruderman-Kittel-Kasuya-Yosida (RKKY) interactions [150] between the localised spins, which lead to a magnetic ordering of the spins. At sufficiently strong coupling, spin-flip scattering of the conduction electrons off the localised spins dominate. As a result, the local spins are screened by the conduction electrons (which is the so-called Kondo screening) and the ground state is a magnetically disordered heavy-Fermi-liquid (HFL).

More recently, studies were done in the coupling regimes where the RKKY interactions and the Kondo screening are competing effects, and the resulting possibly existing novel phases and (quantum) phase transitions between them are not well understood [148, 151, 152]. Ultra-cold fermionic alkaline-earth-metal atoms allow to simulate the KLM and to study these phases and phase transitions.

There are three main reasons why fermionic alkaline-earth-metal atoms are especially suitable to simulate the KLM:

- ▷ The excited state $^3P_0$ is metastable; it couples to the ground state $^1S_0$ through an ultra-narrow doubly forbidden transition. Thus, these two states are available in experiments to address the orbital degree of freedom. Furthermore, both states can be trapped independently by two different optical lattice potentials with the same spatial periodicity [91]. This allows to trap atoms in one state inside a deep lattice (e. g. one at each lattice site) such that they mimic the localised spins. And using a very shallow lattice for the atoms in the other state allows to simulate the mobile conduction electrons.

- ▷ Both the metastable excited and the ground state have a vanishing electronic angular momentum ($J = 0$). This implies an almost perfect [153] decoupling of

the nuclear spin I from J in these two states and results in an $SU(\mathcal{N})$ symmetry in the (hyperfine) spin degree of freedom, where $\mathcal{N} = 2I + 1$.

- ▷ The spin multiplicities can be as large as $\mathcal{N} = 10$ for ^{87}Sr ($I = 9/2$) and $\mathcal{N} = 8$ for ^{43}Ca ($I = 7/2$). Moreover, the particular value of $\mathcal{N}$ can be chosen through the controlled population of a subset of the hyperfine states [39]. Hence, fermionic alkaline-earth-metal atoms offer the unique possibility to employ controlled large-$\mathcal{N}$ expansions in quantum field theory for the study of both, static and dynamical properties [147, 154, 155, 156].

Due to these properties, ultra-cold gases of fermionic alkaline-earth-metal atoms in optical lattice potentials open the unique possibility to study, besides the static properties of Kondo lattice systems, also dynamical properties in a controlled way. Transport phenomena both close to and far from thermal equilibrium can be induced through external as well as internal boundary conditions, e. g. by varying additional linear or harmonic trapping potentials or modifying interaction strengths by use of Feshbach resonances or lattice depths, respectively. Dynamical correlations like the evolution of spectral densities can be measured to characterise non-equilibrium properties. This is of particular interest in regimes where strong correlations are present such as close to equilibrium phase transitions, where the dynamical properties have been explored to a limited extent so far.

Using $1/\mathcal{N}$ expansions [154, 155, 156], the $SU(\mathcal{N})$ symmetric KLM has been theoretically investigated in the large-$\mathcal{N}$ limit [147, 157] (in these studies, $\mathcal{N}$ is the degeneracy of the localised spins), and experimentally observed properties of the HFL were successfully reproduced. In the large-$\mathcal{N}$ limit, only the leading order (LO) of the $1/\mathcal{N}$ expansion is kept, which eases the analyses of the model a lot. In LO, the spin-flip scattering contribution of the interaction, which give rise to the HFL properties, is taken into account; in contrast, the direct interaction contributions appear almost exclusively at next-to-leading order (this is especially true for $\mathcal{N} \gg 2$). Since it is tedious to go beyond the LO in most of these $1/\mathcal{N}$ expansions, this explains why, so-far, only very little is known about the KLM away from the HFL regime.

In the 2PI effective action approach that we employ, the full next-to-leading order contribution in the $1/\mathcal{N}$ expansions can be taken into account. This contributions includes not only the direct interactions missed at LO but also off-energy-shell scattering effects. Thus, applying the $1/\mathcal{N}$ expansion of the 2PI effective action beyond the leading-order approximation is a promising tool to study dynamics, new phases and phase transitions possibly appearing outside the HFL regime.

4.2 The Kondo lattice model

In this section, we review the Kondo lattice model (KLM) more formally. We show how different representations of the Kondo lattice Hamiltonian that are commonly

used in the literature are linked with each other and discuss the symmetries of the Hamiltonian. Thereafter, we introduce a decomposition of the interaction vertex, which will be crucial for the $1/\mathcal{N}$ expansion of the effective action that we discuss later in this chapter.

4.2.1 The model Hamiltonian and its symmetries

We consider the dynamical evolution of an ultra-cold Fermi gas of atoms in a d-dimensional optical lattice. The atoms are assumed to be, internally, in two different electronic states $s \in \{c, f\}$, and $\mathcal{N} = 2I + 1$ different hyperfine states $\alpha \in \{-I/2, -I/2 + 1, \ldots, I/2\}$. Hence, the fermionic many-body system can be described by complex Graßmann-valued fields $\psi_{s\alpha}(\mathbf{n})$, where $\mathbf{n}$ labels the lattice sites, obeying

$$\psi_{s\alpha}(t, \mathbf{n})\psi_{s'\alpha'}(t', \mathbf{m}) + \psi_{s'\alpha'}(t', \mathbf{m})\psi_{s\alpha}(t, \mathbf{n}) = 0 \tag{4.1}$$

$$\psi_{s\alpha}(t, \mathbf{n})\psi^*_{s'\alpha'}(t', \mathbf{m}) + \psi^*_{s'\alpha'}(t', \mathbf{m})\psi_{s\alpha}(t, \mathbf{n}) = 0 \tag{4.2}$$

for any combination of s, s', α, α', t, t', $\mathbf{n}$, and $\mathbf{m}$.

The Kondo lattice is characterised by the distinction between a localised band of immobile atoms in electronic states f and a conduction band of mobile atoms in electronic states c. In the Kondo lattice, the dynamics is defined through the two-orbital single-band Hubbard Hamiltonian

$$H = H_0 + H_{\text{int}} \tag{4.3}$$

with

$$H_0 = \sum_{\langle \mathbf{n}, \mathbf{m} \rangle} \left[-J \Big(\psi^*_{c\alpha}(x_0, \mathbf{n})\psi_{c\alpha}(x_0, \mathbf{m}) + \text{c.c.} \Big) + V_{\text{ext},s}(x)\psi^*_{s\alpha}(x)\psi_{s\alpha}(x) \right], \tag{4.4}$$

where $x \equiv (x_0, \mathbf{n})$ denotes the lattice space-time coordinate, c.c. the complex conjugate, and the sum $\langle \mathbf{n}, \mathbf{m} \rangle$ is over pairs of nearest-neighbour sites $\mathbf{n}$ and $\mathbf{m}$. J characterises the hopping rate with which the conducting c-atoms tunnel from site to site. $V_{\text{ext},s}(x)$ are possibly time-dependent trapping potentials or other external fields that are identical for all hyperfine states $\alpha \in \{1, \ldots, \mathcal{N}\}$. Summations over the indices s and α are implied.

Elastic s-wave collisions between atoms in different hyperfine states are assumed, while Pauli's principle forbids s-wave interactions between fermions that are internally in the same state. If one further assumes the scattering lengths to be independent from the nuclear spin, it follows that the most general interaction Hamiltonian must be $SU(\mathcal{N})$ symmetric. In this approximation, with a possibly time-dependent coupling strength $U(t)$ between the electronic states c and f, the interaction Hamiltonian reads

$$H_{\text{int}}(t) = \frac{U(t)}{\mathcal{N}} \sum_{\mathbf{n}} \left[\Big(\psi^*_{c\alpha}(x)(T_k)_{\alpha\alpha'}\psi_{c\alpha'}(x) \Big) \Big(\psi^*_{f\beta}(x)(T_k)_{\beta\beta'}\psi_{f\beta'}(x) \Big) \right], \tag{4.5}$$

where $U(t)/\mathcal{N}$ is a possibly time dependent coupling constant, $\sum_{\mathbf{n}}$ is a sum over all lattice sites, and sums over repeated indices, besides c and f, are implied. The T_k, $k \in \{1, \ldots, \mathcal{N}^2 - 1\}$, form the algebra of generators of the $SU(\mathcal{N})$ group in the fundamental representation in which the group elements act on complex vectors with $\mathcal{N}$ entries. Before rewriting the interaction Hamiltonian in a more suitable form for the following discussion, we look into the symmetries of the Hamiltonian H in more detail.

▷ H is symmetric under global $U(1)$ transformations of the complex-valued fields $\psi_{s\alpha}(x)$,

$$\psi_{s\alpha}(x) \to \exp[\mathrm{i}\phi]\psi_{s\alpha}(x)\,. \tag{4.6}$$

This $U(1)$ symmetry is associated with the elasticity of collisions regarding the electronic state. The total population in each of the electronic states c and f is conserved.

▷ The interaction term (4.5) is chosen such that the Hamiltonian has an $SU(\mathcal{N})$ symmetry in the space of all hyperfine levels,

$$\psi_{s\alpha}(x) \to \exp[\mathrm{i}\xi_k T_k]_{\alpha\beta}\psi_{s\beta}(x)\,. \tag{4.7}$$

Note that the independence of the coupling $U(t)$ from the hyperfine states—aside from the restrictions imposed by Pauli's principle of fermionic anti-symmetry, which is taken into account by the Graßmann nature of the field—is crucial for the fulfilment of the $SU(\mathcal{N})$ symmetry of the Hamiltonian. As we discussed in the previous section, this independence is available in the case of fermionic alkaline-earth-metal atoms in the metastable excited state ${}^3P_0$ and the ground state ${}^1S_0$ since both states have a vanishing electronic angular momentum J and therefore the nuclear spin I (almost perfectly [153]) decouples from J. In contrast, assuming an $SU(\mathcal{N} > 2)$ symmetric model with alkali atoms is a substantial idealisation due to strong hyperfine coupling generally present in these atoms.

▷ As a distinct feature of the $SU(\mathcal{N})$ symmetry, the total population in a given hyperfine state α is conserved. This implies that atoms with large nuclear spin I can be used to reproduce the dynamics of atoms with smaller I by a controlled initial population of only a subset of the hyperfine states.

Also note that a factor of $1/\mathcal{N}$ has been taken out of the couplings U in Eq. (4.5) in order that the interaction Hamiltonian H_{int} scales as $\mathcal{N}$ like the free Hamiltonian H_0. This makes the relative weight of the interaction term invariant under a rescaling of $\mathcal{N}$. To see that the interaction Hamiltonian H_{int} scales as $\mathcal{N}$ note that the $SU(\mathcal{N})$ symmetry allows to diagonalise the terms in the round bracket of Eq. (4.5) within the hyperfine index space, cf. Eq. (4.7). This way, only one of the two sums over the hyperfine indices remains in each round bracket. Thus, the term in the square

brackets scales quadratic in $\mathcal{N}$ such that $H_{\rm int}$ as a whole scales linear.

The interaction Hamiltonian in Eq. (4.5) is written in a form that makes the $SU(\mathcal{N})$ symmetry obvious. For the following discussion, we want to rewrite the interaction Hamiltonian in the standard form used in the literature. For this purpose, we need to rewrite the so-called projection operator $(T_k)_{\alpha\alpha'}(T_k)_{\beta\beta'}$ and, therefore, have to get familiar with some properties of the T_k, which are discussed in more detail in Refs. [158, 159, 160]. Choosing the normalisation

$$\mathrm{Tr}[T_k T_l] = 2\delta_{kl}\,, \tag{4.8}$$

one has a multiplication law of the type

$$T_k T_l = \frac{2}{\mathcal{N}}\delta_{kl} + (d_{klm} + \mathrm{i}f_{klm})T_m \tag{4.9}$$

since T_k and the unit matrix I together span the space of all complex $\mathcal{N}\times\mathcal{N}$ matrices with a unit determinant. The latter fact implies that the projection operator can be written as

$$(T_k)_{\alpha\alpha'}(T_k)_{\beta\beta'} = 2\left(\delta_{\alpha\beta'}\delta_{\beta\alpha'} - \frac{1}{\mathcal{N}}\delta_{\alpha\alpha'}\delta_{\beta\beta'}\right). \tag{4.10}$$

The above relations imply the commutation relations

$$[T_k, T_l]_- = 2\mathrm{i}f_{klm}T_m\,, \tag{4.11}$$

$$[T_k, T_l]_+ = \frac{4}{\mathcal{N}}\delta_{kl} + 2\mathrm{i}d_{klm}T_m\,. \tag{4.12}$$

From the commutation relations follows that the structure constants d_{klm} and f_{klm} are totally symmetric and anti-symmetric, respectively. Since $SU(\mathcal{N})$ is compact, one has

$$f_{klm}f_{nlm} = \mathcal{N}\delta_{kn}\,, \tag{4.13}$$

$$d_{klm}d_{nlm} = \frac{\mathcal{N}^2-4}{\mathcal{N}}\delta_{kn}\,. \tag{4.14}$$

With Eq. (4.10), the interaction Hamiltonian in Eq. (4.5) can be rewritten as

$$\begin{aligned} H_{\rm int} = \frac{2U(t)}{\mathcal{N}}\sum_{\mathbf{n}}\Bigg(&\psi^*_{c\alpha}(x)\psi_{c\alpha'}(x)\psi^*_{f\alpha'}(x)\psi_{f\alpha}(x) \\ &- \frac{1}{\mathcal{N}}\psi^*_{c\alpha}(x)\psi_{c\alpha}(x)\psi^*_{f\alpha'}(x)\psi_{f\alpha'}(x)\Bigg)\,. \end{aligned} \tag{4.15}$$

The Hamiltonian defined in Eqs. (4.3), (4.4), and (4.15) was proposed by Coqblin and Schrieffer [147], and is usually referred to as the Kondo lattice model. It was later used, for example, to describe strongly correlated electron systems such as manganese

oxide perovskite [161], and rare-earth and actinoide compounds characterised as heavy-fermion materials [148]. As pointed out by Zhang and Yu [162], the first term in (4.15) (for $\alpha \neq \alpha'$) corresponds to the spin-flip scatterings that gives rise to the local Kondo screening effect, and has been investigated, e. g. in approaches based on a $1/\mathcal{N}$ expansion [154, 155, 156]. The second term, together with the $\alpha = \alpha'$ contributions of the first term, describes direct interactions causing a polarisation of the conduction atoms by the local impurity spins, which leads to a magnetic instability [157]. In a $1/\mathcal{N}$ expansion, these two phenomena are not treated on equal footings since spin-flip scattering terms occur at first order in the expansion, whereas most of the direct scattering terms occur only at second order. Especially for $\mathcal{N} \gg 2$ this imbalance in the treatment of these two types of scattering becomes more and more dominant.

Using the form of the interaction in Eq. (4.15), the Lagrangian for the Kondo lattice model can be expressed as

$$\begin{aligned} L(x_0) = \sum_{\mathbf{n}} \Bigg[& \frac{\mathrm{i}}{2} \Big(\psi^*_{s\alpha}(x)(\partial_{x_0}\psi_{s\alpha}(x)) - \text{c.c.} \Big) - V_{\text{ext},s}(x)\psi^*_{s\alpha}(x)\psi_{s\alpha}(x) \\ & - \frac{2U(x)}{\mathcal{N}} \Bigg(\psi^*_{c\alpha}(x)\psi_{c\alpha'}(x)\psi^*_{f\alpha'}(x)\psi_{f\alpha}(x) \\ & \qquad + \frac{1}{\mathcal{N}} \psi^*_{c\alpha}(x)\psi_{c\alpha}(x)\psi^*_{f\alpha'}(x)\psi_{f\alpha'}(x) \Bigg) \Bigg] \\ & + \sum_{\langle \mathbf{n},\mathbf{m} \rangle} J \Big(\psi^*_{c\alpha}(x_0,\mathbf{n})\psi_{c\alpha}(x_0,\mathbf{m}) + \text{c.c.} \Big) \,, \end{aligned} \tag{4.16}$$

where ∂_{x_0} denotes the partial derivative with respect to time. In the functional-integral approach we adopt, we will employ the action $S[\psi]$,

$$S[\psi] = \int_{x_0} L(x_0) \,, \tag{4.17}$$

where $\int_{x_0} \equiv \int \mathrm{d}x_0$. Inserting the Lagrangian (4.16), we write the action in the compact form

$$S[\psi] = \frac{1}{2} \int_{xy} \psi^*_a(x) \mathrm{i} G^{-1}_{0,ab}(x,y) \psi_b(y) + S_{\text{int}}[\psi] \,, \tag{4.18}$$

where $\int_x \equiv \int \mathrm{d}x_0 \sum_{\mathbf{n}}$ denotes the integration/summation over the region of space-time under consideration. Also, we have introduced a triple index $a = (s\alpha, i)$, $i \in \{1, 2\}$, with

$$\psi_{s\alpha,1}(x) \equiv \psi_{s\alpha}(x) \,, \qquad \psi_{s\alpha,2}(x) \equiv \psi^*_{s\alpha}(x) \,, \tag{4.19}$$

such that the inverse free propagator in Eq. (4.18) is given by

$$\mathrm{i} G^{-1}_{0,ab}(x,y) = \mathrm{i}\delta_{ab}\delta(x-y)\partial_{x_0} - \delta_{s_a s_b}\delta_{\alpha_a \alpha_b}\sigma_{3,i_a i_b} H^{\text{1B}}_{s_a}(x,y) \tag{4.20}$$

with the one-body Hamiltonian

$$H_s^{\mathrm{1B}}(x,y) = -J\delta_{\langle \mathbf{n},\mathbf{m}\rangle}\delta(x_0-y_0) + \delta(x-y)V_{\mathrm{ext},s}(x)\,. \tag{4.21}$$

Here, $\delta(x-y) = \delta_{\mathbf{nm}}\delta(x_0-y_0)$ and $\delta_{\langle \mathbf{n},\mathbf{m}\rangle} = 1$ if and only if $\mathbf{n}$ and $\mathbf{m}$ denote adjacent lattice sites in the single-band approximation, otherwise it is zero. Moreover, here and in the following, σ_1, σ_2, and σ_3 are the standard Pauli matrices. The interaction part $S_{\mathrm{int}}[\psi]$ corresponding to the Lagrangian (4.16) is written as

$$\begin{aligned} S_{\mathrm{int}}[\psi] = -\frac{U(x)}{2\mathcal{N}}\sigma_{1,ij}\sigma_{1,ss'}\int_x\Bigg(&\psi_{s\alpha,i}(x)\psi_{s\alpha',j}(x)\psi_{s'\alpha',i}(x)\psi_{s'\alpha,j}(x) \\ &- \frac{1}{\mathcal{N}}\psi_{s\alpha,i}(x)\psi_{s\alpha,j}(x)\psi_{s'\alpha',i}(x)\psi_{s'\alpha',j}(x)\Bigg)\,. \end{aligned} \tag{4.22}$$

With this, we are in the position to adopt the 2PI effective action formalism and employ the $1/\mathcal{N}$ expansion. Before doing so, we introduce a graphical decomposition of the interaction vertex, which will simplify this discussion.

4.2.2 Structure of the interaction vertex

For the following discussion, where we look into a diagrammatic expansion of the 2PI part of the effective action, it is convenient to reveal the specific structure of the interaction vertex

$$S^{(4)}_{abcd} = \frac{\delta^4 S_{\mathrm{int}}}{\delta\psi_a(x_a)\delta\psi_b^*(x_b)\delta\psi_c(x_c)\delta\psi_d^*(x_d)} \tag{4.23}$$

and to represent the vertex by a squiggly line for the "spin-exchange" term (proportional to $U(x)/(8\mathcal{N})$) and a dashed line for the "direct" term (proportional to $U(x)/(8\mathcal{N}^2)$) of the vertex. The form of the interaction part of the considered Lagrangian density in Eq. (4.16) allows us to require that spins are conserved at each end of the vertex. The possible index contractions at each vertex are depicted in Fig. 4.1. Note that, beside drawing the interaction vertices as squiggly and dashed lines, each interaction vertex is still local in space and time.

4.3 2PI effective action approach to non-equilibrium dynamics reviewed

To derive the non-equilibrium dynamical equations of motion for the Kondo lattice gas, we use the 2PI effective action approach, which we introduced in Ch. 1, with two minor modifications: we keep a complex field basis, and use a discrete space. As a result of the former modification, the dynamic equations look slightly different. And for completeness, we review the relevant formulae leading to the dynamic equations in this section.

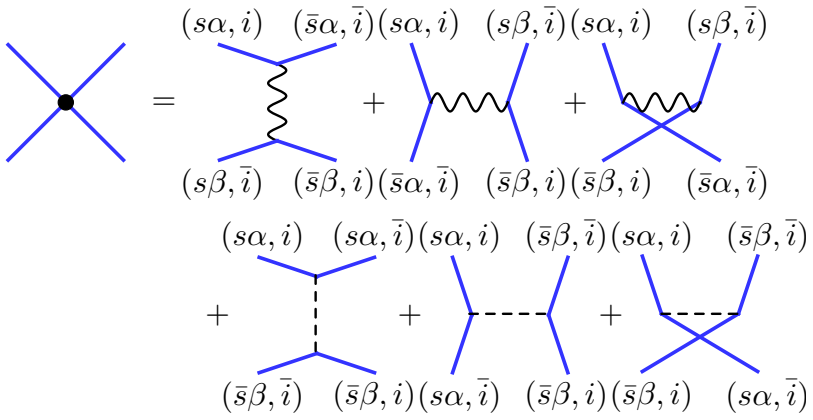

Figure 4.1: Decomposition of the bare vertex S^4 (black dot) as a sum of the six possible index contractions. The point interaction vertex is represented by a squiggly line for the spin-exchange interaction vertex $U(x)/(2\mathcal{N})$ and a dashed line for the direct interaction vertex $U(x)/(2\mathcal{N}^2)$. At each end of the squiggly and the dashed line, the spin index is conserved, and it is summed over the indices s, α, β, and i in each diagram.

4.3.1 2PI effective action

Using the complex field operators $\hat{\Psi}_{s\alpha}(\mathbf{n},t)$ and $\hat{\Psi}^\dagger_{s\alpha}(\mathbf{n},t)$ that obey the equal-time anti-commutation relations, i. e.

$$[\hat{\Psi}_{s\alpha}(\mathbf{n},t),\hat{\Psi}^\dagger_{s'\alpha'}(\mathbf{m},t)]_+ = \delta_{ss'}\delta_{\alpha\alpha'}\delta_{\mathbf{nm}}\,, \tag{4.24}$$

and introducing the field operator $\hat{\Psi}_a$ with triple index $a=(s\alpha,i)$ such that $\hat{\Psi}_{s\alpha,1}=\hat{\Psi}_{s\alpha}$ and $\hat{\Psi}_{s\alpha,2}=\hat{\Psi}^\dagger_{s\alpha}$, the non-equilibrium generating functional $Z[K;\hat{\rho}_D]$ is now given by

$$Z[K;\hat{\rho}_D] \equiv \mathrm{Tr}\left[\hat{\rho}_D(t_0)\mathcal{T}_\mathcal{C} e^{\frac{\mathrm{i}}{2}\int_{\mathcal{C},xy}\hat{\Psi}^\dagger_a(x)K_{ab}(x,y)\hat{\Psi}_b(y)}\right], \tag{4.25}$$

where $\hat{\rho}_D(t_0)$ is the normalised density matrix of the system at the initial time t_0. $\mathcal{C}=\mathcal{C}^+\cup\mathcal{C}^-$ indicates that the temporal integrals are to be taken along the closed (Schwinger-Keldysh) time path (CTP) [40, 44] from the initial time t_0 to infinity (path $\mathcal{C}^+$) and back to t_0 ($\mathcal{C}^-$) such that $\int_{\mathcal{C},x}=\int_{\mathcal{C},x_0}\sum_{\mathbf{n}}$ with $\int_{\mathcal{C},x_0}=\int_{\mathcal{C}^+}\mathrm{d}x_0-\int_{\mathcal{C}^-}\mathrm{d}x_0$. $\mathcal{T}_\mathcal{C}$ denotes time-ordering along the closed time path, implying that operators evaluated at later times stand to the left of those evaluated at earlier times. The classical external two-point field $K_{ab}(x,y)$ is introduced to allow for the generation of correlation functions of order $2n$.

The two-particle irreducible (2PI) effective action defined by a Legendre transformation of the Schwinger functional $W[K]=-\mathrm{i}\ln Z[K]$ with respect to K has the same form as in the real field basis,

$$\Gamma[G] = -\frac{\mathrm{i}}{2}\,\mathrm{Tr}\left[\ln(G^{-1})+G_0^{-1}G\right]+\Gamma_2[G]+\text{const.}\,. \tag{4.26}$$

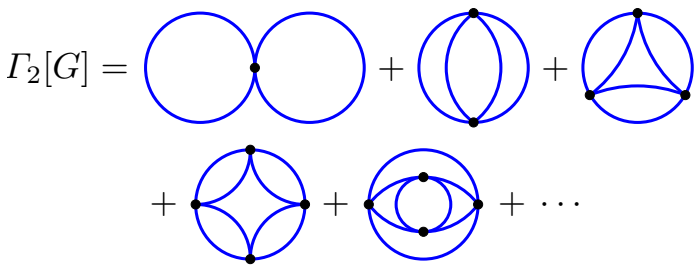

Figure 4.2: Diagrammatic expansion of the two-particle irreducible (2PI) part Γ_2 of the effective action (4.26) in terms of 2PI graphs. (Blue) solid lines stand for the Green function G, and (black) dots for the interaction vertex $S^{(4)}$. Explicitly shown are all diagrams that contain up to four vertices. All statistical factors are omitted.

The 2PI part Γ_2 of the effective action is depicted in Fig. 4.2. In Eq. (4.26), unlike before, the two-point Green function G is now defined as the time-ordered expectation value of two complex fields at two points in space-time,

$$G_{ab}(x,y) = \langle \mathcal{T}_{\mathcal{C}} \hat{\Psi}_a^\dagger(x) \hat{\Psi}_b(y) \rangle \,, \tag{4.27}$$

where the time-ordering is defined as

$$\mathcal{T}_{\mathcal{C}} \hat{\Psi}_a^\dagger(x) \hat{\Psi}_b(y) = \begin{cases} \hat{\Psi}_a^\dagger(x) \hat{\Psi}_b(y) & \text{if } \operatorname{sgn}_{\mathcal{C}}(x_0 - y_0) = 1 \\ -\hat{\Psi}_b(y) \hat{\Psi}_a^\dagger(x) & \text{if } \operatorname{sgn}_{\mathcal{C}}(x_0 - y_0) = -1 \,. \end{cases} \tag{4.28}$$

The spectral function ρ and the statistical propagator F are defined as

$$F_{ab}(x,y) \equiv \frac{1}{2} \langle \big[\hat{\Psi}_a^\dagger(x), \hat{\Psi}_b(y) \big]_- \rangle \,, \tag{4.29}$$

$$\rho_{ab}(x,y) \equiv \mathrm{i} \langle \big[\hat{\Psi}_a^\dagger(x), \hat{\Psi}_b(y) \big]_+ \rangle \,. \tag{4.30}$$

The symmetry properties of the two-point functions are now given as

$$G_{ab}(x,y) = -G_{\bar{b}\bar{a}}(y,x) = -G_{ba}^*(y,x) \,, \tag{4.31a}$$

$$F_{ab}(x,y) = -F_{\bar{b}\bar{a}}(y,x) = -F_{ba}^*(y,x) \,, \tag{4.31b}$$

$$\rho_{ab}(x,y) = \rho_{\bar{b}\bar{a}}(y,x) = \rho_{ba}^*(y,x) \,, \tag{4.31c}$$

where $\bar{a} = (\alpha s, 3-i)$ for $a = (\alpha s, i)$. And for the spectral density function, one finds

$$\rho_{ab}(x,y)\big|_{x_0=y_0} = \delta_{s_a s_b} \delta_{\alpha\beta} \mathrm{i} \sigma_{3,i_a i_b} \delta_{\mathbf{nm}} \,, \tag{4.32}$$

where $x = (x_0, \mathbf{n})$ and $y = (y_0, \mathbf{m})$.

4.3.2 Dynamic equations

Since the effective action has the same form in the complex-field basis as in the real-field basis, also the dynamical equations for the Green function G, which are derived from the effective action, will not change. The inverse free propagator G_0^{-1} appearing therein has, however, different representations in the two bases. And as a result of this, the dynamical equations for the statistical correlation function F and the spectral function ρ have a slightly different form—compared to Eqs. (1.84) and (1.85), the τ matrices are now missing. They read

$$\begin{aligned} \mathrm{i}\partial_{x_0} F_{ab}(x,y) = &\int_z M_{ac}(x,z) F_{cb}(z,y) + \int_{t_0}^{x_0} \mathrm{d}z\, \overline{\Sigma}^{\rho}_{ac}(x,z) F_{cb}(z,y) \\ &- \int_{t_0}^{y_0} \mathrm{d}z\, \overline{\Sigma}^{F}_{ac}(x,z) \rho_{cb}(z,y)\,, \end{aligned} \tag{4.33}$$

$$\mathrm{i}\partial_{x_0} \rho_{ab}(x,y) = \int_z M_{ac}(x,z) \rho_{cb}(z,y) + \int_{y_0}^{x_0} \mathrm{d}z\, \overline{\Sigma}^{\rho}_{ac}(x,z) \rho_{cb}(z,y)\,, \tag{4.34}$$

where $\int_t^{t'} \mathrm{d}x \equiv \int_t^{t'} \mathrm{d}x_0 \sum_{\mathbf{n}}$,

$$M_{ab}(x,y) = \delta_{\mathcal{C}}(x-y) \Sigma^{(0)}_{ab}(x) + \sigma_{3,i_a i_b} \delta_{s_a s_b} \delta_{\alpha_a \alpha_b} H^{\mathrm{1B}}_{s_a}(x,y)\,, \tag{4.35}$$

and $\Sigma^{(0)}$ and $\overline{\Sigma}$ are, as before, the local and non-local parts of the proper self-energy.

4.4 Non-equilibrium dynamic equations for the Kondo lattice gas

In this section, we study the dynamical evolution of two-point function G and its statistical and spectral components F and ρ. In particular, we will discuss the dynamic equations obtained from the two-particle irreducible (2PI) effective action, Eqs. (4.33) and (4.34), in a $1/\mathcal{N}$ expansion beyond the leading order (mean-field) approximation.

To derive an expansion of the 2PI part Γ_2 of the effective action in powers of the inverse number of hyperfine levels $\mathcal{N}$, the $SU(\mathcal{N})$ symmetry can be used. This becomes apparent when considering the powers of $\mathcal{N}$ in the diagrams in Fig. 4.3. In each diagram, each squiggly vertex line contributes a factor of $1/\mathcal{N}$ and each dashed vertex line a factor of $1/\mathcal{N}^2$, cf. Eq. (4.16). Each propagator loop contributes a factor of $\mathcal{N}$, which can be seen as follows: Since the hyperfine index is conserved at each end of the vertices, each propagator loop can be written as a trace of a matrix product in the hyperfine space, e. g. $G_{\alpha\beta} G_{\beta\gamma} G_{\gamma\delta} = \mathrm{tr}\,(G^3)$ for a loop out of three propagators, and where we skipped all other indices that are irrelevant for the moment. For spin balanced mode populations, one can diagonalise the product of Green functions inside the trace using the $SU(\mathcal{N})$ symmetry. As a result, only one sum over the hyperfine

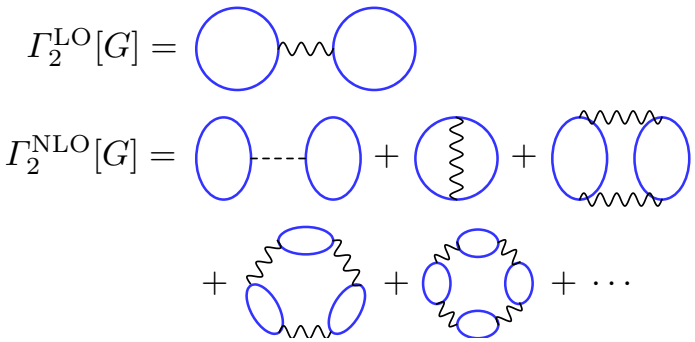

Figure 4.3: Diagrammatic representation of the leading order (LO) and next-to-leading order (NLO) contributions to Γ_2 in the $1/\mathcal{N}$ expansion. All statistical factors are omitted.

levels remains in the trace, which means that each propagator loop contributes a factor of $\mathcal{N}$. Hence, propagator loops can be attached to each other to form 2PI diagrams which are of the same order in $\mathcal{N}$, provided that for every new loop there is precisely one new squiggly vertex line appearing. Note that the dynamic equations, Eqs. (4.33) and (4.34), conserve the property of spin balanced mode populations in time, i. e. choosing spin balaced mode population at the initial time ensures that the $SU(\mathcal{N})$ symmetry can be used at all later times to diagonalise the propagator loops.

In the following, we derive explicit expressions for the leading-order (LO) and next-to-leading-order (NLO) contribution of the 2PI part Γ_2 of the effective action in the $1/\mathcal{N}$ expansion, i. e.

$$\Gamma_2[G] = \Gamma_2^{\mathrm{LO}}[G] + \Gamma_2^{\mathrm{NLO}}[G] + \cdots , \tag{4.36}$$

as well as the resulting proper self-energies.

4.4.1 Leading-order $1/\mathcal{N}$ approximation

As a first step, we derive the dynamic equations in the leading-order (LO) approximation of the $1/\mathcal{N}$ expansion. As depicted in Fig. 4.3, the LO contribution to Γ_2 consists of a single double-bubble diagram with a squiggly vertex. It reads

$$\Gamma_2^{\mathrm{LO}}[G] = -\int_x \frac{U(x)}{2\mathcal{N}} G_{(s\alpha,\bar{i})(\bar{s}\alpha,\bar{i})}(x,x) G_{(s\alpha',i)(\bar{s}\alpha',i)}(x,x) , \tag{4.37}$$

where $\bar{i} = 3 - i$ summations over s, i, α, and α' are implied. As there are two sums over $\alpha, \alpha' = 1, \ldots, \mathcal{N}$, this contribution is of the same order in $\mathcal{N}$ as the one-loop part of the action.

The proper self-energy derived from Eq. (4.37) is

$$\Sigma_{ab}^{\mathrm{LO}}(x,y) = -\mathrm{i}\Sigma_{ab}^{\mathrm{LO}(0)}(x)\delta_{\mathcal{C}}(x-y) \tag{4.38}$$

with

$$\Sigma^{\mathrm{LO}(0)}_{ab}(x) = -\frac{2U(x)}{\mathcal{N}}\sigma_{1,s_a s_b}\delta_{\alpha_a\alpha_b}\delta_{i_a i_b}G_{(s_b\alpha',\bar{i}_a)(s_a\alpha',\bar{i}_b)}(x,x)\,. \tag{4.39}$$

Hence, in the LO $1/\mathcal{N}$ approximation the proper self-energy has only a temporally and spatially local part $\Sigma^{\mathrm{LO}(0)}$, which contributes to the energy matrix M defined in Eq. (4.35). Therefore, in the limit $\mathcal{N}\to\infty$, the dynamics is entirely mean-field or classical. The dynamic equations for F and ρ reduce to

$$\mathrm{i}\partial_{x_0}F_{ab}(x,y) = \int_z M^{\mathrm{LO}}_{ac}(x,z)F_{cb}(z,y)\,, \tag{4.40}$$

$$\mathrm{i}\partial_{x_0}\rho_{ab}(x,y) = \int_z M^{\mathrm{LO}}_{ac}(x,z)\rho_{cb}(z,y)\,, \tag{4.41}$$

where $M^{\mathrm{LO}}(x,y) = M(x,y)$ is defined in Eq. (4.35) with $\Sigma^{(0)}(x;G) = \Sigma^{\mathrm{LO}(0)}(x;G)$ given in Eq. (4.39). As the non-local proper self-energy contribution $\overline{\Sigma}$ vanishes, the dynamic equations for F and ρ decouple. The dynamic equation for F, Eq. (4.40), can be written as

$$\begin{aligned}\mathrm{i}\partial_{x_0}F_{ab}(x,y) = (-1)^{i_a}&\int_z H^{\mathrm{1B}}_{s_a}(x,z)F_{ab}(z,y)\\ &-\frac{2U(x)}{\mathcal{N}}F_{(\bar{s}_a\alpha',\bar{i}_a)(s_a\alpha',\bar{i}_a)}(x,x)F_{(\bar{s}_a\alpha_a,i_a)b}(x,y)\,,\end{aligned} \tag{4.42}$$

where the bar over the orbital index is meant in the sense that $\bar{c}=f$ and $\bar{f}=c$.

Since more frequently used in the literature, we want to derive the dynamical equations for the single-particle density matrix

$$n_{(s\alpha)(s'\alpha')}(\mathbf{n},\mathbf{m};t) = \langle\hat{\Psi}^\dagger_{s\alpha}(\mathbf{n})\hat{\Psi}_{s'\alpha'}(\mathbf{m})\rangle_t\,, \tag{4.43}$$

which includes the density of particles at lattice site $\mathbf{n}$, $n_\alpha(\mathbf{n},t) = n_{(s\alpha)(s\alpha)}(\mathbf{n},\mathbf{n};t)$, and the anomalous density matrix or pair function

$$m_{(s\alpha)(s'\alpha')}(\mathbf{n},\mathbf{m};t) = \langle\hat{\Psi}_{s\alpha}(\mathbf{n})\hat{\Psi}_{s'\alpha'}(\mathbf{m})\rangle_t\,. \tag{4.44}$$

Both the single-particle density matrix and the pair function are solely determined by the statistical correlation function since

$$\begin{aligned}\tilde{n}_{(s\alpha)(s'\alpha')}(\mathbf{n},\mathbf{m};t) &= n_{(s\alpha)(s'\alpha')}(\mathbf{n},\mathbf{m};t) - \frac{1}{2}\delta_{ss'}\delta_{\alpha\alpha'}\delta_{\mathbf{nm}}\\ &= F_{(s\alpha,1)(s'\alpha',1)}(\mathbf{n},\mathbf{m};t)\end{aligned} \tag{4.45}$$

and

$$m_{(s\alpha)(s'\alpha')}(\mathbf{n},\mathbf{m};t) = F_{(s\alpha,2)(s'\alpha',1)}(\mathbf{n},\mathbf{m};t)\,, \tag{4.46}$$

and where we used the fact that the spectral function ρ is fixed by the anti-commutation relations (4.32) at equal times. Thus, their dynamics is determined by the equal-time dynamic equation for F. In LO $1/\mathcal{N}$ approximation, the latter is obtained by adding Eq. (4.42) and its transpose,

$$\begin{aligned}\mathrm{i}\partial_t F_{ab}(\mathbf{n},\mathbf{m};t) = \sum_{\mathbf{l}}\Big(&(-1)^{i_a} H^{\mathrm{1B}}_{s_a}(\mathbf{n},\mathbf{l};t) F_{ab}(\mathbf{l},\mathbf{m};t) \\ &+ (-1)^{i_b} H^{\mathrm{1B}}_{s_b}(\mathbf{m},\mathbf{l};t) F^*_{ba}(\mathbf{l},\mathbf{n};t)\Big) \\ &- \left\{\frac{2U(t)}{\mathcal{N}} F_{(\bar{s}_a\gamma,\bar{i}_a)(s_a\gamma,i_a)}(\mathbf{n},\mathbf{n};t) F_{(\bar{s}_a\alpha_a,i_a)b}(\mathbf{n},\mathbf{m};t)\right\} \\ &- \Big\{(a,\mathbf{n}) \leftrightarrow (b,\mathbf{m})\Big\}^*,\end{aligned} \tag{4.47}$$

where $x = (x_0, \mathbf{n})$, $y = (y_0, \mathbf{m})$, and the last term represents the complex conjugate of the first term in curly brackets with a and b, and $\mathbf{n}$ and $\mathbf{m}$ interchanged, respectively. The resulting time evolution of $\tilde{n}_{(s\alpha)(s'\alpha')}(\mathbf{n},\mathbf{m};t)$ and $m_{(s\alpha)(s'\alpha')}(\mathbf{n},\mathbf{m};t)$ is thus given by

$$\begin{aligned}&\sum_{\mathbf{l}}\Big(\mathrm{i}\partial_t\delta_{\mathbf{ln}}\delta_{\mathbf{km}} + H^{\mathrm{1B}}_s(\mathbf{n},\mathbf{l};t)\delta_{\mathbf{km}} - H^{\mathrm{1B}}_{s'}(\mathbf{m},\mathbf{k};t)\delta_{\mathbf{ln}}\Big)\tilde{n}_{(s\alpha)(s'\alpha')}(\mathbf{l},\mathbf{k};t) \\ &= \left\{\frac{2U(t)}{\mathcal{N}}\tilde{n}_{(s\beta)(\bar{s}\beta)}(\mathbf{n},\mathbf{n};t)\tilde{n}_{(\bar{s}\alpha)(s'\alpha')}(\mathbf{n},\mathbf{m};t)\right\} - \Big\{(s,\alpha,\mathbf{n}) \leftrightarrow (s',\alpha',\mathbf{m})\Big\},\end{aligned} \tag{4.48}$$

$$\begin{aligned}&\sum_{\mathbf{l}}\Big(\mathrm{i}\partial_t\delta_{\mathbf{ln}}\delta_{\mathbf{km}} - H^{\mathrm{1B}}_s(\mathbf{n},\mathbf{l};t)\delta_{\mathbf{km}} - H^{\mathrm{1B}}_{s'}(\mathbf{m},\mathbf{k};t)\delta_{\mathbf{ln}}\Big)m_{(s\alpha)(s'\alpha')}(\mathbf{l},\mathbf{k};t) \\ &= -\left\{\frac{2U(t)}{\mathcal{N}}\tilde{n}_{(\bar{s}\beta)(s\beta)}(\mathbf{n},\mathbf{n};t)m_{(\bar{s}\alpha)(s'\alpha')}(\mathbf{n},\mathbf{m};t)\right\} + \Big\{(s,\alpha,\mathbf{n}) \leftrightarrow (s',\alpha',\mathbf{m})\Big\}.\end{aligned} \tag{4.49}$$

The last term in Eq. (4.47), Eq. (4.48), and Eq. (4.49) denotes the first term in curly brackets with s and s', α and α', and $\mathbf{n}$ and $\mathbf{m}$ interchanged.

LO $1/\mathcal{N}$ and the $U = 0$ Anderson model

Before proceeding to the next-to-leading order contributions, we show that the equation of motion for F, Eq. (4.42), derived from the LO approximation in the $\mathcal{N}$ expansion of the 2PI effective action is equivalent to the equation of motion found from the mean-field Hamiltonian

$$\begin{aligned}H_{\mathrm{MFT}} = &-J\sum_{\langle\mathbf{n},\mathbf{m}\rangle,\alpha}\psi^*_{c\alpha}(x_0,\mathbf{n})\psi_{c\alpha}(x_0,\mathbf{m}) - U(x)\sum_{\mathbf{n},\alpha}\Big(V(x)\psi^*_{c\alpha}(x)\psi_{f\alpha}(x) + \mathrm{h.c.}\Big) \\ &+ \frac{U(x)\mathcal{N}}{2}\sum_{\mathbf{n}}V^*(x)V(x) + \sum_{\mathbf{n},s,\alpha}V_{\mathrm{ext}}(x)\psi^*_{s\alpha}(x)\psi_{s\alpha}(x)\,,\end{aligned}$$

(4.50)

where $x = (x_0, \mathbf{n})$ and V is a non-fluctuating bosonic field that in the operator formulation is given as the hybridisation

$$V(x) = (2/\mathcal{N}) \sum_{\alpha} \left\langle \hat{\Psi}^{\dagger}_{f\alpha}(x) \hat{\Psi}_{c\alpha}(x) \right\rangle . \tag{4.51}$$

For $\mathcal{N} = 2$, the mean-field Hamiltonian H_{MFT} defines the $U = 0$ Anderson model. It can be derived from the original Hamiltonian defined in Eqs. (4.3), (4.4), and (4.15), written in terms of fermionic field operators, by means of a Hubbard-Stratonovich transformation. Dropping the second term in the interaction Hamiltonian (4.15), which contributes only beyond the LO $1/\mathcal{N}$ approximation, H_{int} can be written as

$$H_{\mathrm{int}} = -\frac{2U(t)}{\mathcal{N}} \sum_{\mathbf{n}} \Big(\psi^{*}_{c\alpha}(\mathbf{n}) \psi_{f\alpha}(\mathbf{n}) \Big) \Big(\psi^{*}_{f\alpha'}(\mathbf{n}) \psi_{c\alpha'}(\mathbf{n}) \Big) \tag{4.52}$$

This is of the form $-[U(t)/(2\mathcal{N})] \sum_{\mathbf{n}} A^{*}(\mathbf{n}) A(\mathbf{n})$ with $A(\mathbf{n}) = \psi^{*}_{f\alpha}(\mathbf{n}) \psi_{c\alpha}(\mathbf{n})$. Using a Hubbard-Stratonovich transformation,

$$-\frac{2U}{\mathcal{N}} A^{*} A \to -U \Big(V^{*} A + A^{*} V \Big) + \frac{U\mathcal{N}}{2} V^{*} V \, , \tag{4.53}$$

and taking V as a non-fluctuating Bose field, one recovers the mean-field Hamiltonian in Eq. (4.50). This transformation would be exact if the $V(x)$ were treated as fluctuating variables inside a path integral—which then would lead to the "Read-Newns" path integral formulation of the Kondo lattice model [156, 163, 164, 165].

In Ref. [93], the dynamic evolution according to H_{MFT} was derived from the Heisenberg equations of motion for the field operators which read

$$\begin{aligned} \mathrm{i}\partial_{x_0} \begin{pmatrix} \hat{\Psi}_{c\alpha}(x) \\ \hat{\Psi}_{f\alpha}(x) \end{pmatrix} = & \begin{pmatrix} \sum_{\mathbf{l}} -J \delta_{\langle \mathbf{n},\mathbf{l} \rangle} \hat{\Psi}_{c\alpha}(\mathbf{l}, x_0) \\ 0 \end{pmatrix} + V_{\mathrm{ext}}(x) \begin{pmatrix} \hat{\Psi}_{c\alpha}(x) \\ \hat{\Psi}_{f\alpha}(x) \end{pmatrix} \\ & - U(x) \begin{pmatrix} V^{*}(x) \hat{\Psi}_{f\alpha}(x) \\ V(x) \hat{\Psi}_{c\alpha}(x) \end{pmatrix} . \end{aligned} \tag{4.54}$$

Applying these dynamic equations of the field operators to the definition of F in Eq. (4.29) yields the dynamic equation for F,

$$\begin{aligned} \mathrm{i}\partial_{x_0} \begin{pmatrix} F_{(c\alpha,1)b}(x,y) \\ F_{(f\alpha,1)b}(x,y) \end{pmatrix} = & \begin{pmatrix} \sum_{\mathbf{l}} J \delta_{\langle \mathbf{n},\mathbf{l} \rangle} F_{(c\alpha,1)b}((\mathbf{l}, x_0), y) \\ 0 \end{pmatrix} \\ & - V_{\mathrm{ext}}(x) \begin{pmatrix} F_{(c\alpha,1)b}(x,y) \\ F_{(f\alpha,1)b}(x,y) \end{pmatrix} + U(x) \begin{pmatrix} V(x) F_{(f\alpha,1)b}(x,y) \\ V^{*}(x) F_{(c\alpha,1)b}(x,y) \end{pmatrix} , \end{aligned} \tag{4.55}$$

$$\begin{aligned} \mathrm{i}\partial_{x_0} \begin{pmatrix} F_{(c\alpha,2)b}(x,y) \\ F_{(f\alpha,2)b}(x,y) \end{pmatrix} = & \begin{pmatrix} \sum_{\mathbf{l}} -J \delta_{\langle \mathbf{n},\mathbf{l} \rangle} F_{(c\alpha,2)b}((\mathbf{l}, x_0), y) \\ 0 \end{pmatrix} \\ & + V_{\mathrm{ext}}(x) \begin{pmatrix} F_{(c\alpha,2)b}(x,y) \\ F_{(f\alpha,2)b}(x,y) \end{pmatrix} - U(x) \begin{pmatrix} V^{*}(x) F_{(f\alpha,2)b}(x,y) \\ V(x) F_{(c\alpha,2)b}(x,y) \end{pmatrix} . \end{aligned} \tag{4.56}$$

These equations are equivalent to the equation of motion for F, Eq. (4.42), derived from the LO approximation in the $\mathcal{N}$ expansion of the 2PI effective action since

$$V(x) = \frac{2}{\mathcal{N}} F_{(c\alpha,2)(f\alpha,2)}(x,x)\,, \tag{4.57}$$

$$V^*(x) = \frac{2}{\mathcal{N}} F_{(f\alpha,1)(c\alpha,1)}(x,x)\,. \tag{4.58}$$

Thus, we conclude that the dynamic equations derived in LO approximation of the $1/\mathcal{N}$ expansion of the 2PI effective action describe the same dynamics as the equations of motion of the $U = 0$ Anderson model.

4.4.2 Next-to-leading order $1/\mathcal{N}$ approximation

As depicted in Fig. 4.3, the next-to-leading order (NLO) contribution to Γ_2 consists of a double-bubble diagram with a dashed vertex line, and all ring diagrams with only squiggly vertex lines. Thus, the "dashed line" vertex contributes only to the local part of the self-energy, i. e. only on-energy-shell scattering contributions are taken into account from this vertex. This implies that the LO "dashed line" vertex contribution does not contribute to a redistribution of the momentum mode occupation numbers during the time-evolution. To include also off-energy-shell scattering contributions from the "dashed line" vertex, it is necessary to beyond NLO.

For large $\mathcal{N}$, most of the direct interactions leaving the spins of the scatterers unaltered are included in the "dashed line" vertex contribution, and only a small fraction is included in the "squiggly line" vertex contribution. At least for $\mathcal{N} = 2$, the direct interactions describe the polarisation of the conduction-band atoms by the local impurity spins, leading to magnetical instability, and are important for RKKY interactions. Thus, it is crucial to include direct interaction contributions if we want to describe physics away from the HFL phase at strong coupling. To find out about the relevance of the direct interactions of the "dashed line" vertex on the dynamics and late-time distribution of the KLM for various $\mathcal{N}$ is part of future studies.

In the remainder of this section, we give the explicit formula for the NLO contribution to the 2PI part Γ_2^{NLO} of the effective action as well as the resulting dynamical equations. Finally, we briefly comment on some aspects relevant for a numerical implementation of the dynamical equations.

The 2PI part Γ_2^{NLO} is depicted in Fig. 4.3 and reads

$$\begin{aligned}\Gamma_2^{\mathrm{NLO}}[G] = \frac{\sigma_{1,ss'}}{2\mathcal{N}^2}\int_x U(x) G_{(s\alpha,i)(s\alpha,i)}(x,x) G_{(s'\beta,i)(s'\beta,i)}(x,x) \\ + \frac{\mathrm{i}}{2}\,\mathrm{Tr}\left[\ln\left[B(x,y;G)\right]\right]\end{aligned} \tag{4.59}$$

with

$$B_{(s,i)(t,j)}(x,y;G) = \delta_{st}\delta_{ij}\delta_{\mathcal{C}}(x-y) - \mathrm{i}\Pi_{(s,i)(t,j)}(x,y) \tag{4.60}$$

and

$$\Pi_{(r,i)(s,j)}(x,y) = \frac{2U(x)}{\mathcal{N}} G_{(r\alpha,\bar{i})(t\beta,k)}(x,y) G_{(\bar{t}\beta,k)(\bar{s}\alpha,\bar{i})}(y,x) h_{(t,k)(s,j)}\,, \tag{4.61}$$

where summations over t, k, α and β are implied and

$$h_{(t,k)(s,j)} = \frac{1}{2}\Big(\sigma_{1,ts}\delta_{kj} - \delta_{ts}\sigma_{1,kj}\Big)\,, \tag{4.62}$$

such that

$$\begin{aligned}
&\mathrm{Tr}\left[\ln\big[B(x,y;G)\big]\right] \\
&= -\mathrm{i}\int_x \Pi_{(s,i)(s,i)}(x,x) \\
&\quad - \frac{\mathrm{i}^2}{2}\int_{xy} \Pi_{(s,i)(t,j)}(x,y)\Pi_{(t,j)(s,i)}(y,x) \\
&\quad - \frac{\mathrm{i}^3}{3}\int_{xyz} \Pi_{(s,i)(t,j)}(x,y)\Pi_{(t,j)(u,k)}(y,z)\Pi_{(u,k)(s,i)}(z,x) \\
&\quad - \cdots .
\end{aligned} \tag{4.63}$$

The resulting proper self-energy contribution Σ^{NLO} has both local and non-local contributions, i. e.

$$\Sigma^{\mathrm{NLO}}_{ab}(x,y;G) = \Sigma^{\mathrm{NLO},(0)}_{ab}(x;G)\delta_{\mathcal{C}}(x-y) + \overline{\Sigma}^{\mathrm{NLO}}_{ab}(x,y;G)\,. \tag{4.64}$$

The local contribution is given by

$$\Sigma^{\mathrm{NLO},(0)}_{ab}(x;G) = \frac{2\mathrm{i}U}{\mathcal{N}^2}\delta_{ab}G_{ba}(x,x) - \frac{4\mathrm{i}U}{\mathcal{N}} h_{(s_a,\bar{i}_a)(s_b,i_b)}(x,y) G_{\bar{a}\bar{b}}(x,y)\,, \tag{4.65}$$

and the non-local contribution reads

$$\overline{\Sigma}^{\mathrm{NLO}}_{ab}(x,y;G) = 2I_{(s_a,i_a)(s_b,i_b)}(x,y) G_{\bar{a}\bar{b}}(x,y)\,, \tag{4.66}$$

where

$$I_{(r,i)(s,j)}(x,y;G) = \int_z \Lambda_{(r,i)(t,k)}(x,z;G)\Pi_{(t,k)(s,j)}(z,y) \tag{4.67}$$

with

$$\Lambda_{(r,i)(s,j)}(x,y) = \Big(2U(x)h_{(r,i)(s,j)}\delta_{\mathcal{C}}(x-y) + \mathrm{i}I_{(r,i)(s,j)}(x,y;G)\Big)\,. \tag{4.68}$$

Finally, we combine the LO and the NLO contributions and express all equations in statistical and spectral components. The local contribution is given by

$$\begin{aligned}\Sigma^{(0)}_{ab}(x;G) = -\frac{2U}{\mathcal{N}}\Big(&\sigma_{1,s_a s_b}\delta_{\alpha_a\alpha_b}\delta_{i_a i_b}F_{(s_b\alpha',\bar{i}_a)(s_a\alpha',\bar{i}_b)}(x,x)\\ &+\frac{\delta_{ab}}{\mathcal{N}}F_{(\bar{s}_a\alpha,i_a)(\bar{s}_a\alpha,i_b)}(x,x) - 2h_{(s_a,\bar{i}_a)(s_b,i_b)}F_{\bar{a}\bar{b}}(x,x)\Big)\,.\end{aligned} \tag{4.69}$$

And the non-local beyond-mean-field contribution of the self-energy is given by

$$\overline{\Sigma}^F_{ab}(x,y) = 2\Big(I^F_{(s_a,\bar{i}_a)(s_b,i_b)}(x,y)F_{\bar{a}\bar{b}}(x,y) - \frac{1}{4}I^\rho_{(s_a,\bar{i}_a)(s_b,i_b)}(x,y)\rho_{\bar{a}\bar{b}}(x,y)\Big)\,, \tag{4.70}$$

$$\overline{\Sigma}^\rho_{ab}(x,y) = 2\Big(I^F_{(s_a,\bar{i}_a)(s_b,i_b)}(x,y)\rho_{(\bar{a}\bar{b}}(x,y) + I^\rho_{(s_a,\bar{i}_a)(s_b,i_b)}(x,y)F_{\bar{a}\bar{b}}(x,y)\Big)\,, \tag{4.71}$$

where

$$\begin{aligned}I^F_{(s_a,i_a)(s_b,i_b)}(x,y) = h_{(s_a,i_a)(r,j)}&\Pi^F_{(r,j)(s_b,i_b)}(x,y)\\ &+\int_0^{x_0}\mathrm{d}z\, I^\rho_{(s_a,i_a)(t,j)}(x,z)\Pi^F_{(t,j)(s_b,i_b)}(z,y)\\ &-\int_0^{y_0}\mathrm{d}z\, I^F_{(s_a,i_a)(t,j)}(x,z)\Pi^\rho_{(t,j)(s_b,i_b)}(z,y)\,,\end{aligned} \tag{4.72}$$

$$\begin{aligned}I^\rho_{(s_a,i_a)(s_b,i_b)}(x,y) = h_{(s_a,i_a)(r,j)}&\Pi^\rho_{(r,j)(s_b,i_b)}(x,y)\\ &+\int_{y_0}^{x_0}\mathrm{d}z\, I^\rho_{(s_a,i_a)(t,j)}(x,z)\Pi^\rho_{(t,j)(s_b,i_b)}(z,y)\,,\end{aligned} \tag{4.73}$$

with

$$\begin{aligned}\Pi^F_{(s_a,i_a)(s_b,i_b)}(x,y) = \frac{2U(x)}{\mathcal{N}}\Big(&F_{(s\alpha,i)(r\beta,j)}(x,y)F_{(\bar{r}\beta,j)(\bar{s}\alpha,i)}(y,x)\\ &+\frac{1}{4}\rho_{(s\alpha,i)(r\beta,j)}(x,y)\rho_{(\bar{r}\beta,j)(\bar{s}\alpha,i)}(y,x)\Big)h_{(r,j)(s_b,i_b)}\,,\end{aligned} \tag{4.74}$$

$$\begin{aligned}\Pi^\rho_{(s_a,i_a)(s_b,i_b)}(x,y) = \frac{2U(x)}{\mathcal{N}}\Big(&\rho_{(s\alpha,i)(r\beta,j)}(x,y)F_{(\bar{r}\beta,j)(\bar{s}\alpha,i)}(y,x)\\ &-F_{(s\alpha,i)(r\beta,j)}(x,y)\rho_{(\bar{r}\beta,j)(\bar{s}\alpha,i)}(y,x)\Big)h_{(r,j)(s_b,i_b)}\,.\end{aligned} \tag{4.75}$$

With this, we derived the dynamical equations for the spectral function ρ and the statistical propagator F of the $SU(\mathcal{N})$ symmetric Kondo lattice model in NLO approximation of the $1/\mathcal{N}$ expansion of the 2PI effective action. The next step would be to implement them on a computer and study their properties. Since the hyperfine space we want to considered in this equations can be quite large, a thoughtless implementation can very easily exceed computational limitations. Therefore, we close this section with a few crucial remarks on how to realise an efficient numerical implementation.

Some considerations for an efficient numerical implementation

When numerically implementing the equations of motion in NLO $1/\mathcal{N}$ approximation, it is crucial to make use of the symmetries in the hyperfine index in order to save memory. For the case of spin balanced initial conditions, for each of the functions F, ρ, $\overline{\Sigma}^F$ and $\overline{\Sigma}^\rho$ only two quantities need to be stored in the hyperfine index space for each combination of field and space-time indices: one for $\alpha = \beta$ and another for $\alpha \neq \beta$. In this case, also the sums over the hyperfine indices in I^F, I^ρ, Π^F, and Π^ρ should be performed analytically in order to save computation power and run time. Taking these ideas into consideration, the resulting code requires the same amount of memory and run time as the code used for the two-component Fermi gas investigated in Ch. 3, independent of the actual value of $\mathcal{N}$.

4.5 Summary

In this chapter, we discussed an ultra-cold Fermi gas on a spatial lattice that can be described by the $SU(\mathcal{N})$ symmetric Kondo lattice model (KLM). We reviewed relevant properties of the KLM and derived non-equilibrium dynamical equations up to next-to-leading order approximation of the $1/\mathcal{N}$ expansion of the 2PI effective action. With this, we laid the foundations for future studies analysing the dynamic equations and exploring the phase diagram of the $SU(\mathcal{N})$ symmetric KLM.

We began with a motivation why the KLM recently attracted more and more attention in the cold atom community: Fermionic alkaline-earth-metal atoms trapped in optical lattice potentials allow to simulate the KLM in the laboratory. In fermionic alkaline-earth-metal atoms, the metastable excited state ${}^3P_0$ and the ground state ${}^1S_0$ are only very weakly coupled and can be trapped independently by two different optical lattice potentials with the same spatial periodicity. This allows to simulate localised spin impurities in a delocalised conduction band of atoms. The vanishing electronic angular momentum J in both of these states results in an almost perfect decoupling of the nuclear spin I from J, which implies an $SU(\mathcal{N})$ symmetry in the (hyperfine) spin degree of freedom with $\mathcal{N} = 2I + 1$. Moreover, the particular value of $\mathcal{N}$, which can be as large as ten for ^{87}Sr, can be chosen through the controlled population of a subset of the hyperfine states. This offers the unique possibility to employ controlled large-$\mathcal{N}$ expansions in quantum field theory for the study of both, static and dynamical properties.

Thereafter, we reviewed the KLM more formally and showed how different representations of the Kondo lattice Hamiltonian are linked with each other. Since we used a complex field basis for our description in this chapter, we briefly showed relevant formulae of the 2PI effective action approach in order to see which formulae change and which do not. Then, we derived the dynamic equations using the $1/\mathcal{N}$ expansion of the 2PI effective action. In leading-order approximation of the $1/\mathcal{N}$, we recovered the mean-field dynamic equations of the $U = 0$ Anderson model used

in Ref. [93] to describe Kondo lattice dynamics. Finally, we derived the dynamic equations in next-to-leading order (NLO) approximation. At NLO, both spin-flip and direct interactions between localised atoms and conduction band atoms are taken into account non-perturbatively into the dynamic equations. Therefore, the $1/\mathcal{N}$ expansion of the 2PI effective action beyond the leading-order approximation is a promising tool to tackle yet outstanding challenges in KLM research, e. g. possible novel phases depending on the coupling strength, filling factors, and size of the degeneracy $\mathcal{N}$, and phase transitions between them. We closed this chapter by rewriting the dynamic equations in next-to-leading order approximation in a way that is suitable for a numerical implementation. Also, we explained how such an implementation can be done very efficiently even for large $\mathcal{N}$.

Conclusion

In this thesis, we addressed the description of far-from-equilibrium dynamics of fermionic quantum gases utilising functional quantum field theoretical methods. We discussed in detail the dynamics of a spin-degenerate Fermi gas in one spatial dimension from a far-from equilibrium initial state. We found that the gas evolves into thermal as well as non-thermal states depending on its total energy. Furthermore, we laid the foundations to study non-equilibrium dynamics and to explore possible new phases in the $SU(\mathcal{N})$ symmetric Kondo lattice model (KLM) by deriving dynamical equations in next-to-leading order approximation of the $1/\mathcal{N}$ expansion of the two-particle irreducible (2PI) effective action.

In the first chapter, we derived exact non-equilibrium dynamical equations—real-time integro-differential Schwinger-Dyson/Kadanoff-Baym dynamic equations—for the two-point correlation functions of a non-relativistic Fermi gas. Thereby, we reviewed the general framework for obtaining these equations from the 2PI effective action Γ. The calculations and formulae in this chapter were model independent in the sense that we did not specify to any particular interaction between the fermions.

We started with a presentation of the general Lagrangian for non-relativistic fermions and remarked on some basic and general properties of the specific models that we investigated in the following chapters of this thesis. In particular, we discussed the symmetries of the Lagrangian since it is crucial that also the dynamic equations derived later on needed to respect them in order to appropriately describe the dynamics.

Our main interest throughout this thesis was in the dynamic evolution of the lowest-order correlation functions since most of the experimentally relevant observables are determined by these functions. Due to the Pauli exclusion principle, which states that no two identical fermions can occupy the same quantum state simultaneously, there is no macroscopic field for fermions unlike it can be the case for bosons. And thus, for fermions, the lowest correlation functions we are interested in are the two-point functions. We introduced the two-point Green function G and its decomposition into the spectral function ρ and the statistical propagator F.

To derive the dynamic equations for the two-point functions, we introduced the non-equilibrium generating functional for connected Green functions using the Schwinger-Keldysh closed time path formulation that is suitable for initial value problems. Specifying to Gaussian initial states, which permit to set (one- and) two-point functions as initial conditions, allowed us to rewrite the generating functional in a much simpler form. However, written in a real-time path integral formulation, the generating functional still involved an integration over a fluctuating field; therefore, it

could not be evaluated directly. A solution was to introduce an effective action that incorporated these fluctuations without requiring an explicit path integral. We saw that the 2PI effective action is a suitable effective action when Gaussian initial states are considered. We showed that, similar to Hamilton's principle for the classical action, one can determine the exact dynamic equation for the two-point Green function from the effective action by solving a variational problem. The resulting dynamic equation for the two-point Green function contained a time integration along the closed time path; however, it could be transformed into two coupled integro-differential equations for the statistical propagator and the spectral function that involved only standard time integrals. This neat feature was especially helpful when solving the (at that time necessarily approximated) dynamic equations numerically for the two-fold spin-degenerate Fermi gas in Ch. 3.

Deriving the dynamic equations from the effective action functional had the substantial advantage that approximations could be made on the level of a functional. The 2PI effective action was constructed in such a way that it, as well as any truncation of it, owned the same global symmetries as the underlying classical action that specifies a model. Thus, starting with any truncation of the functional, the variational procedure then ensured that the resulting equations of motion still preserved the global symmetries. And hence, the Noether currents associated with these symmetries were also conserved. This is crucial for an accurate description of long-time and out-of-equilibrium dynamics. Then, we discussed and derived explicit expressions for the conserved total particle number and the energy-momentum tensor.

The real-time Schwinger-Dyson/Kadanoff-Baym dynamic equations for the two-point correlation functions are generally unsolvable due to the non-local proper self-energy contribution $\overline{\Sigma}$ appearing therein. The approximations necessary to (numerically) solve these equations are model dependent. To investigate the dynamic equations further, we looked at two specific models in this thesis, the spin degenerate Fermi gas and the Kondo lattice gas.

In the second and third chapter, we studied the non-equilibrium dynamics of a non-relativistic Fermi gas with $\mathcal{N}$-fold spin degeneracy in which the spin components mutually interact through local s-wave scattering. In Ch. 2, we discussed different possible approximation schemes of the 2PI effective action Γ, which lead to an approximated proper self-energy. Each of these schemes was characterised by a certain truncation of the expansion of the 2PI part Γ_2 of the 2PI effective action in terms of 2PI diagrams. We first approximated the functional Γ_2 and then derived the corresponding proper self-energy from Γ_2 rather than directly approximating the proper self-energy. This had the advantage that the resulting dynamic equation still preserved the global symmetries of the original model and, therefore, fulfilled the conservation laws associated with these symmetries.

We described two approximation schemes of the 2PI effective action in detail. The first approximation scheme was a loop expansion. In this expansion, the contributions to the 2PI part Γ_2 of the 2PI effective action were ordered as a power series in the number of explicitly appearing bare coupling constants λ. This is very similar to the

standard loop or coupling expansion with the only difference that only 2PI graphs were considered and the full propagator G was used for all propagator lines in a diagram. And since the full propagator itself contained the bare coupling constant λ to all orders, the loop expansion using the full propagator was non-perturbative in the coupling even for small λ. We discussed the first-order (Hartree-Fock-Bogoliubov) approximation in the loop expansion and obtained dynamic equations for the single particle density and an anomalous pair-correlation function. In the next order of this approximation, the resulting coupled equations for the statistical propagator F and spectral function ρ generalised the quantum Boltzmann kinetic equation for multi-component fermions by including non-Markovian corrections to the propagation kernel as well as many-body corrections to the two-body T matrix. We also briefly commented on higher-order loop approximations. We pointed out that the loop expansion requires a small coupling constant in order to be a controlled approximation.

The second approximation scheme was a controlled non-perturbative approximation, in which the expansion parameter was not superficially based on the coupling, and which was, therefore, not necessarily restricted to the weak coupling regime. Instead, the 2PI part Γ_2 of the effective action was expanded in powers of the inverse number of spin states $\mathcal{N}$, i. e. in powers of $1/\mathcal{N}$. We computed the 2PI effective action to next-to-leading order (NLO) in this $1/\mathcal{N}$ expansion. At NLO, an infinite number of diagrams was resummed and both scattering and memory effects were included. We briefly discussed how to go beyond the NLO approximation of the $1/\mathcal{N}$ expansion.

In the third chapter, we thoroughly studied the long-time evolution of a homogeneous Fermi gas with two-fold spin-degeneracy in one spatial dimension after an initial preparation far from thermal equilibrium. For this purpose, we adopted the different approximation schemes to numerically solve the dynamic equations.

The Fermi gas was initially assumed to be non-interacting and prepared far from equilibrium, characterised by a non-equilibrium single-particle momentum distribution. We assumed the interactions to be switched on at the initial time and investigated the long-time evolution of the interacting gas towards equilibrium. All runs that we performed evolved into a stationary state once they were insensitive to numerical parameters like the discrete time step size. These stationary states were insensitive to the details of the initial state—they were solely determined by the total energy E_{tot}, the line density n_{1D}, and the interaction strength γ. In the stationary states, we found that the occupation numbers of the lowest momentum modes coincided with a Fermi-Dirac distribution with which thermodynamic quantities like the temperature and the chemical potential are connected. The extracted thermodynamic quantities converged to the ideal gas results for high temperatures and deviate from them for lower temperatures. These deviations were expected since the finite coupling constant becomes more significant at lower temperatures. In the stationary states, the occupation numbers of the higher momentum modes deviated from a Fermi-Dirac distribution. This deviation were more pronounced at lower total energies, and a power-law tail was replacing the exponential decay of the Fermi-Dirac distribution. The power law is reminiscent of the p^{-4} power law for the high-momentum tail of the

single-particle momentum distribution in both one of Tan's relations for a strongly correlated two-component Fermi gas and BCS theory. Our results do not rule out that a power law ultimately appears also at higher energies in a range of momenta beyond the momentum cut off present in our numerics.

To address the question whether or not the late-time stationary states can be described by a standard statistical ensemble, we investigated the fluctuation-dissipation relation (FDR) for our data. For this purpose, it is convenient to look into the FDR rather than at, for example, the single-particle momentum mode occupation numbers since only the the occupation numbers of the eigenmodes need to be Fermi-Dirac distributed in order for the system to be in a thermal state. Thus, the single-particle momentum distribution is likely not to be Fermi-Dirac distributed once the interactions become a pronounced feature of the system, which is generically the case at sufficiently low energies. For the runs with very low total energies, i. e. those where the single particle momentum distribution deviates the most from a Fermi-Dirac distribution, we also found deviations from the FDR. This indicated that the Fermi gas approached a non-thermal state at large times.

In the fourth chapter, we discussed an ultra-cold Fermi gas on a spatial lattice that can be described by the $SU(\mathcal{N})$ symmetric Kondo lattice model (KLM). We reviewed relevant properties of the KLM and derived non-equilibrium dynamical equations up to next-to-leading order approximation of the $1/\mathcal{N}$ expansion of the 2PI effective action. With this, we laid the foundations for future studies analysing the dynamic equations and exploring the phase diagram of the $SU(\mathcal{N})$ symmetric KLM.

The KLM recently attracted attention in the cold atom community because fermionic alkaline-earth-metal atoms trapped in optical lattice potentials allow to simulate the KLM in the laboratory. In fermionic alkaline-earth-metal atoms, the metastable excited state ${}^3P_0$ and the ground state ${}^1S_0$ are only very weakly coupled and can be trapped independently by two different optical lattice potentials with the same spatial periodicity. This allows to simulate localised spin impurities in a delocalised conduction band of atoms. The vanishing electronic angular momentum J in both of these states results in an almost perfect decoupling of the nuclear spin I from J, which implies an $SU(\mathcal{N})$ symmetry in the (hyperfine) spin degree of freedom with $\mathcal{N} = 2I + 1$. Moreover, the particular value of $\mathcal{N}$, which can be as large as ten for ^{87}Sr, can be chosen through the controlled population of a subset of the hyperfine states. This offers the unique possibility to employ controlled large-$\mathcal{N}$ expansions in quantum field theory for the study of both, static and dynamical properties.

Thereafter, we reviewed the KLM more formally and showed how different representations of the Kondo lattice Hamiltonian are linked with each other. Then, we derived the dynamic equations using the $1/\mathcal{N}$ expansion of the 2PI effective action. In leading-order approximation of the $1/\mathcal{N}$, we recovered the mean-field dynamic equations of the $U = 0$ Anderson model used in Ref. [93] to describe Kondo lattice dynamics. Finally, we derived the dynamic equations in next-to-leading order approximation. At next-to-leading order (NLO), both spin-flip and direct interactions between localised atoms and conduction band atoms are taken into account non-

perturbatively. Therefore, the $1/\mathcal{N}$ expansion of the 2PI effective action beyond the leading-order approximation is a promising tool to tackle yet outstanding challenges in KLM research, e. g. possible novel phases depending on the coupling strength, filling factors, and size of the degeneracy $\mathcal{N}$, and phase transitions between these phases. We closed this chapter by rewriting the dynamic equations in next-to-leading order approximation in a way that is suitable for a numerical implementation. Also, we explained how such an implementation can be done very efficiently even for large $\mathcal{N}$.

In conclusion, with our research we extended existing work on the study of non-equilibrium real-time dynamics based on approximations of the 2PI effective action to systems of non-relativistic Fermi gases. With our numerical investigations of the ultra-cold Fermi gas with two spin components in one spatial dimension, we demonstrated the possibility for equilibration to non-thermal states outside the Tomonaga-Luttinger liquid (TLL) regime, and thereby contributed to the ongoing discussion on the long-time properties of such a system in view of quantum integrability. Our work on the KLM laid the foundation for future studies on static and dynamical properties of this model particular in regimes where strong correlations are present and beyond-mean-field approximations are required.

Appendix A

Ideal non-relativistic Fermi gas in d spatial dimensions

The ideal non-relativistic Fermi gas in three dimensions is discussed in nearly every textbook on statistical mechanics, e. g. the book by F. Schwabl [166]. The generalisation to d dimensions is straightforward, but rarely shown explicitly; therefore, we provide some of the corresponding formulae in this appendix.

A.1 Grand-canonical potential

The state of N non-interacting particles can be written as a tensor product of the one-particle states $|p_i\rangle$, $i = 1, \ldots, N$. And to simplify the discussion, it is convenient to characterise the N-particle state by the occupation numbers n_p of the one-particle states.

To derive thermodynamic quantities, it is most convenient to determine the grand-canonical potential. In the formalism of the second quantisation, the grand-canonical partition function is given by

$$Z_G = \mathrm{Tr} \exp[-\beta(H - \mu\hat{N})] \,, \tag{A.1}$$

where the Hamiltonian H and the particle number operator $\hat{N}$ in second quantisation are given by

$$H = \sum_p \varepsilon_p \hat{a}_p^\dagger \hat{a}_p \qquad \text{and} \qquad \hat{N} = \sum_p \hat{a}_p^\dagger \hat{a}_p \,, \tag{A.2}$$

where the sum is over all possible one-particle states $p = (\mathbf{p}, m_s)$ characterised by the momentum $\mathbf{p}$ and the z-component m_s of the spin s; m_s takes $2s + 1$ values. For fermions, it follows

$$\begin{aligned} Z_G &= \mathrm{Tr} \prod_p \exp[-\beta(\varepsilon_p - \mu)\hat{a}_p^\dagger \hat{a}_p] = \mathrm{Tr} \prod_p \exp[-\beta(\varepsilon_p - \mu)\hat{n}_p] \\ &= \prod_p \Big(1 + \mathrm{e}^{-\beta(\varepsilon_p - \mu)}\Big) \,. \end{aligned} \tag{A.3}$$

The grand-canonical potential is

$$\Phi = -\beta^{-1} \ln Z_G = -\beta^{-1} \sum_p \ln\left[1 + \mathrm{e}^{-\beta(\varepsilon_p - \mu)}\right]. \tag{A.4}$$

In discrete momentum space, each momentum $\mathbf{p}$ occupies the volume $(2\pi\hbar/L)^d$. For large volumes $V = L^d$, the sum over one-particle states can be replaced by an integral. If the integrand depends only on the absolute value of $\mathbf{p}$ then it is convenient to evaluate the integral in spherical coordinates. In this case, one can integrate out all but the radial component p_r:

$$\begin{aligned}\sum_p &= \sum_{m_s=-s}^{s} \sum_{\mathbf{p}} \\ &\approx \frac{V}{(2\pi\hbar)^d} \sum_{m_s=-s}^{s} \int \mathrm{d}^d p = \frac{V}{(2\pi\hbar)^d} \frac{2\pi^{d/2}}{\Gamma(d/2)} \sum_{m_s=-s}^{s} \int_0^\infty \mathrm{d}p_r \, p_r^{d-1} \\ &= \int_0^\infty \mathrm{d}\varepsilon \, g(\varepsilon)\end{aligned} \tag{A.5}$$

with energy density

$$g(\varepsilon) = \frac{g_s V}{(2\pi\hbar)^d} \frac{2\pi^{d/2}}{\Gamma(d/2)} p_r^{d-1}(\varepsilon) \left(\frac{\partial \varepsilon}{\partial p_r}\right)^{-1}. \tag{A.6}$$

Here, $g_s = 2s + 1$ is the degeneracy factor, which appears since we assumed the mode energy ε_p to be independent of the spin s. $\Gamma(\nu)$ is the Euler Gamma function with, for example, $\Gamma(1/2) = \sqrt{\pi}$, $\Gamma(1) = 1$, $\Gamma(3/2) = \sqrt{\pi}/2$, and $\Gamma(5/2) = 3\sqrt{\pi}/4$.

For the special case of non-relativistic particles with dispersion relation

$$\varepsilon = \frac{\mathbf{p}^2}{2m} \left[= \frac{p_r^2}{2m}\right], \tag{A.7}$$

the energy density is

$$g(\varepsilon) = \frac{g_s V}{\lambda_T^d} \frac{\beta^{d/2}}{\Gamma(d/2)} \varepsilon^{d/2-1} \tag{A.8}$$

with the thermal wavelength

$$\lambda_T = \frac{2\pi\hbar}{\sqrt{2\pi m \beta^{-1}}}. \tag{A.9}$$

A.2 Fermi-Dirac functions

For the following discussion, it is convenient to define the so-called Fermi-Dirac functions $f_\nu(z)$, which are generalisations of the Riemann zeta function $\zeta(\alpha) = \sum_k k^{-\alpha}$

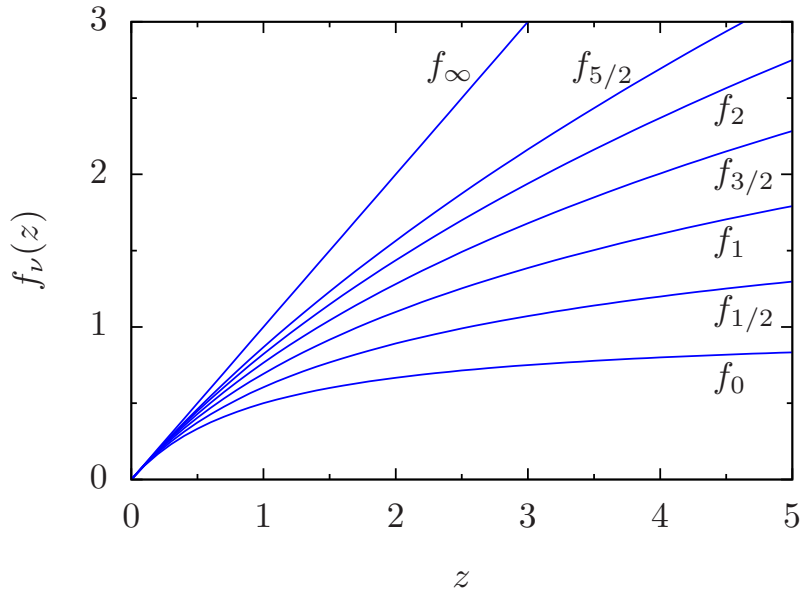

Figure A.1: Illustration of some of the Fermi-Dirac functions $f_\nu(z)$ defined in Eq. (A.10).

for $\mathrm{Re}[\alpha] > 1$. The Fermi-Dirac functions are defined as

$$f_\nu(z) = \frac{1}{\Gamma(\nu)} \int_0^\infty \mathrm{d}x \, \frac{x^{\nu-1}}{z^{-1}\mathrm{e}^x + 1}\,, \qquad 0 \le z < \infty\,. \tag{A.10}$$

For $\nu \ge 1$, they fulfil the recurrence relation

$$z f_\nu'(z) = f_{\nu-1}(z)\,. \tag{A.11}$$

Some special cases are

$$f_0(z) = \frac{z}{z+1}\,, \qquad f_1(z) = \ln(z+1)\,, \qquad f_\infty(z) = z\,. \tag{A.12}$$

For $0 \le z \le 1$, a series expansion exists,

$$f_\nu(z) = \sum_{k=1}^{\infty} (-1)^k \frac{z^k}{k^\nu}\,. \tag{A.13}$$

And the asymptotic expansion for $z \gg 1$ is

$$f_\nu(z) = \frac{(\ln z)^\nu}{\Gamma(\nu+1)} \left(1 + \sum_{k=1}^{\infty} \frac{2(1-2^{1-2k}) n! \zeta(2k)}{(n-2k)! (\ln z)^{2k}} \right). \tag{A.14}$$

Some of the Fermi-Dirac functions are shown in Fig. A.1.

A.3 Total particle number

The mean particle number is

$$N \equiv -\left(\frac{\partial \Phi}{\partial \mu}\right)_{\beta} = \sum_{p} n(\varepsilon_p)\,, \tag{A.15}$$

where

$$n(\varepsilon_p) \equiv \frac{1}{\mathrm{e}^{\beta(\varepsilon_p-\mu)}+1} \tag{A.16}$$

is the mean occupation number of the state $|p\rangle$. The uncertainty in the occupation numbers is

$$\big(\Delta n(\varepsilon_p)\big)^2 = \beta^{-1}\frac{\partial n(\varepsilon_p)}{\partial \mu} = n(\varepsilon_p)\big(1-n(\varepsilon_p)\big)\,, \tag{A.17}$$

which vanishes for $n(\varepsilon_p)=0$ and $n(\varepsilon_p)=1$.

Replacing the sum over $\mathbf{p}$ by an integral, one finds for the total particle number

$$N = \frac{g_s V}{\lambda_T^d} f_{d/2}(z)\,, \tag{A.18}$$

where $z=\exp[\mu\beta]$ is the fugacity. As we will see, the ratio $N\lambda_T^d/(g_s V)$ can be replaced in favour of an expression that solely depends on the dimension d and the temperature β^{-1}, see Eq. (A.40). Since $f_{d/2}(z)$ is invertible for non-negative z and diverges to positive infinity for $d>0$, the fugacity z is thus uniquely fixed for given d and β.

For later use, note that the mean occupation number in Eq. (A.16) simplifies to

$$n(\varepsilon_p) = \begin{cases} 1, & \text{for } \varepsilon_p < \mu \\ 0, & \text{for } \varepsilon_p \geq \mu \end{cases} \tag{A.19}$$

for $\beta^{-1}=0$.

A.4 Fugacity

The fugacity z is defined as

$$z = \mathrm{e}^{\mu\beta}\,. \tag{A.20}$$

The fugacity as a function of temperature is shown in Fig. A.2.

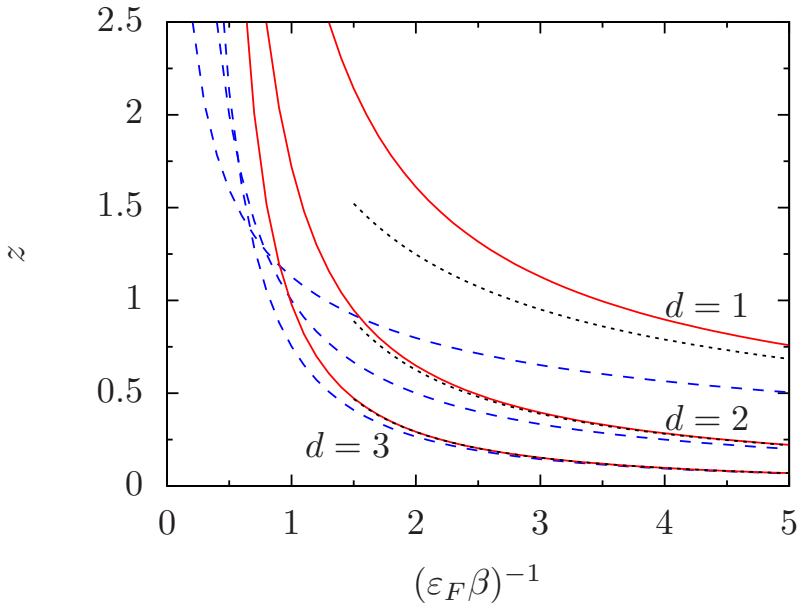

Figure A.2: Fugacity as a function of temperature for the ideal Fermi gas (red solid lines) and the ideal classical gas (blue dashed lines) in d dimensions. The asymptotic behaviour of the ideal Fermi gas for high temperatures is shown as black dotted lines.

Quantum limit ($z \gg 1$):

For $z \gg 1$, the Fermi function asymptotically reaches

$$f_\nu(z) = \frac{(\ln z)^\nu}{\Gamma(\nu+1)}\Big(1 + \mathcal{O}\big[(\ln z)^{-2}\big]\Big)\,. \tag{A.21}$$

Combining this equation with Eq. (A.40) gives

$$z \approx \exp[\varepsilon_F\beta]\,. \tag{A.22}$$

Classical limit ($z \ll 1$):

The fugacity can be calculated from the series expansion of $f_{d/2}(z)$,

$$f_{d/2}(z) = z - \frac{z^2}{2^{d/2}} + \mathcal{O}\big[z^3\big]\,. \tag{A.23}$$

As we will shortly see, one can write $N\lambda^d/(g_s V)$ in Eq. (A.18) as an expression with d and β as the only parameters, cf. Eq. (A.40). Combining Eq. (A.23) and Eq. (A.40), one finds

$$z = z_{\text{classical}} + \frac{2^{2-d/2}/d^2}{\Gamma^2(d/2)}(\varepsilon_F\beta)^d + \mathcal{O}\big[(\varepsilon_F\beta)^{3d/2}\big] \tag{A.24}$$

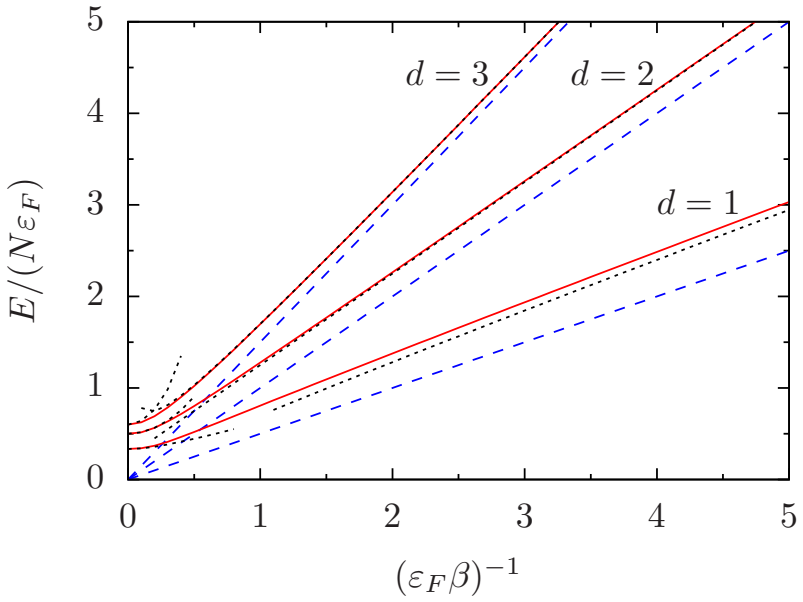

Figure A.3: Mean energy per particle as a function of temperature for the ideal Fermi gas (red solid lines) and the ideal classical gas (blue dashed lines) in d dimensions. The asymptotic behaviour of the ideal Fermi gas for low and high temperatures is shown as black dotted lines.

with

$$z_{\text{classical}} = \frac{2/d}{\Gamma(d/2)}(\varepsilon_F\beta)^{d/2}\,. \tag{A.25}$$

A.5 Mean energy per particle

The internal energy E is given by

$$E = \left(\frac{\partial(\Phi\beta)}{\partial\beta}\right)_{\beta\mu} = \sum_p \varepsilon_p n(\varepsilon_p)\,. \tag{A.26}$$

Replacing the sum over $\mathbf{p}$ by an integral, one finds for the mean energy per particle

$$\frac{E}{N} = \frac{d}{2}\beta^{-1}\frac{f_{d/2+1}(z)}{f_{d/2}(z)}\,. \tag{A.27}$$

The mean energies per particle as a function of temperature in $d = 1$, 2, and 3 dimensions are shown in Fig. A.3.

Quantum limit ($z \gg 1$):

The asymptotic behaviour for large z, i. e. $\beta^{-1} \ll 1$, allows to define a characteristic energy, the Fermi energy ε_F. For $z \gg 1$, we find

$$\frac{f_{d/2+1}(z)}{f_{d/2}(z)} \approx \frac{d}{d+2} \ln z = \frac{d}{d+2} \beta\mu \,. \tag{A.28}$$

Thus, for $\beta^{-1} \to 0$, we find from Eq. (A.27),

$$\frac{E}{N} \to \frac{d}{d+2} \mu(\beta^{-1} \to 0) \,. \tag{A.29}$$

We call the chemical potential at zero temperature the Fermi energy ε_F,

$$\varepsilon_F \equiv \mu(\beta^{-1} = 0) \,, \tag{A.30}$$

which allows to rewrite Eq. (A.29) as

$$E(\beta^{-1} = 0) = N\varepsilon_F \frac{d}{d+2} \,. \tag{A.31}$$

Classical limit ($z \ll 1$):

For $z \ll 1$, the series expansion (A.13) allows the approximation

$$\begin{aligned} \frac{f_{\nu+1}(z)}{f_\nu(z)} &= \frac{z - z^2/2^{\nu+1}}{z - z^2/2^\nu} + \mathcal{O}\big[z^2\big] = \left(1 - \frac{z}{2^{\nu+1}}\right)\left(1 + \frac{z}{2^\nu}\right) + \mathcal{O}\big[z^2\big] \\ &= 1 + \frac{z}{2^{\nu+1}} + \mathcal{O}\big[z^2\big] \,. \end{aligned} \tag{A.32}$$

Using $z \approx f_{d/2}(z)$ and Eq. (A.40) gives

$$\frac{f_{d/2+1}(z)}{f_{d/2}(z)} \approx 1 + \frac{2^{-d/2}/d}{\Gamma(d/2)} (\varepsilon_F\beta)^{d/2} \,. \tag{A.33}$$

Thus, we find

$$\frac{E}{N\varepsilon_F} = \frac{E_{\text{classical}}}{N\varepsilon_F} \left(1 + \frac{2^{-d/2}/d}{\Gamma(d/2)} (\varepsilon_F\beta)^{d/2}\right) \tag{A.34a}$$

$$= \frac{E_{\text{classical}}}{N\varepsilon_F} + \frac{2^{-d/2-1}}{\Gamma(d/2)} (\varepsilon_F\beta)^{d/2-1} \tag{A.34b}$$

with

$$\frac{E_{\text{classical}}}{N\varepsilon_F} = \frac{d}{2} (\varepsilon_F\beta)^{-1} \,. \tag{A.35}$$

From Eq. (A.34a) follows $E/E_{\text{classical}} \to 1$ at high temperatures for all $d > 0$; however, the behaviour of the difference $(E - E_{\text{classical}})$ is dimension dependent:

$$\frac{E - E_{\text{classical}}}{N\varepsilon_F} \to \begin{cases} \text{diverges} \sim (\varepsilon_F\beta)^{d/2-1} \,, & \text{for } d < 2 \\ 1/4 \,, & \text{for } d = 2 \\ 0 \,, & \text{for } d > 2 \,. \end{cases} \tag{A.36}$$

$f_{d/2}(z)$ in terms of d and β:

For $\beta^{-1} = 0$, the mean energy can be directly obtained from the defining integral,

$$\begin{aligned} E(\beta^{-1}=0) &= \sum_p \varepsilon_p n(\varepsilon_p) \quad \text{with } n(\varepsilon_p) \text{ given in Eq. (A.19)} \\ &\approx \frac{g_s V}{(2\pi\hbar)^d} \frac{(2\pi m)^{d/2}}{\Gamma(d/2)} \int_0^\infty \mathrm{d}\varepsilon\, \varepsilon^{d/2-1} n(\varepsilon) \\ &= \frac{g_s V}{(2\pi\hbar)^d} \frac{(2\pi m)^{d/2}}{\Gamma(d/2)} \int_0^{\varepsilon_F} \mathrm{d}\varepsilon\, \varepsilon^{d/2-1} \\ &= \frac{g_s V}{(2\pi\hbar)^d} \frac{(2\pi m)^{d/2}}{\Gamma(d/2)} \frac{\varepsilon_F^{d/2+1}}{d/2+1}\,. \end{aligned} \tag{A.37}$$

Combining Eqs. (A.31) and (A.37),

$$N\varepsilon_F \frac{d}{d+2} = g_s \left(\frac{L}{2\pi\hbar}\right)^d (2\pi m)^{d/2} \frac{1}{\Gamma(d/2)} \frac{1}{d/2+1} \varepsilon_F^{d/2+1} \tag{A.38}$$

$$\Leftrightarrow \qquad \frac{d}{2} N \Gamma(d/2) = g_s \left(\frac{L}{2\pi\hbar}\right)^d (2\pi m \varepsilon_F)^{d/2} = \frac{g_s V}{\lambda_T^d} (\varepsilon_F \beta)^{d/2}\,, \tag{A.39}$$

allows to express $f_{d/2}(z)$ can be expressed in terms of d and β,

$$f_{d/2}(z) \overset{\text{(A.18)}}{=} \frac{N\lambda_T^d}{g_s V} \overset{\text{(A.39)}}{=} \frac{2/d}{\Gamma(d/2)} (\varepsilon_F \beta)^{d/2}\,. \tag{A.40}$$

For later use, we note that the last equation implies

$$\frac{\partial f_\nu(z)}{\partial(\beta^{-1})} = -\nu\beta f_\nu(z)\,. \tag{A.41}$$

A.6 Heat capacity

The heat capacity C_V at constant volume is defined as

$$\frac{C_V}{N k_B} \equiv \frac{1}{N} \frac{\partial E}{\partial \beta^{-1}}\,. \tag{A.42}$$

Using Eq. (A.27) and Eq. (A.41), one finds

$$\frac{C_V}{N k_B} = \left(\frac{d}{2} + \frac{d^2}{4}\right) \frac{f_{d/2+1}(z)}{f_{d/2}(z)} - \frac{d^2}{4} \frac{f'_{d/2+1}(z)}{f'_{d/2}(z)}\,. \tag{A.43}$$

The chemical potentials as a function of temperature in $d = 1$, 2, and 3 dimensions are shown in Fig. A.4.

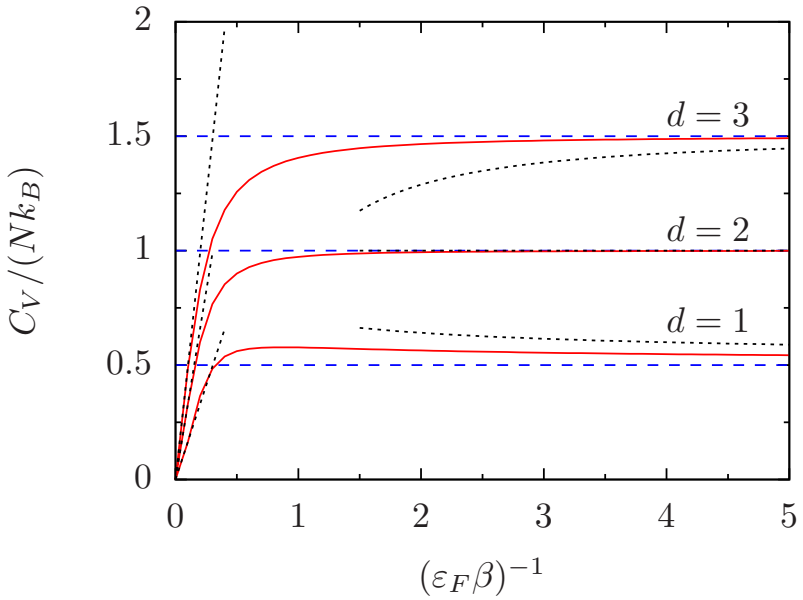

Figure A.4: Heat capacity per particle as a function of temperature for the ideal Fermi gas (red solid lines) and the ideal classical gas (blue dashed lines) in d dimensions. The asymptotic behaviour of the ideal Fermi gas for low and high temperatures is shown as black dotted lines.

Quantum limit ($z \gg 1$):

At low temperatures, C_V goes linearly to zero according to

$$\frac{C_V}{Nk_B} = \frac{\pi^2 d}{6}(\varepsilon_F\beta)^{-1} + \mathcal{O}\left[(\varepsilon_F\beta)^{-2}\right]. \tag{A.44}$$

Classical limit ($z \ll 1$):

From the $\beta^{-1} \gg 1$ behaviour of the energy E, it follows that C_V converges to the classical result in all dimensions:

$$\frac{C_V}{Nk_B} = \frac{C_{V,\text{classical}}}{Nk_B} + \frac{2^{-d/2}d(1-d/2)}{\Gamma(d/2)}(\varepsilon_F\beta)^{d/2} + \mathcal{O}\left[(\varepsilon_F\beta)^{d}\right] \tag{A.45}$$

with

$$\frac{C_{V,\text{classical}}}{Nk_B} = \frac{d}{2}. \tag{A.46}$$

A.7 Chemical potential

Since the fugacity z can be calculated according to Eq. (A.40) for a given $(\varepsilon_F\beta)^{-1}$, the chemical potential as a function of temperature is given by the definition of the

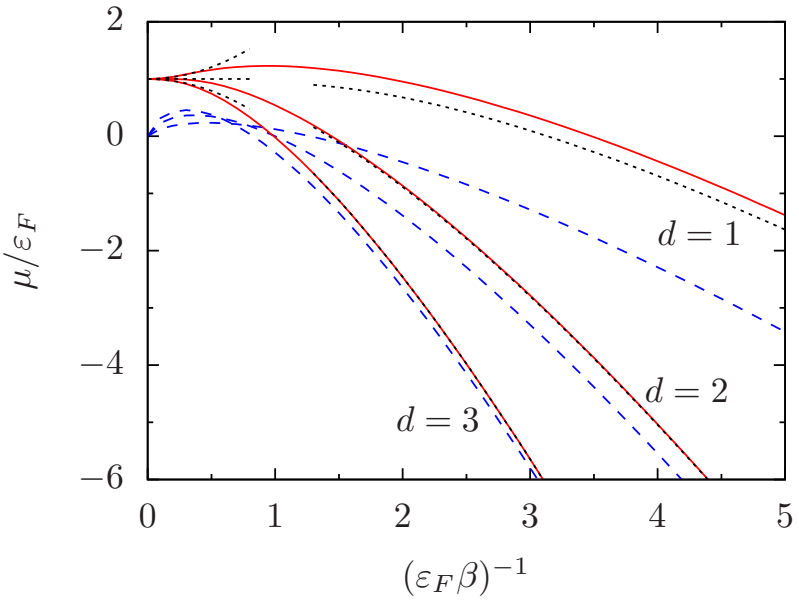

Figure A.5: Chemical potential as a function of temperature for the ideal Fermi gas (red solid lines) and the ideal classical gas (blue dashed lines) in d dimensions. The asymptotic behaviour of the ideal Fermi gas for low and high temperatures is shown as black dotted lines.

fugacity,

$$\frac{\mu}{\varepsilon_F} = (\varepsilon_F\beta)^{-1} \ln z \,. \tag{A.47}$$

The chemical potentials as a function of temperature in $d = 1$, 2, and 3 dimensions are shown in Fig. A.5.

Quantum limit ($z \gg 1$):

Per definition of the Fermi energy, it is $\mu/\varepsilon_F = 1$ at zero temperature. Including second-order corrections, one finds

$$\frac{\mu}{\varepsilon_F} = 1 + \frac{\pi^2}{6}\left(1 - \frac{d}{2}\right)(\varepsilon_F\beta)^{-2} + \mathcal{O}\left[(\varepsilon_F\beta)^{-4}\right]. \tag{A.48}$$

Classical limit ($z \ll 1$):

Using Eq. (A.24), one finds

$$\frac{\mu}{\varepsilon_F} = \frac{\mu_{\text{classical}}}{\varepsilon_F} + \frac{2^{1-d/2}/d}{\Gamma(d/2)}(\varepsilon_F\beta)^{d/2-1} \tag{A.49}$$

with

$$\frac{\mu_{\text{classical}}}{\varepsilon_F} = (\varepsilon_F\beta)^{-1} \ln\left[\frac{2/d}{\Gamma(d/2)}(\varepsilon_F\beta)^{d/2}\right] . \tag{A.50}$$

The high-temperature behaviour of the difference $(\mu - \mu_{\text{classical}})$ is dimension dependent:

$$\frac{\mu - \mu_{\text{classical}}}{\varepsilon_F} \to \begin{cases} \text{diverges} \sim (\varepsilon_F\beta)^{d/2-1}\,, & \text{for } d < 2 \\ 1/2\,, & \text{for } d = 2 \\ 0\,, & \text{for } d > 2. \end{cases} \tag{A.51}$$

A.8 Pressure

The grand-canonical potential Φ can be written in terms of the total energy E,

$$\begin{aligned} \Phi &= -\frac{g_s V}{\lambda_T^d}\frac{\beta^{d/2}}{\Gamma(d/2)}\int_0^\infty \varepsilon^{d/2-1}\ln\left[1 + z\mathrm{e}^{-\beta\varepsilon}\right]\mathrm{d}\varepsilon \\ &= -\frac{g_s V}{\lambda_T^d}\frac{\beta^{d/2}}{\Gamma(d/2)}\frac{2}{d}\left\{\left[\varepsilon^{d/2}\ln\left[1 + z\mathrm{e}^{-\beta\varepsilon}\right]\right]_0^\infty + \beta\int_0^\infty \frac{\varepsilon^{d/2}}{z^{-1}\mathrm{e}^{\beta\varepsilon}+1}\right\} \\ &= -\frac{2}{d}\frac{g_s V}{\lambda_T^d}\beta^{-1}\frac{\Gamma(1+d/2)}{\Gamma(d/2)}f_{1+d/2}(z) \\ &= -\frac{2}{d}E\,. \end{aligned} \tag{A.52}$$

Thus, one finds for the pressure P, defined by $PV = -\Phi$,

$$PV = \frac{2}{d}E\,. \tag{A.53}$$

The last equation is the so-called energy-momentum relation. Note that, for an ideal quantum gas, it can be shown that this relation is independent of the statistics (Fermi-Dirac, Bose-Einstein, Maxwell-Boltzmann).

Appendix B

Graßmann variables and coherent states for fermions

In this appendix, we list properties of Graßmann variables that are needed in the context of our discussion of non-relativistic fermionic path integrals. For a rigorous and more detailed discussion of Graßmann variables in the context of path integrals, see, for example, Ref. [109]. Furthermore, we briefly review coherent states for fermions, which are discussed in more detail, for example, in Ref. [95].

B.1 Graßmann variables

To distinguish anti-commuting Graßmann variables from commuting real and complex numbers, the latter will be called c-numbers in this appendix, where c stands for commuting.

Anti-commutation relation

A set of complex Graßmann variables θ_a, $a \in \{1, \ldots, n\}$, satisfies

$$\theta_a \theta_b + \theta_b \theta_a = 0 \tag{B.1}$$

with $a, b \in \{1, 2, \ldots, n\}$. This implies that Graßmann variables are nilpotent,

$$(\theta_a)^2 = 0\,. \tag{B.2}$$

Any Graßmann variable commutes with any c-number. Zero is the only number that is a c-number as well as a Graßmann variable simultaneously.

Complex conjugation

For any pair of Graßmann variables θ and ϑ, complex conjugation (denoted by an asterisk) is defined by

$$(\theta\vartheta)^* = \vartheta^* \theta^*\,, \tag{B.3}$$

which ensures the reality condition $(\theta\theta^*)^* = \theta\theta^*$.

Functions of Graßmann variables

A function of Graßmann variables is defined as a Taylor expansion of the function. Since Graßmann variables are nilpotent, Eq. (B.2), there is only a finite number of Taylor coefficients for a function the depends on a finite number of Graßmann variables.

For a function $f(\theta)$ of a single Graßmann variable θ, it is

$$f(\theta) = a + b\theta \tag{B.4}$$

with c-numbered Fourier coefficients a and b. We find

$$a = f(0) \tag{B.5}$$

$$b = \frac{\partial}{\partial\theta} f(\theta)\,. \tag{B.6}$$

Since any function $f(\theta)$ of a single Graßmann variable is θ at most linear in θ, the two fundamental integrals

$$\int \mathrm{d}\theta = 0 \tag{B.7}$$

$$\int \mathrm{d}\theta\,\theta = 1 \tag{B.8}$$

determine completely the integral of f. Note that differentiation and integration with respect to a Graßmann gives the same result,

$$\frac{\partial}{\partial\theta} f(\theta) = b = \int \mathrm{d}\theta\, f(\theta)\,. \tag{B.9}$$

Differentiation and integration

Since Graßmann variables anti-commute, it is necessary to choose an order for differentiation and integration. The common choice is

$$\frac{\partial}{\partial\theta}\theta\vartheta = \vartheta = -\frac{\partial}{\partial\theta}\vartheta\theta \qquad \Leftrightarrow \qquad \int \mathrm{d}\theta\,\theta\vartheta = \vartheta = -\int \mathrm{d}\theta\,\vartheta\theta\,, \tag{B.10}$$

$$\frac{\partial}{\partial\theta}\frac{\partial}{\partial\vartheta} = -\frac{\partial}{\partial\vartheta}\frac{\partial}{\partial\theta} \qquad \Leftrightarrow \qquad \int \mathrm{d}\theta\mathrm{d}\vartheta = -\int \mathrm{d}\theta\mathrm{d}\vartheta\,, \tag{B.11}$$

where θ and ϑ are Graßmann variables.

Change of variables

Since differentiation and integration coincides for Graßmann variables, the integral needs to be transformed with the *inverse* of the usual Jacobian if Graßmann integration variables are changed,

$$\int \mathrm{d}\theta_n \cdots \mathrm{d}\theta_1 = \int \mathrm{d}\theta'_n \cdots \mathrm{d}\theta'_1 \left[\frac{\partial\vec{\theta}}{\partial\vec{\theta}'}\right]^{-1}. \tag{B.12}$$

Functional derivative

We consider a Graßmann variable $\theta(t)$ that depends on a c-number parameter t, i. e. $\theta(t)$ is a so-called Graßmann field. Let $F[\theta(t)]$ be a functional of $\theta(t)$. The functional derivative of $F[\theta(t)]$ with respect to the Graßmann field $\theta(s)$ is then defined as

$$\frac{\delta F[\theta(t)]}{\delta\theta(s)} \equiv \frac{F[\theta(t)+\varepsilon\delta(t-s)]-F[\theta(t)]}{\varepsilon}\,, \tag{B.13}$$

where ε is a Graßmann variable that anti-commutes with Graßmann field. As mentioned above, the Taylor expansion of $F[\psi(t)+\varepsilon\delta(t-s)]-F[\psi(t)]$ with respect to ε is linear in ε since $\varepsilon^2=0$. Since the numerator is proportional to ε, the division by ε is to be understood as picking up the coefficient of ε in the numerator. Note, however, that a division by a Graßmann variable is not well defined in general.

Real and imaginary parts of complex Graßmann variables

The real and imaginary parts of a complex Graßmann variable θ are defined as

$$\frac{1}{\sqrt{2}}\theta_1 = \mathrm{Re}[\theta] \equiv \frac{1}{2}\Big(\theta+\theta^*\Big)\,, \tag{B.14}$$

$$\frac{1}{\sqrt{2}}\theta_2 = \mathrm{Im}[\theta] \equiv \frac{1}{2\mathrm{i}}\Big(\theta-\theta^*\Big)\,. \tag{B.15}$$

From this definition of θ_1 and θ_2, and property (B.1) of θ and θ^* follows immediately

$$\theta_1\theta_1 = \theta_2\theta_2 = 0\,, \tag{B.16}$$

$$\mathrm{i}\theta_1\theta_2 = -\mathrm{i}\theta_2\theta_1 = \theta^*\theta\,, \tag{B.17}$$

which implies that $\mathrm{i}\theta_1\theta_2$ rather than $\theta_1\theta_2$ is real. This motivates to introduce the bared notation,

$$\overline{\theta}_1 = -\mathrm{i}\theta_2 = \frac{1}{\sqrt{2}}\Big(\theta^*-\theta\Big)\,, \tag{B.18}$$

$$\overline{\theta}_2 = \mathrm{i}\theta_1 = \frac{\mathrm{i}}{\sqrt{2}}\Big(\theta^*+\theta\Big)\,, \tag{B.19}$$

such that

$$\theta_i\overline{\theta}_j = -\overline{\theta}_j\theta_i \in \mathbb{R} \tag{B.20}$$

for $i,j\in\{1,2\}$ and

$$\theta^*\theta = \frac{1}{2}\Big(\overline{\theta}_1\theta_1+\overline{\theta}_2\theta_2\Big)\,. \tag{B.21}$$

The measure of integration in $\int \mathrm{d}\theta^*\mathrm{d}\theta$ and $\int \mathrm{d}\theta_1\mathrm{d}\theta_2$ are related by

$$\int \mathrm{d}\theta^*\mathrm{d}\theta = \frac{\mathrm{i}}{2}\int \mathrm{d}\theta_1\mathrm{d}\theta_2\,, \tag{B.22}$$

where we used Eq. (B.12).

B.2 Coherent states for fermions

Coherent states, i. e. eigenstates of the annihilation operator $\hat{a}$, for fermions are defined as

$$|\theta\rangle \equiv \mathrm{e}^{-\theta^*\theta/2}\mathrm{e}^{\hat{a}^\dagger\theta}|0\rangle = \mathrm{e}^{-\theta^*\theta/2}\big(|0\rangle - \theta|1\rangle\big)\,, \tag{B.23}$$

and their adjoint states read

$$\langle\theta| \equiv \mathrm{e}^{-\theta^*\theta/2}\langle 0|\mathrm{e}^{\theta^*\hat{a}} = \mathrm{e}^{-\theta^*\theta/2}\big(\langle 0| + \theta^*\langle 1|\big)\,. \tag{B.24}$$

Note that the Graßmann variable θ anti-commutes with the fermionic operators $\hat{a}$ and $\hat{a}^\dagger$. The coherent states $|\theta\rangle$ are indeed an eigenstates of the annihilation operator $\hat{a}$ since

$$\begin{aligned}\hat{a}|\theta\rangle &= \hat{a}\mathrm{e}^{-\theta^*\theta/2}\big(|0\rangle - \theta|1\rangle\big) = \mathrm{e}^{-\theta^*\theta/2}\hat{a}\big(|0\rangle - \theta|1\rangle\big) = \mathrm{e}^{-\theta^*\theta/2}\theta\hat{a}|1\rangle \\ &= \mathrm{e}^{-\theta^*\theta/2}\theta|0\rangle \overset{\text{(B.2)}}{=} \mathrm{e}^{-\theta^*\theta/2}\theta\big(|0\rangle - \theta|1\rangle\big) = \theta\mathrm{e}^{-\theta^*\theta/2}\big(|0\rangle - \theta|1\rangle\big) \\ &= \theta|\theta\rangle\,.\end{aligned} \tag{B.25}$$

The coherent states $|\theta\rangle$ form an over-complete set in the one-fermion Hilbert space. They fulfil the identity

$$\begin{aligned}&\int \mathrm{d}\theta^*\mathrm{d}\theta\,|\theta\rangle\langle\theta| \\ &= \int \mathrm{d}\theta^*\mathrm{d}\theta\,\mathrm{e}^{-\theta^*\theta}\big(|0\rangle\langle 0| - \theta|1\rangle\langle 0| + \theta^*|0\rangle\langle 1|\big) \\ &= \int \mathrm{d}\theta^*\mathrm{d}\theta\,\Big(|0\rangle\langle 0| + |1\rangle\langle 0|\theta + \theta^*|0\rangle\langle 1| + \theta\theta^*\big(|0\rangle\langle 0| + |1\rangle\langle 1|\big)\Big) = 1\,.\end{aligned} \tag{B.26}$$

For an operator $\hat{O}$, the trace can be evaluated using the integral over the *anti-diagonal* elements

$$\begin{aligned}\mathrm{Tr}\left[\hat{O}\right] &= \int \mathrm{d}\theta^*\mathrm{d}\theta\,\langle -\theta|\hat{O}|\theta\rangle = \int \mathrm{d}\theta^*\mathrm{d}\theta\,\mathrm{e}^{-\theta^*\theta}\big(\langle 0| - \theta^*\langle 1|\big)\hat{O}\big(|0\rangle - \theta|1\rangle\big) \\ &= \langle 0|\hat{O}|0\rangle + \langle 1|\hat{O}|1\rangle\,.\end{aligned} \tag{B.27}$$

Bibliography

[1] J. Berges, *What the inflaton might tell us about RHIC/LHC*, Nucl. Phys. A **820** (2009), 65c–73c.

[2] R. Micha and I. I. Tkachev, *Turbulent thermalization*, Phys. Rev. D **70** (2004), 043538.

[3] U. W. Heinz and P. F. Kolb, *Early thermalization at RHIC*, Nucl. Phys. A **702** (2002), 269.

[4] Y. V. Kovchegov and A. Taliotis, *Early time dynamics in heavy-ion collisions from AdS/CFT correspondence*, Phys. Rev. C **76** (2007), 014905.

[5] E. Shuryak, *Physics of strongly coupled quark-gluon plasma*, Prog. Part. Nucl. Phys. **62** (2009), 48.

[6] R. D. Levine, *Molecular Reaction Dynamics*, Cambridge University Press, Cambridge, 2005.

[7] P. H. Bucksbaum, *The future of attosecond spectroscopy*, Science **317** (2007), 766.

[8] A. L. Cavalieri, N. Müller, T. Uphues, V. S. Yakovlev, A. Baltuška, B. Horvath, B. Schmidt, L. Blümel, R. Holzwarth, S. Hendel, M. Drescher, U. Kleineberg, P. M. Echenique, R. Kienberger, F. Krausz, and U. Heinzmann, *Attosecond spectroscopy in condensed matter*, Nature **449** (2007), 1029–1032.

[9] M. Hentschel, R. Kienberger, C. Spielmann, G. A. Reider, N. Milosevic, T. Brabec, P. Corkum, U. Heinzmann, M. Drescher, and F. Krausz, *Attosecond metrology*, Nature **414** (2001), 509–513.

[10] I. Bloch, J. Dalibard, and W. Zwerger, *Many-body physics with ultracold gases*, Rev. Mod. Phys. **80** (2008), 885–964.

[11] E. Fermi, J. Pasta, and S. Ulam *Studies of nonlinear problems* Technical report, Los Alamos report LA-1940, Mai 1955 (published later in Collected Papers of Enrico Fermi, E. Segré (Ed.), University of Chicago Press (1965)).

[12] J. Ford, *The Fermi-Pasta-Ulam problem: Paradox turns discovery*, Physics Reports **213** (1992), 271.

[13] M. Greiner, O. Mandel, T. W. Hänsch, and I. Bloch, *Collapse and revival of the matter wave field of a Bose-Einstein condensate*, Nature (London) **419** (2002), 51.

[14] S. Hofferberth, I. Lesanovsky, B. Fischer, T. Schumm, and J. Schmiedmayer, *Non-equilibrium coherence dynamics in one-dimensional Bose gases*, Nature **449** (2007), 324.

[15] T. Kinoshita, T. Wenger, and D. S. Weiss, *A quantum Newton's cradle*, Nature **440** (2006), 900.

[16] A. J. Leggett, *Bose-Einstein condensation in the alkali gases: Some fundamental concepts*, Rev. Mod. Phys. **73** (2001), 307–356.

[17] L. P. Pitaevskii and S. Stringari, *Bose-Einstein Condensation*, Clarendon Press, 2003.

[18] M. P. A. Fisher and L. I. Glazman, *Transport in a one-dimensional Luttinger liquid*, in Mesoscopic Electron Transport, (L. Kowenhoven, G. Schoen, and L. Sohn, eds.) NATO ASI Series E, Kluwer, Dordrecht, 1996.

[19] V. E. Korepin, N. M. Bogoliubov, and A. G. Izergin, *Quantum Inverse Scattering Method and Correlation Functions*, Cambridge University Press, Cambridge, 1997.

[20] K. Burnett, *Tailor-made condensates*, Nature **392** (1998), 125.

[21] U. Fano, *On the absorption spectrum of noble gases at the arc spectrum limit*, Nuovo Cimento [J. Res. NIST 110, 583 (2005)] **12** (1935), 154.

[22] ———, *Effects of configuration interaction on intensities and phase shifts*, Phys. Rev. **124** (1961), 1866.

[23] E. Tiesinga, A. J. Moerdijk, B. J. Verhaar, and H. T. C. Stoof, *Conditions for Bose-Einstein condensation in magnetically trapped atomic cesium*, Phys. Rev. A **46** (1992), R1167–R1170.

[24] I. Bloch, *Quantum gases in optical lattices*, Phys. World **17** (2004), 25–29.

[25] D. Jaksch, C. Bruder, J. I. Cirac, C. W. Gardiner, and P. Zoller, *Cold bosonic atoms in optical lattices*, Phys. Rev. Lett. **81** (1998), 3108–3111.

[26] O. Morsch and M. K. Oberthaler, *Dynamics of Bose-Einstein condensates in optical lattices*, Rev. Mod. Phys. **78** (2006), 179.

[27] T. Bergeman, M. G. Moore, and M. Olshanii, *Atom-atom scattering under cylindrical harmonic confinement: Numerical and analytic studies of the confinement induced resonance*, Phys. Rev. Lett. **91** (2003), 163201.

[28] M. Olshanii, *Atomic scattering in the presence of an external confinement and a gas of impenetrable bosons*, Phys. Rev. Lett. **81** (1998), 938–941.

[29] B. Paredes, A. Widera, V. Murg, O. Mandel, S. Fölling, I. Cirac, G. V. Shlyapnikov, T. W. Hänsch, and I. Bloch, *Tonks-Girardeau gas of ultracold atoms in an optical lattice*, Nature **429** (2004), 277–281.

[30] J. Schmiedmayer and R. Folman, C. R. Acad. Sci. Paris IV **2** (2001), 333.

[31] Q. Chen, J. Stajic, S. Tan, and K. Levin, *BCS-BEC crossover: From high temperature superconductors to ultracold superfluids*, Phys. Reports **412** (2005), 1–88.

[32] S. Diehl, S. Flörchinger, H. Gies, J. M. Pawlowski, and C. Wetterich, *Functional renormalization group approach to the BCS-BEC crossover*, Annalen Phys. **522** (2010), 615–656.

[33] S. Giorgini, L. P. Pitaevskii, and S. Stringari, *Theory of ultracold Fermi gases*, Rev. Mod. Phys. **80** (2008), 1215.

[34] R. Grimm, *Ultracold Fermi gases in the BEC-BCS crossover: A review from the Innsbruck perspective*, in Proceedings of the International School of Physics - Enrico Fermi, (M. Inguscio, W. Ketterle, and C. Salomon, eds.), IOS Press, Amsterdam, 2008.

[35] (M. Inguscio, W. Ketterle, and C. Salomon, eds.), *Ultracold Fermi gases, Proceedings of the International School of Physics "Enrico Fermi", Course CLXIV, Varenna, 2006*, IOS Press, Amsterdam, 2008.

[36] C. A. Regal, M. Greiner, and D. S. Jin, *Lifetime of molecule-atom mixtures near a Feshbach resonance in* ^{40}K, Phys. Rev. Lett. **92** (2004), 083201.

[37] C. A. Regal and D. S. Jin, *Experimental realization of the BCS-BEC crossover with a Fermi gas of atoms*, Adv. At. Mol. Opt. Phys. **54** (2006), 1.

[38] M. W. Zwierlein, C. A. Stan, C. H. Schunck, S. M. F. Raupach, A. J. Kerman, and W. Ketterle, *Condensation of pairs of fermionic atoms near a Feshbach resonance*, Phys. Rev. Lett. **92** (2004), 120403.

[39] A. V. Gorshkov, M. Hermele, V. Gurarie, C. Xu, P. S. Julienne, J. Ye, P. Zoller, E. Demler, M. D. Lukin, and A. M. Rey, *Two-orbital $SU(N)$ magnetism with ultracold alkaline-earth atoms*, Nature Phys. **6** (2010), 289–295.

[40] J. Schwinger, *Brownian motion of a quantum oscillator*, J. Math. Phys. **2** (1961), 407–432.

[41] P. M. Bakshi and K. T. Mahanthappa, *Expectation value formalism in quantum field theory. I*, J. Math. Phys. **4** (1963), 1–11.

[42] ———, *Expectation value formalism in quantum field theory. II*, J. Math. Phys. **4** (1963), 12–16.

[43] K. T. Mahanthappa, *Multiple production of photons in quantum electrodynamics*, Phys. Rev. **126** (1962), 329–340.

[44] L. V. Keldysh, *Diagram technique for nonequilibrium processes*, [Sov. Phys. JETP **20**, 1018 (1965)] Zh. Eksp. Teor. Fiz. **47** (1964), 1515.

[45] F. Cooper, J. Dawson, S. Habib, and R. D. Ryne, *Chaos in time-dependent variational approximations to quantum dynamics*, Phys. Rev. E **57** (1998), 1489–1498.

[46] A. V. Ryzhov and L. G. Yaffe, *Large N quantum time evolution beyond leading order*, Phys. Rev. D **62** (2000), 125003.

[47] T. Altherr and D. Seibert, *Problems of perturbation series in non-equilibrium quantum field theories*, Phys. Lett. B **333** (1994), 149–152.

[48] G. Aarts, G. F. Bonini, and C. Wetterich, *Exact and truncated dynamics in nonequilibrium field theory*, Phys. Rev. D **63** (2000), 025012.

[49] B. Mihaila, T. Athan, F. Cooper, J. Dawson, and S. Habib, *Exact and approximate dynamics of the quantum mechanical $O(N)$ model*, Phys. Rev. D **62** (2000), 125015.

[50] B. Mihaila, J. F. Dawson, and F. Cooper, *Order $1/N$ corrections to the time-dependent Hartree approximation for a system of $N+1$ oscillators*, Phys. Rev. D **56** (1997), 5400–5412.

[51] M. Sallé and J. Smit, *Hartree ensemble approximation revisited: The "symmetric phase"*, Phys. Rev. D **67** (2003), 116006.

[52] M. Sallé, J. Smit, and J. C. Vink, *Thermalization in a Hartree ensemble approximation to quantum field dynamics*, Phys. Rev. D **64** (2001), 025016.

[53] G. Baym, *Self-consistent approximations in many-body systems*, Phys. Rev. **127** (1962), 1391–1401.

[54] J. Berges and J. Cox, *Thermalization of quantum fields from time-reversal invariant evolution equations*, Phys. Lett. B **517** (2001), 369.

[55] E. Calzetta and B. L. Hu, *Nonequilibrium quantum fields: Closed-time-path effective action, Wigner function, and Boltzmann equation*, Phys. Rev. D **37** (1988), 2878–2900.

[56] J. M. Cornwall, R. Jackiw, and E. Tomboulis, *Effective action for composite operators*, Phys. Rev. D **10** (1974), 2428–2445.

[57] J. M. Luttinger and J. C. Ward, *Ground-state energy of a many-fermion system. II*, Phys. Rev. **118** (1960), 1417–1427.

[58] L. Hedin, *New method for calculating the one-particle Green's function with application to the electron-gas problem*, Phys. Rev. **139** (1965), A796–A823.

[59] G. Aarts, D. Ahrensmeier, R. Baier, J. Berges, and J. Serreau, *Far-from-equilibrium dynamics with broken symmetries from the* $1/N$ *expansion of the 2PI effective action*, Phys. Rev. D **66** (2002), 045008.

[60] J. Berges, *Controlled nonperturbative dynamics of quantum fields out of equilibrium*, Nucl. Phys. A **699** (2002), 847–886.

[61] A. Arrizabalaga, J. Smit, and A. Tranberg, *Equilibration in* φ^4 *theory in* $3+1$ *dimensions*, Phys. Rev. D **72** (2005), 025014.

[62] F. Cooper, J. F. Dawson, and B. Mihaila, *Dynamics of broken symmetry* $\lambda\varphi^4$ *field theory*, Phys. Rev. D **67** (2003), 051901.

[63] ———, *Quantum dynamics of phase transitions in broken symmetry* $\lambda\varphi^4$ *field theory*, Phys. Rev. D **67** (2003), 056003.

[64] J. Berges, S. Borsányi, and J. Serreau, *Thermalization of fermionic quantum fields*, Nucl. Phys. B **660** (2003), 51.

[65] J. Berges, S. Borsányi, and C. Wetterich, *Prethermalization*, Phys. Rev. Lett. **93** (2004), 142002.

[66] J. Berges and T. Gasenzer, *Quantum versus classical statistical dynamics of an ultracold Bose gas*, Phys. Rev. A **76** (2007), 033604.

[67] A. Branschädel and T. Gasenzer, *2PI nonequilibrium versus transport equations for an ultracold Bose gas*, J. Phys. B **41** (2008), 135302.

[68] T. Gasenzer, J. Berges, M. G. Schmidt, and M. Seco, *Nonperturbative dynamical many-body theory of a Bose-Einstein condensate*, Phys. Rev. A **72** (2005), 063604.

[69] A. M. Rey, B. L. Hu, E. Calzetta, A. Roura, and C. W. Clark, *Nonequilibrium dynamics of optical-lattice-loaded Bose-Einstein-condensate atoms: Beyond the Hartree-Fock-Bogoliubov approximation*, Phys. Rev. A **69** (2004), 033610.

[70] C. Scheppach, J. Berges, and T. Gasenzer, *Matter-wave turbulence: Beyond kinetic scaling*, Phys. Rev. A **81** (2010), 033611.

[71] K. Temme and G. Gasenzer, *Non-equilibrium dynamics of condensates in a lattice from the 2PI effective action in* $1/\mathcal{N}$ *expansion*, Phys. Rev. A **74** (2006), 053603.

[72] T. Gasenzer, S. Keßler, and J. M. Pawlowski, *Far-from-equilibrium quantum many-body dynamics*, Eur. Phys. J. C.

[73] T. Gasenzer and J. M. Pawlowski, *Functional renormalisation group approach to far-from-equilibrium quantum field dynamics*, Phys. Lett. B **670**.

[74] J. Berges, *Introduction to nonequilibrium quantum field theory*, AIP Conf. Proc. **739** (2005), 3–62.

[75] T. Gasenzer, *Ultracold gases far from equilibrium*, Eur. Phys. J. ST **168** (2009), 89–148.

[76] H. Kleinert, *Field theory of collective excitations II – Large-amplitude phenomena*, Lett. al Nuovo Cimento **31** (1981), 521–527.

[77] ———, *Field theory of collective excitations III – Condensation of four-particle clusters*, Phys. Lett. **84A** (1981), 199–201.

[78] C. N. Yang, *Some exact results for the many-body problem in one dimension with repulsive delta-function interaction*, Phys. Rev. Lett. **19** (1967), 1312–1315.

[79] D. M. Gangardt and M. Pustilnik, *Correlations in an expanding gas of hard-core bosons*, Phys. Rev. A **77** (2008), 041604.

[80] S. R. Manmana, A. Muramatsu, and R. M. Noack, *Time evolution of one-dimensional quantum many body systems*, AIP Conf. Proc. **789** (2005), 269.

[81] S. R. Manmana, S. Wessel, R. M. Noack, and A. Muramatsu, *Strongly correlated fermions after a quantum quench*, Phys. Rev. Lett. **98** (2007), 210405.

[82] M. Rigol, V. Dunjko, V. Yurovsky, and M. Olshanii, *Relaxation in a completely integrable many-body quantum system: An ab initio study of the dynamics of the highly excited states of 1D lattice hard-core bosons*, Phys. Rev. Lett. **98** (2007), 050405.

[83] S. Tomonaga, *Remarks on Bloch's method of sound waves applied to many-fermion problems*, Prog. Theor. Phys. **5** (1950), 544.

[84] M. Cazalilla, *Effect of suddenly turning on interactions in the Luttinger model*, Phys. Rev. Lett. **97** (2006), 156403.

[85] D. M. Kennes and V. Meden, *Relaxation dynamics of an exactly solvable electron-phonon model*, arXiv:1006.0927v1 [cond-mat.str-el].

[86] P. Calabrese and J. Cardy, *Quantum quenches in extended systems*, J. Stat. Mech. **P06008**.

[87] M. Eckstein and M. Kollar, *Nonthermal steady states after an interaction quench in the Falicov-Kimball model*, Phys. Rev. Lett. **100** (2008), 120404.

[88] C. Kollath, A. M. Läuchli, and E. Altman, *Quench dynamics and nonequilibrium phase diagram of the Bose-Hubbard model*, Phys. Rev. Lett. **98** (2007), 180601.

[89] M. Moeckel and S. Kehrein, *Interaction quench in the Hubbard model*, Phys. Rev. Lett. **100** (2008), 175702.

[90] M. Kronenwett and T. Gasenzer, *Far-from-equilibrium dynamics of an ultracold Fermi gas*, to be published in Appl. Phys. B.

[91] A. J. Daley, M. M. Boyd, J. Ye, and P. Zoller, *Quantum computing with alkaline-earth-metal atoms*, Phys. Rev. Lett. **101** (2008), 170504.

[92] M. Foss-Feig, M. Hermele, V. Gurarie, and A. M. Rey, *Heavy fermions in an optical lattice.*

[93] M. Foss-Feig, M. Hermele, and A. M. Rey, *Probing the Kondo lattice model with alkaline-earth-metal atoms*, Phys. Rev. A **81** (2010), 051603.

[94] P. A. M. Dirac, *Lectures on Quantum Mechanics*, Dover Publications, New York, 2001.

[95] H. Kleinert, *Path Integrals in Quantum Mechanics, Statistics, Polymer Physics, and Financial Markets*, World Scientific Publishing Company, Singapore, 2009.

[96] J. D. Bjorken, *Applications of the chiral* $U(6) \bigotimes U(6)$ *algebra of current densities*, Phys. Rev. **148** (1966), 1467–1478.

[97] K. Johnson and F. E. Low, *Current algebras in a simple model*, Prog. Theor. Phys. Suppl. **37** (1966), 74–93.

[98] H. B. Callen and T. A. Welton, *Irreversibility and generalized noise*, Phys. Rev. **83** (1951), 34–40.

[99] J. Jin, S. Welack, J. Luo, X.-Q. Li, P. Cui, R.-X. Xu, and Y. Yan, *Dynamics of quantum dissipation systems interacting with fermion and boson grand canonical bath ensembles: Hierarchical equations of motion approach*, J. Chem. Phys. **126** (2007), 134113.

[100] J. Berges, *n-PI effective action techniques for gauge theories*, Phys. Rev. D **70** (2004), 105010.

[101] J. Berges, S. Borsányi, D. Sexty, and I.-O. Stamatescu, *Lattice simulations of real-time quantum fields*, Phys. Rev. D **75** (2007), 045007.

[102] S. Chandrasekharan and U.-J. Wiese, *Meron-cluster solution of fermion sign problems*, Phys. Rev. Lett. **83** (1999), 3116–3119.

[103] T. D. Kieu and C. J. Griffin, *Monte Carlo simulations with indefinite and complex-valued measures*, Phys. Rev. E **49** (1994), 3855–3859.

[104] P. B. Blakie, A. S. Bradley, M. J. Davis, R. J. Ballagh, and C. W. Gardiner, *Dynamics and statistical mechanics of ultra-cold Bose gases using c-field techniques*, Adv. Phys. **57** (2008), 363–472.

[105] C. W. Gardiner and P. Zoller, *Quantum Noise*, 3. edition, Springer, Heidelberg, Heidelberg, 2004.

[106] M. Hillery, R. F. O'Connell, M. O. Scully, and E. P. Wigner, *Distribution functions in physics: Fundamentals*, Phys. Rept. **106** (1984), 121–167.

[107] A. Polkovnikov, *Phase space representation of quantum dynamics*, Annals of Physics **325** (2010), 1790–1852.

[108] U. Mosel, *Path Integrals in Field Theory*, Springer, Berlin, 2004.

[109] J. Zinn Justin, *Path Integrals in Quantum Mechanics*, Oxford University Press, Oxford, Jan 2005.

[110] R. J. Rivers, *Path integral methods in Quantum Field Theory*, Cambridge University Press, Cambridge, 1987.

[111] G. Baym and L. P. Kadanoff, *Conservation laws and correlation functions*, Phys. Rev. **124** (1961), 287–299.

[112] D. J. Bedingham, *Out-of-equilibrium quantum fields with conserved charge*, Phys. Rev. D **69** (2004), 105013.

[113] Y. B. Ivanov, J. Knoll, and D. N. Voskresensky, *Self-consistent approximations to non-equilibrium many-body theory*, Nuclear Physics A **657** (1999), 413 – 445.

[114] A. M. Rey, B. L. Hu, E. Calzetta, and C. W. Clark, *Quantum kinetic theory of a Bose-Einstein gas confined in a lattice*, Phys. Rev. A **72** (2005), 023604.

[115] J. Berges and S. Borsányi, *Range of validity of transport equations*, Phys. Rev. D **74** (2006), 045022.

[116] M. Bonitz, *Quantum Kinetic Theory*, Teubner, Stuttgart, 1998.

[117] L. P. Kadanoff and G. Baym, *Quantum Statistical Mechanics*, Benjamin, New York, 1962.

[118] D. R. Hartree, *The wave mechanics of an atom with a non-Coulomb central field*, Proc. Cambridge Phil. Soc. **24** (1928), 89.

[119] V. Fock, *Näherungsmethode zur Lösung des quantenmechanischen Mehrkörperproblems*, Z. Phys. **61** (1930), 126–148.

[120] N. N. Bogoliubov, *On the theory of superfluidity*, J. Phys. (USSR) **11** (1947), 23–32.

[121] M. Holland, J. Park, and R. Walser, *Formation of pairing fields in resonantly coupled atomic and molecular Bose-Einstein condensates*, Phys. Rev. Lett. **86** (2001), 1915–1918.

[122] T. Köhler and K. Burnett, *Microscopic quantum dynamics approach to the dilute condensed Bose gas*, Phys. Rev. A **65** (2002), 033601.

[123] P. Naidon and F. Masnou-Seeuws, *Pair dynamics in the formation of molecules in a Bose-Einstein condensate*, Phys. Rev. A **68** (2003), 033612.

[124] N. P. Proukakis, K. Burnett, and H. T. C. Stoof, *Microscopic treatment of binary interactions in the nonequilibrium dynamics of partially Bose-condensed trapped gases*, Phys. Rev. A **57** (1998), 1230–1247.

[125] N. N. Bogoliubov, *Kinetic equations*, J. Phys. (USSR) **10** (1946), 265–274.

[126] M. Born and H. S. Green, Proc. Roy. Soc. A **188** (1946), 10.

[127] J. G. Kirkwood, *The statistical mechanical theory of transport processes I. General theory*, J. Chem. Phys. **14** (1946), 180.

[128] ———, *The statistical mechanical theory of transport processes II. Transport in gases*, J. Chem. Phys. **15** (1947), 72.

[129] J. Yvon, *Théorie statistique des fluides et l'équation d'état*, Act. sci. et ind. **203**.

[130] K. Balzer, S. Bauch, and M. Bonitz, *Time-dependent second-order Born calculations for model atoms and molecules in strong laser fields*, Phys. Rev. A **82** (2010), 033427.

[131] S. Coleman, R. Jackiw, and H. D. Politzer, *Spontaneous symmetry breaking in the $O(N)$ model for large N*, Phys. Rev. D **10** (1974), 2491–2499.

[132] L. F. Abbott, J. S. Kang, and H. J. Schnitzer, *Bound states, tachyons, and restoration of symmetry in the $1/N$ expansion*, Phys. Rev. D **13** (1976), 2212–2226.

[133] B. Mihaila, J. F. Dawson, and F. Cooper, *Resumming the large-N approximation for time evolving quantum systems*, Phys. Rev. D **63** (2001), 096003.

[134] G. Aarts and A. Tranberg, *Nonequilibrium dynamics in the $O(N)$ model to next-to-next-to-leading order in the $1/N$ expansion*, Phys. Rev. D **74** (2006), 025004.

[135] G. Aarts, N. Laurie, and A. Tranberg, *Effective convergence of the two-particle irreducible $1/N$ expansion for nonequilibrium quantum fields*, Phys. Rev. D **78** (2008), 125028.

[136] M. Kollar and M. Eckstein, *Relaxation of a one-dimensional Mott insulator after an interaction quench*, Phys. Rev. A **78** (2008), 013626.

[137] J. Sabio and S. Kehrein, *Sudden interaction quench in the quantum sine-Gordon model*, New J. Phys. **12** (2010), 055008.

[138] P. Reimann, *Foundation of statistical mechanics under experimentally realistic conditions*, Phys. Rev. Lett. **101** (2008), 190403.

[139] J. M. Luttinger, *An exactly soluble model of a many-fermion system*, J. Math. Phys. **4** (1963), 1154–1162.

[140] D. C. Mattis and E. H. Lieb, *Exact solution of a many-fermion system and its associated boson field*, J. Math. Phys. **6** (1965), 304–312.

[141] A. Iucci and M. A. Cazalilla, *Quantum quench dynamics of the Luttinger model*, Phys. Rev. A **80** (2009), 063619.

[142] L. Viverit, S. Giorgini, L. Pitaevskii, and S. Stringari, *Momentum distribution of a trapped Fermi gas with large scattering length*, Phys. Rev. A **69** (2004), 013607.

[143] S. Tan, *Energetics of a strongly correlated Fermi gas*, Annals of Physics **323** (2008), 2952–2970.

[144] ———, *Large momentum part of a strongly correlated Fermi gas*, Annals of Physics **323** (2008), 2971–2986.

[145] ———, *Generalized virial theorem and pressure relation for a strongly correlated Fermi gas*, Annals of Physics **323** (2008), 2987–2990.

[146] E. Braaten and L. Platter, *Exact relations for a strongly interacting Fermi gas from the operator product expansion*, Phys. Rev. Lett. **100** (2008), 205301.

[147] B. Coqblin and J. R. Schrieffer, *Exchange interaction in alloys with cerium impurities*, Phys. Rev. **185** (1969), 847.

[148] P. Coleman, *Heavy fermions: Electrons at the edge of magnetism*, in Handbook of Magnetism and Advanced Magnetic Materials. Vol 1: Fundamentals and Theory, (H. Kronmuller and S. Parkin, eds.) John Wiley and Sons, 2007, p. 95.

[149] F. Steglich, J. Aarts, C. D. Bredl, W. Lieke, D. Meschede, W. Franz, and H. Schäfer, *Superconductivity in the presence of strong Pauli paramagnetism:* $CeCu_2Si_2$, Phys. Rev. Lett. **43** (1979), 1892–1896.

[150] M. A. Ruderman and C. Kittel, *Indirect exchange coupling of nuclear magnetic moments by conduction electrons*, Phys. Rev. **96** (1954), 99.

[151] P. Gegenwart, Q. Si, and F. Steglich, *Quantum criticality in heavy-fermion metals*, Nature Phys. **4** (2008), 186–197.

[152] H. v. Löhneysen, A. Rosch, M. Vojta, and P. Wölfle, *Fermi-liquid instabilities at magnetic quantum phase transitions*, Rev. Mod. Phys. **79** (2007), 1015–1075.

[153] M. M. Boyd, T. Zelevinsky, A. D. Ludlow, S. Blatt, T. Zanon-Willette, S. M. Foreman, and J. Ye, *Nuclear spin effects in optical lattice clocks*, Phys. Rev. A **76** (2007), 022510.

[154] P. Coleman, $1/N$ *expansion for the Kondo lattice*, Phys. Rev. B **28** (1983), 5255.

[155] ———, *New approach to the mixed-valence problem*, Phys. Rev. B **29** (1984), 3035–3044.

[156] N. Read and D. Newns, *On the solution of the Coqblin-Schrieffer Hamiltonian by the large-N expansion technique*, J. Phys. C **16** (1983), 3273–3295.

[157] S. Doniach, *Magnetic instability of a highly degenerate Kondo lattice*, Phys. Rev. B **35** (1987), 1814–1821.

[158] P. Cvitanović, *Group theory for Feynman diagrams in non-Abelian gauge theories*, Phys. Rev. D **14** (1976), 1536.

[159] ———, *Methods in Theoretical Quantum Optics*, Princeton University Press, 2008.

[160] A. J. Macfarlane, A. Sudbery, and P. H. Weisz, *On Gell-Mann's λ-matrices, d- and f-tensors, octets, and parametrizations of $su(3)$*, Commun. math. Phys **11** (1968), 77.

[161] (Y. Tokura, ed.), *Colossal Magnetoresistive Oxides*, Gordon and Breach, New York, 2000.

[162] G.-M. Zhang and L. Yu, *Kondo singlet state coexisting with antiferromagnetic long-range order: A possible ground state for Kondo insulators*, Phys. Rev. B **62** (2000), 76.

[163] A. Auerbach and K. Levin, *Kondo bosons and the Kondo lattice: Microscopic basis for the heavy Fermi liquid*, Phys. Rev. Lett. **57** (1986), 877–880.

[164] C. Lacroix and M. Cyrot, *Phase diagram of the Kondo lattice*, Phys. Rev. B **20** (1979), 1969–1976.

[165] Z.-z. Li and Y. Qiu, *Self-consistent theory of heavy-fermion alloys*, Phys. Rev. B **43** (1991), 12906–12913.

[166] F. Schwabl, *Statistische Mechanik*, 3. edition, Springer, Berlin Heidelberg New York, 2006.